Summary of the Bulletin of the International Seismological Centre

2020

January – June

Volume 57 Issue I

www.isc.ac.uk

ISSN 2309-236X

2023

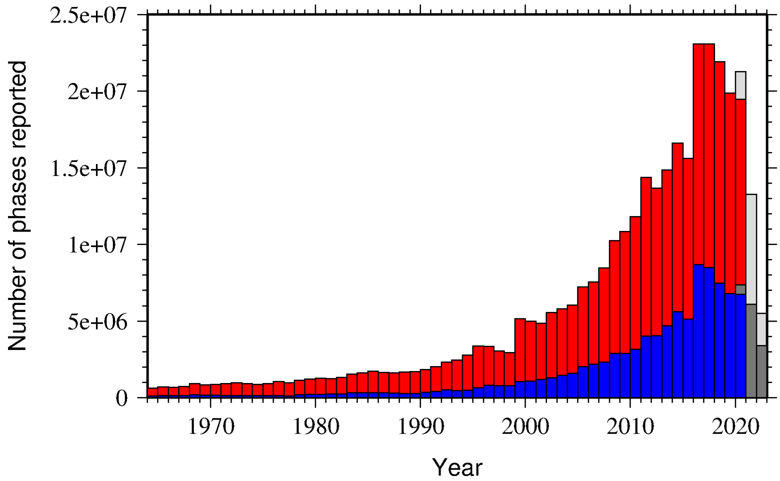

The number of phases (red) and number of amplitudes (blue) collected by the ISC for events each year since 1964. The data in grey covers the current period where data are still being collected before the ISC review takes place and are accurate at the time of publication. See Section 7.3.

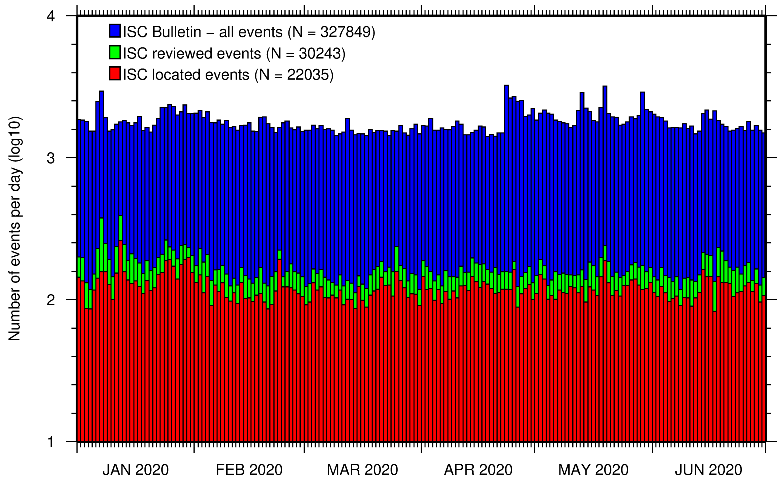

The number of events within the Bulletin for the current summary period. The vertical scale is logarithmic. See Section 8.1.

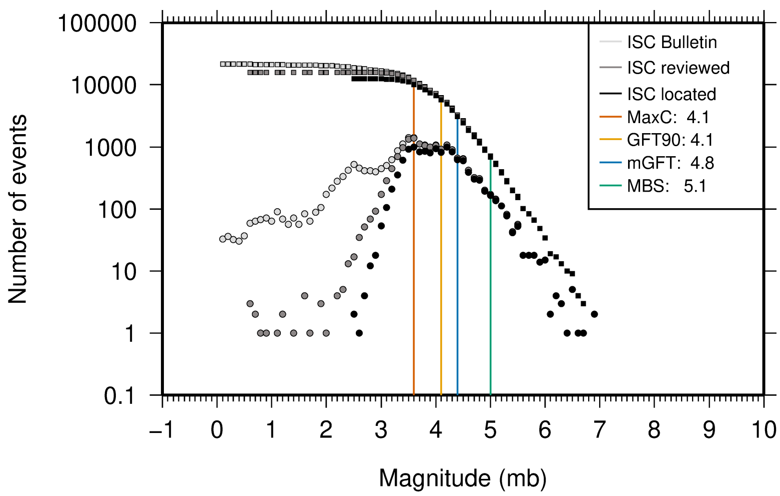

Frequency and cumulative frequency magnitude distribution for all events in the ISC Bulletin, ISC reviewed events and events located by the ISC. The magnitude of completeness (M_C) is shown for the ISC Bulletin. Note: only events with values of m_b are represented in the figure. See Section 8.4.

Summary of the Bulletin of the International Seismological Centre

2020

January - June

Volume 57 Issue I

Produced and edited by:
Kathrin Lieser, James Harris, Natalia Poiata and Dmitry Storchak

Published by
International Seismological Centre

The International Seismological Centre (ISC) is a Charitable Incorporated Organization (CIO) registered with The Charity Commission for England and Wales. Registered charity number: 1188971.

ISC Data Products

http://www.isc.ac.uk/products/

ISC Bulletin:
  http://www.isc.ac.uk/iscbulletin/search

ISC Bulletin and Catalogue monthly files, to the last reviewed month in FFB or ISF1 format:
  http://download.isc.ac.uk/[isf|ffb]/[bulletin|catalogue]/*yyyy*/*yyyymm*.gz
  ftp://www.isc.ac.uk/pub/[isf|ffb]/[bulletin|catalogue]/*yyyy*/*yyyymm*.gz

Datafiles for the ISC data before the rebuild:
  http://download.isc.ac.uk//prerebuild/[isf|ffb]/[bulletin|catalogue]/*yyyy*/*yyyymm*.gz
  ftp://www.isc.ac.uk/pub/prerebuild/[isf|ffb]/[bulletin|catalogue]/*yyyy*/*yyyymm*.gz

ISC-EHB Bulletin:
  http://www.isc.ac.uk/isc-ehb/search/

IASPEI Reference Event List (GT bulletin):
  http://www.isc.ac.uk/gtevents/search/

ISC-GEM Global Instrumental Earthquake Catalogue:
  http://www.isc.ac.uk/iscgem/download.php

ISC Event Bibliography:
  http://www.isc.ac.uk/event_bibliography/bibsearch.php

International Seismograph Station Registry:
  http://www.isc.ac.uk/registries/search/

Seismological Contacts:
  http://www.isc.ac.uk/projects/seismocontacts/

Copyright © 2023 by International Seismological Centre

Permission granted to reproduce for personal and educational use only. Commercial copying, hiring, lending is prohibited.

International Seismological Centre
Pipers Lane
Thatcham
RG19 4NS
United Kingdom
www.isc.ac.uk

The International Seismological Centre (ISC) is a Charitable Incorporated Organization (CIO) registered with The Charity Commission for England and Wales. Registered charity number: 1188971.

ISSN 2309-236X

Printed and bound in Wales by Cambrian Printers.

Contents

1 Preface 1

2 The International Seismological Centre 2

2.1 The ISC Mandate . . . 2
2.2 Brief History of the ISC . . . 3
2.3 Former Directors of the ISC and its U.K. Predecessors . . . 4
2.4 Member Institutions of the ISC . . . 5
2.5 Sponsoring Organisations . . . 10
2.6 Data Contributing Agencies . . . 11
2.7 ISC Staff . . . 18

3 Availability of the ISC Bulletin 23

4 Citing the International Seismological Centre 24

4.1 The ISC Bulletin . . . 24
4.2 The Summary of the Bulletin of the ISC . . . 25
4.3 The historical printed ISC Bulletin (1964-2009) . . . 25
4.4 The IASPEI Reference Event List . . . 25
4.5 The ISC-GEM Catalogue . . . 25
4.6 The ISC-EHB Dataset . . . 27
4.7 The ISC Event Bibliography . . . 27
4.8 International Registry of Seismograph Stations . . . 27
4.9 Seismological Dataset Repository . . . 27
4.10 Data transcribed from ISC CD-ROMs/DVD-ROMs . . . 27

5 Notes from ISC Data Users 28

5.1 Correct Assignment of Rayleigh Waves to Seismic Events . . . 28

6 Summary of Seismicity, January – June 2020 37

7 Statistics of Collected Data 42

7.1 Introduction . . . 42
7.2 Summary of Agency Reports to the ISC . . . 42
7.3 Arrival Observations . . . 47
7.4 Hypocentres Collected . . . 54

7.5 Collection of Network Magnitude Data . . . 56
7.6 Moment Tensor Solutions . . . 62
7.7 Timing of Data Collection . . . 64

8 Overview of the ISC Bulletin 66
8.1 Events . . . 66
8.2 Seismic Phases and Travel-Time Residuals . . . 75
8.3 Seismic Wave Amplitudes and Periods . . . 80
8.4 Completeness of the ISC Bulletin . . . 82
8.5 Magnitude Comparisons . . . 83

9 The Leading Data Contributors 88
9.1 The Largest Data Contributors . . . 88
9.2 Contributors Reporting the Most Valuable Parameters . . . 91
9.3 The Most Consistent and Punctual Contributors . . . 95

10 Appendix 97
10.1 ISC Operational Procedures . . . 97
10.1.1 Introduction . . . 97
10.1.2 Data Collection . . . 97
10.1.3 ISC Automatic Procedures . . . 98
10.1.4 ISC Location Algorithm . . . 102
10.1.5 Review Process . . . 112
10.1.6 Probabilistic Point Source Model (ISC-PPSM) . . . 114
10.1.7 History of Operational Changes . . . 114
10.2 IASPEI Standards . . . 115
10.2.1 Standard Nomenclature of Seismic Phases . . . 115
10.2.2 Flinn-Engdahl Regions . . . 123
10.2.3 IASPEI Magnitudes . . . 130
10.2.4 The IASPEI Seismic Format (ISF) . . . 134
10.2.5 Ground Truth (GT) Events . . . 136
10.2.6 Nomenclature of Event Types . . . 138
10.3 Tables . . . 139

11 Glossary of ISC Terminology 157

12 Acknowledgements 161

References 162

1

Preface

Dear Colleague,

This is the first 2020 issue of the Summary of the ISC Bulletin, which remains the most fundamental reason for continued operations at the ISC. This issue covers earthquakes and other seismic events that occurred during the period from January to June 2020. Users can search the ISC Bulletin on the ISC website. The monthly Bulletin files are available from the ISC ftp site. For instructions, please see the www.isc.ac.uk/iscbulletin/.

This publication contains information on the ISC, its staff, Members, Sponsors and Data providers. It offers analysis of the data contributed to the ISC by many seismological agencies worldwide as well as analysis of the data in the ISC Bulletin itself. This issue also includes seismological standards and procedures used by the ISC in its operations.

I would like to reiterate here that all ISC hypocenter solutions (1964-present) are now based on the *ak135* velocity model and all ISC magnitudes (1964-present) are based on the latest robust procedures.

As another note from the ISC data users, we included an invited article from the Institute of Geophysics and Geology of the University of Leipzig in Germany on correct assignment of Rayleigh waves to seismic events.

We hope that you find this publication useful in your work. If your home-institution or company is unable, for one reason or another, to support the long-term international operations of the ISC in full by becoming a Member or a Sponsor, then, please, consider subscribing to this publication by contacting us at admin@isc.ac.uk.

With kind regards to our Data Contributors, Members, Sponsors and users,

Dr Dmitry A. Storchak
Director
International Seismological Centre (ISC)

The ISC is a Charitable Incorporated Organization (CIO) registered with The Charity Commission for England and Wales. Registered charity number: 1188971.

2

The International Seismological Centre

2.1 The ISC Mandate

The International Seismological Centre (ISC) was set up in 1964 with the assistance of UNESCO as a successor to the International Seismological Summary (ISS) to carry forward the pioneering work of Prof. John Milne, Sir Harold Jeffreys and other British scientists in collecting, archiving and processing seismic station and network bulletins and preparing and distributing the definitive summary of world seismicity.

Under the umbrella of the International Association of Seismology and Physics of the Earth Interior (IASPEI/IUGG), the ISC has played an important role in setting international standards such as the International Seismic Bulletin Format (ISF), the IASPEI Standard Seismic Phase List (SSPL) and both the old and New IASPEI Manual of the Seismological Observatory Practice (NMSOP-2) (www.iaspei.org/projects/NMSOP.html).

The ISC has contributed to scientific research and prominent scientists such as John Hodgson, Eugine Herrin, Hal Thirlaway, Jack Oliver, Anton Hales, Ola Dahlman, Shigeji Suehiro, Nadia Kondorskaya, Vit Karnik, Stephan Müller, David Denham, Bob Engdahl, Adam Dziewonski, John Woodhouse and Guy Masters all considered it an important duty to serve on the ISC Executive Committee and the Governing Council.

The current mission of the ISC is to maintain:

- the ISC **Bulletin** – the longest continuous definitive summary of World seismicity (collaborating with 130 seismic networks and data centres around the world). (www.isc.ac.uk/iscbulletin/)
- the International Seismographic Station Registry (**IR**, jointly with the World Data Center for Seismology, Denver). (www.isc.ac.uk/registries/)
- the IASPEI Reference Event List (Ground Truth, **GT**, jointly with IASPEI). (www.isc.ac.uk/gtevents/)

These are fundamentally important tasks. Bulletin data produced, archived and distributed by the ISC for almost 50 years are the definitive source of such information and are used by thousands of seismologists worldwide for seismic hazard estimation, for tectonic studies and for regional and global imaging of the Earth's structure. Key information in global tomographic imaging is derived from the analysis of ISC data. The ISC Bulletin served as a major source of data for such well known products as the ak135 global 1-D velocity model and the EHB (*Engdahl et al.*, 1998) and Centennial (*Engdahl and Villaseñor*, 2002) catalogues. It presents an important quality-control benchmark for the Comprehensive Nuclear-Test-Ban Treaty Organization (CTBTO). Hypocentre parameters from the ISC Bulletin are used by the Data Management Center of the Incorporated Research Institutions for Seismology (IRIS DMC) to serve event-oriented user-requests for waveform data. The ISC-GEM Bulletin is a cornerstone of the ISC-GEM Global Instrumental Reference Earthquake Catalogue for Global Earthquake risk Model (GEM).

The ISC Bulletin contains over 8 million seismic events: earthquakes, chemical and nuclear explosions, mine blasts and mining induced events. Almost 2 million of them are regional and teleseismically recorded events that have been reviewed by the ISC analysts. The ISC Bulletin contains approximately 255 million individual seismic station readings of arrival times, amplitudes, periods, SNR, slowness and azimuth, reported by approximately 19,000 seismic stations currently registered in the IR. Over 9,000 stations have contributed to the ISC Bulletin in recent years. This number includes the numerous sites of the USArray. The IASPEI GT List currently contains 10187 events for which latitude, longitude and depth of origin are known with high confidence (to 5 km or better) and seismic signals were recorded at regional and/or teleseismic distances.

2.2 Brief History of the ISC

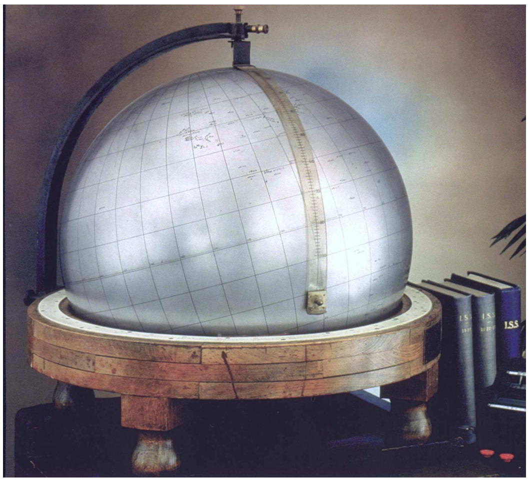

Figure 2.1: *The steel globe bearing positions of early seismic stations was used for locating positions of earthquakes for the International Seismological Summaries.*

Earthquake effects have been noted and documented from the earliest times, but it is only since the development of earthquake recording instruments in the latter half of the 19th century that a proper study of their occurrence has been possible. After the first teleseismic observation of an earthquake in 1889, the need for international exchange of readings was recognised in 1895 by Prof. John Milne and by Ernst von Rebeur Paschwitz together with Georg Gerland, resulting in the publication of the first international seismic bulletins. Milne's "Shide Circulars" were issued under the auspices of the Seismological Committee of the British Association for the Advancement of Science (BAAS), while co-workers of Gerland at the Central Bureau of the International Association of Seismology worked independently in Strasbourg (BCIS).

Following Milne's death in 1913, Seismological Bulletins of the BAAS were continued under Prof. H.H. Turner, later based at Oxford University. Upon formal post-war dissolution of the International Association of Seismology in 1922 the newly founded Seismological Section of the International Union of Geodesy and Geophysics (IUGG) set up the International Seismological Summary (ISS) to continue at Oxford under Turner, to produce the definitive global catalogues from the 1918 data-year onwards, under the auspices of IUGG and with the support of the BAAS.

ISS production, led by several professors at Oxford University, and Sir Harold Jeffreys at Cambridge

University, continued until it was superseded by the ISC Bulletin, after the ISC was formed in Edinburgh in 1964 with Dr P.L. Willmore as its first director.

During the period 1964 to 1970, with the help of UNESCO and other international scientific bodies, the ISC was reconstituted as an international non-governmental body, funded by interested institutions from various countries. Initially there were supporting members from seven countries, now there are almost 70, and member institutions include national academies, research foundations, government departments and research institutes, national observatories and universities. Each member, contributing a minimum unit of subscription or more, appoints a representative to the ISC's Governing Council, which meets every two years to decide the ISC's policy and operational programme. Representatives from the International Association of Seismology and Physics of the Earth's Interior also attend these meetings. The Governing Council appoints the Director and a small Executive Committee to oversee the ISC's operations.

Figure 2.2: *ISC building in Thatcham, Berkshire, UK.*

In 1975, the ISC moved to Newbury in southern England to make use of better computing facilities there. The ISC subsequently acquired its own computer and in 1986 moved to its own building at Pipers Lane, Thatcham, near Newbury. The internal layout of the new premises was designed for the ISC and includes not only office space but provision for the storage of extensive stocks of ISS and ISC publications and a library of seismological observatory bulletins, journals and books collected over many tens of years.

In 1997 the first set of the ISC Bulletin CD-ROMs was produced (not counting an earlier effort at USGS). The first ISC website appeared in 1998 and the first ISC database was put in day-to-day operations from 2001.

Throughout 2009-2011 a major internal reconstruction of the ISC building was undertaken to allow for more members of staff working in mainstream ISC operations as well as major development projects such as the CTBTO Link, ISC-GEM Catalogue and the ISC Bulletin Rebuild.

2.3 Former Directors of the ISC and its U.K. Predecessors

John Milne
Publisher of the Shide Cicular Reports on Earthquakes
1899-1913

Herbert Hall Turner

Seismological Bulletins of the BAAS

1913-1922
Director of the ISS
1922-1930

Harry Hemley Plaskett
Director of the ISS
1931-1946

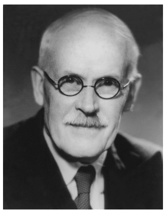

Harold Jeffreys
Director of the ISS
1946-1957

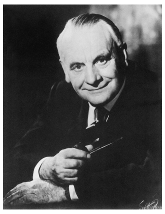

Robert Stoneley
Director of the ISS
1957-1963

P.L. (Pat) Willmore
Director of the ISS
1963-1970
Director of the ISC
1964-1970

Edouard P. Arnold
Director of the ISC
1970-1977

Anthony A. Hughes
Director of the ISC
1977-1997

Raymond J. Willemann
Director of the ISC
1998-2003

Avi Shapira
Director of the ISC
2004-2007

2.4 Member Institutions of the ISC

Article IV(a-b) of the ISC Working Statutes stipulates that any national academy, agency, scientific institution or other non-profit organisation may become a Member of the ISC on payment to the ISC of a sum equal to at least one unit of subscription and the nomination of a voting representative to serve on the ISC's governing body. Membership shall be effective for one year from the date of receipt at the ISC of the annual contribution of the Member and is thereafter renewable for periods of one year.

The ISC is currently supported with funding from its 70 Member Institutions and a four-year Grant Award EAR-1811737 from the US National Science Foundation.

Figures 2.3 and 2.4 show major sectors to which the ISC Member Institutions belong and proportional financial contributions that each of these sectors make towards the ISC's annual budget.

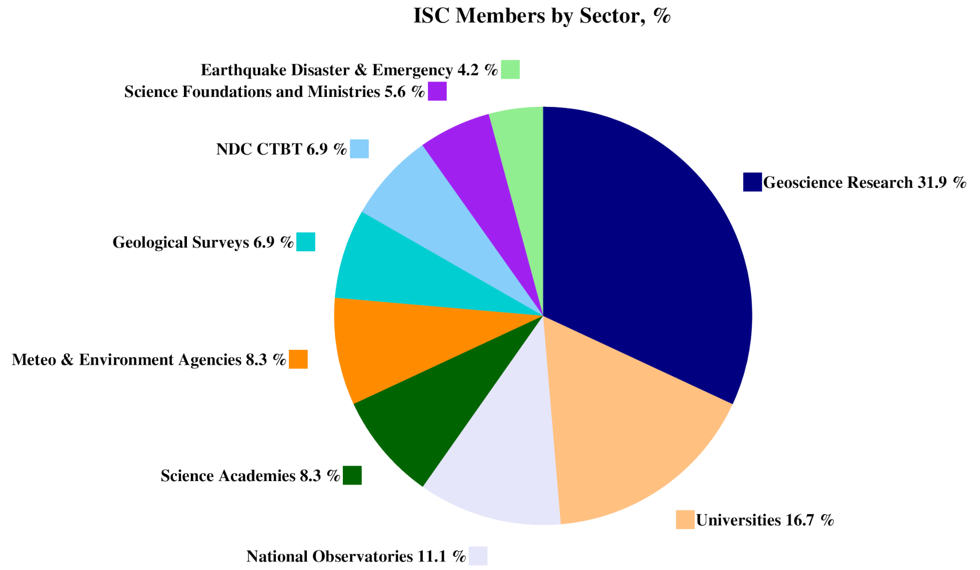

Figure 2.3: *Distribution of the ISC Member Institutions by sector during the review of data in this Summary as a percentage of total number of Members.*

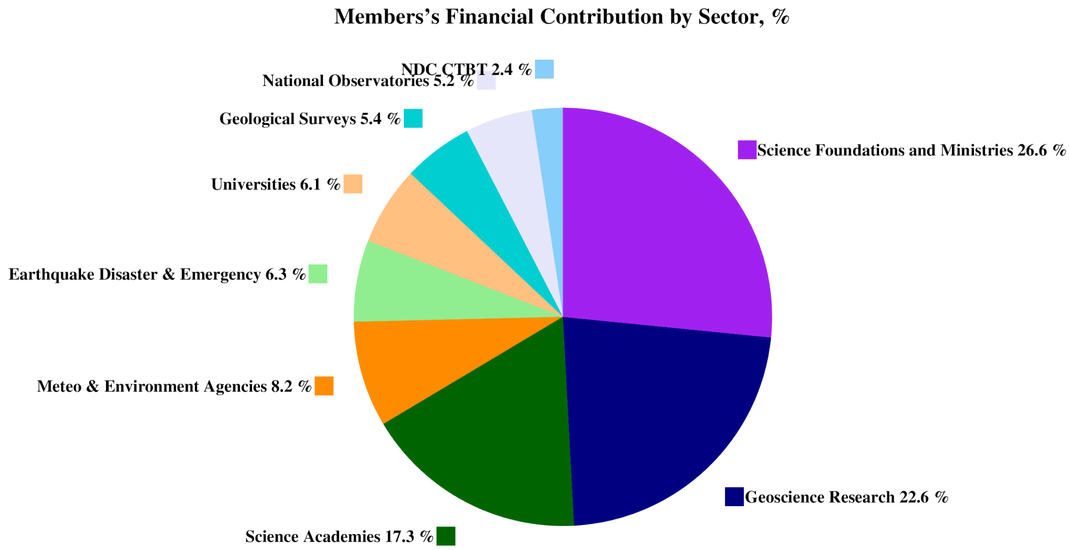

Figure 2.4: *Distribution of Member's financial contributions to the ISC by sector during the review of data in this Summary as a percentage of total annual Member contributions.*

There follows a list of all current Member Institutions with a category (1 through 9) assigned according to the ISC Working Statutes. Each category relates to the number of membership units contributed.

Centre de Recherche en Astronomie, Astrophysique et Géophysique (CRAAG)
Algeria
www.craag.dz
Category: 1

Geoscience Australia
Australia
www.ga.gov.au
Category: 4

Federal Ministry for Education, Science and Research
Austria

Category: 2

Centre of Geophysical Monitoring (CGM) of the National Academy of Sciences of Belarus
Belarus
www.cgm.org.by
Category: 1

Belgian Science Policy Office (BELSPO)
Belgium

Category: 1

Observatorio Nacional
Brazil
www.on.br
Category: 1

Universidade de São Paulo, Centro de Sismologia
Brazil
www.sismo.iag.usp.br
Category: 1

Seismological Observatory, Institute of Geosciences, University of Brasilia
Brazil
www.obsis.unb.br
Category: 1

National Institute of Geophysics, Geodesy and Geography (NIGGG), Bulgarian Academy of Sciences
Bulgaria
www.niggg.bas.bg
Category: 1

The Geological Survey of Canada
Canada
gsc.nrcan.gc.ca
Category: 4

Centro Sismologico Nacional, Universidad de Chile
Chile

Category: 1

China Earthquake Administration
China
www.cea.gov.cn
Category: 4

Institute of Earth Sciences, Academia Sinica
Chinese Taipei
www.earth.sinica.edu.tw
Category: 1

Geological Survey Department
Cyprus
www.moa.gov.cy
Category: 1

Institute of Geophysics, Czech Academy of Sciences
Czech Republic

Category: 1

Geological Survey of Denmark and Greenland (GEUS)
Denmark
www.geus.dk
Category: 2

National Research Institute for Astronomy and Geophysics (NRIAG), Cairo
Egypt
www.nriag.sci.eg
Category: 1

The University of Helsinki
Finland
www.helsinki.fi
Category: 2

Laboratoire de Détection et de Géophysique/CEA
France
www-dase.cea.fr
Category: 2

Institute of Radiological and Nuclear Safety (IRSN), joint authority of the Ministries of Defense, the Environment, Industry, Research, and Health
France

Category: 1

Institute National des Sciences de l'Univers
France
www.insu.cnrs.fr
Category: 4

GeoForschungsZentrum Potsdam
Germany
www.gfz-potsdam.de
Category: 2

Bundesanstalt für Geowissenschaften und Rohstoffe
Germany
www.bgr.bund.de
Category: 4

The Seismological Institute, National Observatory of Athens
Greece
www.noa.gr
Category: 1

Institute of Earth Physics and Space Science (EPSS), Hungarian Research Network (ELKH)
Hungary

Category: 1

The Icelandic Meteorological Office
Iceland
www.vedur.is
Category: 1

National Geophysical Research Institute (NGRI), Council of Scientific and Industrial Research (CSIR)
India

Category: 2

National Centre for Seismology, Ministry of Earth Sciences of India
India
www.moes.gov.in
Category: 4

Iraqi Meteorological Organization and Seismology
Iraq
www.imos-tm.com
Category: 1

Dublin Institute for Advanced Studies
Ireland
www.dias.ie
Category: 1

Geological Survey of Israel
Israel

Category: 1

Soreq Nuclear Research Centre (SNRC)
Israel
www.soreq.gov.il
Category: 1

Istituto Nazionale di Oceanografia e di Geofisica Sperimentale
Italy
www.ogs.trieste.it
Category: 1

Istituto Nazionale di Geofisica e Vulcanologia
Italy
www.ingv.it
Category: 3

University of the West Indies at Mona
Jamaica
www.mona.uwi.edu
Category: 1

The Japan Meteorological Agency (JMA)
Japan
www.jma.go.jp
Category: 5

Japan Agency for Marine-Earth Science and Technology (JAMSTEC)
Japan
www.jamstec.go.jp
Category: 2

Earthquake Research Institute, University of Tokyo
Japan
www.eri.u-tokyo.ac.jp
Category: 3

National Institute of Polar Research (NIPR)
Japan
www.nipr.ac.jp
Category: 1

Institute of Geophysics, National University of Mexico
Mexico
www.igeofcu.unam.mx
Category: 1

Centro de Investigación Científica y de Educación Superior de Ensenada (CICESE)
Mexico
resnom.cicese.mx
Category: 1

The Royal Netherlands Meteorological Institute (KNMI)
Netherlands
www.knmi.nl
Category: 2

GNS Science
New Zealand
www.gns.cri.nz
Category: 3

The Centre for Earth Evolution and Dynamics (CEED), the University of Oslo
Norway

Category: 1

The University of Bergen
Norway
www.uib.no
Category: 2

Stiftelsen NORSAR
Norway
www.norsar.no
Category: 2

Institute of Geophysics, Polish Academy of Sciences
Poland
www.igf.edu.pl
Category: 1

Instituto Português do Mar e da Atmosfera
Portugal
www.ipma.pt
Category: 2

Red Sísmica de Puerto Rico
Puerto Rico
redsismica.uprm.edu
Category: 1

Korean Meterological Administration
Republic of Korea
www.kma.go.kr
Category: 1

National Institute for Earth Physics
Romania
www.infp.ro
Category: 1

Russian Academy of Sciences
Russia
www.ras.ru
Category: 5

Earth Observatory of Singapore (EOS), an autonomous Institute of Nanyang Technological University
Singapore
www.earthobservatory.sg
Category: 1

Environmental Agency of Slovenia
Slovenia
www.arso.gov.si
Category: 1

Council for Geoscience
South Africa
www.geoscience.org.za
Category: 1

Instituto Geografico Nacional
Spain

Category: 3

Institut Cartogràfic i Geològic de Catalunya (ICGC)
Spain
www.icgc.cat
Category: 1

Institute of Marine Sciences (ICM-CSIC)
Spain

Category: 1

National Defence Research Establishment (FOI)
Sweden
www.foi.se
Category: 1

Uppsala Universitet
Sweden
www.uu.se
Category: 2

The Swiss Academy of Sciences
Switzerland
www.scnat.ch
Category: 2

Disaster and Emergency Management Authority (AFAD)
Turkey
www.deprem.gov.tr
Category: 2

Kandilli Observatory and Earthquake Research Institute
Turkey
www.koeri.boun.edu.tr
Category: 1

AWE Blacknest
United Kingdom
www.blacknest.gov.uk
Category: 1

British Geological Survey
United Kingdom
www.bgs.ac.uk
Category: 2

The Royal Society
United Kingdom
www.royalsociety.org
Category: 6

National Earthquake Information Center, U.S. Geological Survey
U.S.A.
www.neic.usgs.gov
Category: 1

Alaska Earthquake Center (AEC), University of Alaska Fairbanks
U.S.A.

Category: 1

University of Utah Seismograph Stations (UUSS)
U.S.A.

Category: 1

The National Science Foundation of the United States. (Grant No. EAR-1811737)
U.S.A.
www.nsf.gov
Category: 9

Texas Seismological Network (TexNet), Bureau of Economic Geology, J.A. and K.G. Jackson School of Geosciences, University of Texas at Austin
U.S.A.
www.beg.utexas.edu
Category: 1

Incorporated Research Institutions for Seismology
U.S.A.
www.iris.edu
Category: 1

In addition the ISC is currently in receipt of grants from the International Data Centre (IDC) of the Preparatory Commission of the Comprehensive Nuclear-Test-Ban Treaty Organization (CTBTO), FM Global, Lighthill Risk Network, and AXA XL.

2.5 Sponsoring Organisations

Article IV(c) of the ISC Working Statutes stipulates any commercial organisation with an interest in the objectives and/or output of the ISC may become an Associate Member of the ISC on payment of an Associate membership fee, but without entitlement to representation with a vote on the ISC's governing body.

GeoSIG swiss made to measure http://www.geosig.com/

GeoSIG provides earthquake, seismic, structural, dynamic and static monitoring and measuring solutions As an ISO Certified company, GeoSIG is a world leader in design and manufacture of a diverse range of high quality, precision instruments for vibration and earthquake monitoring. GeoSIG instruments are at work today in more than 100 countries around the world with well-known projects such as the NetQuakes installation with USGS and Oresund Bridge in Denmark. GeoSIG offers off-the-shelf solutions as well as highly customised solutions to fulfil the challenging requirements in many vertical markets including the following:

- Earthquake Early Warning and Rapid Response (EEWRR)
- Seismic and Earthquake Monitoring and Measuring
- Industrial Facility Seismic Monitoring and Shutdown
- Structural Analysis and Ambient Vibration Testing
- Induced Vibration Monitoring
- Research and Scientific Applications

sara electronic instruments http://www.sara.pg.it

SARA designs and manufactures seismometers, accelerometers and portable multichannel seismographs for both seismology and applied geophysics. Since 2002 we provided over 5,000 seismic units, 15,000 acceleration transducers and 15,000 geophysical exploration channels, to thousands of professionals and researchers who are using our equipment with success. Providing low-cost instrumentation for developing countries is our main goal. We developed our seismological software SEISMOWIN which provides full support for all international file formats and communication standards like miniSEED, GSE, SeedLink and a number of tools for earthquake location and site assessment. The GEOEXPLORER software suite offers a number of modules for geological surveys.

In 2023 we introduced our new compact broadband seismometer to the market, suitable for surface, posthole and borehole installation, and new versions of our popular SL06 recorder with rack mount housing and ADC with PGA offering 24 or 32 bit streaming.

Visit our web site and download the free tools available at: www.sara.pg.it

MS&AD InterRisk Research & Consulting

http://www.irric.co.jp/en/corporate/

MS&AD InterRisk Research & Consulting, Inc. is responsible for the core of risk-related service businesses in the MS&AD group. We provide services which meet various expectations of the clients, including consulting, research and investigation, seminars and publications for risk management in addition to the think-tank functions.

2.6 Data Contributing Agencies

In addition to its Members and Sponsors, the ISC owes its existence and successful long-term operations to its 150 seismic bulletin data contributors. These include government agencies responsible for national seismic networks, geoscience research institutions, geological surveys, meteorological agencies, universities, national data centres for monitoring the CTBT and individual observatories. There would be no ISC Bulletin available without the regular stream of data that are unselfishly and generously contributed to the ISC on a free basis.

Institute of Geosciences, Polytechnic University of Tirana
Albania
TIR

Centre de Recherche en Astronomie, Astrophysique et Géophysique
Algeria
CRAAG

Universidad Nacional de La Plata
Argentina
LPA

Instituto Nacional de Prevención Sísmica
Argentina
SJA

National Survey of Seismic Protection
Armenia
NSSP

Geoscience Australia
Australia
AUST

Curtin University
Australia
CUPWA

Zentralanstalt für Meteorologie und Geodynamik (ZAMG)
Austria
VIE

International Data Centre, CTBTO
Austria
IDC

Republican Seismic Survey Center of Azerbaijan National Academy of Sciences
Azerbaijan
AZER

Royal Observatory of Belgium
Belgium
UCC

Observatorio San Calixto
Bolivia
SCB

Republic Hydrometeorological Service, Seismological Observatory, Banja Luka
Bosnia and Herzegovina
RHSSO

Botswana Geoscience Institute
Botswana
BGSI

Observatory Seismological of the University of Brasilia
Brazil
OSUNB

Instituto Astronomico e Geofísico
Brazil
VAO

National Institute of Geophysics, Geology and Geography
Bulgaria
SOF

Canadian Hazards Information Service, Natural Resources Canada
Canada
OTT

Centro Sismológico Nacional, Universidad de Chile
Chile
GUC

China Earthquake Networks Center
China
BJI

Institute of Earth Sciences, Academia Sinica
Chinese Taipei
ASIES

Central Weather Bureau (CWB)
Chinese Taipei
TAP

Red Sismológica Nacional de Colombia
Colombia
RSNC

Sección de Sismología, Vulcanología y Exploración Geofísica
Costa Rica
UCR

Seismological Survey of the Republic of Croatia
Croatia
ZAG

Servicio Sismológico Nacional Cubano
Cuba
SSNC

Cyprus Geological Survey Department
Cyprus
NIC

The Institute of Physics of the Earth (IPEC)
Czech Republic
IPEC

Institute of Geophysics, Czech Academy of Sciences
Czech Republic
PRU

Institute of Geophysics, Czech Academy of Sciences
Czech Republic
WBNET

Korea Earthquake Administration
Democratic People's Republic of Korea
KEA

Geological Survey of Denmark and Greenland
Denmark
DNK

Universidad Autonoma de Santo Domingo
Dominican Republic
SDD

Observatorio Sismologico Politecnico Loyola
Dominican Republic
OSPL

Servicio Nacional de Sismología y Vulcanología
Ecuador
IGQ

National Research Institute of Astronomy and Geophysics
Egypt
HLW

Servicio Nacional de Estudios Territoriales
El Salvador
SNET

Institute of Seismology, University of Helsinki
Finland
HEL

Institut de Physique du Globe de Paris
France
IPGP

EOST / RéNaSS
France
STR

Laboratoire de Détection et de Géophysique/CEA
France
LDG

Laboratoire de Géophysique/CEA
French Polynesia
PPT

Institute of Earth Sciences/ National Seismic Monitoring Center
Georgia
TIF

Alfred Wegener Institute for Polar and Marine Research
Germany
AWI

Geophysikalisches Observatorium Collm
Germany
CLL

Bundesanstalt für Geowissenschaften und Rohstoffe
Germany
BGR

Seismological Observatory Berggießhübel, TU Bergakademie Freiberg
Germany
BRG

Helmholtz Centre Potsdam GFZ German Research Centre For Geosciences
Germany
GFZ

National Observatory of Athens
Greece
ATH

Department of Geophysics, Aristotle University of Thessaloniki
Greece
THE

University of Patras, Department of Geology
Greece
UPSL

INSIVUMEH
Guatemala
GCG

Hong Kong Observatory
Hong Kong
HKC

Geodetic and Geophysical Reasearch Institute, Hungarian Academy of Sciences
Hungary
KRSZO

Icelandic Meteorological Office
Iceland
REY

National Centre for Seismology of the Ministry of Earth Sciences of India
India
NDI

National Geophysical Research Institute
India
HYB

Badan Meteorologi, Klimatologi dan Geofisika
Indonesia
DJA

Tehran University
Iran
TEH

International Institute of Earthquake Engineering and Seismology (IIEES)
Iran
THR

Iraqi Meteorological and Seismology Organisation
Iraq
ISN

Dublin Institute for Advanced Studies
Ireland
DIAS

The Geophysical Institute of Israel
Israel
GII

Laboratory of Research on Experimental and Computational Seimology
Italy
RISSC

Istituto Nazionale di Geofisica e Vulcanologia
Italy
ROM

SARA Electronic Instrument s.r.l.
Italy
SARA

MedNet Regional Centroid - Moment Tensors
Italy
MED_RCMT

Dipartimento per lo Studio del Territorio e delle sue Risorse (RSNI)
Italy
GEN

Istituto Nazionale di Oceanografia e di Geofisica Sperimentale (OGS)
Italy
TRI

Jamaica Seismic Network
Jamaica
JSN

National Institute of Polar Research
Japan
SYO

National Research Institute for Earth Science and Disaster Resilience
Japan
NIED

Japan Meteorological Agency
Japan
JMA

Jordan Seismological Observatory
Jordan
JSO

Seismological Experimental Methodological Expedition
Kazakhstan
SOME

National Nuclear Center
Kazakhstan
NNC

Institute of Seismology, Academy of Sciences of Kyrgyz Republic
Kyrgyzstan
KRNET

Kyrgyz Seismic Network
Kyrgyzstan
KNET

Latvian Seismic Network
Latvia
LVSN

National Council for Scientific Research
Lebanon
GRAL

Geological Survey of Lithuania
Lithuania
LIT

Macao Meteorological and Geophysical Bureau
Macao, China
MCO

Antananarivo
Madagascar
TAN

Instituto de Geofísica de la UNAM
Mexico
MEX

Centro de Investigación Científica y de Educación Superior de Ensenada
Mexico
ECX

Institute of Hydrometeorology and Seismology of Montenegro
Montenegro
PDG

Centre National de Recherche
Morocco
CNRM

The Geological Survey of Namibia
Namibia
NAM

National Seismological Centre, Nepal
Nepal
DMN

IRD Centre de Nouméa
New Caledonia
NOU

Institute of Geological and Nuclear Sciences
New Zealand
WEL

Central American Tsunami Advisory Center
Nicaragua
CATAC

Seismological Observatory Skopje
North Macedonia
SKO

University of Bergen
Norway
BER

Stiftelsen NORSAR
Norway
NAO

Sultan Qaboos University
Oman
OMAN

Universidad de Panama
Panama
UPA

Manila Observatory
Philippines
QCP

Philippine Institute of Volcanology and Seismology
Philippines
MAN

Private Observatory of Pawel Jacek Wiejacz, D.Sc.
Poland
PJWWP

Institute of Geophysics, Polish Academy of Sciences
Poland
WAR

Instituto Dom Luiz, University of Lisbon
Portugal
IGIL

Sistema de Vigilância Sismológica dos Açores
Portugal
SVSA

Instituto Português do Mar e da Atmosfera, I.P.
Portugal
INMG

Centre of Geophysical Monitoring of the National Academy of Sciences of Belarus
Republic of Belarus
BELR

Inst. of Seismology and Geodynamics, V.I. Vernadsky Crimean Federal University
Republic of Crimea
CFUSG

Korea Meteorological Administration
Republic of Korea
KMA

National Institute for Earth Physics
Romania
BUC

North Eastern Regional Seismological Centre, Magadan, GS RAS
Russia
NERS

Federal Center for Integrated Arctic Research
Russia
FCIAR

Kola Regional Seismic Centre, GS RAS
Russia
KOLA

Kamchatka Branch of the Geophysical Survey of the RAS
Russia
KRSC

Baykal Regional Seismological Centre, GS SB RAS
Russia
BYKL

Yakutiya Regional Seismological Center, GS SB RAS
Russia
YARS

Altai-Sayan Seismological Centre, GS SB RAS
Russia
ASRS

Sakhalin Experimental and Methodological Seismological Expedition, GS RAS
Russia
SKHL

Geophysical Survey of Russian Academy of Sciences
Russia
MOS

Mining Institute of the Ural Branch of the Russian Academy of Sciences
Russia
MIRAS

Saudi Geological Survey
Saudi Arabia
SGS

Republicki seizmoloski zavod
Serbia
BEO

Geophysical Institute, Slovak Academy of Sciences
Slovakia
BRA

Slovenian Environment Agency
Slovenia
LJU

Council for Geoscience
South Africa
PRE

Real Instituto y Observatorio de la Armada
Spain
SFS

Instituto Geográfico Nacional
Spain
MDD

Institut Cartogràfic i Geològic de Catalunya
Spain
MRB

University of Uppsala
Sweden
UPP

Swiss Seismological Service (SED)
Switzerland
ZUR

Thai Meteorological Department
Thailand
BKK

The Seismic Research Centre
Trinidad and Tobago
TRN

Institut National de la Météorologie
Tunisia
TUN

Disaster and Emergency Management Presidency
Turkey
AFAD

Kandilli Observatory and Earthquake Research Institute
Turkey
ISK

IRIS Data Management Center
U.S.A.
IRIS

The Global CMT Project
U.S.A.
GCMT

National Earthquake Information Center
U.S.A.
NEIC

Texas Seismological Network, University of Texas at Austin
U.S.A.
TXNET

Pacific Northwest Seismic Network
U.S.A.
PNSN

Pacific Tsunami Warning Center
U.S.A.
PTWC

Red Sísmica de Puerto Rico
U.S.A.
RSPR

Subbotin Institute of Geophysics, National Academy of Sciences
Ukraine
SIGU

Main Centre for Special Monitoring
Ukraine
MCSM

Dubai Seismic Network
United Arab Emirates
DSN

International Seismological Centre
United Kingdom
ISC

British Geological Survey
United Kingdom
BGS

International Seismological Centre Probabilistic Point Source Model
United Kingdom
ISC-PPSM

Institute of Seismology, Academy of Sciences, Republic of Uzbekistan
Uzbekistan
ISU

Fundación Venezolana de Investigaciones Sismológicas
Venezuela
FUNV

Institute of Geophysics, Viet Nam Academy of Science and Technology
Viet Nam
PLV

Goetz Observatory
Zimbabwe
BUL

2.7 ISC Staff

Listed below are the staff (and their country of origin) who were employed at the ISC during the time period when the ISC worked on the data covered by this issue of the Summary.

- Dmitry Storchak
- Director
- Russia / United Kingdom

- Lynn Elms
- Administration Officer
- United Kingdom

- James Harris
- Senior System and Database Administrator
- United Kingdom

- Oliver Rea
- System Administrator
- United Kingdom

- Calum Clague
- Data Collection Officer
- South Africa

- Domenico Di Giacomo
- Senior Seismologist
- Italy/UK

- Tom Garth
- Seismologist / Senior Developer
- United Kingdom

- Ryan Gallacher
- Seismologist / Developer
- United Kingdom

- Natalia Poiata
- Seismologist / Developer
- Moldova

- Adrian Armstrong
- Software Engineer
- United Kingdom

- Rosemary Hulin
- Analyst
- United Kingdom

- Blessing Shumba
- Seismologist / Senior Analyst
- Zimbabwe

- Rebecca Verney
- Analyst
- United Kingdom

- Elizabeth Ayres
- Analyst / Historical Data Officer
- United Kingdom

- Kathrin Lieser
- Analyst Administrator / Summary Editor / Seismologist
- Germany

- Burak Sakarya
- Seismologist / Analyst
- Turkey

- Rian Harris
- Historical Data Officer
- United Kingdom

- Susana Carvalho
- Historical Data Officer
- Portugal

3

Availability of the ISC Bulletin

The ISC Bulletin is available from the following sources:

- Web searches
  The entire ISC Bulletin is available directly from the ISC website via tailored searches.
  (www.isc.ac.uk/iscbulletin/search)
  (isc-mirror.iris.washington.edu/iscbulletin/search)
  - Bulletin search - provides the most verbose output of the ISC Bulletin in ISF or QuakeML.
  - Event catalogue - only outputs the prime hypocentre for each event, producing a simple list of events, locations and magnitudes.
  - Arrivals - search for arrivals in the ISC Bulletin. Users can search for specific phases for selected stations and events.
- CD-ROMs/DVD-ROMs

  CDs/DVDs can be ordered from the ISC for any published volume (one per year), or for all back issues of the Bulletin (not including the latest volume). The data discs contain the Bulletin as a PDF, in IASPEI Seismic Format (ISF), and in Fixed Format Bulletin (FFB) format. An event catalogue is also included, together with the International Registry of seismic station codes.
- FTP site

  The ISC Bulletin is also available to download from the ISC ftp site, which contains the Bulletin in PDF, ISF and FFB formats.
  (ftp://www.isc.ac.uk)
  (ftp://isc-mirror.iris.washington.edu)
  and
  (http://download.isc.ac.uk

Mirror service

A mirror of the ISC database, website and ftp site is available at IRIS DMC (isc-mirror.iris.washington.edu), which benefits from their high-speed internet connection, providing an alternative method of accessing the ISC Bulletin.

4

Citing the International Seismological Centre

Data from the ISC should always be cited. This includes use by academic or commercial organisations, as well as individuals. A citation should show how the data were retrieved and may be in one of these suggested forms:

The ISC is named as a valid data centre for citations within American Geophysical Union (AGU) publications. As such, please follow the AGU guidelines when referencing ISC data in one of their journals. The ISC may be cited as both the institutional author of the Bulletin and the source from which the data were retrieved.

4.1 The ISC Bulletin

International Seismological Centre (2023), On-line Bulletin, `https://doi.org/10.31905/D808B830`

The procedures used for producing the ISC Bulletin have been described in a number of scientific articles. Depending on the use of the Bulletin, users are encouraged to follow the citation suggestions below:

a) For current ISC location procedure:

Bondár, I. and D.A. Storchak (2011). Improved location procedures at the International Seismological Centre, *Geophys. J. Int.*, *186*, 1220-1244, `https://doi.org/10.1111/j.1365-246X.2011.05107.x`

b) For Rebuilt ISC Bulletin:

Storchak, D.A., Harris, J., Brown, L., Lieser, K., Shumba, B., Verney, R., Di Giacomo, D., Korger, E. I. M. (2017). Rebuild of the Bulletin of the International Seismological Centre (ISC), part 1: 1964–1979. *Geosci. Lett.* (2017) 4: 32. `https://doi.org/10.1186/s40562-017-0098-z`

Storchak, D.A., Harris, J., Brown, L., Lieser, K., Shumba, B., Di Giacomo, D. (2020) Rebuild of the Bulletin of the International Seismological Centre (ISC), part 2: 1980–2010. *Geosci. Lett.* (2020) 7: 18, `https://doi.org/10.1186/s40562-020-00164-6`

c) For principles of the ISC data collection process:

R J Willemann, D A Storchak (2001). Data Collection at the International Seismological Centre, *Seis. Res. Lett.*, *72*, 440-453, `https://doi.org/10.1785/gssrl.72.4.440`

d) For interpretation of magnitudes:

Di Giacomo, D., and D.A. Storchak (2016). A scheme to set preferred magnitudes in the ISC Bulletin, *J. Seism.*, *20(2)*, 555-567, `https://doi.org/10.1007/s10950-015-9543-7`

e) For use of source mechanisms:

Lentas, K., Di Giacomo, D., Harris, J., and Storchak, D. A. (2020). The ISC Bulletin as a comprehensive source of earthquake source mechanisms, *Earth Syst. Sci. Data*, *11*, 565-578,https://doi.org/10.5194/essd-11-565-2020

Lentas, K. (2018). Towards routine determination of focal mechanisms obtained from first motion P-wave arrivals, *Geophys. J. Int.*, *212(3)*, 1665–1686.https://doi.org/10.1093/gji/ggx503

f) For use of the original (pre-Rebuild) ISC Bulletin as a historical perspective:

Adams, R.D., Hughes, A.A., and McGregor, D.M. (1982). Analysis procedures at the International Seismological Centre. *Phys. Earth Planet. Inter. 30:* 85-93,https://doi.org/10.1016/0031-9201(82)90093-0

4.2 The Summary of the Bulletin of the ISC

International Seismological Centre (2023), Summary of the Bulletin of the International Seismological Centre, January - June 2020, *57(I)*,https://doi.org/10.31905/NWKNMBLN

4.3 The historical printed ISC Bulletin (1964-2009)

International Seismological Centre, Bull. Internatl. Seismol. Cent., 46(9-12), Thatcham, United Kingdom, 2009.

4.4 The IASPEI Reference Event List

International Seismological Centre (2023), IASPEI Reference Event (GT) List, https://doi.org/10.31905/32NSJF7V

Bondár, I. and K.L. McLaughlin (2009). A New Ground Truth Data Set For Seismic Studies, *Seismol. Res. Lett.*, *80*, 465-472, https://doi.org/10.1785/gssrl.80.3.465

Bondár, E. Engdahl, X. Yang, H. Ghalib, A. Hofstetter, V. Kirichenko, R. Wagner, I. Gupta, G. Ekström, E. Bergman, H. Israelsson, and K. McLaughlin (2004). Collection of a reference event set for regional and teleseismic location calibration, *Bull. Seismol. Soc. Am.*, *94*, 1528-1545, https://doi.org/10.1785/012003128

Bondár, E. Bergman, E. Engdahl, B. Kohl, Y.-L. Kung, and K. McLaughlin (2008). A hybrid multiple event location technique to obtain ground truth event locations, *Geophys. J. Int.*, *175*, https://doi.org/10.1111/j.1365-246X.2011.05011.x

4.5 The ISC-GEM Catalogue

International Seismological Centre (2023), ISC-GEM Earthquake Catalogue, https://doi.org/10.31905/d808b825, 2023.

Depending on the use of the Catalogue, to quote the appropriate scientific articles, as suggested below.

a) For a general use of the catalogue, please quote the following three papers (Storchak et al., 2013; 2015; Di Giacomo et al., 2018):

Storchak, D.A., D. Di Giacomo, I. Bondár, E.R. Engdahl, J. Harris, W.H.K. Lee, A. Villaseñor and P. Bormann (2013). Public Release of the ISC-GEM Global Instrumental Earthquake Catalogue (1900-2009). *Seism. Res. Lett.*, *84*, 5, 810-815, `https://doi.org/10.1785/0220130034`

Storchak, D.A., D. Di Giacomo, E.R. Engdahl, J. Harris, I. Bondár, W.H.K. Lee, P. Bormann and A. Villaseñor (2015). The ISC-GEM Global Instrumental Earthquake Catalogue (1900-2009): Introduction, *Phys. Earth Planet. Int.*, *239*, 48-63, `https://doi.org/10.1016/j.pepi.2014.06.009`

Di Giacomo, D., E.R. Engdahl and D.A. Storchak (2018). The ISC-GEM Earthquake Catalogue (1904–2014): status after the Extension Project, *Earth Syst. Sci. Data*, *10*, 1877-1899, `https://doi.org/10.5194/essd-10-1877-2018`

b) For use of location parameters, please quote (Bondár et al., 2015):

Bondár, I., E.R. Engdahl, A. Villaseñor, J. Harris and D.A. Storchak, 2015. ISC-GEM: Global Instrumental Earthquake Catalogue (1900-2009): II. Location and seismicity patterns, *Phys. Earth Planet. Int.*, *239*, 2-13, `https://doi.org/10.1016/j.pepi.2014.06.002`

c) For use of magnitude parameters, please quote (Di Giacomo et al., 2015a; 2018):

Di Giacomo, D., I. Bondár, D.A. Storchak, E.R. Engdahl, P. Bormann and J. Harris (2015a). ISC-GEM: Global Instrumental Earthquake Catalogue (1900-2009): III. Re-computed MS and mb, proxy MW, final magnitude composition and completeness assessment, *Phys. Earth Planet. Int.*, *239*, 33-47, `https://doi.org/10.1016/j.pepi.2014.06.005`

Di Giacomo, D., E.R. Engdahl and D.A. Storchak (2018). The ISC-GEM Earthquake Catalogue (1904–2014): status after the Extension Project, *Earth Syst. Sci. Data*, *10*, 1877-1899, `https://doi.org/10.5194/essd-10-1877-2018`

d) For use of station data from historical bulletins, please quote (Di Giacomo et al., 2015b; 2018):

Di Giacomo, D., J. Harris, A. Villaseñor, D.A. Storchak, E.R. Engdahl, W.H.K. Lee and the Data Entry Team (2015b). ISC-GEM: Global Instrumental Earthquake Catalogue (1900-2009), I. Data collection from early instrumental seismological bulletins, *Phys. Earth Planet. Int.*, *239*, 14-24, `https://doi.org/10.1016/j.pepi.2014.06.005`

Di Giacomo, D., E.R. Engdahl and D.A. Storchak (2018). The ISC-GEM Earthquake Catalogue (1904–2014): status after the Extension Project, *Earth Syst. Sci. Data*, *10*, 1877-1899, `https://doi.org/10.5194/essd-10-1877-2018`

e) For use of direct values of M0 from the literature, please quote (Lee and Engdahl, 2015):

Lee, W.H.K. and E.R. Engdahl (2015). Bibliographical search for reliable seismic moments of large earthquakes during 1900-1979 to compute MW in the ISC-GEM Global Instrumental Reference Earthquake Catalogue (1900-2009), *Phys. Earth Planet. Int.*, *239*, 25-32, `https://doi.org/10.1016/j.pepi.2014.06.004`

4.6 The ISC-EHB Dataset

International Seismological Centre (2023), ISC-EHB Dataset, https://doi.org/10.31905/PY08W6S3

Engdahl, E.R., R. van der Hilst, and R. Buland (1998). Global teleseismic earthquake relocation with improved travel times and procedures for depth determination, *Bull. Seism. Soc. Am.*, *88*, 3, 722-743. http://www.bssaonline.org/content/88/3/722.abstract

Weston, J., Engdahl, E.R., Harris, J., Di Giacomo, D. and Storchack, D.A. (2018). ISC-EHB: Reconstruction of a robust earthquake dataset, *Geophys. J. Int.*, *214*, 1, 474-484, https://doi.org/10.1093/gji/ggy155

Engdahl, E. R., Di Giacomo, D., Sakarya, B., Gkarlaouni, C. G., Harris, J., and Storchak, D. A. (2020). ISC-EHB 1964-2016, an Improved Data Set for Studies of Earth Structure and Global Seismicity, *Earth and Space Science*, *7(1)*, e2019EA000897, https://doi.org/10.1029/2019EA000897

4.7 The ISC Event Bibliography

International Seismological Centre (2023), On-line Event Bibliography, https://doi.org/10.31905/EJ3B5LV6

Also, please reference the following SRL article that describes the details of this service:

Di Giacomo, D., Storchak, D.A., Safronova, N., Ozgo, P., Harris, J., Verney, R. and Bondár, I., 2014. A New ISC Service: The Bibliography of Seismic Events, *Seismol. Res. Lett.*, *85*, 2, 354-360, https://doi.org/10.1785/0220130143

4.8 International Registry of Seismograph Stations

International Seismological Centre (2023), International Seismograph Station Registry (IR), https://doi.org/10.31905/EL3FQQ40

4.9 Seismological Dataset Repository

International Seismological Centre (2023), Seismological Dataset Repository, https://doi.org/10.31905/6TJZECEY

4.10 Data transcribed from ISC CD-ROMs/DVD-ROMs

International Seismological Centre, Bulletin Disks 1-30 [CD-ROM], Internatl. Seismol. Cent., Thatcham, United Kingdom, 2023.

5

Notes from ISC Data Users

5.1 Correct Assignment of Rayleigh Waves to Seismic Events

Petra Buchholz and Siegfried Wendt
Institute for Geophysics and Geology, University of Leipzig, Germany

Siegfried Wendt and Petra Buchholz

Theoretical travel-time tables can be helpful for phase identification of seismograms. First onsets of P/PKP waves generally have residuals not greater than several seconds. For a correct assignment of the surface wave group to an event, estimating the time difference between the first onsets and the surface waves ($t_{Rmax} - t_{P/PKP}$) is important. Here, t_{Rmax} represents the arrival time of the maximum amplitude inside the Rayleigh wave group (R_{max}) and $t_{P/PKP}$ is the arrival time of the first longitudinal body wave, which may correspond to P, Pdif or PKP phase. Tables with ($t_{Rmax} - t_{P/PKP}$) as a function of epicentral distance were published by *Arkangelskaya* (1959) and *Willmore* (1979). The New Manual of Seismological Observatory Practice (NMSOP, *Bormann*, 2012) contains this table in Data Sheet (DS) 3.1. The time accuracy of these published values ($t_{Rmax} - t_{P/PKP}$) is about one minute.

In this short note we used data from Collm geophysical observatory (CLL) in Germany. The station was established in 1935, providing high-quality seismic data and manually reviewed body and surface wave arrivals (*Wendt and Buchholz*, 2014). Not only waveforms corresponding to tectonic earthquakes are analysed but also those of anthropogenic events. An example of such a case, including a seismogram from CLL showing clear arrival of surface waves despite the event being a nuclear explosion, is presented in Figure 5.1. We have interpreted about 81,000 seismograms of teleseismic earthquakes in an epicentral distance range of 10 - 170 deg (Fig. 5.2) recorded at CLL between 2006 and 2019. This makes a unique homogeneous database that contains about 13,000 events with Rayleigh wave measurements. All

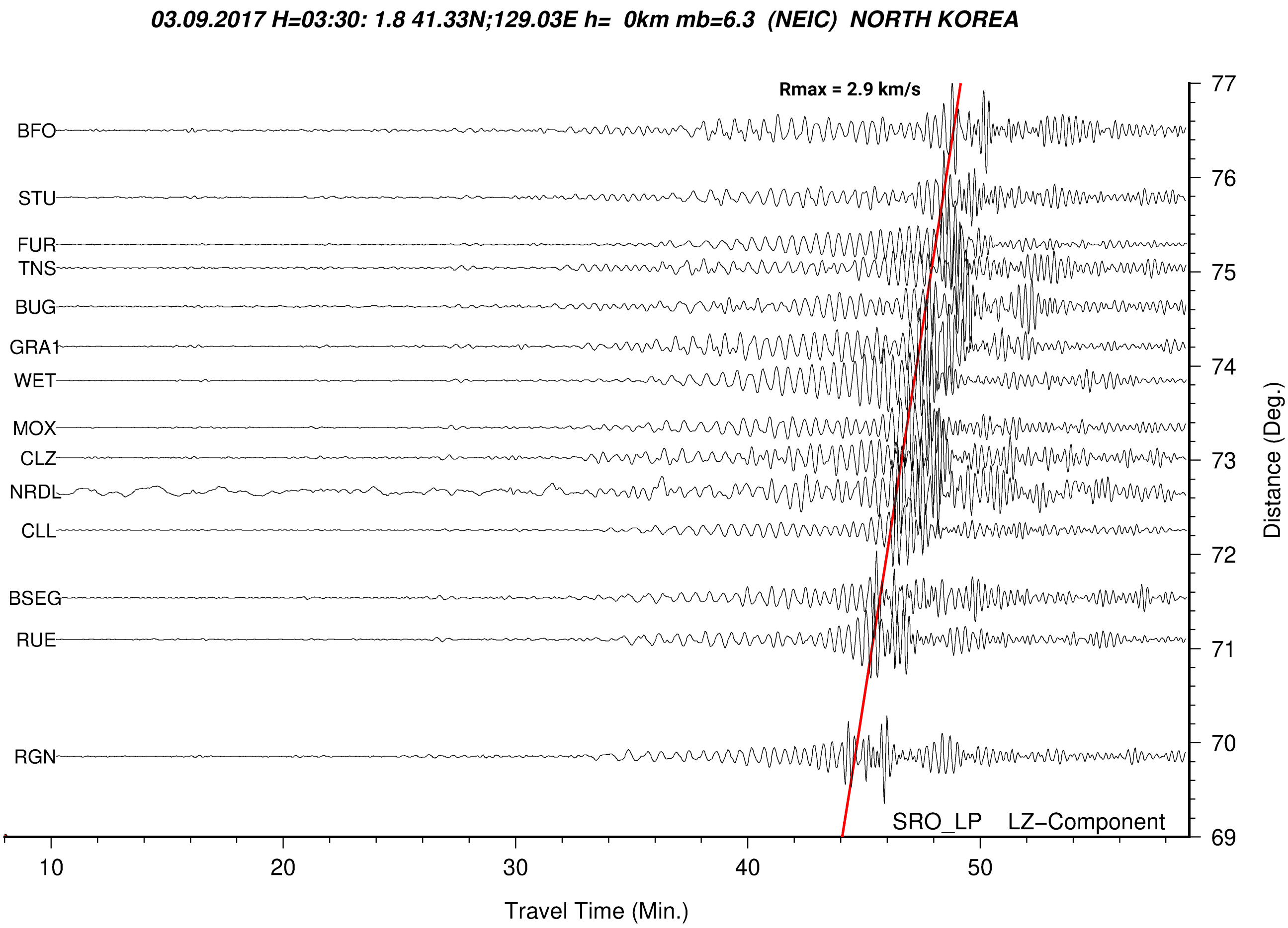

Figure 5.1: *Seismograms of an underground explosion in DPRK sorted with respect to distance for stations of the German Regional Seismic Network (GRSN) and GEOFON Network. Horizontal axis shows travel time (in minutes) relative to the origin time of the event (September 3, 2017 03:30:01.8 UTC). The size of event corresponds to mb=6.3 or Ms=5.1 (NEIC).*

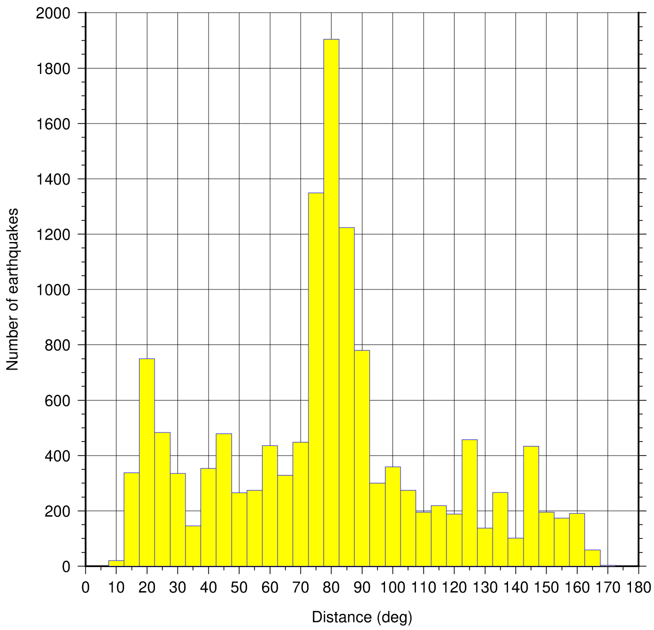

Figure 5.2: *Distribution of all events with measured Rmax on CLL with respect to epicentral distance.*

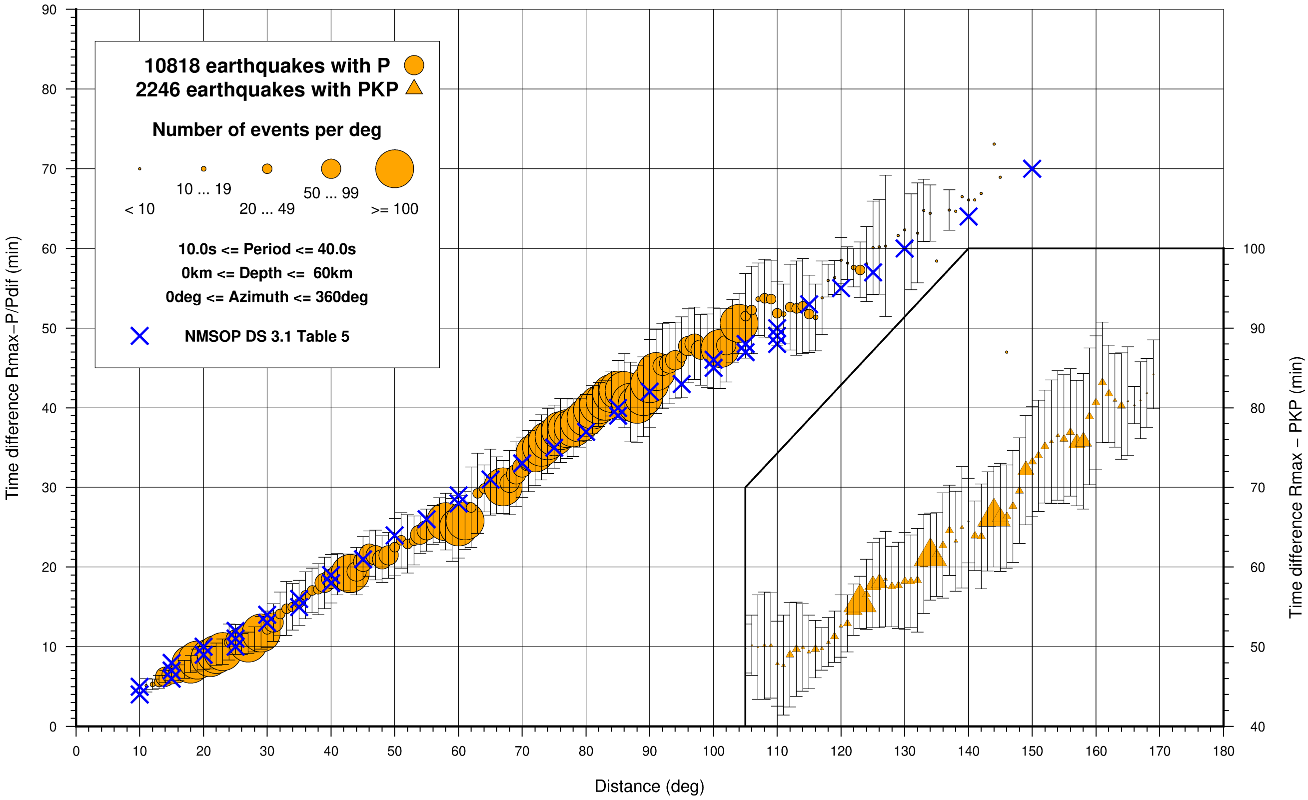

Figure 5.3: *Average time differences $t_{Rmax} - t_{P/PKP}$ as function of epicentral distance. Orange circles correspond to $t_{Rmax} - t_P$ values, orange triangles to $t_{Rmax} - t_{PKP}$. Symbol size is proportional to the number of values in the average calculation and thin gray vertical bars represent their standard deviations. Blue crosses represent the values reported in Table 5 of Data Sheet 3.1 from the NMSOP (Bormann, 2012).*

Rayleigh waves arrivals were manually picked. Figure 5.3 shows the average time differences between t_{Rmax} and $t_{P/PKP}$ from our dataset as a function of epicentral distance and without differentiating for Rayleigh wave period or ray path (continental or oceanic). There is a general agreement between our values and those reported in the NMSOP (blue crosses). For epicentral distances larger than 105 deg we included Pdif and PKP as the first body wave arrivals and we extended our observations up to 170 deg.

However, the distribution of the average velocities of the Rayleigh wave group calculated for the events recorded at CLL station in grid cells of 2 deg by 5 deg in epicentral distance and azimuth, respectively, highlights significant differences in the group velocities depending on the path (Fig. 5.4). More specifically, predominantly continental paths, such as those within the red sector in Figure 5.4 (epicenters going from the Middle East to the Western Sunda Arc), are characterized by group velocities below 3 km/s. Instead, the blue sector in Figure 5.4 (epicenters including the North Atlantic Ridge and the Caribbean Islands) shows group velocities above 3 km/s for oceanic or mainly oceanic paths (i.e., less than 20% continental path). Some internal, smaller scale variations can also be observed inside the blue coloured sector with the velocities getting smaller due to a larger proportion of continental paths for earthquakes in Iceland or the Mid-Atlantic Ridge.

The histograms shown in Figure 5.5(a) are further highlighting the difference in the Rmax group velocities depending on the path. Indeed, there is a clear shift to values higher than 3.1 km/s and lower than 3.0 km/s for the oceanic and continental paths, respectively. Figure 5.5(b) shows the average group

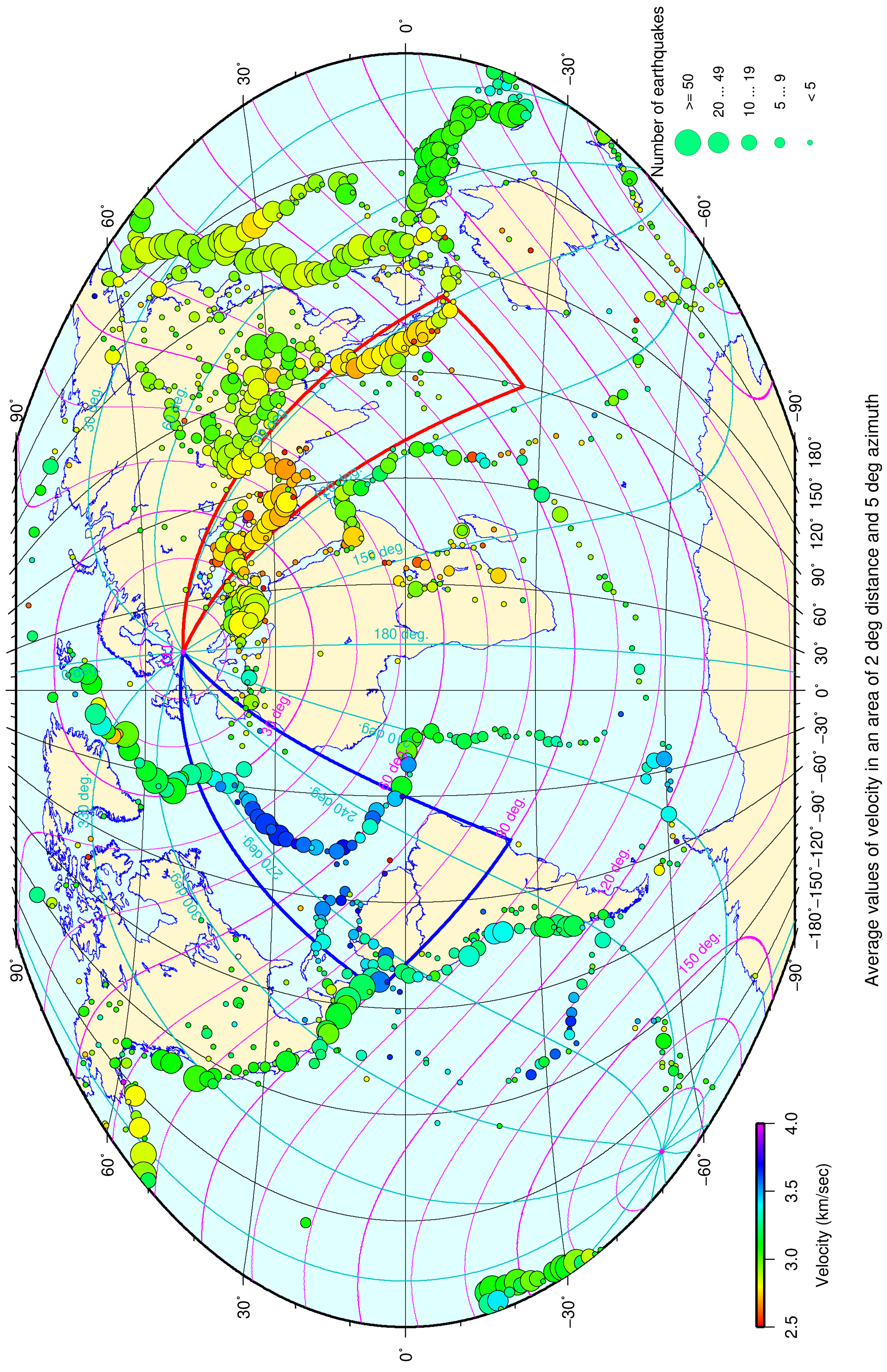

Figure 5.4: *Global distribution of maximum Rayleigh wave group (Rmax) velocity estimated as* $(t_{Rmax} - t_0)/distance$*; with* t_0 = *origin time of the earthquake. Circles correspond to the averaged individual velocities estimated over 2 deg epicentral distance and 5 deg station azimuth increments for events recorded at station CLL. Size of the circles indicates the number of measurements included in the average calculation. Cyan lines = azimuth, magenta lines = epicentral distance.*

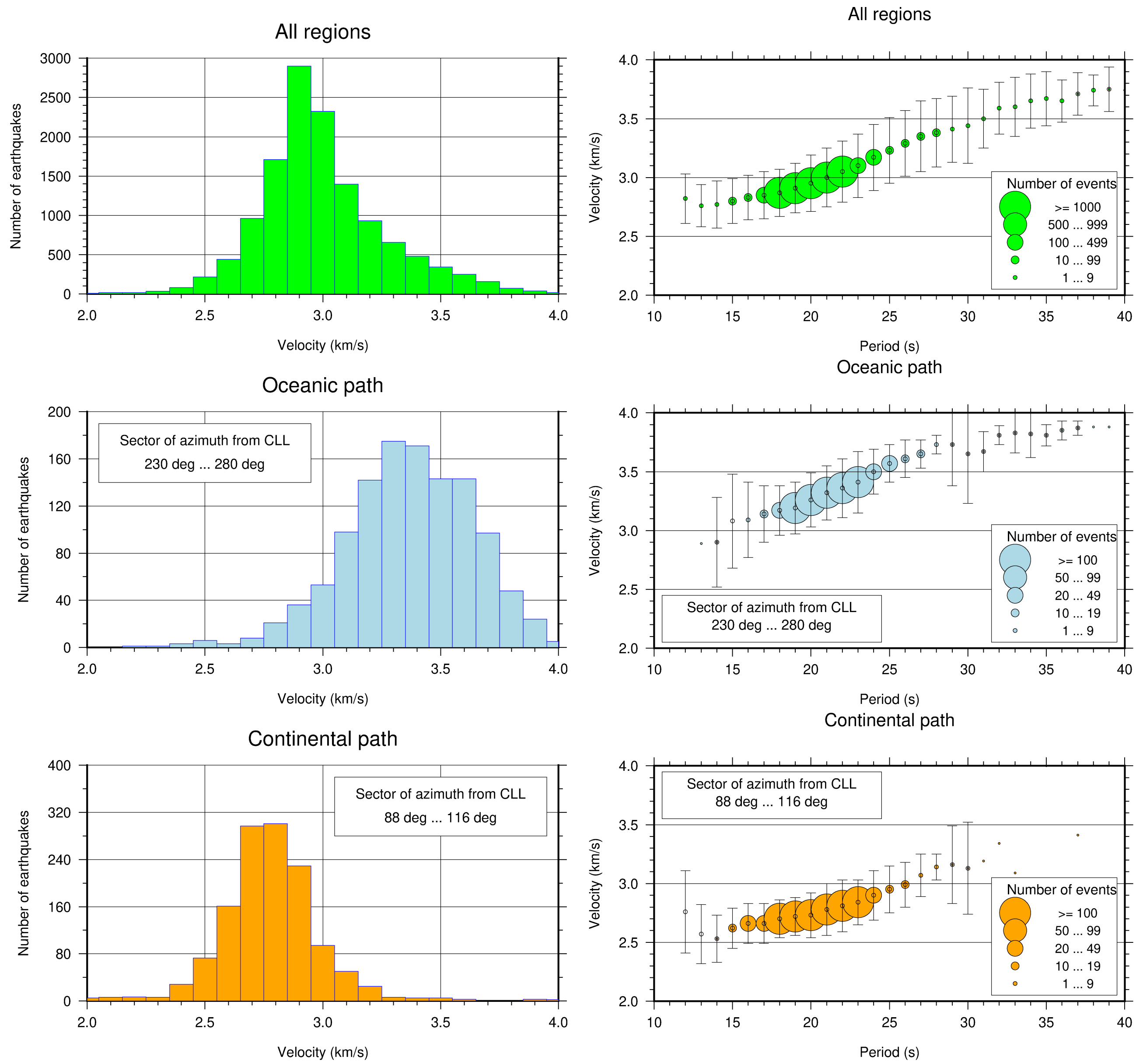

(a) Rmax velocities (b) Dispersion curves

Figure 5.5: *Histograms of Rmax velocities (a) and dispersion curves (b) for: all earthquakes in the database regardless of the region of occurrence (green); sector of 230 – 280 deg azimuth from CLL, corresponding to the predominant oceanic path (blue Fig. 5.4)) and sector of 88 – 116 deg azimuth from CLL, corresponding to the predominant continental path (red in Fig. 5.4).*

velocities of Rmax as a function of the period T for all earthquakes and for the sectors considered in Figure 5.4. We can observe, as expected, that the velocities increase with the period and that the difference between predominantly continental or oceanic paths persist (i.e., higher velocities for oceanic paths and lower for the continental ones).

Considering the results discussed for Figures 5.4 and 5.5, it follows that the dependence of Rmax velocity on its path should be taken into consideration when estimating the theoretical travel-times t_{Rmax}. With the velocities for period T for continental path and oceanic path defined as $v_{cont}(T)$ and $v_{oce}(T)$, respectively, the theoretical t_{Rmax} for the overall path D, decomposed in a continental part D_{cont} and an oceanic part D_{oce}, can be estimated as follows:

$$t_R max = \frac{D_{cont}}{v_{cont}(T)} + \frac{D_{oce}}{v_{oce}(T)}.$$

We calculate the continental (D_{cont}) and oceanic (D_{oce}) parts of the path D as the intersections of the horizontal component of the ray-path with the coastal lines using the Generic Mapping Tool (command "spatial"; *Wessel et al.*, 2019). Our measurements indicate that such an approach, although it should be considered as a simple and quick approximation, works well when calculating t_{Rmax} for different paths to CLL. However, other more precise approaches can be used. The proposed expression for the travel-time calculation considers the dependence of the Rayleigh wave on period and path and, as such, it is an improvement compared to the travel times estimations by *Archangelskaya* (1959) and provided in Table 5 of DS 3.1 from the NMSOP (*Bormann*, 2012).

Additional challenges in t_{Rmax} estimations may appear due to the complexity of the recorded waveforms. E.g., the superposition of surface waves from two different earthquakes can make the association of the Rayleigh wave measurements to the correct event difficult or impossible by using just time differences. In such instances, sorting the seismograms with respect to epicentral distance can be helpful, especially if there is a distinct difference in the event-station azimuth for the overlapping earthquakes. Figure 5.6

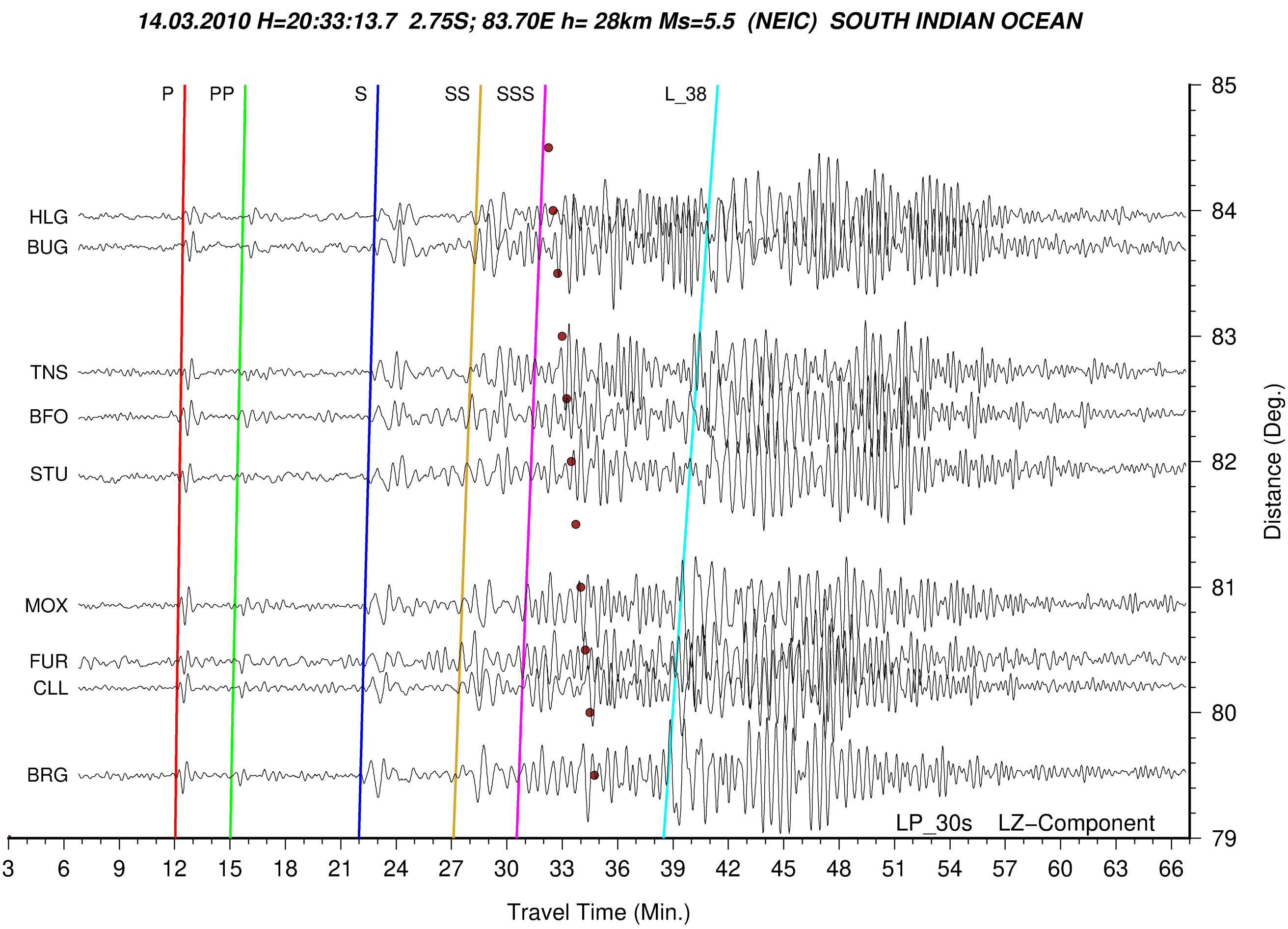

Figure 5.6: *Superposition of seismograms of two events: South Indian Ocean (2010-03-14 20:33:11.5) Ms=5.5 and Central Chile (2010-03-14 20:04:55.5) Ms=5.4 (origin times from ISC) on stations of GRSN and GEOFON networks. cyan line = Rayleigh waves of South Indian Ocean event; brown circles =* t_{Rmax} *of Chile event. See text for more details.*

shows a superposition of seismograms for two events: one from South Indian Ocean (MS=5.5, epicentral distance to CLL = 80 deg) and the other from Central Chile (MS=5.4, epicentral distance to CLL = 117 deg) occurring about 28 minutes before the South Indian Ocean earthquake. These two events have a difference of 134 degrees in back azimuth to CLL. Seismograms of the South Indian Ocean event are sorted with respect to the epicentral distances for stations belonging to the German Regional Seismic Network (*GRSN*) and *GEOFON* Network. Long, periodic initial part of Rayleigh waves is marked by a cyan line with a slope of 3.8 km/s. Body waves (SS, SSS) of this earthquake are superposed by surface waves of the Central Chile earthquake. Its t_{Rmax} timings are marked by brown circles. The surface waves of the two events can be distinguished by their arrivals on the stations sloping in different directions (cyan line and brown circles). Without sorting seismograms by epicentral distance, the identification and correct association of the surface wave for the Central Chile earthquake may not be possible or it may contain erroneous measurements.

It is also worth mentioning that surface waves can travel around the Earth several times and be observed as returning waves after large earthquakes. This can occur on the short path from the hypocenter to seismic station (360 deg + D) as well as on the long path (360 deg + (360 deg - D), where D is the epicentral distance in degrees. Such waves can add complexity to the seismic recordings and hinder the association of surface waves to the correct event. Figure 5.7 shows an example where seismograms of GRSN stations are sorted with respect to the epicentral distance. Surface wave trains L, L3 and L5

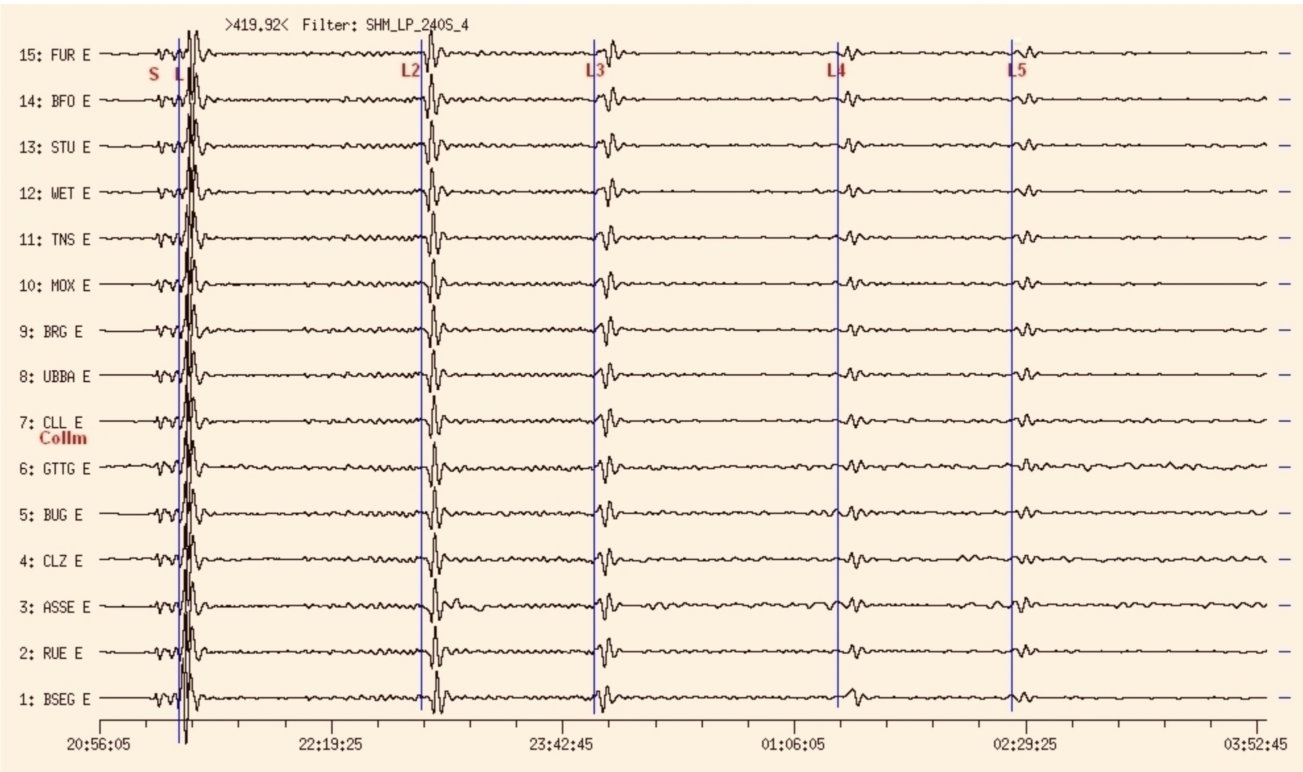

Figure 5.7: *Seismograms showing surface waves of a strong earthquake (mb=7.0, MS=7.6, ISC) south of Alaska on October 19, 2020, 20:54:39.0 GMT. The surface waves travelled up to two times around the globe along the short and long path from the earthquake to CLL. L, L3 and L5 – travelled along (multiples of) the short path, L2 and L4 – along (multiples of) the long path. Blue line = arrival time at CLL. Please note that L(m/V) is an older notation for the maximum of the surface wave and does not refer to Love waves specifically here.*

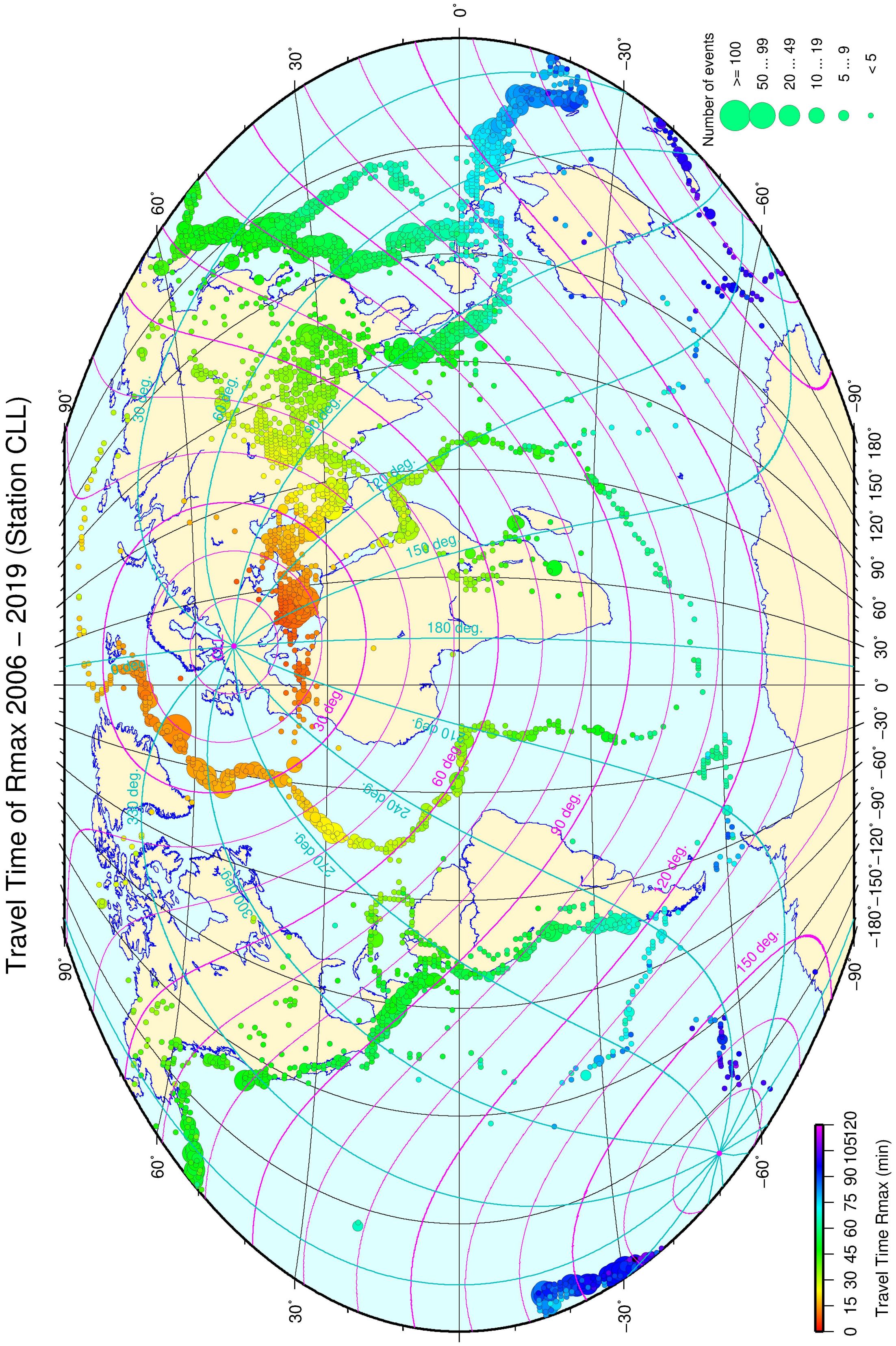

Figure 5.8: *Overview of global Rmax travel times ($t_{Rmax} - t_{P/PKP}$) recorded in CLL. Circles = number of events in cell, cyan lines = azimuth, magenta lines = epicentral distance.*

correspond to the travel-paths along the short path while L2 and L4 to the travel-paths along the long path (L2 = 360 deg - D, L3 = 360 deg + D, L4 = 360 deg + (360 deg - D), L5 = (2 * 360 deg) + D, i.e. L5 travelled around the Earth twice before arriving at CLL station). The path of the wave-train can be identified from the seismograms: L, L3 and L5 arrive first at the closest station (BSEG) in Northern Germany, while L2 and L4 arrive first at the furthest station FUR in Southern Germany.

In this short note we presented our database of teleseismic Rayleigh wave travel-time observations (t_{Rmax}) at station CLL in Germany and provided a procedure to better estimate the expected arrival times of t_{Rmax} by separating the wave propagation path into the continental and oceanic sections. The database provided can serve for the observation-based Rayleigh wave travel-time estimations at CLL station for future earthquakes. The summary of the global Rayleigh wave travel-times included in the database is provided in Figure 5.7. The dataset containing all the associated picks used in this study is publicly available in the ISC Dataset Repository (*Wendt and Buchholz*, 2023). By creating a 1 deg by 1 deg grid of this map, we can estimate a time window when Rmax should arrive at the station when analysing the seismograms. This map is of course only based on the measurements at CLL station, but with a large enough dataset, this principle could be used by other observatories and institutions, which would lead to more accurate estimations of the Rayleigh wave arrivals on a global scale.

Acknowledgements

The authors are very grateful to Natalia Poiata and Kathrin Lieser from the International Seismological Centre (ISC) for their constructive suggestions, which helped improve this contribution.

The authors thank Prof. Dr. Michael Korn for a critical reading of the manuscript and useful hints.

References

Arkangelskaya, V .M. (1959), The dispersion of surface waves in the Earth's crust, *Izv. Akad. Nauk SSSR*, *Seriya Geofiz.*, *9* (in Russian).

Bormann, P. (Ed.)(2012), New Manual of Seismological Observatory Practice (NMSOP-2), *Potsdam : Deutsches GeoForschungszentrum GFZ; IASPEI*, `https://doi.org/10.2312/GFZ.NMSOP-2`.

GEOFON Data Centre (1993), GEOFON Seismic Network, GFZ Data Services, GFZ German Research Centre for Geosciences, Potsdam, Germany, `https://doi.org/10.14470/TR560404`.

GRSN, Federal Institute for Geosciences and Natural Resources (1976), German Regional Seismic Network (GRSN), Bundesanstalt für Geowissenschaften und Rohstoffe (BGR), Hanover, Germany, `https://doi.org/10.25928/mbx6-hr74`.

Willmore, P. L. (Ed.)(1979), Manual of Seismological Observatory Practice, *World Data Center A for Solid Earth Geophysics*, *Report SE-20*, Boulder, Colorado.

Wendt, S. and P. Buchholz (2017), Collm Geophysical Observatory, *Summ. Bull. Internatl. Seismol. Cent.*, January - June 2014, *51*(I), pp. 32–44, `https://doi.org/10.5281/zenodo.996043`.

Wendt, S. and P. Buchholz (2023), Rayleigh wave travel times measured at Collm Geophysical Observatory, Germany, between 2006 and 2019, ISC Seismological Dataset Repository, `https://doi.org/10.31905/PHF064PS`.

Wessel, P., J. F. Luis, L. Uieda, R. Scharroo, F. Wobbe, W. H. F. Smith and D. Tian (2019), The Generic Mapping Tools version 6, *Geochem. Geophys. Geosyst.*, *20*, 5556–5564, `https://doi.org/10.1029/2019GC008515`.

6

Summary of Seismicity, January – June 2020

The period between January and June 2020 produced 5 earthquakes with $M_W \geq 7$; these are listed in Table 6.1. The largest one was the M_W 7.7 strike-slip earthquake along the Oriente fault where the North American and Caribbean plates meet in the Caribbean on 28 January 2020 (19:10:23.76 UTC, 19.3775°N, 78.7539°W, 6 km, 2043 stations (ISC)). The study of Tadapansawutet et al. (2021) of the rupture found an unusually complex rupture process for a transform fault earthquake. They suggest that the complex geometry of the fault system caused changes in rupture speed and direction and triggered successive rupture episodes that included a supershear rupture, where the rupture speed exceeds shear wave velocity.

The most discussed earthquake in the scientific community during this Summary's time period was the M_W6.8 Elazig event in Turkey (24/01/2020 17:55:15.54 UTC, 38.2987°N, 39.1475°E, 12 km, 2113 stations (ISC)) with currently 41 entries in the ISC Event Bibliography (*Di Giacomo et al.*, 2014; *International Seismological Centre*, 2023). At the time, it was the largest event in that area along the East Anatolian Fault Zone for about a century. The strike-slip event lasted for about 20 s, propagated from north-east to south-west at a relatively slow rupture speed of 2-2.5 km/s but did not cause any surface slip (e.g., *Konca et al.*, 2021; *Melgar et al.*, 2020; *Pousse-Beltran et. al.*, 2020). Three years later, about 220 km to the southwest the disastrous M_W7.8 earthquake and its aftershocks struck southern Turkey and Syria in February 2023 causing tens of thousands of people to lose their lives, injuring more than 100,000 people and destroying tens of thousands of buildings (*USGS*, 2023).

The number of events in this Bulletin Summary categorised by type are given in Table 6.2.

Figure 6.1 shows the number of moderate and large earthquakes in the first half of 2020. The distribution of the number of earthquakes should follow the Gutenberg-Richter law.

Figures 6.2 to 6.5 show the geographical distribution of moderate and large earthquakes in various magnitude ranges.

Table 6.1: *Summary of the earthquakes of magnitude Mw $\geq$ 7 between January and June 2020.*

Date	lat	lon	depth	Mw	Flinn-Engdahl Region
2020-01-28 19:10:23	19.38	-78.75	5	7.7	Cuba region
2020-03-25 02:49:19	48.85	157.76	49	7.5	East of Kuril Islands
2020-06-18 12:49:55	-33.37	-177.84	19	7.4	South of Kermadec Islands
2020-06-23 15:29:02	15.82	-96.03	12	7.4	Near coast of Oaxaca
2020-02-13 10:33:44	45.53	148.84	150	7.0	Kuril Islands

Table 6.2: *Summary of events by type between January and June 2020.*

felt earthquake	6883
known earthquake	160953
known chemical explosion	8109
known induced event	3673
known landslide	3
known mine explosion	2183
known rockburst	153
known experimental explosion	39
suspected earthquake	133571
suspected chemical explosion	5693
suspected induced event	67
suspected mine explosion	5769
suspected rockburst	190
suspected experimental explosion	373
suspected ice-quake	186
unknown	4
total	327849

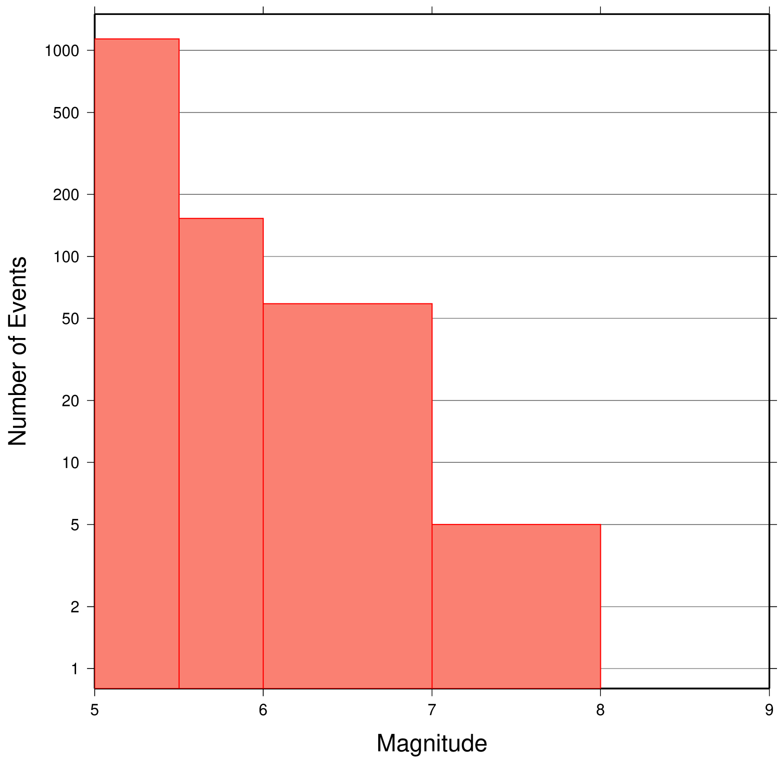

Figure 6.1: *Number of moderate and large earthquakes between January and June 2020. The non-uniform magnitude bias here correspond with the magnitude intervals used in Figures 6.2 to 6.5.*

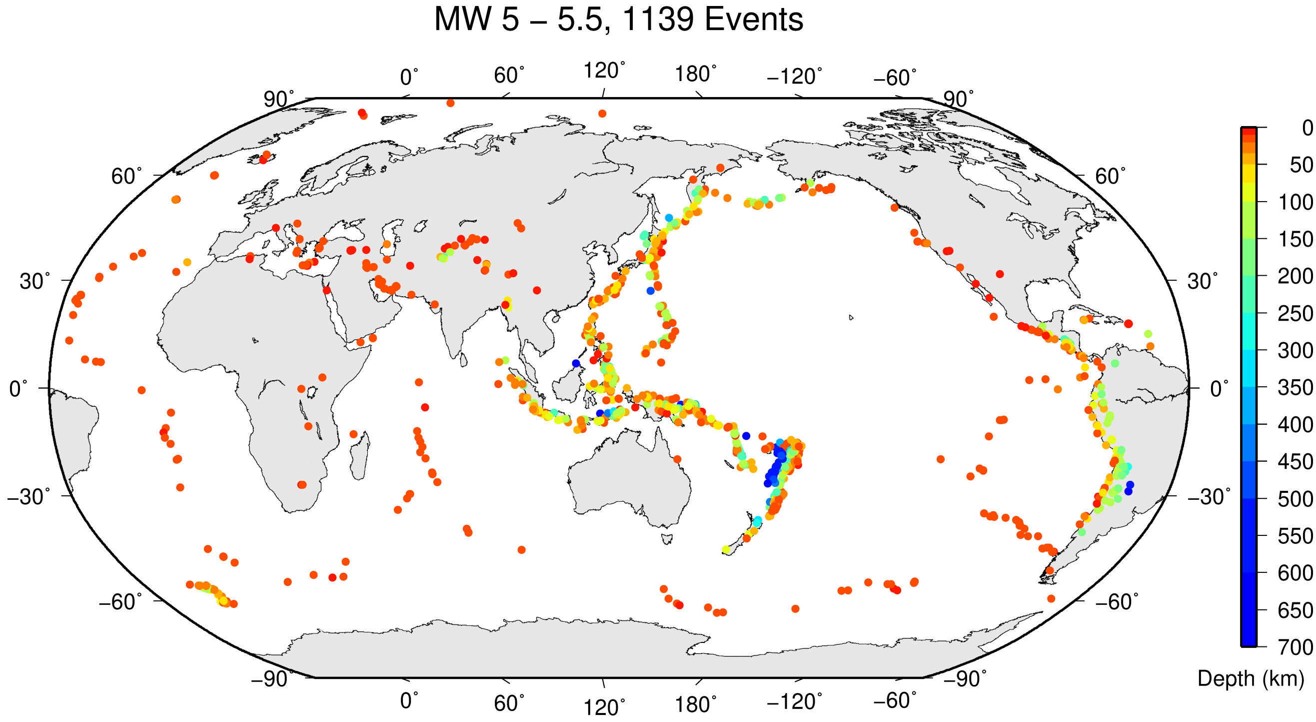

Figure 6.2: *Geographic distribution of magnitude 5-5.5 earthquakes between January and June 2020.*

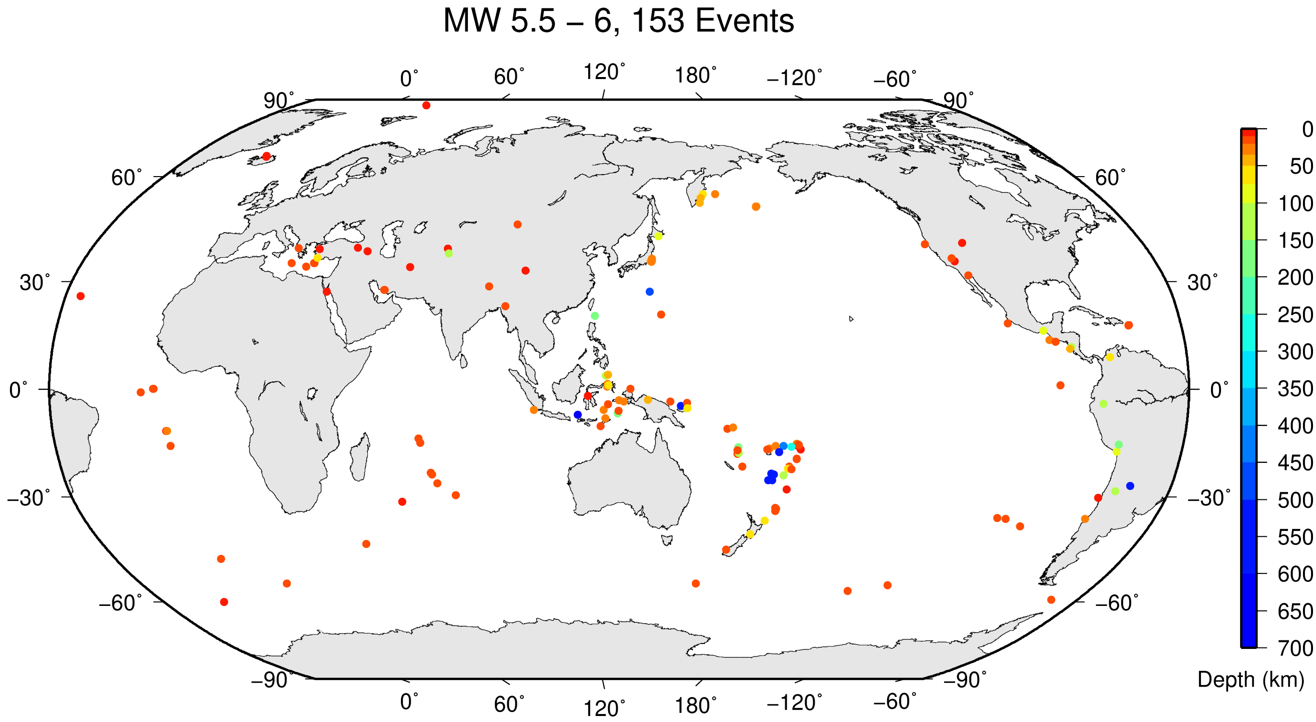

Figure 6.3: *Geographic distribution of magnitude 5.5-6 earthquakes between January and June 2020.*

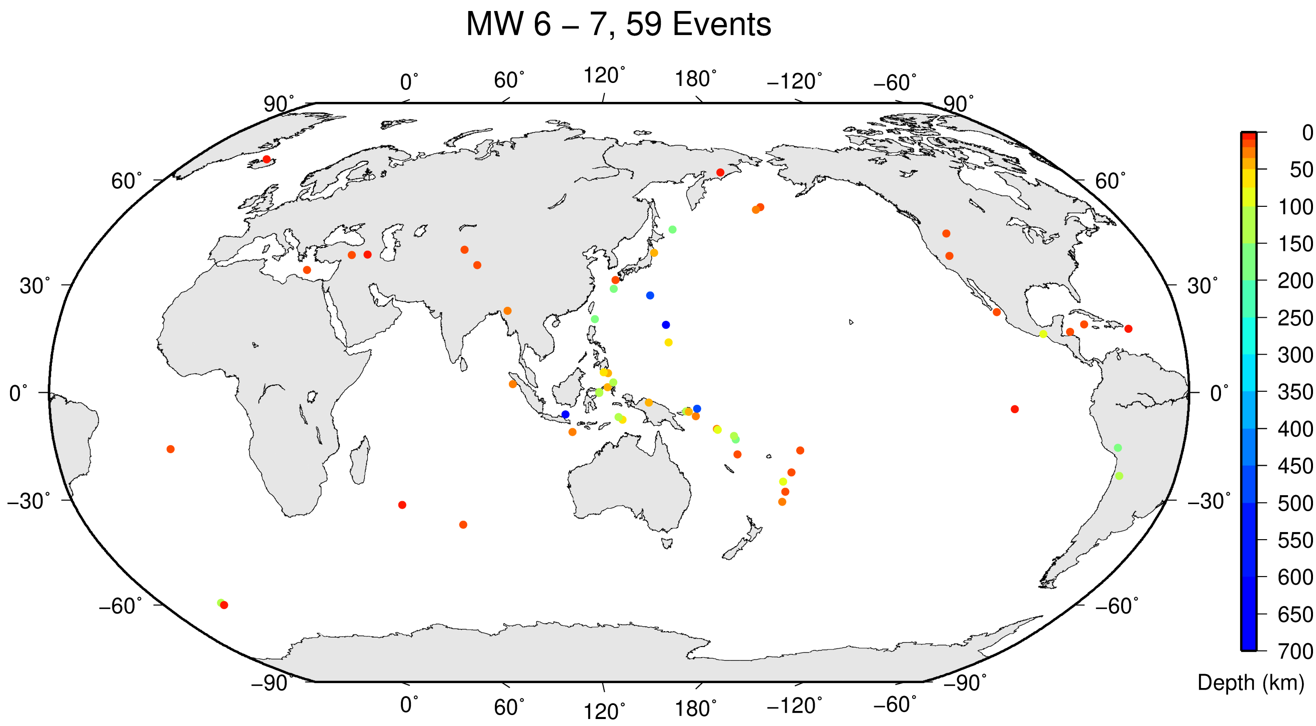

Figure 6.4: *Geographic distribution of magnitude 6-7 earthquakes between January and June 2020.*

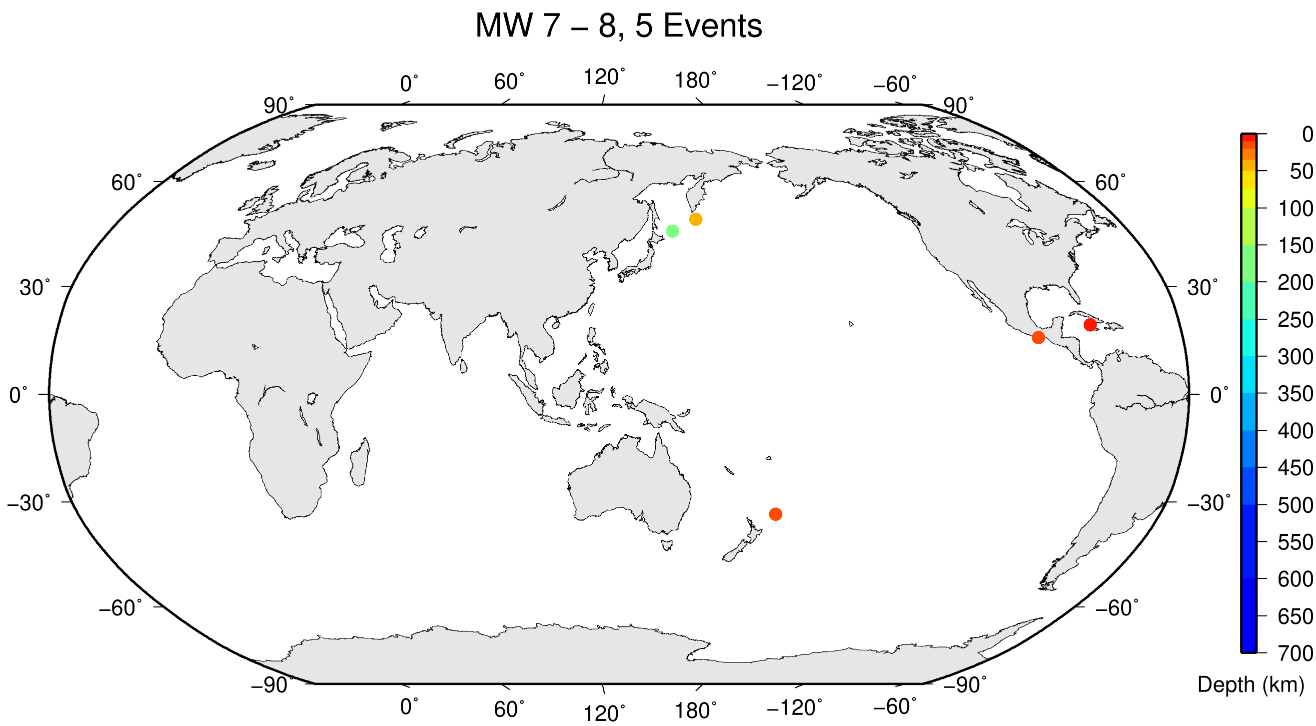

Figure 6.5: *Geographic distribution of magnitude 7-8 earthquakes between January and June 2020.*

References

Di Giacomo, D., D.A. Storchak, N. Safronova, P. Ozgo, J. Harris, R. Verney and I. Bondár (2014), A New ISC Service: The Bibliography of Seismic Events, *Seismol. Res. Lett.*, *85*(2), 354–360, https://doi.org/10.1785/0220130143.

International Seismological Centre (2023), On-line Event Bibliography, https://doi.org/10.31905/EJ3B5LV6.

Konca, A. Ö., H. Karabulut, S.E. Güvercin, F. Eskiköy, S. Özarpacı, A. Özdemir, M. Floyd, S Ergintav and U. Doğan (2021), From interseismic deformation with near-repeating earthquakes to co-seismic rupture: A unified view of the 2020 Mw6.8 Sivrice (Elazığ) eastern Turkey earthquake, *J. Geophys. Res. Solid Earth*, *126*, e2021JB021830, https://doi.org/10.1029/2021JB021830.

Melgar, D., A. Ganas, T. Taymaz, S. Valkaniotis, B.W. Crowell, V. Kapetanidis, V. Tsironi, S. Yolsal-Çevikbilen and T. Öcalan (2020), Rupture kinematics of 2020 January 24 Mw 6.7 Doğanyol-Sivrice, Turkey earthquake on the East Anatolian Fault Zone imaged by space geodesy, *Geophys. J. Int.*, *223*(2), 862–874, https://doi.org/10.1093/gji/ggaa345.

Pousse-Beltran, L., E. Nissen, E.A. Bergman, M.D. Cambaz, É. Gaudreau, E. Karasözen and F. Tan (2020), The 2020 Mw 6.8 Elazığ (Turkey) earthquake reveals rupture behavior of the East Anatolian Fault, *Geophys. Res. Lett.*, *47*, e2020GL088136, https://doi.org/10.1029/2020GL088136.

Tadapansawut, T., R. Okuwaki, Y. Yagi and S. Yamashita (2021), Rupture process of the 2020 Caribbean earthquake along the Oriente transform fault, involving supershear rupture and geometric complexity of fault. *Geophys. Res. Lett.*, *48*, e2020GL090899, urlhttps://doi.org/10.1029/2020GL090899.

USGS (2023), https://earthquake.usgs.gov/earthquakes/eventpage/us6000jllz, (08/03/23).

7

Statistics of Collected Data

7.1 Introduction

The ISC Bulletin is based on the parametric data reports received from seismological agencies around the world. With rare exceptions, these reports include the results of waveform review done by analysts at network data centres and observatories. These reports include combinations of various bulletin elements such as event hypocentre estimates, moment tensors, magnitudes, event type and felt and damaging data as well as observations of the various seismic waves recorded at seismic stations.

Data reports are received in different formats that are often agency specific. Once an authorship is recognised, the data are automatically parsed into the ISC database and the original reports filed away to be accessed when necessary. Any reports not recognised or processed automatically are manually checked, corrected and re-processed. This chapter describes the data that are received at the ISC before the production of the reviewed Bulletin.

Notably, the ISC integrates all newly received data reports into the automatic ISC Bulletin (available on-line) soon after these reports are made available to ISC, provided it is done before the submission deadline that currently stands at 12 months following an event occurrence.

With data constantly being reported to the ISC, even after the ISC has published its review, the total data shown as collected, in this chapter, is limited to two years after the time of the associated reading or event, i.e. any hypocentre data collected two years after the event are not reflected in the figures below.

7.2 Summary of Agency Reports to the ISC

A total of 150 agencies have reported data for January 2020 to June 2020. The parsing of these reports into the ISC database is summarised in Table 7.1.

Table 7.1: *Summary of the parsing of reports received by the ISC from a total of 150 agencies, containing data for this summary period.*

	Number of reports
Total collected	6783
Automatically parsed	5843
Manually parsed	936

Data collected by the ISC consists of multiple data types. These are typically one of:

- Bulletin, hypocentres with associated phase arrival observations.

- Catalogue, hypocentres only.
- Unassociated phase arrival observations.

In Table 7.2, the number of different data types reported to the ISC by each agency is listed. The number of each data type reported by each agency is also listed. Agencies reporting indirectly have their data type additionally listed for the agency that reported it. The agencies reporting indirectly may also have 'hypocentres with associated phases' but with no associated phases listed - this is because the association is being made by the agency reporting directly to the ISC. Summary maps of the agencies and the types of data reported are shown in Figure 7.1 and Figure 7.2.

Table 7.2: *Agencies reporting to the ISC for this summary period. Entries in bold are for new or renewed reporting by agencies since the previous six-month period.*

Agency	Country	Directly or indirectly reporting (D/I)	Hypocentres with associated phases	Hypocentres without associated phases	Associated phases	Unassociated phases	Amplitudes
TIR	Albania	D	848	0	12098	0	2935
CRAAG	Algeria	D	207	0	2606	24	0
LPA	Argentina	D	0	0	0	954	0
SJA	Argentina	D	946	1	46598	0	13935
NSSP	Armenia	D	166	0	3052	0	0
AUST	Australia	D	940	0	55885	0	54987
CUPWA	Australia	D	27	0	353	0	0
IDC	Austria	D	18445	0	626061	0	556245
VIE	Austria	D	5137	59	51300	379	50980
AZER	Azerbaijan	D	4432	0	60742	0	0
UCC	Belgium	D	1663	0	11581	35	3671
SCB	Bolivia	D	826	0	12840	0	1880
RHSSO	Bosnia and Herzegovina	D	298	0	5087	3268	0
BGSI	Botswana	D	476	2	5426	1	1456
OSUNB	Brazil	D	79	0	2263	0	0
VAO	Brazil	D	883	21	21479	555	0
SOF	Bulgaria	D	225	0	2801	2948	0
OTT	Canada	D	1343	32	36861	0	4850
PGC	Canada	I OTT	681	0	20702	0	0
GUC	Chile	D	3672	363	106526	8185	33230
BJI	China	D	1230	52	109784	30652	76253
ASIES	Chinese Taipei	D	0	34	0	0	0
TAP	Chinese Taipei	D	13373	0	700250	0	0
RSNC	Colombia	D	17434	217	264071	863	66276
UCR	Costa Rica	D	348	0	17897	0	0
ZAG	Croatia	D	0	0	0	54752	0
SSNC	Cuba	D	4009	1	60893	16	23438
NIC	Cyprus	D	348	0	12934	0	5347
IPEC	Czech Republic	D	531	0	5602	22055	2605
PRU	Czech Republic	D	4759	0	44978	182	10322
WBNET	Czech Republic	D	218	0	3934	0	3934
KEA	Democratic People's Republic of Korea	D	123	0	1368	0	679
DNK	Denmark	D	2556	2056	37304	26898	9513
OSPL	Dominican Republic	D	2254	0	25684	12	8637
SDD	Dominican Republic	D	4032	0	77420	380	29087
IGQ	Ecuador	D	140	0	6656	0	0
HLW	Egypt	D	139	0	1320	0	0
SNET	El Salvador	D	1260	4	19231	91	395
EST	Estonia	I HEL	216	25	0	0	0
FIA0	Finland	I HEL	7	0	0	0	0
HEL	Finland	D	6867	1344	172318	19	32038
CSEM	France	I AWI	2511	176	0	0	0
IPGP	France	D	0	103	0	0	0
LDG	France	D	1983	65	28112	1	12284

Table 7.2: *(continued)*

Agency	Country	Directly or indirectly reporting (D/I)	Hypocentres with associated phases	Hypocentres without associated phases	Associated phases	Unassociated phases	Amplitudes
STR	France	D	3796	1	72453	93	0
PPT	French Polynesia	D	977	20	6309	34	6324
TIF	Georgia	D	0	136	0	2894	0
AWI	Germany	D	4365	9	17344	1086	7572
BGR	Germany	D	559	208	14420	0	5922
BNS	Germany	I BGR	2	21	0	0	0
BRG	Germany	D	0	0	0	9981	3495
CLL	Germany	D	2	0	86	7992	2671
GDNRW	Germany	I BGR	1	4	0	0	0
GFZ	Germany	D	2490	1329	137239	0	153275
HLUG	Germany	I BGR	6	5	0	0	0
LEDBW	Germany	I BGR	22	9	0	0	0
ATH	Greece	D	7898	34	236933	0	66315
THE	Greece	D	3168	0	70293	3507	53759
UPSL	Greece	D	0	4	0	0	0
GCG	Guatemala	D	1459	0	17224	0	2102
HKC	Hong Kong	D	0	0	0	32	0
KRSZO	Hungary	D	705	11	10339	0	4724
REY	Iceland	D	96	3	3493	0	0
HYB	India	D	587	3	1688	7	101
NDI	India	D	973	566	38630	58	15081
DJA	Indonesia	D	5089	49	69497	0	67688
TEH	Iran	D	1902	0	20316	0	0
THR	Iran	D	81	0	2163	0	967
ISN	Iraq	D	148	0	1110	0	359
DIAS	Ireland	D	0	0	0	1163	0
GII	Israel	D	2319	0	53806	0	0
GEN	Italy	D	932	0	22816	21	0
MED_RCMT	Italy	D	0	185	0	0	0
RISSC	Italy	D	6	0	92	0	0
ROM	Italy	D	8636	129	719389	249075	477855
SARA	**Italy**	**D**	**20**	**0**	**256**	**0**	**0**
TRI	Italy	D	0	0	0	10006	0
JSN	Jamaica	D	450	8	2280	0	0
JMA	Japan	D	109188	5570	680112	0	15104
NIED	Japan	D	0	678	0	0	0
SYO	Japan	D	0	0	0	762	0
JSO	Jordan	D	651	7	10543	0	15846
NNC	Kazakhstan	D	9002	68	89761	0	84059
SOME	Kazakhstan	D	4922	108	57575	4	49348
KNET	Kyrgyzstan	D	1117	0	8989	0	2928
KRNET	Kyrgyzstan	D	2872	0	46669	30	0
LVSN	Latvia	D	154	0	2425	0	1438
GRAL	Lebanon	D	149	0	1382	1293	0
LIT	Lithuania	D	863	861	5513	668	0
MCO	Macao, China	D	0	0	0	28	0
TAN	Madagascar	D	671	0	6065	4	0
ECX	Mexico	D	588	0	15776	0	3226
MEX	Mexico	D	17543	235	305339	22	0
PDG	Montenegro	D	624	1	13351	0	6717
CNRM	Morocco	D	1341	0	14918	0	0
NAM	Namibia	D	111	0	1319	32	382
DMN	Nepal	D	72	0	1267	0	535
DBN	**Netherlands**	**I BGR**	**0**	**3**	**0**	**0**	**0**
NOU	New Caledonia	D	3804	0	69005	0	4563
WEL	New Zealand	D	11231	65	381720	98397	275872
CATAC	Nicaragua	D	2244	1	92698	31	0
SKO	North Macedonia	D	0	456	2884	2053	1302
BER	Norway	D	2289	1919	47401	4133	11792
NAO	Norway	D	1962	959	5636	0	1786
OMAN	Oman	D	572	0	28805	0	0
UPA	Panama	D	1561	68	20261	58	985
ARE	Peru	I RSNC	2	0	0	0	0
MAN	Philippines	D	0	6726	0	54273	13641
QCP	Philippines	D	0	0	0	42	0
PJWWP	Poland	D	152	0	366	5	22

Table 7.2: *(continued)*

Agency	Country	Directly or indirectly reporting (D/I)	Hypocentres with associated phases	Hypocentres without associated phases	Associated phases	Unassociated phases	Amplitudes
WAR	Poland	D	0	0	0	20098	906
IGIL	Portugal	D	776	0	3569	0	1187
INMG	Portugal	D	1683	0	79463	15503	40298
PDA	**Portugal**	**I SVSA**	**1**	**0**	**0**	**0**	**0**
SVSA	Portugal	D	1219	0	40381	10817	32115
BELR	Republic of Belarus	D	0	0	0	22552	7569
CFUSG	Republic of Crimea	D	112	0	3214	287	2104
KMA	Republic of Korea	D	12	0	306	0	1
BUC	Romania	D	499	0	13517	55188	6152
ASRS	Russia	D	128	3347	4208	0	1581
BYKL	Russia	D	52	0	6934	0	2391
DRS	Russia	I MOS	178	134	0	0	0
FCIAR	Russia	D	170	0	1338	993	602
IDG	Russia	I MOS	0	3	0	0	0
IGKR	**Russia**	**I MOS**	**0**	**3**	**0**	**0**	**0**
KOLA	Russia	D	2159	146	17684	72	0
KRSC	Russia	D	1125	0	31031	0	0
MIRAS	Russia	D	37	0	1158	0	595
MOS	Russia	D	2838	3757	320632	0	109980
NERS	Russia	D	83	4	2116	0	1011
NORS	Russia	I MOS	28	147	0	0	0
SKHL	Russia	D	995	995	21825	26	9303
YARS	Russia	D	354	9	6841	0	4435
SGS	Saudi Arabia	D	1868	0	28768	0	0
BEO	Serbia	D	1023	0	22149	0	0
BRA	Slovakia	D	0	0	0	19319	0
LJU	Slovenia	D	1257	0	19219	3072	6831
PRE	South Africa	D	2004	0	39998	552	13387
MDD	Spain	D	3134	0	74455	0	21079
MRB	Spain	D	714	0	20076	273	8636
SFS	Spain	D	1036	0	17806	41	0
UPP	Sweden	D	2829	1784	33049	0	0
ZUR	Switzerland	D	609	24	14848	0	8943
BKK	Thailand	D	186	5	1328	0	2028
TRN	Trinidad and Tobago	D	4892	13	27572	32375	0
TUN	Tunisia	D	30	1	198	5	0
AFAD	Turkey	D	19352	0	540093	0	188447
ISK	Turkey	D	18598	0	275857	1713	159772
AEIC	U.S.A.	I NEIC	646	2518	65048	0	0
ANF	U.S.A.	I IRIS	223	769	0	0	0
BUT	U.S.A.	I NEIC	0	582	4907	0	0
GCMT	U.S.A.	D	0	2324	0	0	0
HVO	U.S.A.	I NEIC	0	537	21910	0	0
IRIS	U.S.A.	D	1979	769	268678	0	0
LDO	U.S.A.	I NEIC	0	6	43	0	0
NCEDC	U.S.A.	I NEIC	0	376	21260	0	0
NEIC	U.S.A.	D	22490	13268	2079689	0	1071254
PAS	U.S.A.	I NEIC	0	405	25443	0	0
PMR	U.S.A.	I IRIS	12	0	0	0	0
PNSN	U.S.A.	D	0	76	0	0	0
PTWC	**U.S.A.**	**D**	**313**	**0**	**4435**	**0**	**0**
REN	U.S.A.	I NEIC	1	1164	19413	0	0
RSPR	U.S.A.	D	10596	2609	199610	0	0
SEA	U.S.A.	I NEIC	0	39	1743	0	0
SLC	**U.S.A.**	**I NEIC**	**0**	**1**	**0**	**0**	**0**
SLM	U.S.A.	I NEIC	0	66	1471	0	0
TUL	**U.S.A.**	**I NEIC**	**0**	**1**	**0**	**0**	**0**
TXNET	U.S.A.	D	853	3	41287	170	22108
UUSS	U.S.A.	I NEIC	1	206	6232	0	0
MCSM	Ukraine	D	1270	230	25199	55	13020
SIGU	Ukraine	D	34	34	1436	0	787
DSN	United Arab Emirates	D	482	0	6934	0	0

Table 7.2: *(continued)*

Agency	Country	Directly or indirectly reporting (D/I)	Hypocentres with associated phases	Hypocentres without associated phases	Associated phases	Unassociated phases	Amplitudes
BGS	United Kingdom	D	348	19	9287	0	3994
ISC-PPSM	United Kingdom	D	0	86	0	0	0
ISU	Uzbekistan	D	611	59	2800	12	0
FUNV	Venezuela	D	888	1	8119	0	0
PLV	Viet Nam	D	15	0	226	39	104
BUL	Zimbabwe	D	252	0	1672	263	0

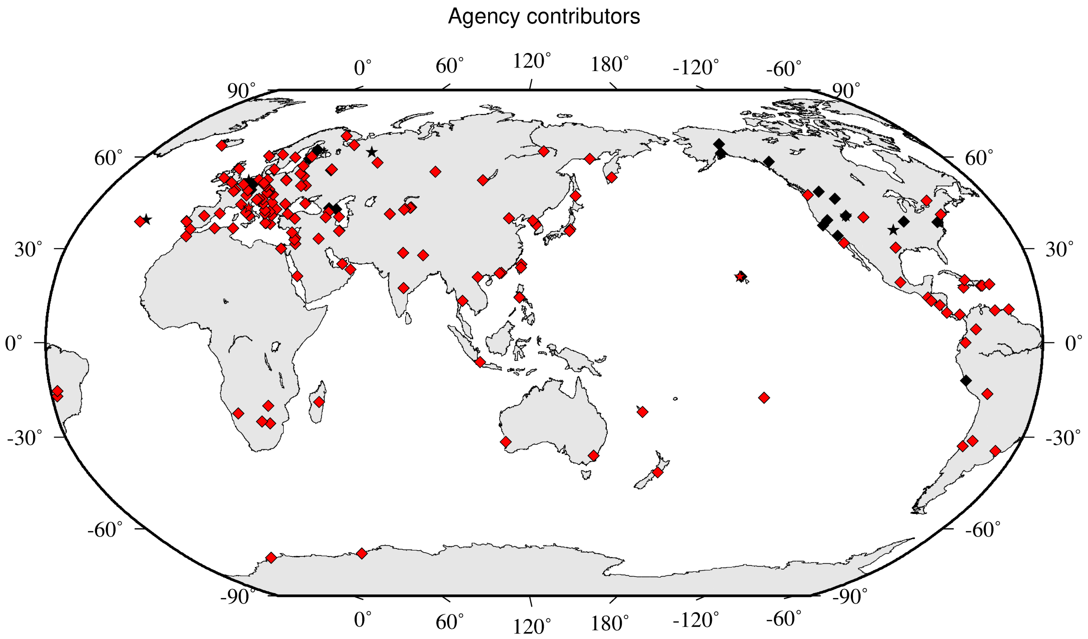

Figure 7.1: *Map of agencies that have contributed data to the ISC for this summary period. Agencies that have reported directly to the ISC are shown in red. Those that have reported indirectly (via another agency) are shown in black. Any new or renewed agencies, since the last six-month period, are shown by a star. Each agency is listed in Table 7.2.*

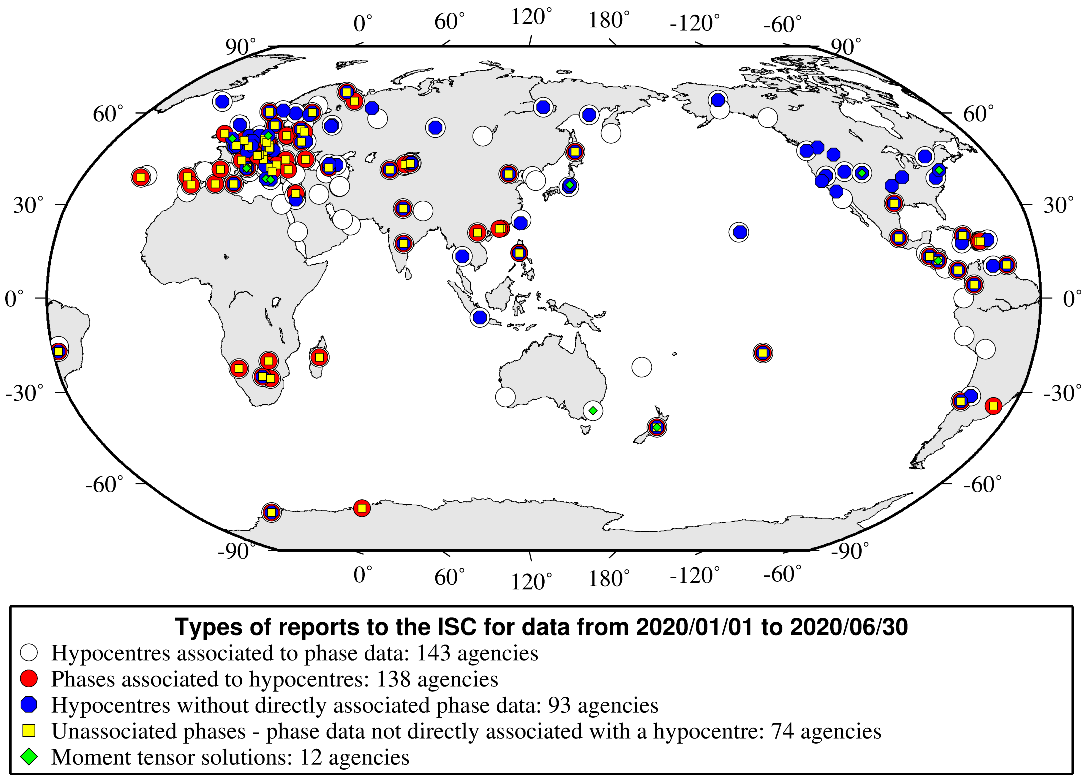

Figure 7.2: *Map of the different data types reported by agencies to the ISC. A full list of the data types reported by each agency is shown in Table 7.2.*

7.3 Arrival Observations

The collection of phase arrival observations at the ISC has increased dramatically with time. The increase in reported phase arrival observations is shown in Figure 7.3.

The reports with phase data are summarised in Table 7.3. This table is split into three sections, providing information on the reports themselves, the phase data, and the stations reporting the phase data. A map of the stations contributing these phase data is shown in Figure 7.4.

The ISC encourages the reporting of phase arrival times together with amplitude and period measurements whenever feasible. Figure 7.5 shows the percentage of events for which phase arrival times from each station are accompanied with amplitude and period measurements.

Figure 7.6 indicates the number of amplitude and period measurement for each station.

Together with the increase in the number of phases (Figure 7.3), there has been an increase in the number of stations reported to the ISC. The increase in the number of stations is shown in Figure 7.7. This increase can also be seen on the maps for stations reported each decade in Figure 7.8.

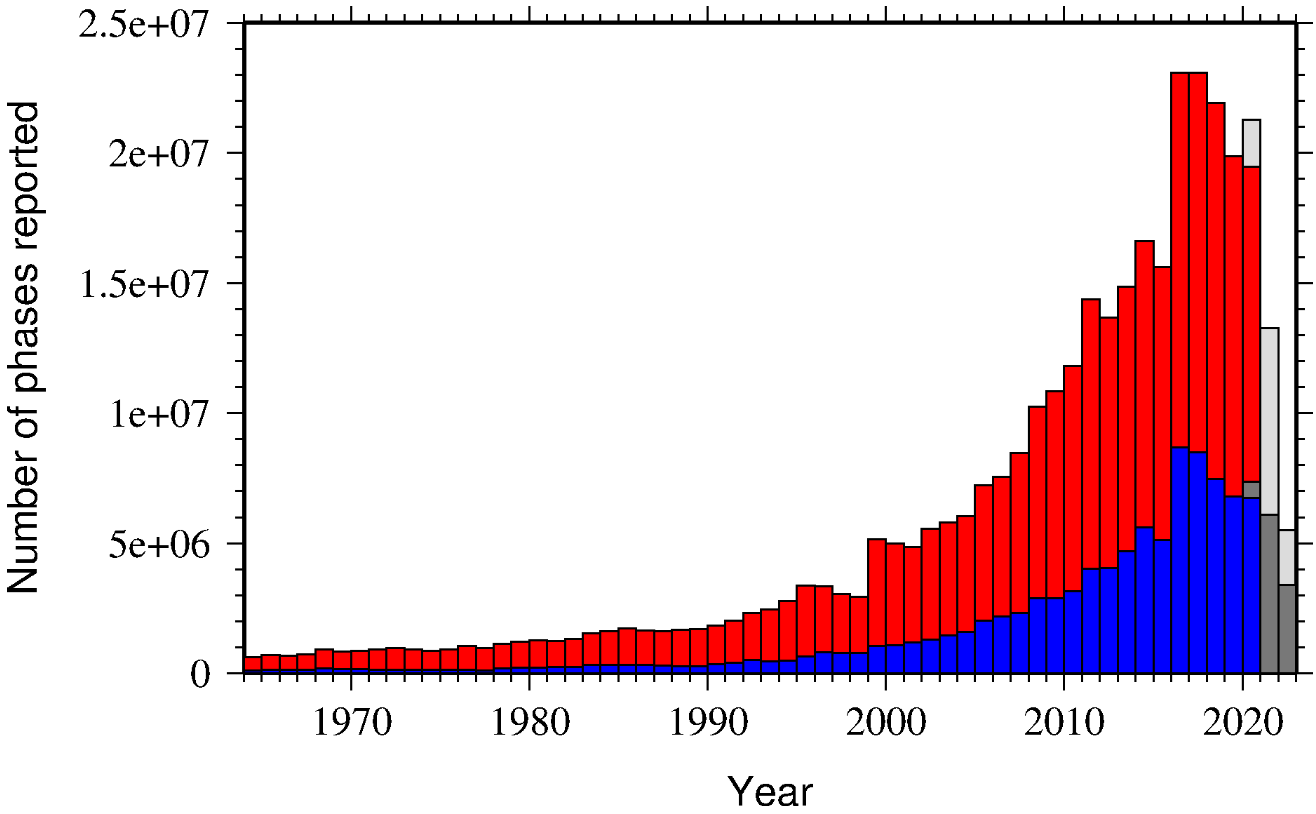

Figure 7.3: *Histogram showing the number of phases (red) and number of amplitudes (blue) collected by the ISC for events each year since 1964. The data in grey covers the current period where data are still being collected before the ISC review takes place and is accurate at the time of publication.*

Table 7.3: *Summary of reports containing phase arrival observations.*

Reports with phase arrivals	5854
Reports with phase arrivals including amplitudes	4953
Reports with only phase arrivals (no hypocentres reported)	171
Total phase arrivals received	10816063
Total phase arrival-times received	9997323
Number of duplicate phase arrival-times	809737 (8.1%)
Number of amplitudes received	3981227
Stations reporting phase arrivals	9880
Stations reporting phase arrivals with amplitude data	5677
Max number of stations per report	2423

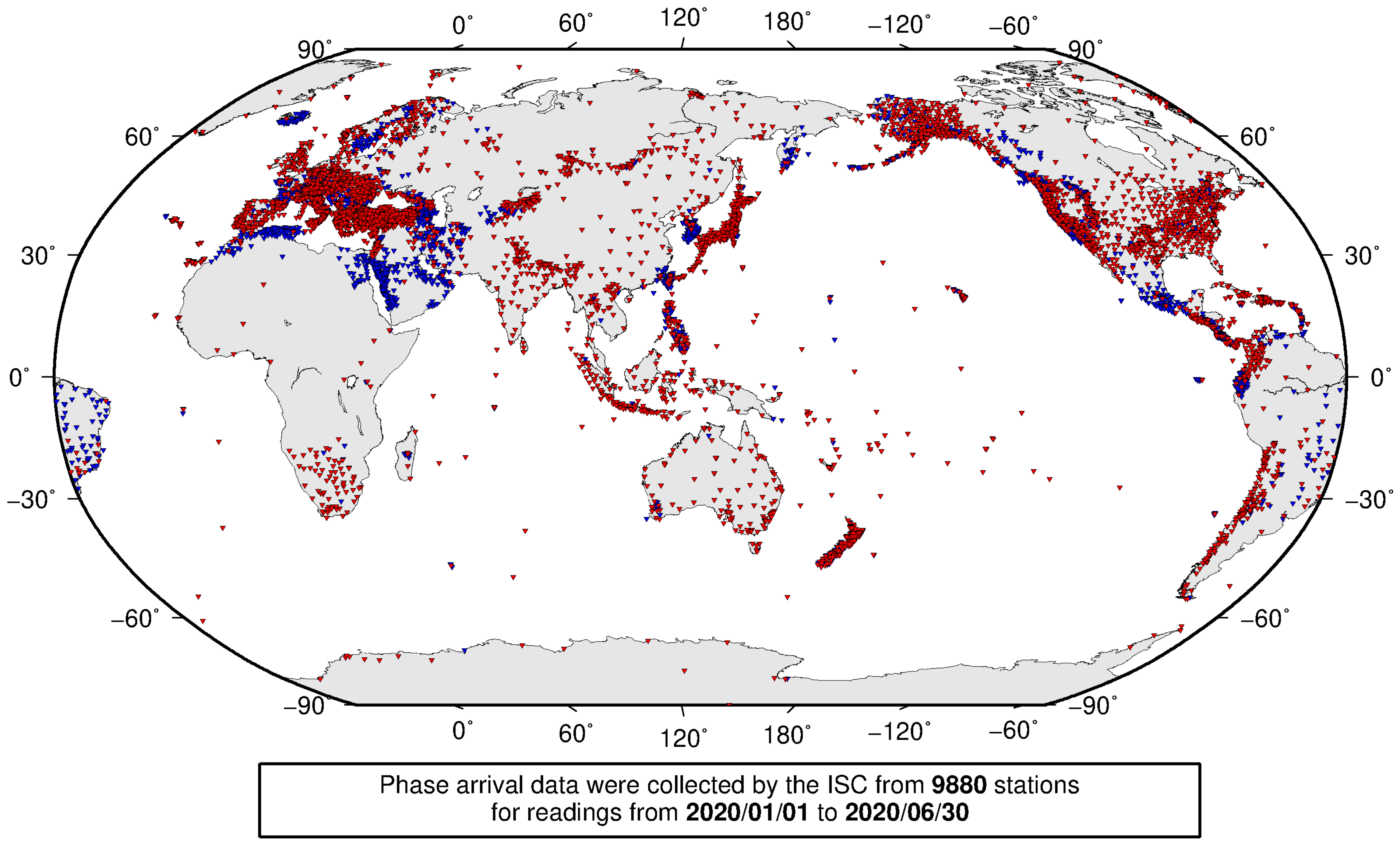

Figure 7.4: *Stations contributing phase data to the ISC for readings from January 2020 to the end of June 2020. Stations in blue provided phase arrival times only; stations in red provided both phase arrival times and amplitude data.*

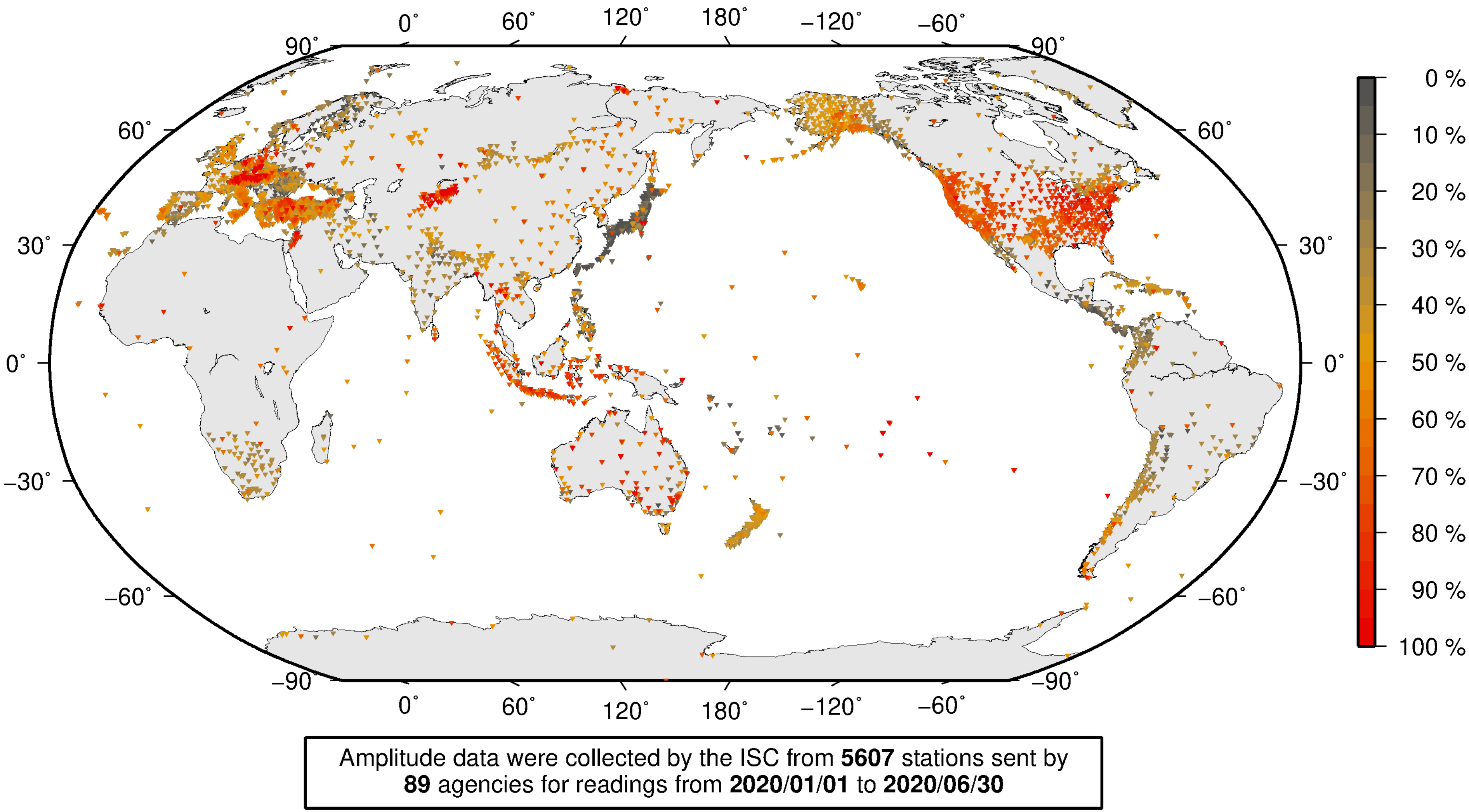

Figure 7.5: *Percentage of events for which phase arrival times from each station are accompanied with amplitude and period measurements.*

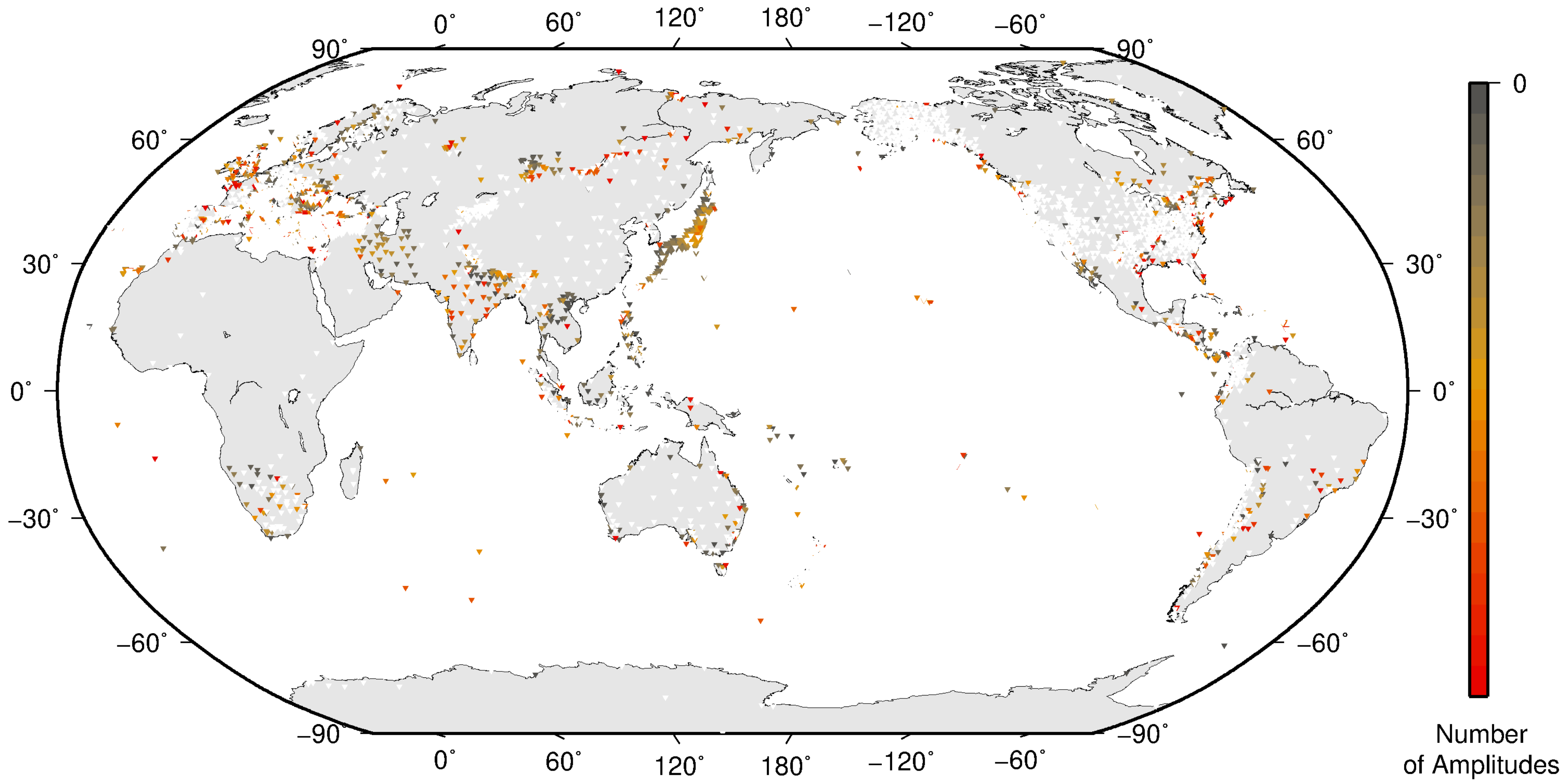

Amplitude data were collected by the ISC from **5607** stations sent by **89** agencies for readings from **2020/01/01** to **2020/06/30**

Figure 7.6: *Number of amplitude and period measurements for each station.*

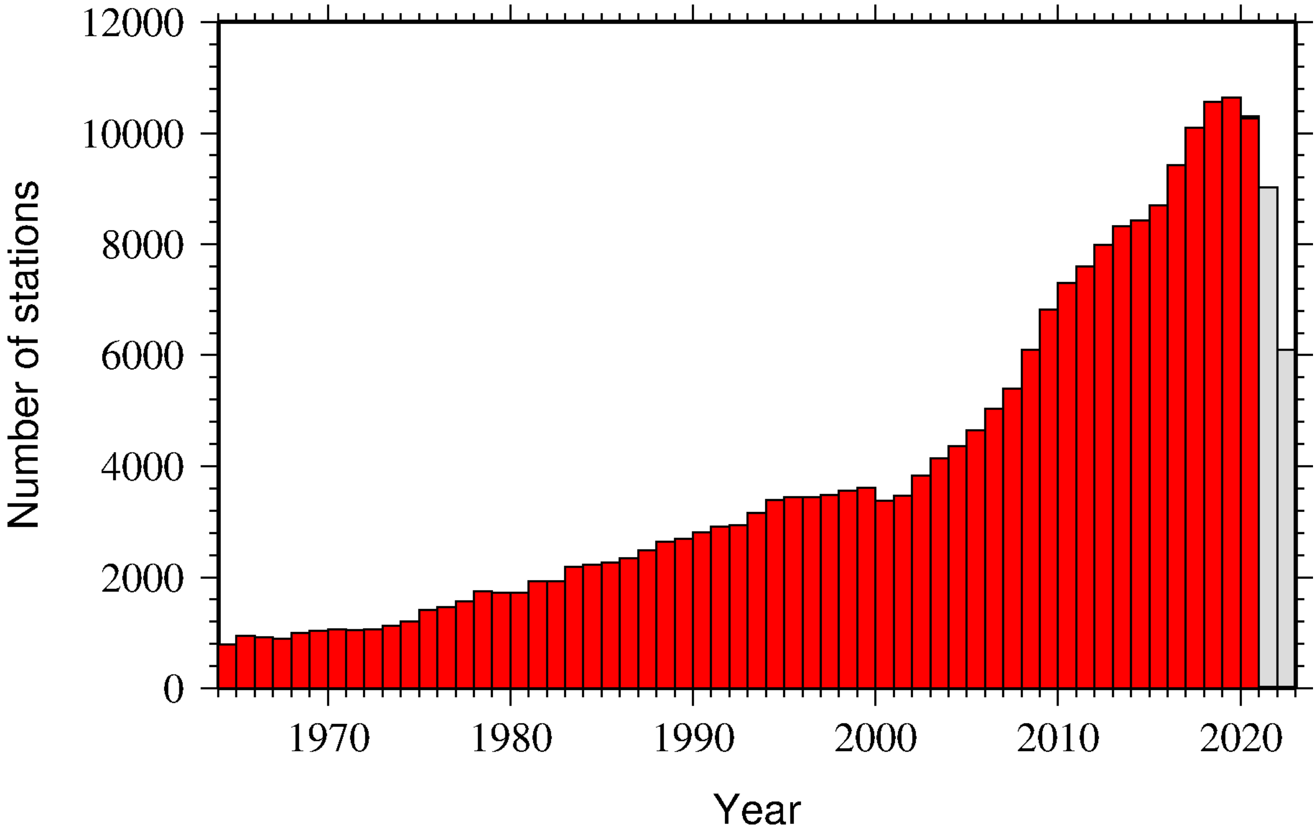

Figure 7.7: *Histogram showing the number of stations reporting to the ISC each year since 1964. The data in grey covers the current period where station information is still being collected before the ISC review of events takes place and is accurate at the time of publication.*

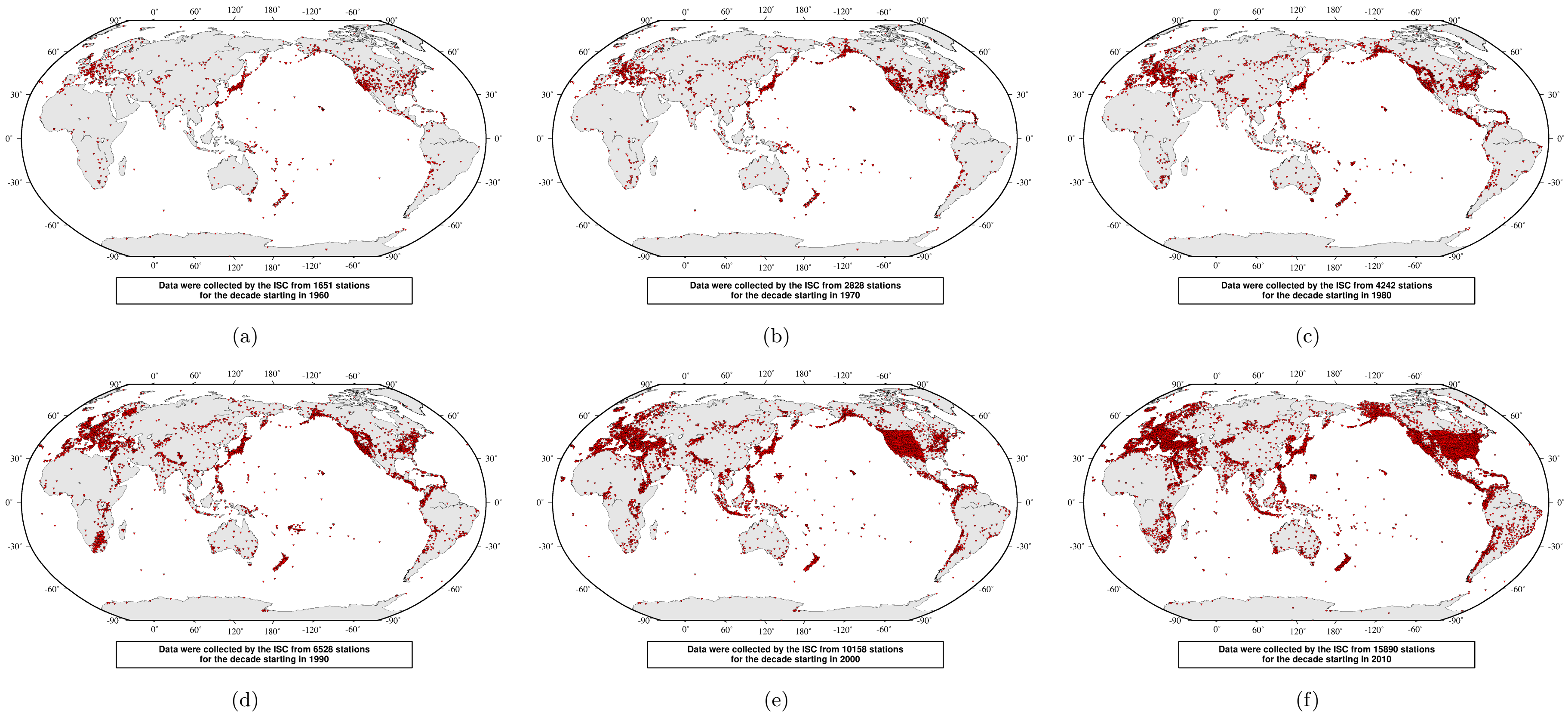

(a) (b) (c)

(d) (e) (f)

Figure 7.8: *Maps showing the stations reported to the ISC for each decade since 1960. Note that the last map covers a shorter time period.*

7.4 Hypocentres Collected

The ISC Bulletin groups multiple estimates of hypocentres into individual events, with an appropriate prime hypocentre solution selected. The collection of these hypocentre estimates are described in this section.

The reports containing hypocentres are summarised in Table 7.4. The number of hypocentres collected by the ISC has also increased significantly since 1964, as shown in Figure 7.9. A map of all hypocentres reported to the ISC for this summary period is shown in Figure 7.10. Where a network magnitude was reported with the hypocentre, this is also shown on the map, with preference given to reported values, first of M_W followed by M_S, m_b and M_L respectively (where more than one network magnitude was reported).

Table 7.4: *Summary of the reports containing hypocentres.*

Reports with hypocentres	6612
Reports of hypocentres only (no phase readings)	929
Total hypocentres received	467166
Number of duplicate hypocentres	12656 (2.7%)
Agencies determining hypocentres	165

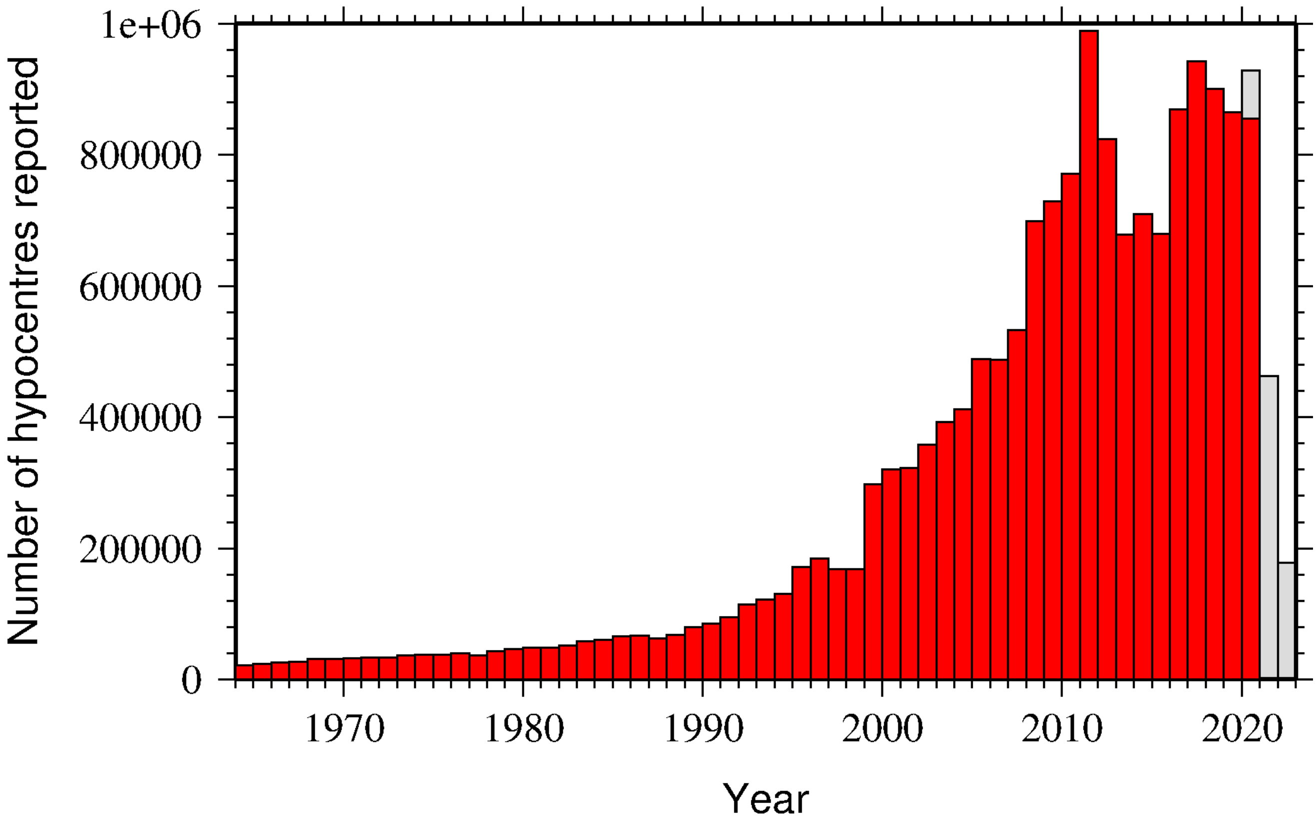

Figure 7.9: *Histogram showing the number of hypocentres collected by the ISC for events each year since 1964. For each event, multiple hypocentres may be reported.*

All the hypocentres that are reported to the ISC are automatically grouped into events, which form the basis of the ISC Bulletin. For this summary period 489933 hypocentres (including ISC) were grouped

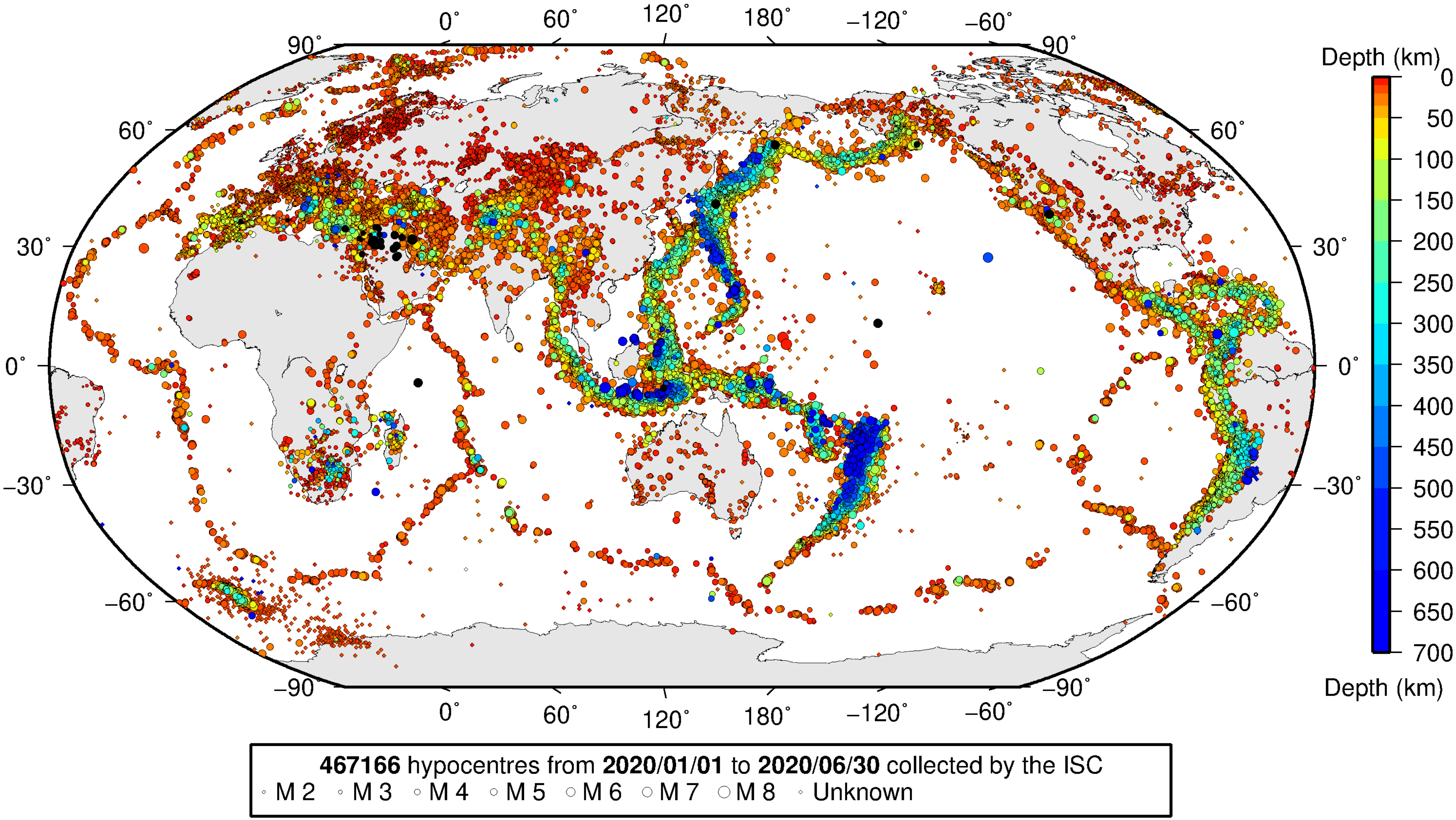

Figure 7.10: *Map of all hypocentres collected by the ISC. The scatter shows the large variation of the multiple hypocentres that are reported for each event. The magnitude corresponds with the reported network magnitude. If more than one network magnitude type was reported, preference was given to values of M_W, M_S, m_b and M_L respectively. Compare with Figure 8.2*

into 338107 events, the largest of these having 58 hypocentres in one event. The total number of events shown here is the result of an automatic grouping algorithm, and will differ from the total events in the published ISC Bulletin, where both the number of events and the number of hypocentre estimates will have changed due to further analysis. The process of grouping is detailed in Section 10.1.3. Figure 8.2 on page 68 shows a map of all prime hypocentres.

7.5 Collection of Network Magnitude Data

Data contributing agencies normally report earthquake hypocentre solutions along with magnitude estimates. For each seismic event, each agency may report one or more magnitudes of the same or different types. This stems from variability in observational practices at regional, national and global level in computing magnitudes based on a multitude of wave types. Differences in the amplitude measurement algorithm, seismogram component(s) used, frequency range, station distance range as well as the instrument type contribute to the diversity of magnitude types. Table 7.5 provides an overview of the complexity of reported network magnitudes reported for seismic events during the summary period.

Table 7.5: *Statistics of magnitude reports to the ISC; M – average magnitude of estimates reported for each event.*

	M<3.0	3.0≤M<5.0	M≥5.0
Number of seismic events	260141	48336	484
Average number of magnitude estimates per event	1.4	3.2	25.0
Average number of magnitudes (by the same agency) per event	1.2	1.8	2.9
Average number of magnitude types per event	1.3	2.5	11.1
Number of magnitude types	26	39	35

Table 7.6 gives the basic description, main features and scientific paper references for the most commonly reported magnitude types.

Table 7.6: *Description of the most common magnitude types reported to the ISC.*

Magnitude type	Description	References	Comments
M	Unspecified		Often used in real or near-real time magnitude estimations
mB	Medium-period and Broad-band body-wave magnitude	*Gutenberg* (1945a); *Gutenberg* (1945b); *IASPEI* (2005); *IASPEI* (2013); *Bormann et al.* (2009); *Bormann and Dewey* (2012)	
mb	Short-period body-wave magnitude	*IASPEI* (2005); *IASPEI* (2013); *Bormann et al.* (2009); *Bormann and Dewey* (2012)	Classical mb based on stations between 21°-100° distance

Table 7.6: *continued*

Magnitude type	Description	References	Comments
mb1	Short-period body-wave magnitude	*IDC* (1999) and references therein	Reported only by the IDC; also includes stations at distances less than 21°
mb1mx	Maximum likelihood short-period body-wave magnitude	*Ringdal* (1976); *IDC* (1999) and references therein	Reported only by the IDC
mbtmp	short-period body-wave magnitude with depth fixed at the surface	*IDC* (1999) and references therein	Reported only by the IDC
mbLg	Lg-wave magnitude	*Nuttli* (1973); *IASPEI* (2005); *IASPEI* (2013); *Bormann and Dewey* (2012)	Also reported as MN
Mc	Coda magnitude		
MD (Md)	Duration magnitude	*Bisztricsany* (1958); *Lee et al.* (1972)	
ME (Me)	Energy magnitude	*Choy and Boatwright* (1995)	Reported only by NEIC
MJMA	JMA magnitude	*Tsuboi* (1954)	Reported only by JMA
ML (Ml)	Local (Richter) magnitude	*Richter* (1935); *Hutton and Boore* (1987); *IASPEI* (2005); *IASPEI* (2013)	
MLSn	Local magnitude calculated for Sn phases	*Balfour et al.* (2008)	Reported by PGC only for earthquakes west of the Cascadia subduction zone
MLv	Local (Richter) magnitude computed from the vertical component		Reported only by DJA and BKK
MN (Mn)	Lg-wave magnitude	*Nuttli* (1973); *IASPEI* (2005)	Also reported as mbLg
MS (Ms)	Surface-wave magnitude	*Gutenberg* (1945c); *Vaněk et al.* (1962); *IASPEI* (2005)	Classical surface-wave magnitude computed from station between 20°-160° distance
Ms1	Surface-wave magnitude	*IDC* (1999) and references therein	Reported only by the IDC; also includes stations at distances less than 20°
ms1mx	Maximum likelihood surface-wave magnitude	*Ringdal* (1976); *IDC* (1999) and references therein	Reported only by the IDC

Table 7.6: *continued*

Magnitude type	Description	References	Comments
Ms7	Surface-wave magnitude	*Bormann et al.* (2007)	Reported only by BJI and computed from records of a Chinese-made long-period seismograph in the distance range 3°-177°
MW (Mw)	Moment magnitude	*Kanamori* (1977); *Dziewonski et al.* (1981)	Computed according to the *IASPEI* (2005) and *IASPEI* (2013) standard formula
Mw(mB)	Proxy Mw based on mB	*Bormann and Saul* (2008)	Reported only by DJA and BKK
Mwp	Moment magnitude from P-waves	*Tsuboi et al.* (1995)	Reported only by DJA and BKK and used in rapid response
mbh	Unknown		
mbv	Unknown		
MG	Unspecified type		Contact contributor
Mm	Unknown		
msh	Unknown		
MSV	Unknown		

Table 7.7 lists all magnitude types reported, the corresponding number of events in the ISC Bulletin and the agency codes along with the number of earthquakes.

Table 7.7: *Summary of magnitude types in the ISC Bulletin for this summary period. The number of events with values for each magnitude type is listed. The agencies reporting these magnitude types are listed, together with the total number of values reported.*

Magnitude type	Events	Agencies reporting magnitude type (number of values)
M	17850	WEL (10575), MOS (3105), CATAC (2104), GFZ (1938), BKK (159), IGQ (103), PRU (24), INMG (23), KRSZO (9), OTT (1)
mb	25393	IDC (16819), NEIC (7375), NNC (4217), KRNET (2869), GFZ (1919), VIE (1860), MOS (1698), DJA (1466), BJI (1009), RSNC (513), NOU (489), VAO (354), CATAC (266), MCSM (238), BGR (234), OMAN (127), MDD (112), CFUSG (98), IASPEI (49), DSN (46), BKK (37), SIGU (34), INMG (33), THE (19), NDI (13), IGQ (11), AUST (11), OSUNB (10), SFS (9), ANF (8), YARS (8), PDG (8), SSNC (7), ROM (7), BGS (4), GUC (4), KMA (3), DNK (2), CRAAG (2), STR (2), IGIL (2), SCB (2), PTWC (1)
mB	2288	BJI (999), DJA (735), WEL (428), RSNC (203), CATAC (195), BKK (34), GFZ (10), IGQ (6), MCSM (2), KRSZO (1)
MB	253	NAO (202), SCB (44), SSNC (7)
mB_BB	26	BGR (26)
mb_Lg	3474	MDD (2984), NEIC (468), OTT (28)

Table 7.7: *Continued.*

Magnitude type	Events	Agencies reporting magnitude type (number of values)
mBc	1	RSNC (1)
mbR	78	VAO (78)
mbtmp	18281	IDC (18281)
Mc	25	KRSC (25)
MD	18659	RSPR (8883), SSNC (3417), SDD (3306), LDG (1524), GCG (1347), TRN (1203), ECX (444), JMA (373), JSN (303), NCEDC (262), GII (226), SOF (192), GRAL (149), TIR (146), MEX (142), ROM (121), UPA (111), CFUSG (104), PDG (82), PNSN (67), SLM (66), HLW (56), HVO (34), SIGU (26), TUN (26), JSO (16), UUSS (10), SNET (10), DNK (8), STR (3), SEA (2), SJA (1)
Mjma	224	BKK (116), IGQ (106), RSNC (4), JSO (3), WEL (1)
ML	148108	AFAD (18761), ISK (18593), RSNC (17225), TAP (13372), IDC (10526), NEIC (10213), WEL (9972), ROM (8284), ATH (7853), HEL (7013), AZER (4422), GUC (3884), UPP (3877), SSNC (3564), SDD (3315), VIE (2981), AEIC (2599), INMG (2271), OSPL (2249), KOLA (1974), PRE (1964), TEH (1901), SGS (1864), LDG (1486), DNK (1453), SFS (1445), BER (1349), SNET (1255), LJU (1196), REN (1181), KRSC (1027), BEO (1019), UPA (941), CNRM (927), SJA (876), GEN (825), TIR (812), SCB (806), TXNET (772), GCG (767), MRB (714), BUT (583), KRSZO (574), PDG (562), ANF (549), IPEC (531), ECX (509), IGIL (508), HVO (500), BUC (499), PGC (484), SKO (436), NDI (404), TAN (403), RSPR (380), PAS (366), NIC (348), YARS (345), NAO (340), BGSI (302), RHSSO (298), UCC (265), AUST (257), KNET (231), OMAN (218), WBNET (216), UUSS (194), DSN (185), PTWC (180), BJI (174), CRAAG (156), LVSN (149), HLW (139), ISN (138), BGS (128), BGR (106), BKK (94), NOU (86), PPT (78), THR (76), IGQ (75), NCEDC (73), SEA (57), KEA (56), DMN (45), MIRAS (36), OTT (33), JSO (27), BNS (23), GFZ (21), SARA (20), CUPWA (19), SIGU (17), PLV (15), RISSC (6), LDO (6), FIA0 (4), KMA (4), NAM (3), REY (3), VAO (2), CSEM (1), CLL (1)
MLh	3747	THE (3127), ZUR (489), ASRS (127), RSNC (4)
MLSn	197	PGC (197)
MLv	26475	WEL (10651), DJA (4378), STR (3791), RSNC (3625), CATAC (2173), NOU (1018), SFS (730), MCSM (256), BKK (165), IGQ (121), JSO (104), GFZ (14), KRSZO (9), OTT (2), OSUNB (2), ASRS (1), AUST (1)
MN	624	OTT (624)
mpv	4596	NNC (4596)
MPVA	208	MOS (174), NORS (173)
mR	49	OSUNB (49)

Table 7.7: *Continued.*

Magnitude type	Events	Agencies reporting magnitude type (number of values)
MS	14692	IDC (8192), MAN (6725), BJI (794), MOS (418), NSSP (165), BGR (148), SOME (39), OMAN (24), INMG (22), VIE (20), IASPEI (17), GUC (6), DSN (5), DNK (4), SSNC (2), YARS (1), IGIL (1), PPT (1), MIRAS (1)
Ms(BB)	89	IGQ (84), RSNC (3), BKK (1), JSO (1)
Ms7	795	BJI (795)
Ms_20	157	NEIC (157)
Ms_VX	1	NEIC (1)
MSH	106	CFUSG (106)
MV	108700	JMA (108700)
MW	9768	SDD (3190), GCMT (1162), SJA (870), UPA (746), NIED (678), FUNV (612), SSNC (556), BER (548), AFAD (536), GFZ (504), NDI (393), UCR (323), PGC (203), GCG (154), MED_RCMT (106), JMA (104), IPGP (103), DJA (80), JSN (66), WEL (63), ASIES (34), ATH (30), ROM (19), INMG (12), UPSL (4), RSNC (3), SNET (1), GUC (1), OS-UNB (1)
Mw(mB)	645	WEL (407), CATAC (190), BKK (33), GFZ (10), IGQ (6)
Mwb	156	NEIC (156)
MwMwp	54	CATAC (47), BKK (4), IGQ (3)
Mwp	309	PTWC (127), DJA (127), CATAC (50), SARA (19), RSNC (19), OMAN (9), THE (7), BKK (4), ROM (4), IGQ (3)
Mwpd	3	ROM (3)
Mwr	704	NEIC (423), SLM (243), GUC (121), NCEDC (41), PAS (38), OTT (10), UUSS (3)
Mws	984	GII (984)
Mww	657	NEIC (657), GUC (12)

The most commonly reported magnitude types are short-period body-wave, surface-wave, local (or Richter), moment, duration and JMA magnitude type. For a given earthquake, the number and type of reported magnitudes greatly vary depending on its size and location. The large earthquake of October 25, 2010 gives an example of the multitude of reported magnitude types for large earthquakes (Listing 7.1). Different magnitude estimates come from global monitoring agencies such as the IDC, NEIC and GCMT, a local agency (GUC) and other agencies, such as MOS and BJI, providing estimates based on the analysis of their networks. The same agency may report different magnitude types as well as several estimates of the same magnitude type, such as NEIC estimates of Mw obtained from W-phase, centroid and body-wave inversions.

Listing 7.1: *Example of reported magnitudes for a large event*

```
Event   15264887 Southern Sumatera
   Date       Time        Err   RMS Latitude Longitude  Smaj  Smin  Az Depth   Err Ndef Nsta Gap  mdist  Mdist Qual   Author      OrigID
2010/10/25 14:42:22.18   0.27 1.813  -3.5248  100.1042 4.045 3.327  54  20.0  1.37 2102 2149  23   0.76 176.43 m i de ISC       01346132
 (#PRIME)

Magnitude  Err Nsta Author      OrigID
mb      6.1       61 BJI       15548963
mB      6.9       68 BJI       15548963
Ms      7.7       85 BJI       15548963
Ms7     7.5       86 BJI       15548963
mb      5.3 0.1   48 IDC       16686694
mb1     5.3 0.1   51 IDC       16686694
mb1mx   5.3 0.0   52 IDC       16686694
```

```
mbtmp   5.3 0.1   51 IDC        16686694
ML      5.1 0.2    2 IDC        16686694
MS      7.1 0.0   31 IDC        16686694
Ms1     7.1 0.0   31 IDC        16686694
ms1mx   6.9 0.1   44 IDC        16686694
mb      6.1      243 ISCJB      01677901
MS      7.3      228 ISCJB      01677901
M       7.1      117 DJA        01268475
mb      6.1 0.2  115 DJA        01268475
mB      7.1 0.1  117 DJA        01268475
MLv     7.0 0.2   26 DJA        01268475
        7.1 0.4  117 DJA        01268475
Mwp     6.9 0.2  102 DJA        01268475
mb      6.4       49 MOS        16742129
MS      7.2       70 MOS        16742129
mb      6.5      110 NEIC       01288303
ME      7.3          NEIC       01288303
MS      7.3      143 NEIC       01288303
MW      7.7          NEIC       01288303
MW      7.8      130 GCMT       00125427
mb      5.9          KLM        00255772
ML      6.7          KLM        00255772
MS      7.6          KLM        00255772
mb      6.4       20 BGR        16815854
Ms      7.2        2 BGR        16815854
mb      6.3 0.3  250 ISC        01346132
MS      7.3 0.1  237 ISC        01346132
```

An example of a relatively small earthquake that occurred in northern Italy for which we received magnitude reports of mostly local and duration type from six agencies in Italy, France and Austria is given in Listing 7.2.

Listing 7.2: *Example of reported magnitudes for a small event*

```
Event 15089710 Northern Italy
   Date       Time        Err   RMS Latitude Longitude  Smaj  Smin  Az Depth   Err Ndef Nsta Gap  mdist  Mdist Qual   Author      OrigID
2010/08/08 15:20:46.22   0.94 0.778  45.4846    8.3212 2.900 2.539 110  28.6  9.22  172  110  82   0.41   5.35 m i ke ISC       01249414
 (#PRIME)

Magnitude  Err Nsta Author      OrigID
ML      2.4       10 ZUR       15925566
Md      2.6 0.2   19 ROM       16861451
Ml      2.2 0.2    9 ROM       16861451
ML      2.5          GEN       00554757
ML      2.6 0.3   28 CSEM      00554756
Md      2.3 0.0    3 LDG       14797570
Ml      2.6 0.3   32 LDG       14797570
```

Figure 7.11 shows a distribution of the number of agencies reporting magnitude estimates to the ISC according to the magnitude value. The peak of the distribution corresponds to small earthquakes where many local agencies report local and/or duration magnitudes. The number of contributing agencies rapidly decreases for earthquakes of approximately magnitude 5.5 and above, where magnitudes are mostly given by global monitoring agencies.

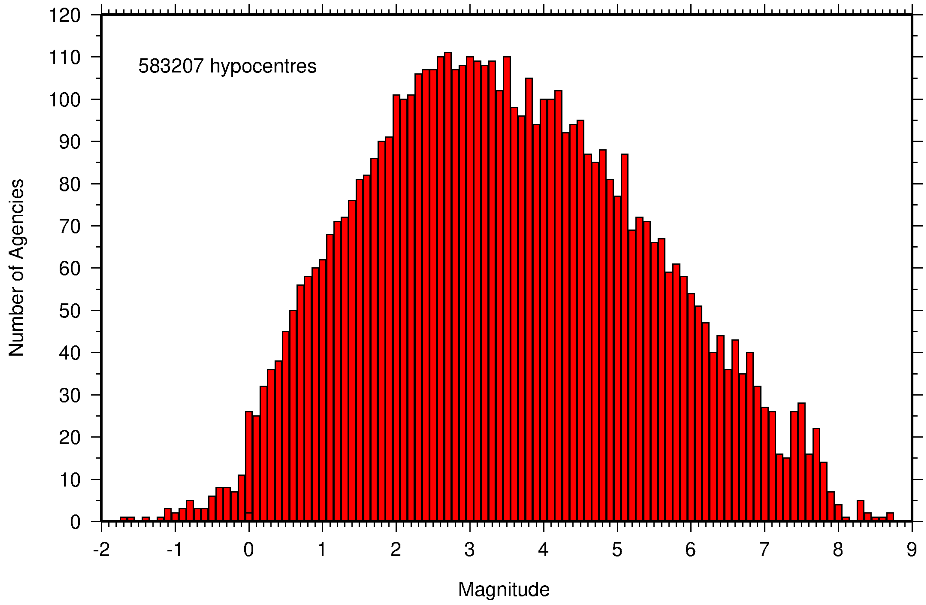

Figure 7.11: *Histogram showing the number of agencies that reported network magnitude values. All magnitude types are included.*

7.6 Moment Tensor Solutions

The ISC Bulletin publishes moment tensor solutions, which are reported to the ISC by other agencies. The collection of moment tensor solutions is summarised in Table 7.8. A histogram showing all moment tensor solutions collected throughout the ISC history is shown in Figure 7.12. Several moment tensor solutions from different authors and different moment tensor solutions calculated by different methods from the same agency may be present for the same event.

Table 7.8: *Summary of reports containing moment tensor solutions.*

Reports with Moment Tensors	1332
Total moment tensors received	10604
Agencies reporting moment tensors	12

The number of moment tensors for this summary period, reported by each agency, is shown in Table 7.9. The moment tensor solutions are plotted in Figure 7.13.

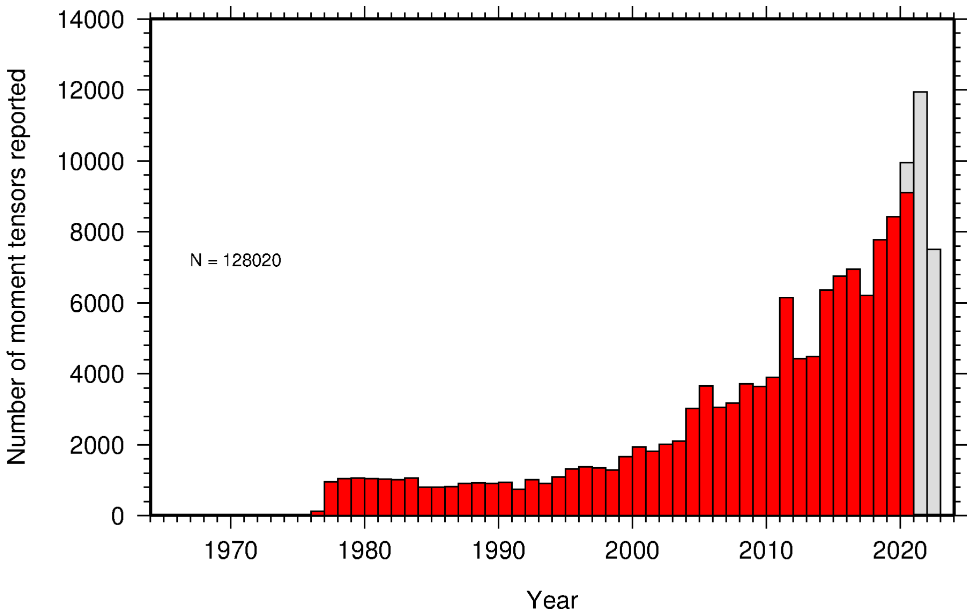

Figure 7.12: *Histogram showing the number of moment tensors reported to the ISC since 1964. The regions in grey represent data that are still being actively collected.*

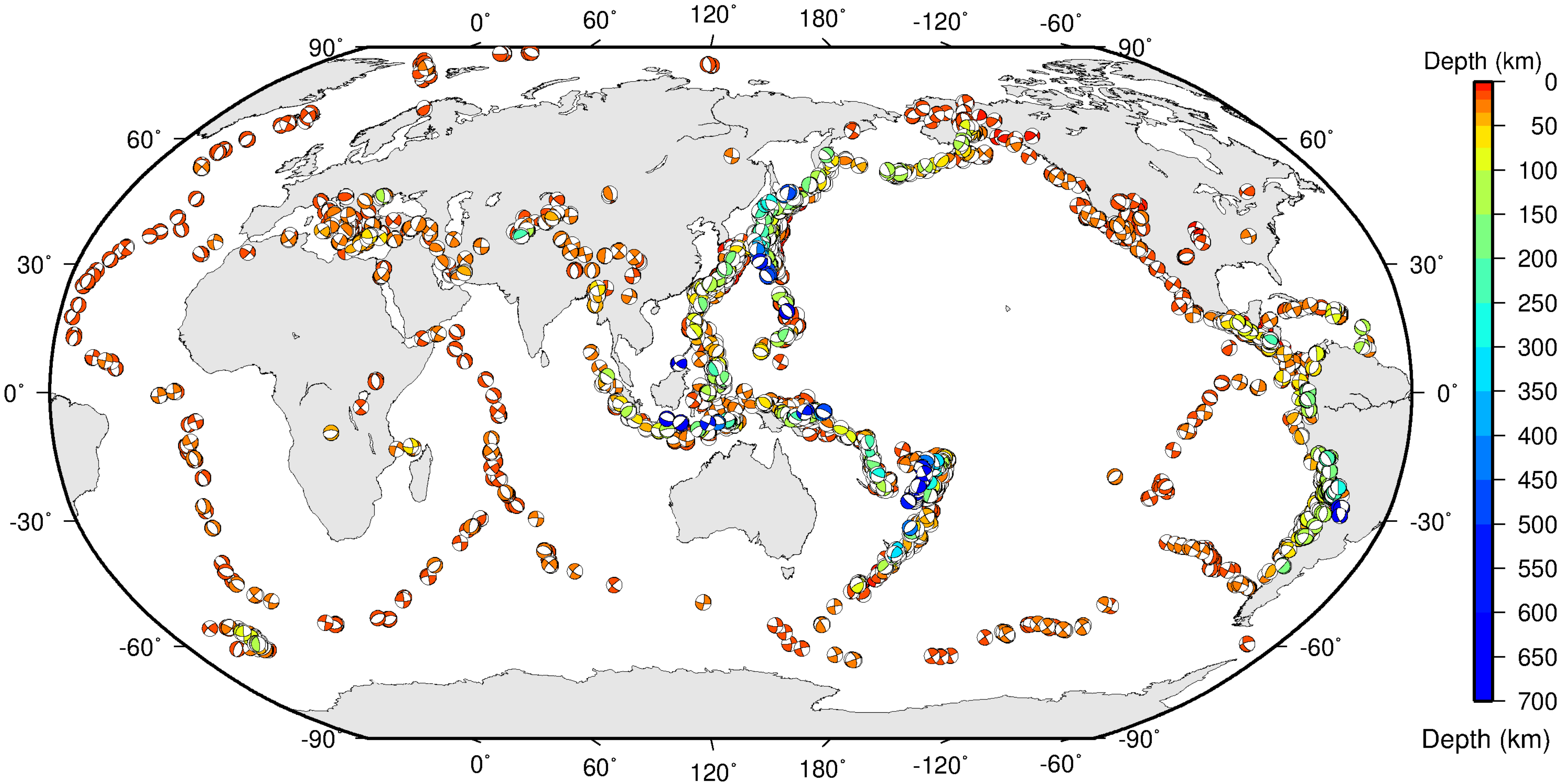

ISC Bulletin: **4560** focal mechanism solutions for **2442** events from **2020/01/01** to **2020/06/30**

Figure 7.13: *Map of all moment tensor solutions in the ISC Bulletin for this summary period.*

Table 7.9: *Summary of moment tensor solutions in the ISC Bulletin reported by each agency.*

Agency	Number of moment tensor solutions		Agency	Number of moment tensor solutions
NEIC	1367		UCR	23
GCMT	1162		ROM	19
NIED	678		UPA	9
CATAC	601		MOS	8
GFZ	443		ECX	5
TAN	355		UPSL	4
IPGP	203		GCG	3
MED_RCMT	106		MEX	3
ISC-PPSM	86		SSNC	2
ASIES	68		PLV	2
PNSN	68		DNK	1
WEL	64		BGS	1
ATH	30			

7.7 Timing of Data Collection

Here we present the timing of reports to the ISC. Please note, this does not include provisional alerts, which are replaced at a later stage. Instead, it reflects the final data sent to the ISC. The absolute timing of all hypocentre reports, regardless of magnitude, is shown in Figure 7.14. In Figure 7.15 the reports are grouped into one of six categories - from within three days of an event origin time, to over one year. The histogram shows the distribution with magnitude (for hypocentres where a network magnitude was reported) for each category, whilst the map shows the geographic distribution of the reported hypocentres.

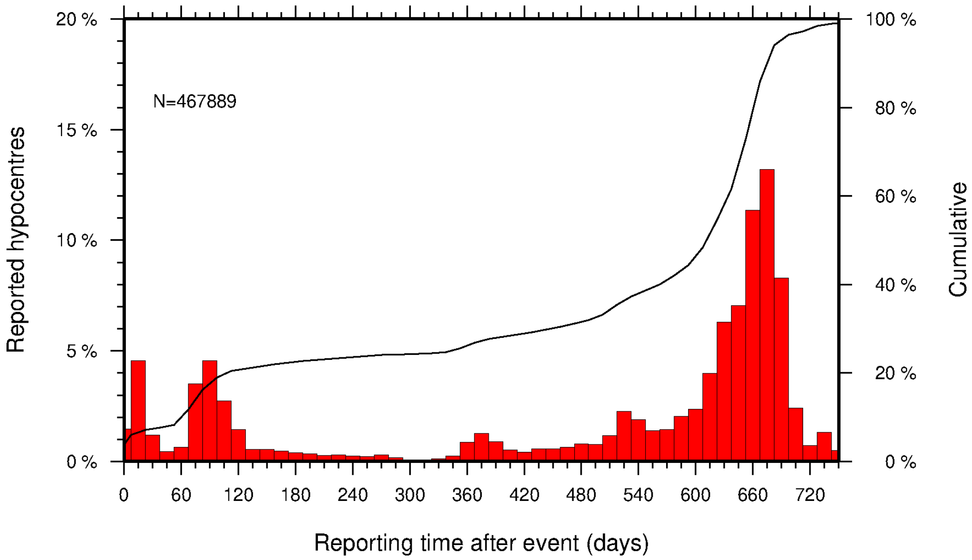

Figure 7.14: *Histogram showing the timing of final reports of the hypocentres (total of N) to the ISC. The cumulative frequency is shown by the solid line.*

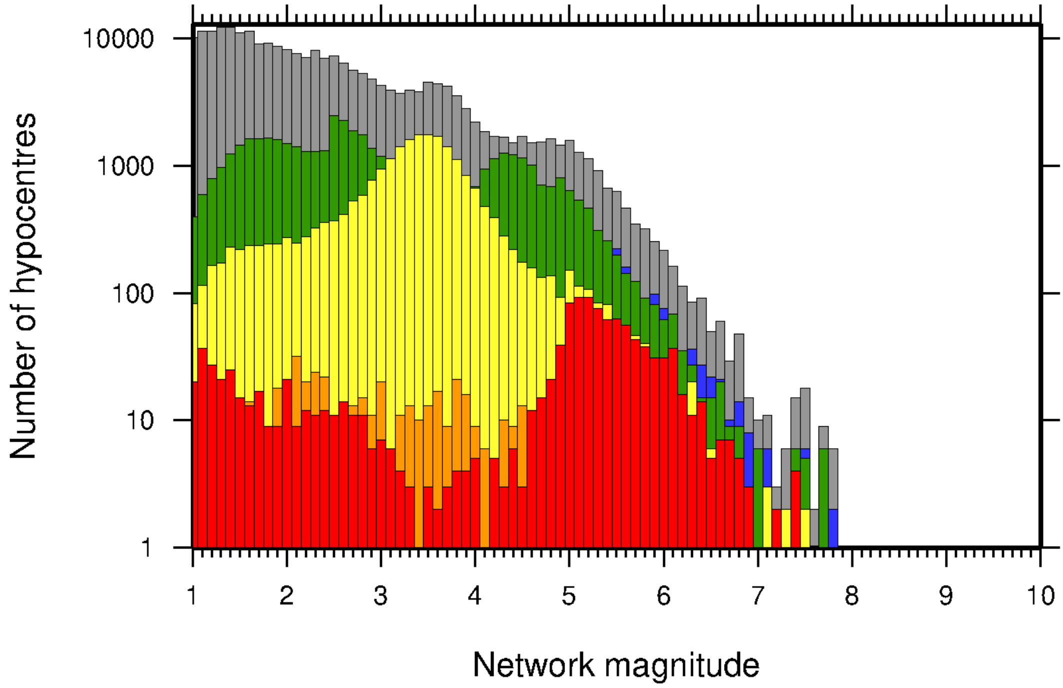

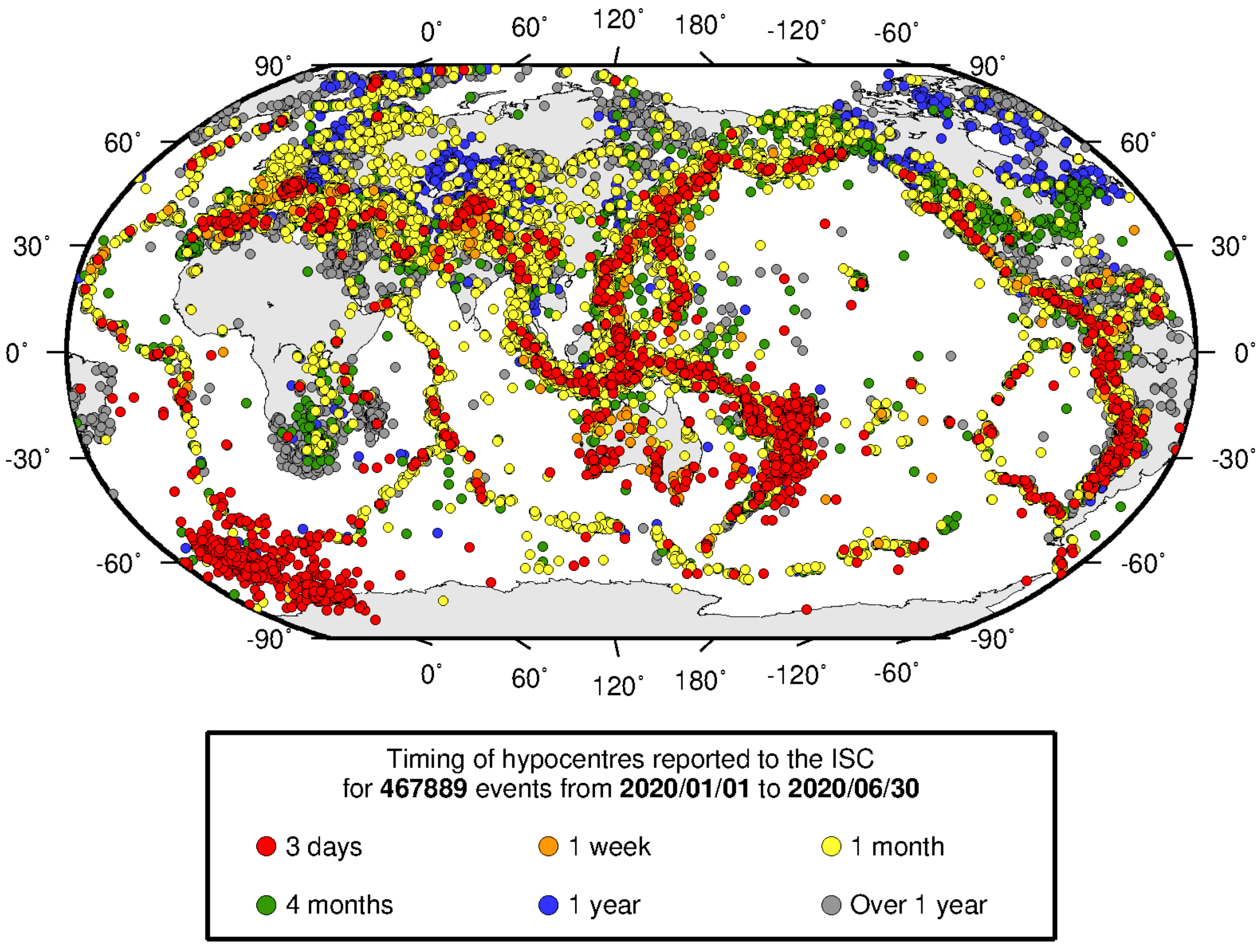

Figure 7.15: *Timing of hypocentres reported to the ISC. The colours show the time after the origin time that the corresponding hypocentre was reported. The histogram shows the distribution with magnitude. If more than one network magnitude was reported, preference was given to a value of* M_W *followed by* M_S*,* m_b *and* M_L *respectively; all reported hypocentres are included on the map. Note: early reported hypocentres are plotted over later reported hypocentres, on both the map and histogram.*

8

Overview of the ISC Bulletin

This chapter provides an overview of the seismic event data in the ISC Bulletin. We indicate the differences between all ISC events and those ISC events that are reviewed or located. We describe the wealth of phase arrivals and phase amplitudes and periods observed at seismic stations worldwide, reported in the ISC Bulletin and often used in the ISC location and magnitude determination. Finally, we make some comparisons of the ISC magnitudes with those reported by other agencies, and discuss magnitude completeness of the ISC Bulletin.

8.1 Events

The ISC Bulletin had 327849 reported events in the summary period between January and June 2020. Some 91% (301407) of the events were identified as earthquakes, the rest (26442) were of anthropogenic origin (including mining and other chemical explosions, rockbursts and induced events) or of unknown origin. As discussed in Section 10.1.3. In this summary period 9% of the events were reviewed and 6% of the events were located by the ISC. For events that are not located by the ISC, the prime hypocentre is identified according to the rules described in Section 10.1.3.

Of the 11114548 reported phase observations, 34% are associated to ISC-reviewed events, and 32% are associated to events selected for ISC location. Note that all large events are reviewed and located by the ISC. Since large events are globally recorded and thus reported by stations worldwide, they will provide the bulk of observations. This explains why only about one-fifth of the events in any given month is reviewed although the number of phases associated to reviewed events has increased nearly exponentially in the past decades.

Figure 8.1 shows the daily number of events throughout the summary period. Figure 8.2 shows the locations of the events in the ISC Bulletin; the locations of ISC-reviewed and ISC-located events are shown in Figures 8.3 and 8.4, respectively.

Figure 8.5 shows the hypocentral depth distributions of events in the ISC Bulletin for the summary period. The vast majority of events occur in the Earth's crust. Note that the peaks at 0, 10, 35 km, and at every 50 km intervals deeper than 100 km are artifacts of analyst practices of fixing the depth to a nominal value when the depth cannot be reliably resolved.

Figure 8.6 shows the depth distribution of free-depth solutions in the ISC Bulletin. The depth of a hypocentre reported to the ISC is assumed to be determined as a free parameter, unless it is explicitly labelled as a fixed-depth solution. On the other hand, as described in Section 10.1.4, the ISC locator attempts to get a free-depth solution if, and only if, there is resolution for the depth in the data, i.e. if there is a local network and/or sufficient depth-sensitive phases are reported.

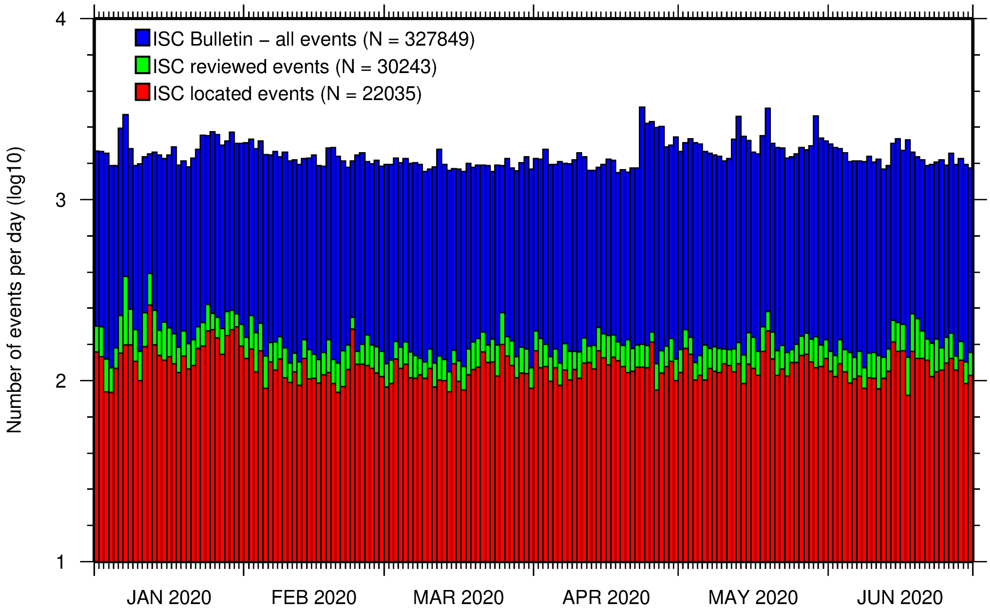

Figure 8.1: *Histogram showing the number of events in the ISC Bulletin for the current summary period. The vertical scale is logarithmic.*

Figure 8.7 shows the depth distribution of fixed-depth solutions in the ISC Bulletin. Except for a fraction of events whose depth is fixed to a shallow depth, this set comprises mostly ISC-located events. If there is no resolution for depth in the data, the ISC locator fixes the depth to a value obtained from the ISC default depth grid file, or if no default depth exists for that location, to a nominal default depth assigned to each Flinn-Engdahl region (see details in Section 10.1.4). During the ISC review editors are inclined to accept the depth obtained from the default depth grid, but they typically change the depth of those solutions that have a nominal (10 or 35 km) depth. When doing so, they usually fix the depth to a round number, preferably divisible by 50.

For events selected for ISC location, the number of stations typically increases as arrival data reported by several agencies are grouped together and associated to the prime hypocentre. Consequently, the network geometry, characterised by the secondary azimuthal gap (the largest azimuthal gap a single station closes), is typically improved. Figure 8.8 illustrates that the secondary azimuthal gap is indeed generally smaller for ISC-located events than that for all events in the ISC Bulletin. Figure 8.9 shows the distribution of the number of associated stations. For large events the number of associated stations is usually larger for ISC-located events than for any of the reported event bulletins. On the other hand, events with just a few reporting stations are rarely selected for ISC location. The same is true for the number of defining stations (stations with at least one defining phase that were used in the location). Figure 8.10 indicates that because the reported observations from multiple agencies are associated to the prime, large ISC-located events typically have a larger number of defining stations than any of the reported event bulletins.

The formal uncertainty estimates are also typically smaller for ISC-located events. Figure 8.11 shows the distribution of the area of the 90% confidence error ellipse for ISC-located events during the summary period. The distribution suffers from a long tail indicating a few poorly constrained event locations. Nevertheless, half of the events are characterised by an error ellipse with an area less than 160 km^2, 90% of the events have an error ellipse area less than 1092 km^2, and 95% of the events have an error ellipse

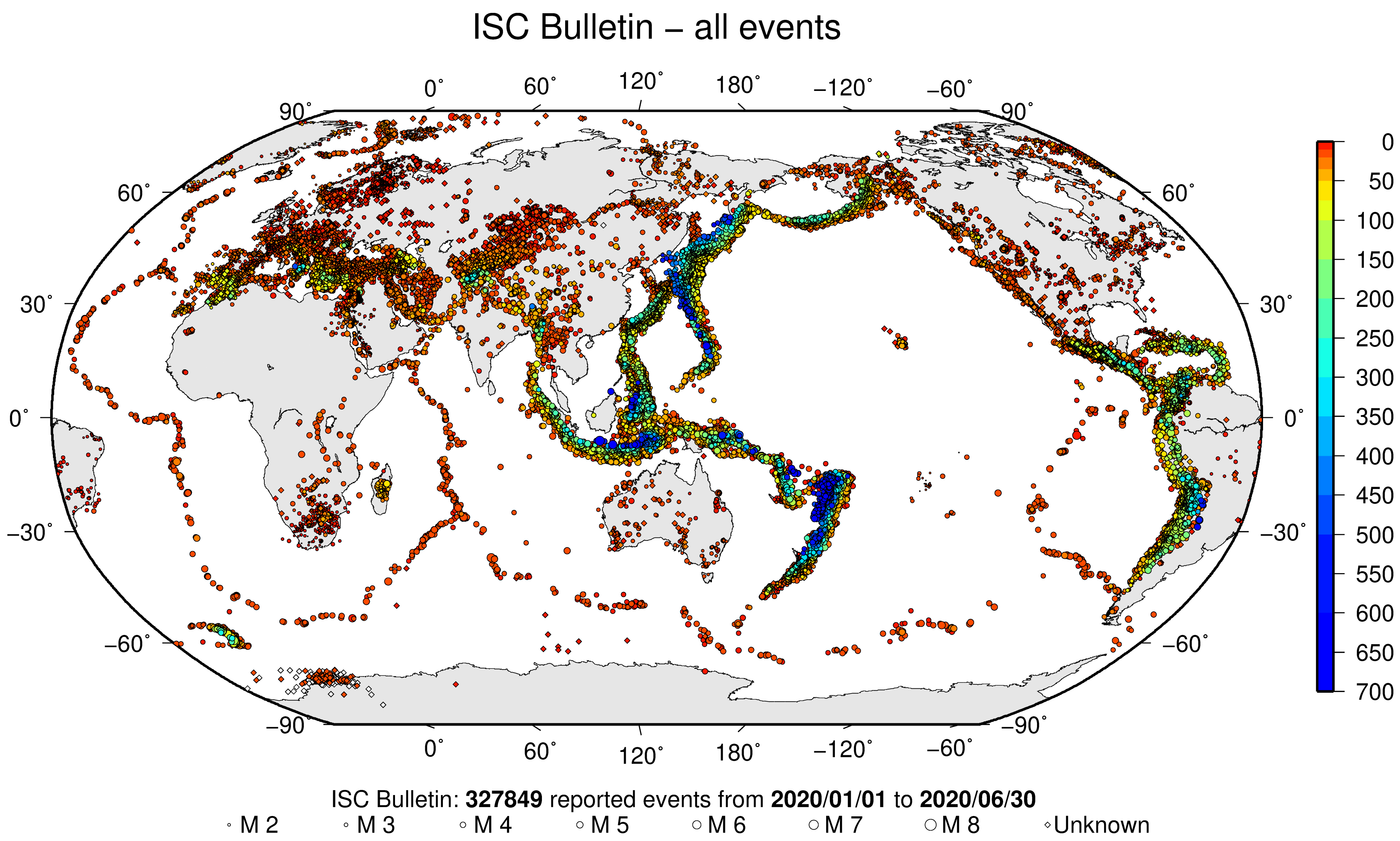

Figure 8.2: *Map of all events in the ISC Bulletin. Prime hypocentre locations are shown. Compare with Figure 7.10.*

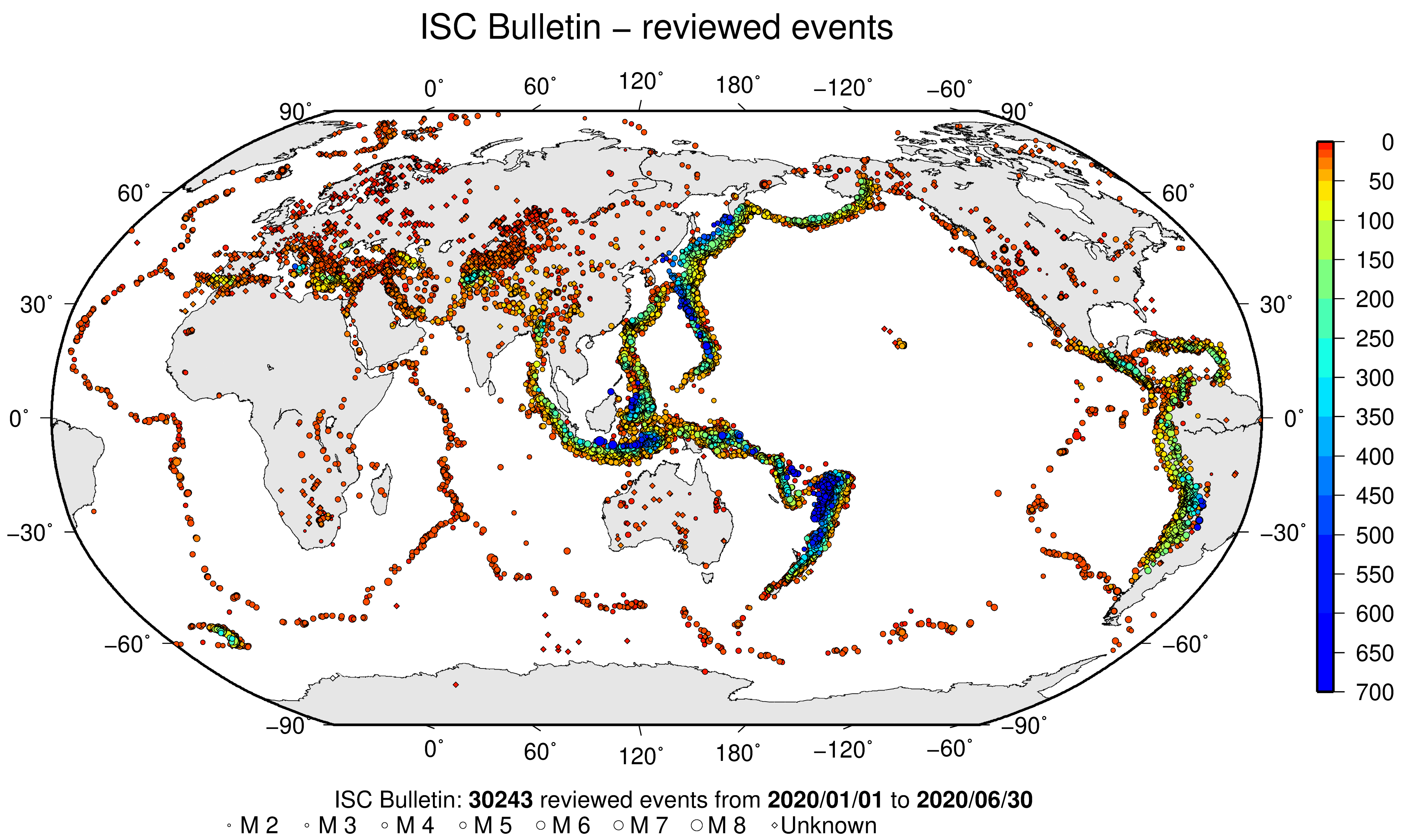

Figure 8.3: *Map of all events reviewed by the ISC for this time period. Prime hypocentre locations are shown.*

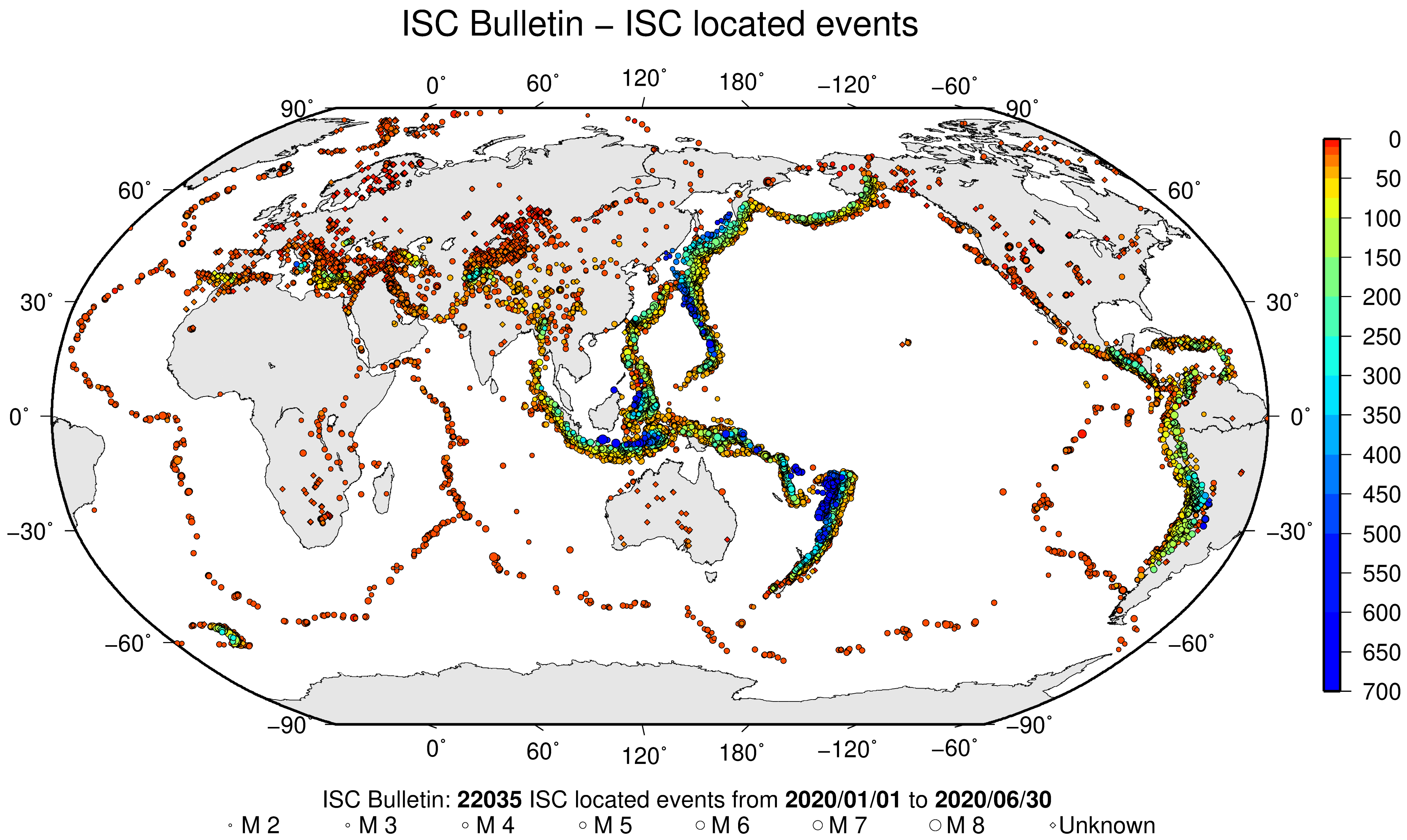

Figure 8.4: *Map of all events located by the ISC for this time period. ISC determined hypocentre locations are shown.*

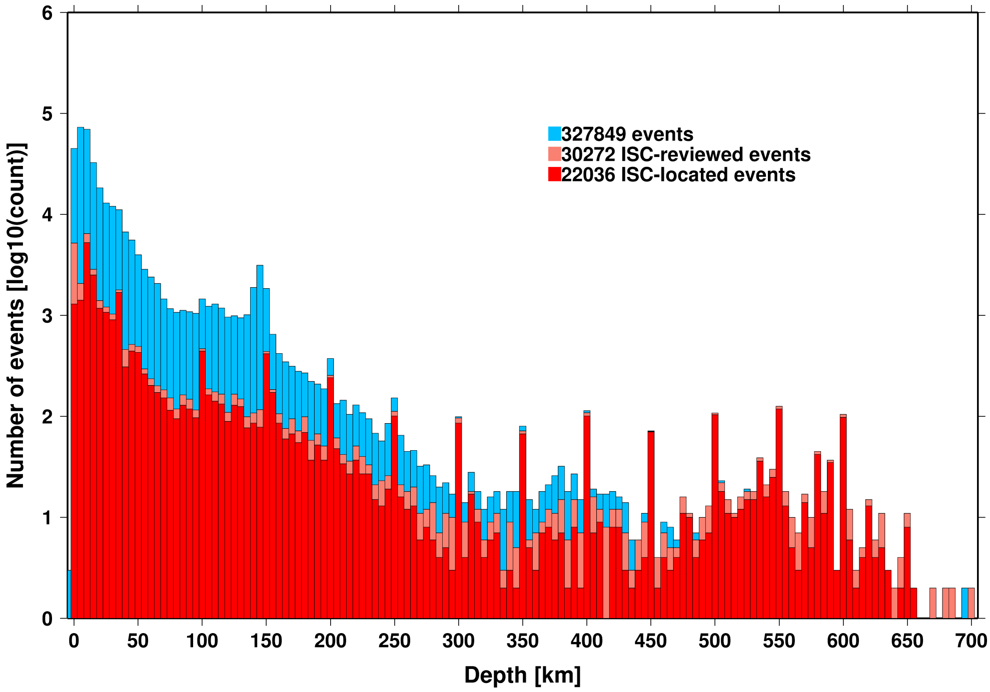

Figure 8.5: *Distribution of event depths in the ISC Bulletin (blue) and for the ISC-reviewed (pink) and the ISC-located (red) events during the summary period. All ISC-located events are reviewed, but not all reviewed events are located by the ISC. The vertical scale is logarithmic.*

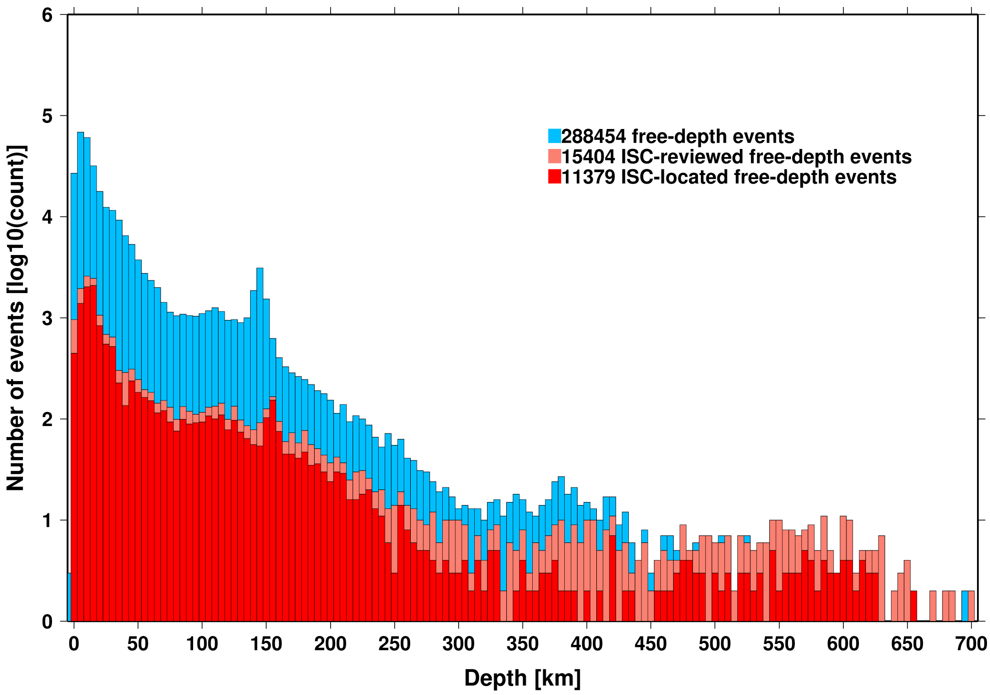

Figure 8.6: *Hypocentral depth distribution of events where the prime hypocentres are reported/located with a free-depth solution in the ISC Bulletin. The vertical scale is logarithmic.*

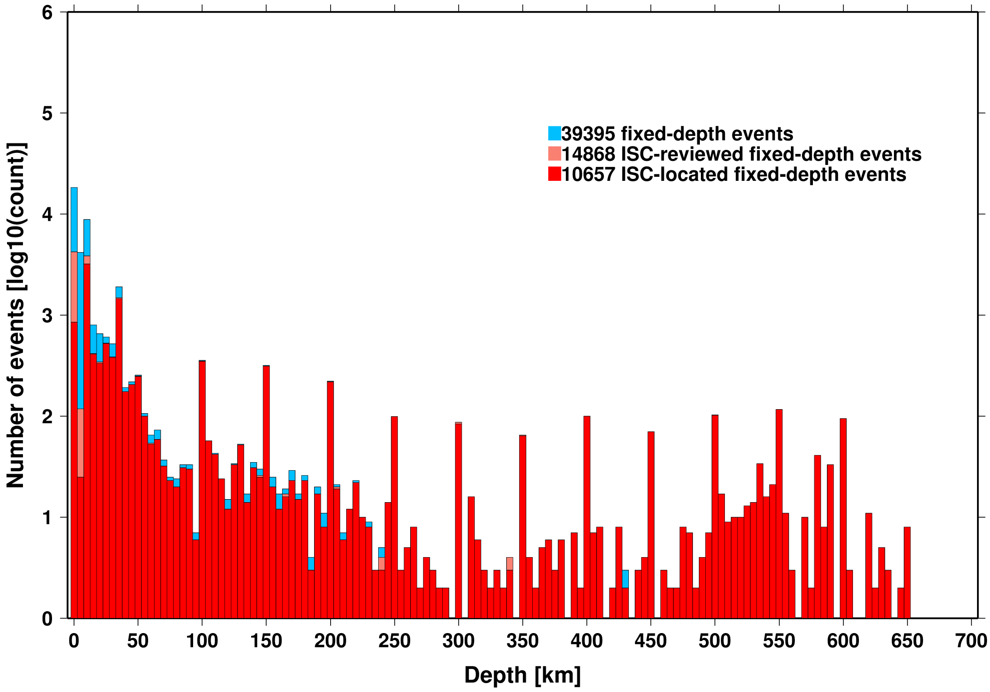

Figure 8.7: *Hypocentral depth distribution of events where the prime hypocentres are reported/located with a fixed-depth solution in the ISC Bulletin. The vertical scale is logarithmic.*

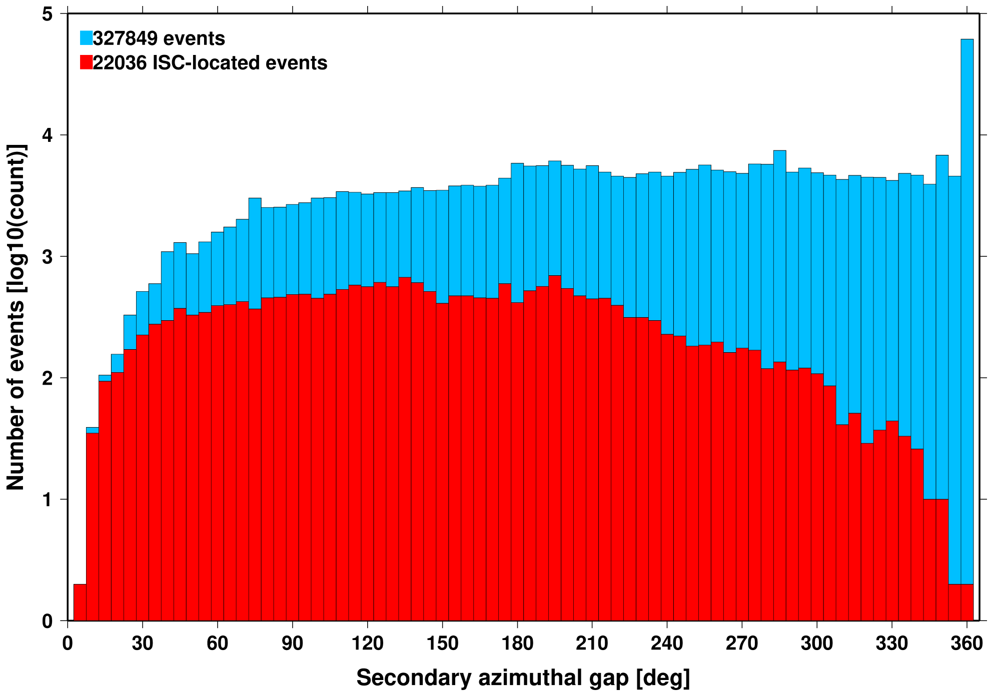

Figure 8.8: *Distribution of secondary azimuthal gap for events in the ISC Bulletin (blue) and those selected for ISC location (red). The vertical scale is logarithmic.*

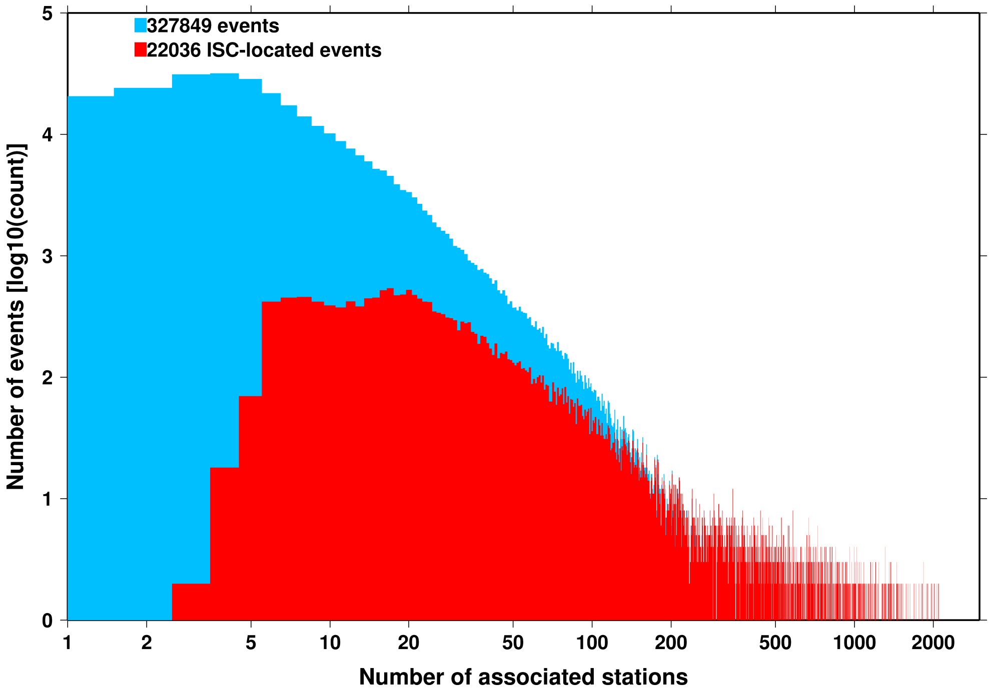

Figure 8.9: *Distribution of the number of associated stations for events in the ISC Bulletin (blue) and those selected for ISC location (red). The vertical scale is logarithmic.*

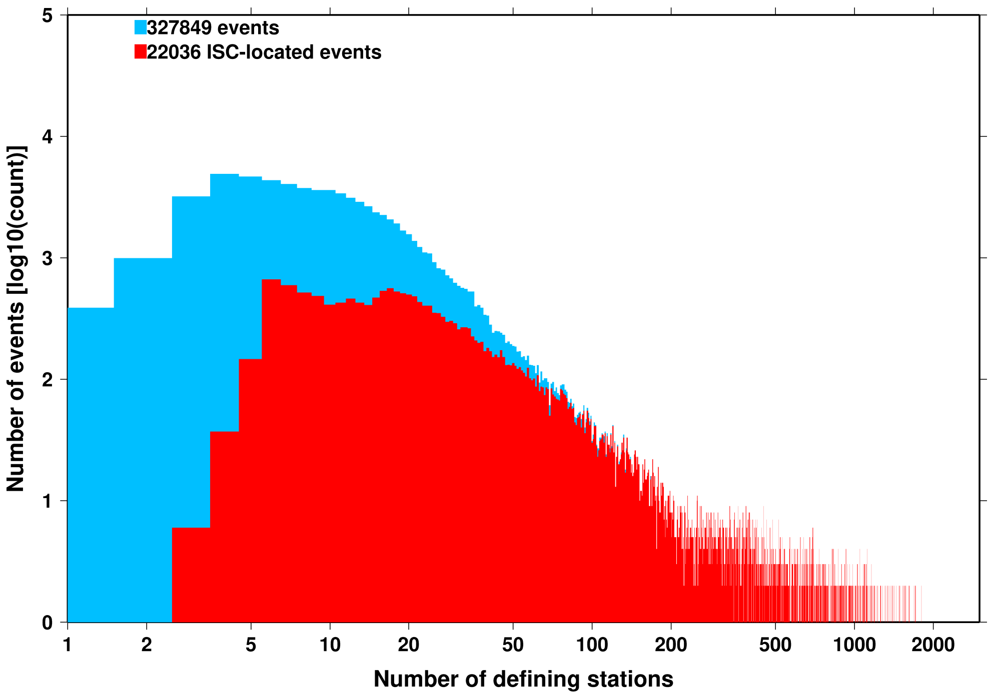

Figure 8.10: *Distribution of the number of defining stations for events in the ISC Bulletin (blue) and those selected for ISC location (red). The vertical scale is logarithmic.*

area less than 2010 km^2.

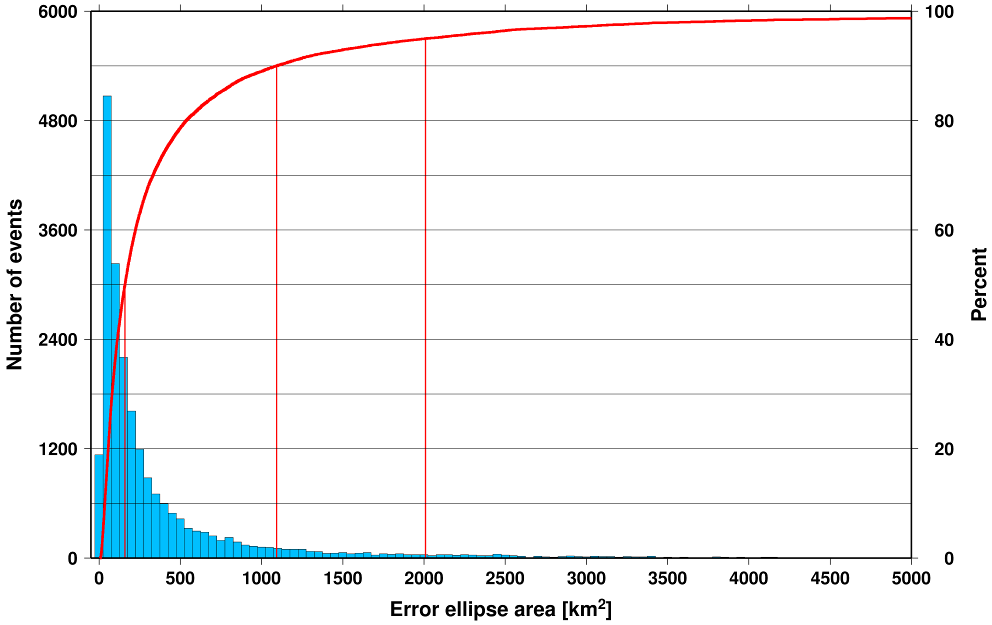

Figure 8.11: *Distribution of the area of the 90% confidence error ellipse of the ISC-located events. Vertical red lines indicate the 50th, 90th and 95th percentile values.*

Figure 8.12 shows one of the major characteristic features of the ISC location algorithm (Bondár and Storchak, 2011). Because the ISC locator accounts for correlated travel-time prediction errors due to unmodelled velocity heterogeneities along similar ray paths, the area of the 90% confidence error ellipse does not decrease indefinitely with increasing number of stations, but levels off once the information carried by the network geometry is exhausted, thus providing more realistic uncertainty estimates.

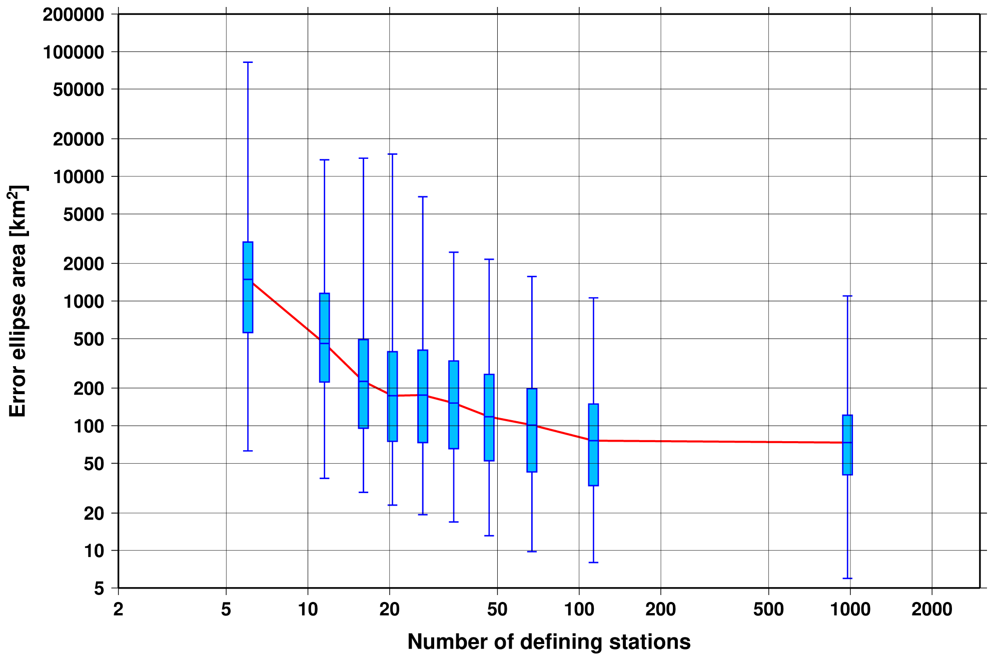

Figure 8.12: *Box-and-whisker plot of the area of the 90% confidence error ellipse of the ISC-located events as a function of the number of defining stations. Each box represents one-tenth-worth of the total number of data. The red line indicates the median 90% confidence error ellipse area.*

8.2 Seismic Phases and Travel-Time Residuals

The number of phases that are associated to events over the summary period in the ISC Bulletin is shown in Figure 8.13. Phase types and their total number in the ISC Bulletin is shown in the Appendix, Table 10.3. A summary of phase types is indicated in Figure 8.14.

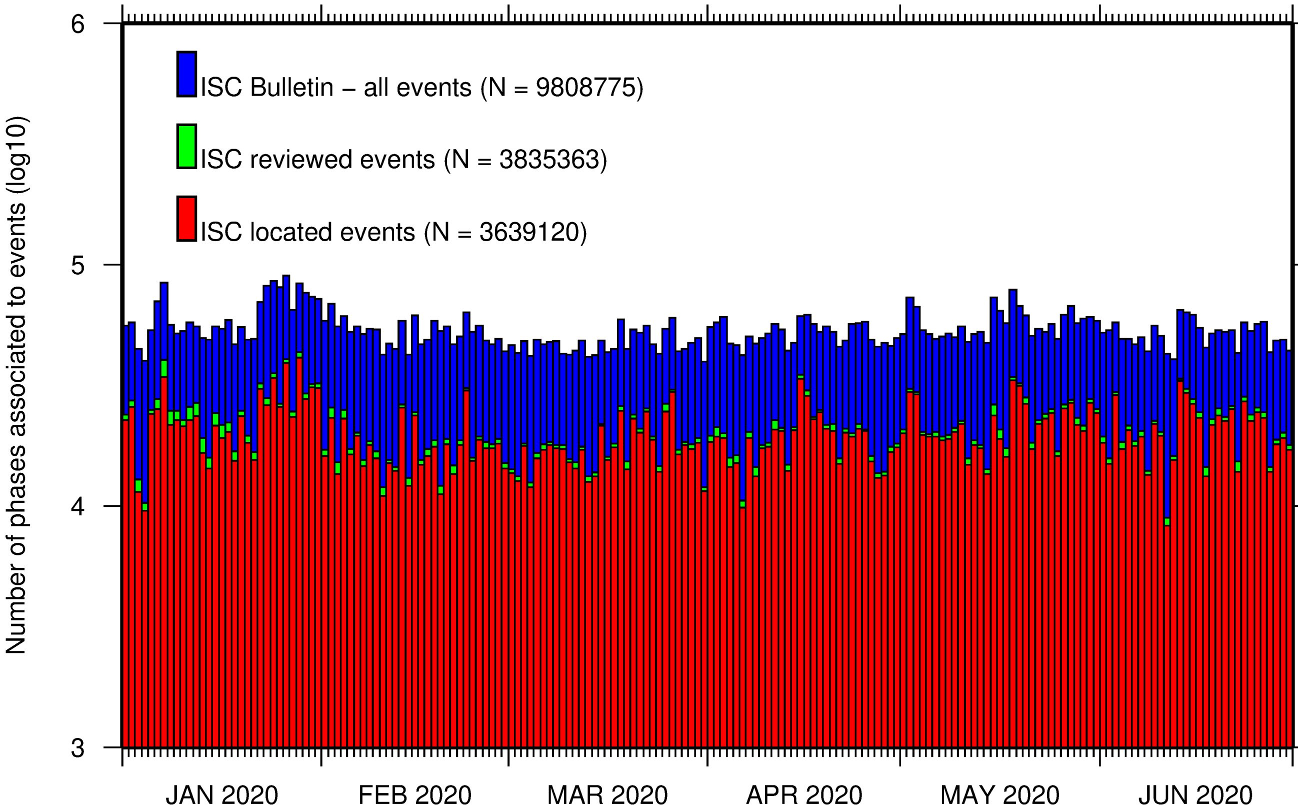

Figure 8.13: *Histogram showing the number of phases (N) that the ISC has associated to events within the ISC Bulletin for the current summary period.*

In computing ISC locations, the current (for events since 2009) ISC location algorithm (*Bondár and Storchak*, 2011) uses all *ak135* phases where possible. Within the Bulletin, the phases that contribute to an ISC location are labelled as *time defining*. In this section, we summarise these time defining phases.

In Figure 8.15, the number of defining phases is shown in a histogram over the summary period. Each defining phase is listed in Table 8.1, which also provides a summary of the number of defining phases per event. A pie chart showing the proportion of defining phases is shown in Figure 8.16. Figure 8.17 shows travel times of seismic waves. The distribution of residuals for these defining phases is shown for the top five phases in Figures 8.18 through 8.22.

Table 8.1: *Numbers of 'time defining' phases (N) within the ISC Bulletin for 22035 ISC located events.*

Phase	Number of 'defining' phases	Number of events	Max per event	Median per event
P	959056	14179	2203	13
Pn	669786	20191	799	16
Sn	225371	17119	205	7
Pb	114478	10228	130	7
Pg	99091	8476	169	7
Sg	74071	7965	147	6
Sb	73007	9670	106	5
S	46251	3562	542	3

Table 8.1: *(continued)*

Phase	Number of 'defining' phases	Number of events	Max per event	Median per event
PKPdf	44854	4190	979	3
PKiKP	26499	3144	268	2
PKPbc	21347	3351	228	2
PKPab	14941	2403	225	2
PcP	13863	3544	88	2
pP	9113	1378	136	3
Pdif	8609	934	366	2
PP	8528	1141	192	2
ScP	4974	1105	225	2
SS	4164	926	53	3
sP	3797	1057	66	2
SKSac	3039	437	172	2
PKKPbc	1917	448	65	2
pwP	1554	534	57	2
SnSn	1274	656	10	1
PnPn	1103	611	15	1
SKPbc	1033	313	81	2
ScS	973	306	27	1
pPKPdf	816	294	35	2
sS	719	374	14	1
P'P'df	598	172	29	2
SKiKP	584	249	47	1
SKPdf	460	136	41	1
PKKPdf	418	210	13	1
PKKPab	401	204	18	1
pPKPbc	369	176	17	1
PS	341	155	33	2
pPKPab	312	133	17	1
SKPab	234	135	17	1
sPKPdf	231	147	19	1
P'P'bc	190	115	5	1
SKSdf	179	148	5	1
PcS	162	100	7	1
PnS	151	114	5	1
SKKSac	139	86	13	1
SP	139	45	34	1
Sdif	130	58	29	1
sPKPab	119	46	24	1
SKKPbc	111	34	16	2
pS	94	82	3	1
pPKiKP	87	28	15	2
pPdif	73	46	12	1
sPKPbc	71	51	4	1
SKKSdf	66	66	1	1
PKSdf	62	45	5	1
P'P'ab	45	29	4	1
sPdif	36	18	18	1
SKKPdf	28	22	3	1
SKKPab	21	12	4	2
SPn	17	14	4	1
SbSb	12	10	2	1
sPn	12	7	4	1
PKSbc	10	6	5	1
sPKiKP	9	8	2	1
sSKSac	9	7	2	1
PbPb	8	7	2	1
PgPg	2	2	1	1
sSdif	2	2	1	1
S'S'ac	2	2	1	1
pSKSdf	1	1	1	1
pSKSac	1	1	1	1
pSdif	1	1	1	1

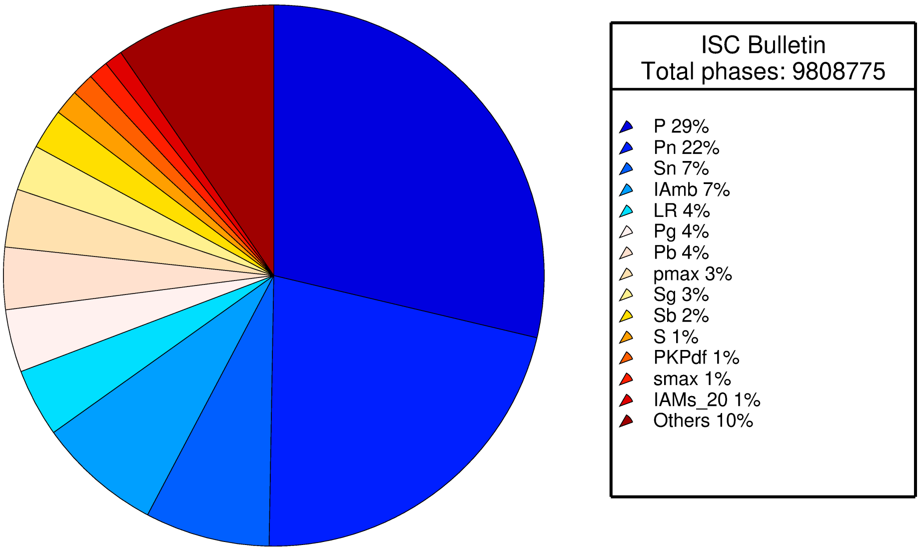

Figure 8.14: *Pie chart showing the fraction of various phase types in the ISC Bulletin for this summary period.*

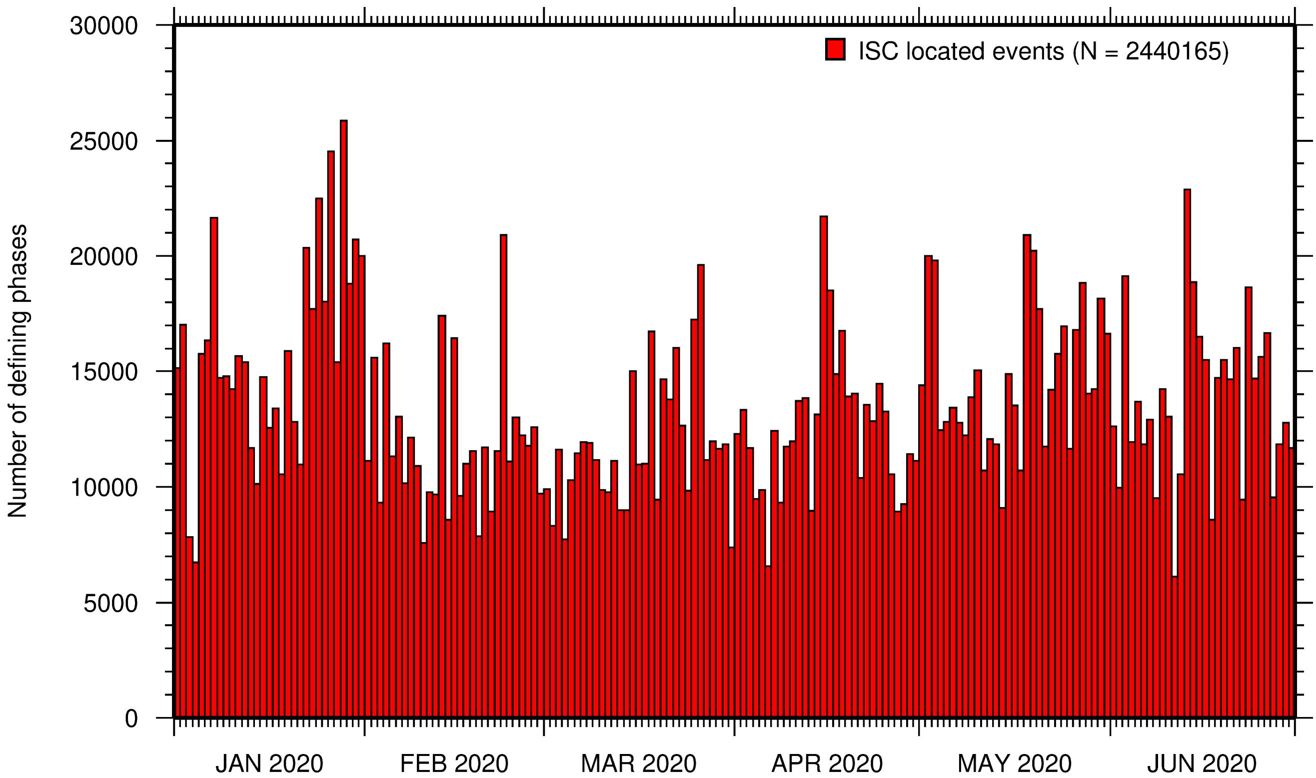

Figure 8.15: *Histogram showing the number of defining phases in the ISC Bulletin, for events located by the ISC.*

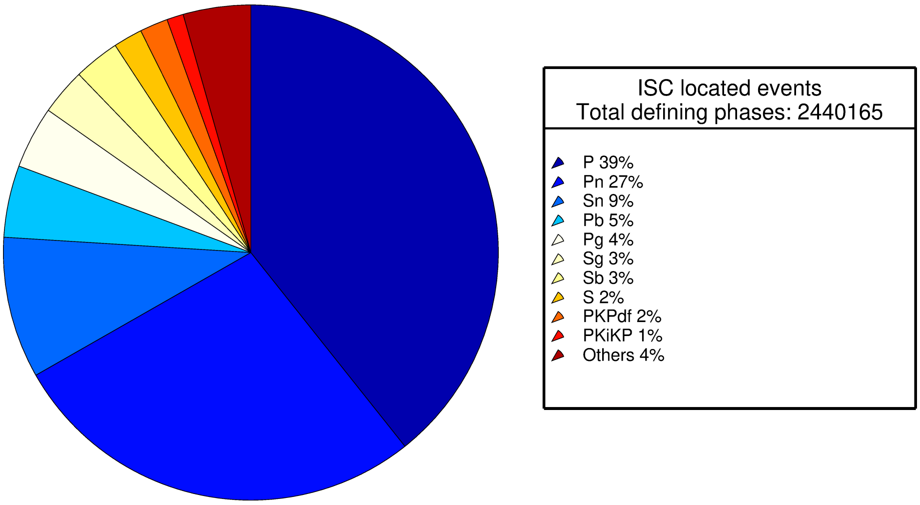

Figure 8.16: *Pie chart showing the defining phases in the ISC Bulletin, for events located by the ISC. A complete list of defining phases is shown in Table 8.1.*

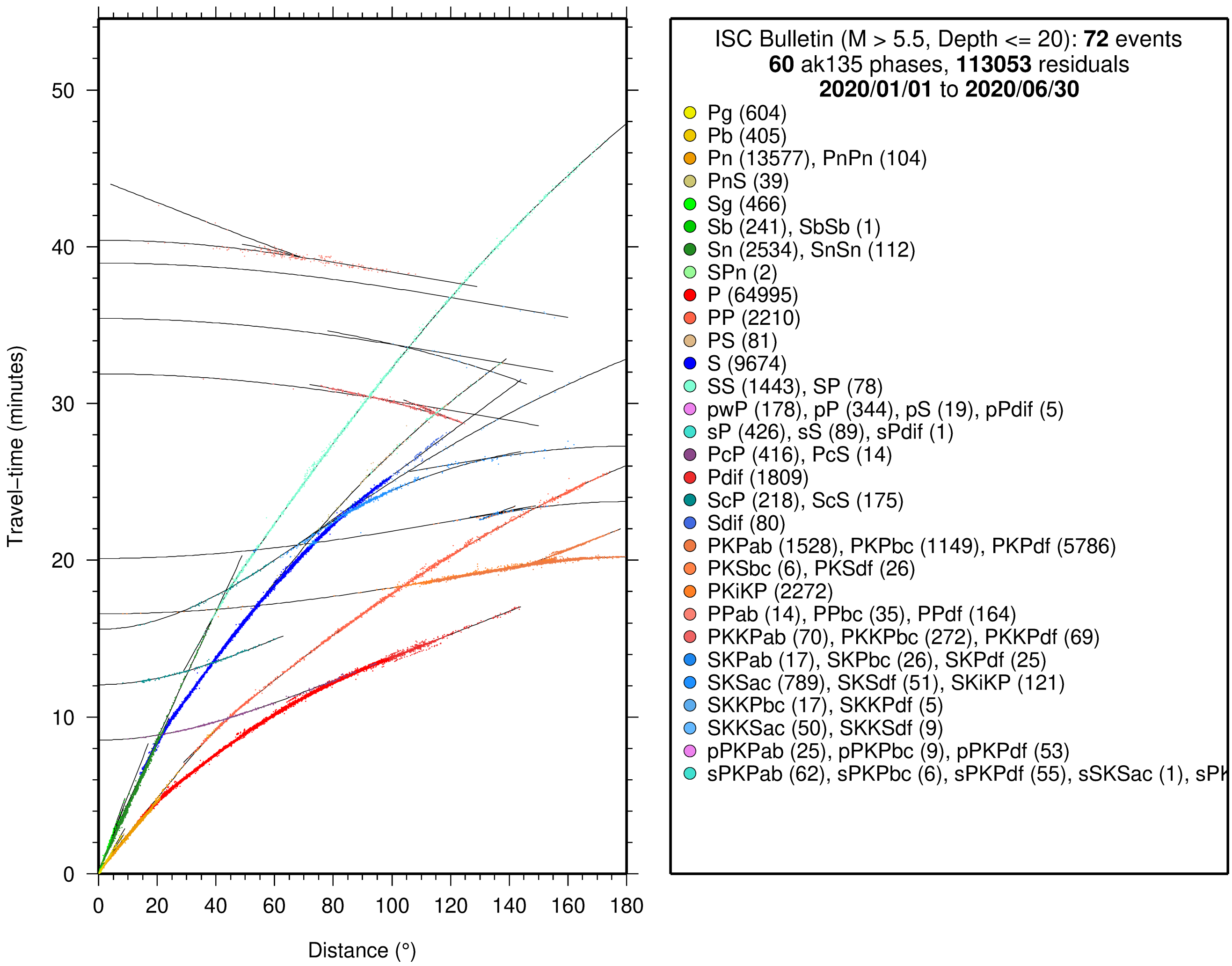

Figure 8.17: *Distribution of travel-time observations in the ISC Bulletin for events with $M > 5.5$ and depth less than 20 km. The travel-time observations are shown relative to a 0 km source and compared with the theoretical ak135 travel-time curves (solid lines). The legend lists the number of each phase plotted.*

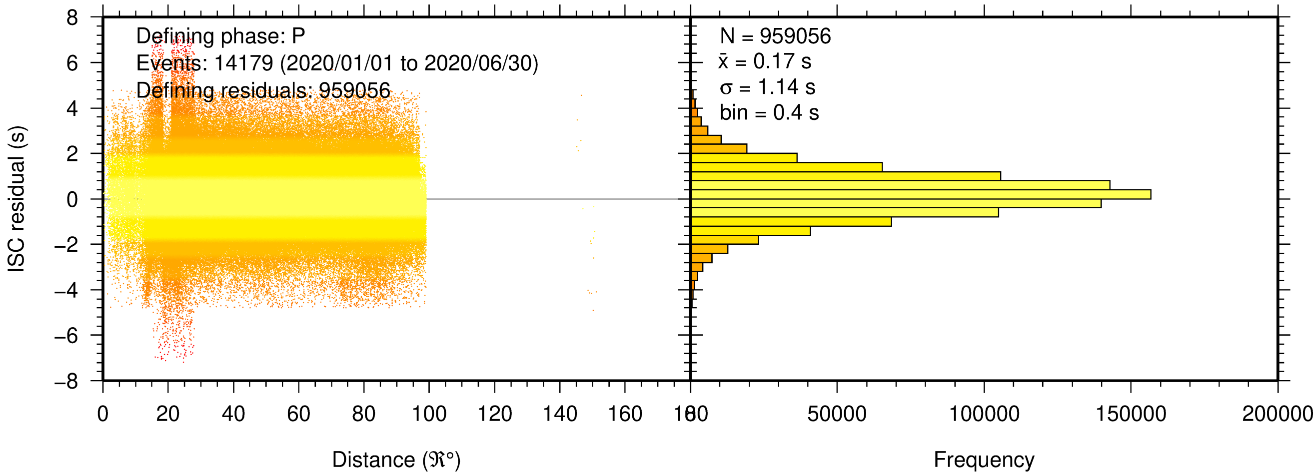

Figure 8.18: *Distribution of travel-time residuals for the defining P phases used in the computation of ISC located events in the Bulletin.*

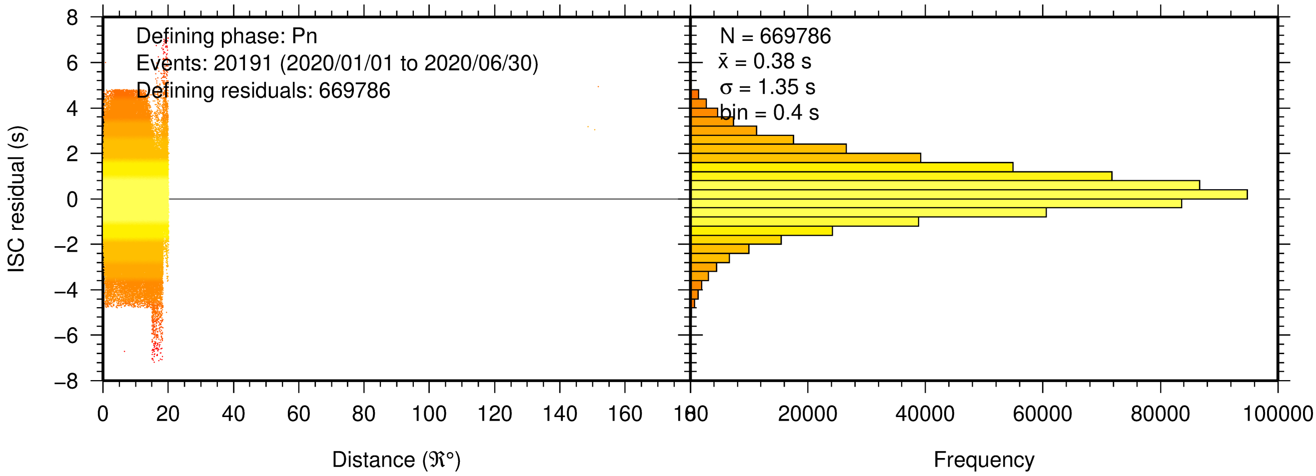

Figure 8.19: *Distribution of travel-time residuals for the defining Pn phases used in the computation of ISC located events in the Bulletin.*

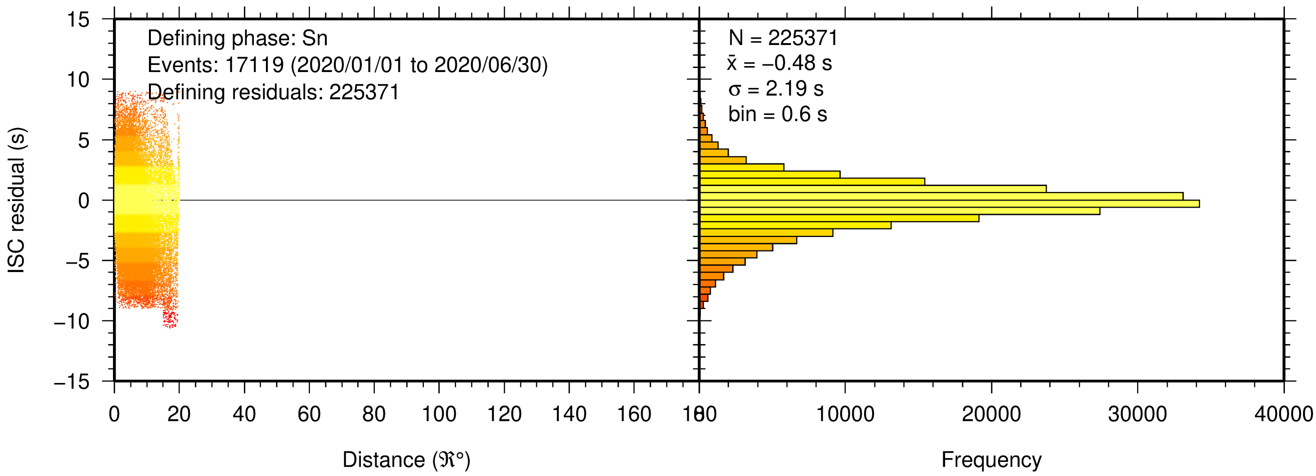

Figure 8.20: *Distribution of travel-time residuals for the defining Sn phases used in the computation of ISC located events in the Bulletin.*

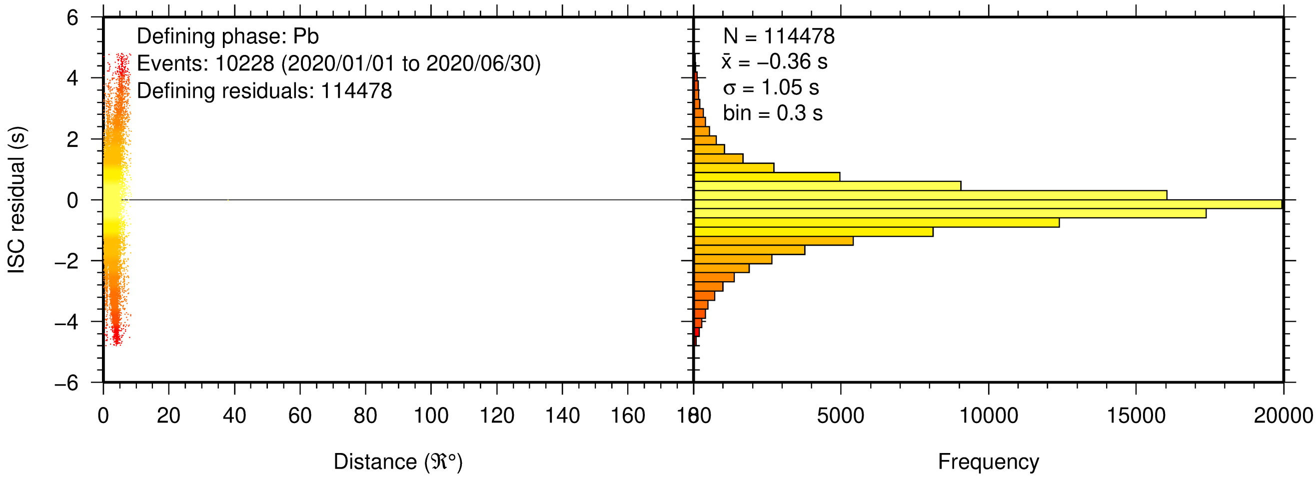

Figure 8.21: *Distribution of travel-time residuals for the defining Pb phases used in the computation of ISC located events in the Bulletin.*

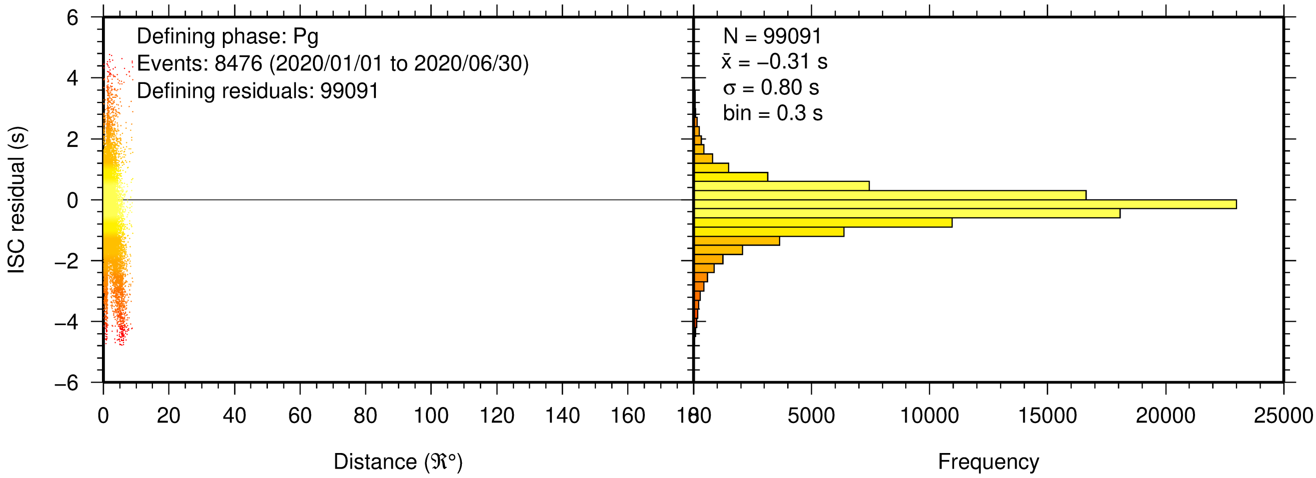

Figure 8.22: *Distribution of travel-time residuals for the defining Pg phases used in the computation of ISC located events in the Bulletin.*

8.3 Seismic Wave Amplitudes and Periods

The ISC Bulletin contains a variety of seismic wave amplitudes and periods measured by reporting agencies. For this Bulletin Summary, the total of collected amplitudes and periods is 3981227 (see Section 7.3). For the determination of the ISC magnitudes MS and mb, only a fraction of such data can be used. Indeed, the ISC network magnitudes are computed only for ISC located events. Here we recall the main features of the ISC procedure for MS and mb computation (see detailed description in Section 10.1.4). For each amplitude-period pair in a reading the ISC algorithm computes the magnitude (a reading can include several amplitude-period measurements) and the reading magnitude is assigned to the maximum A/T in the reading. If more than one reading magnitude is available for a station, the station magnitude is the median of the reading magnitudes. The network magnitude is computed then as the 20% alpha-trimmed median of the station magnitudes (at least three required). MS is computed for shallow earthquakes (depth $\leq$ 60 km) only and using amplitudes and periods on all three components (when available) if the period is within 10-60 s and the epicentral distance is between 20° and 160°. mb is computed also for deep earthquakes (depth down to 700 km) but only with amplitudes on the vertical component measured at periods ≤ 3 s in the distance range 21°-100°.

Table 8.2 is a summary of the amplitude and period data that contributed to the computation of station and ISC MS and mb network magnitudes for this Bulletin Summary.

Table 8.2: *Summary of the amplitude-period data used by the ISC Locator to compute MS and mb.*

	MS	mb
Number of amplitude-period data	150513	492330
Number of readings	132307	488325
Percentage of readings in the ISC located events with qualifying data for magnitude computation	14.0	41.0
Number of station magnitudes	127878	448695
Number of network magnitudes	3610	12501

A small percentage of the readings with qualifying data for MS and mb calculation have more than one amplitude-period pair. Notably, only 14% of the readings for the ISC located (shallow) events included qualifying data for MS computation, whereas for mb the percentage is much higher at 41%. This is due to the seismological practice of reporting agencies. Agencies contributing systematic reports of amplitude and period data are listed in Appendix Table 10.4. Obviously the ISC Bulletin would benefit if more agencies included surface wave amplitude-period data in their reports.

Figure 8.23 shows the distribution of the number of station magnitudes versus distance. For mb there is a significant increase in the distance range 70°-90°, whereas for MS most of the contributing stations are below 100°. The increase in number of station magnitude between 70°-90° for mb is partly due to the very dense distribution of seismic stations in North America and Europe with respect to earthquake occurring in various subduction zones around the Pacific Ocean.

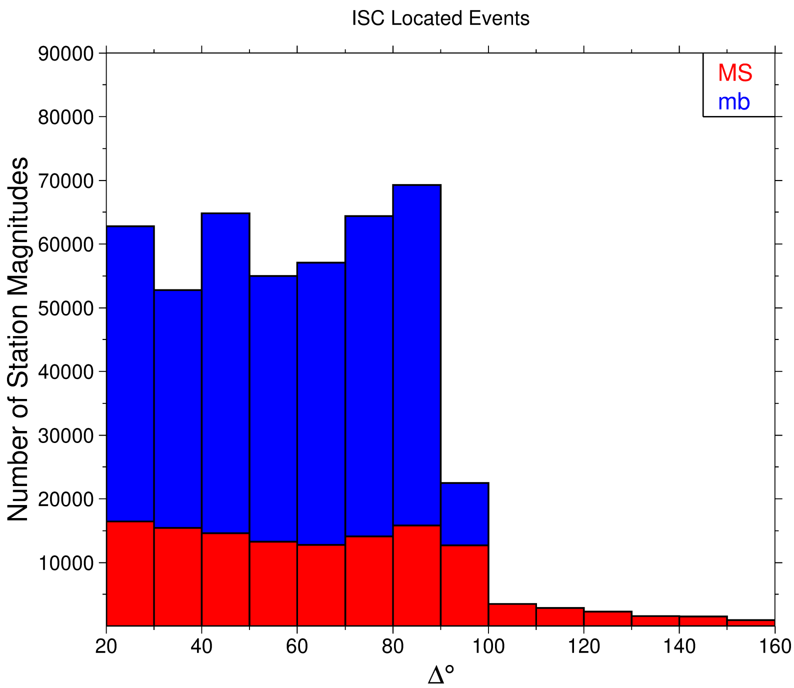

Figure 8.23: *Distribution of the number of station magnitudes computed by the ISC Locator for mb (blue) and MS (red) versus distance.*

Finally, Figure 8.24 shows the distribution of network MS and mb as well as the median number of stations for magnitude bins of 0.2. Clearly with increasing magnitude the number of events is smaller but with a general tendency of having more stations contributing to the network magnitude.

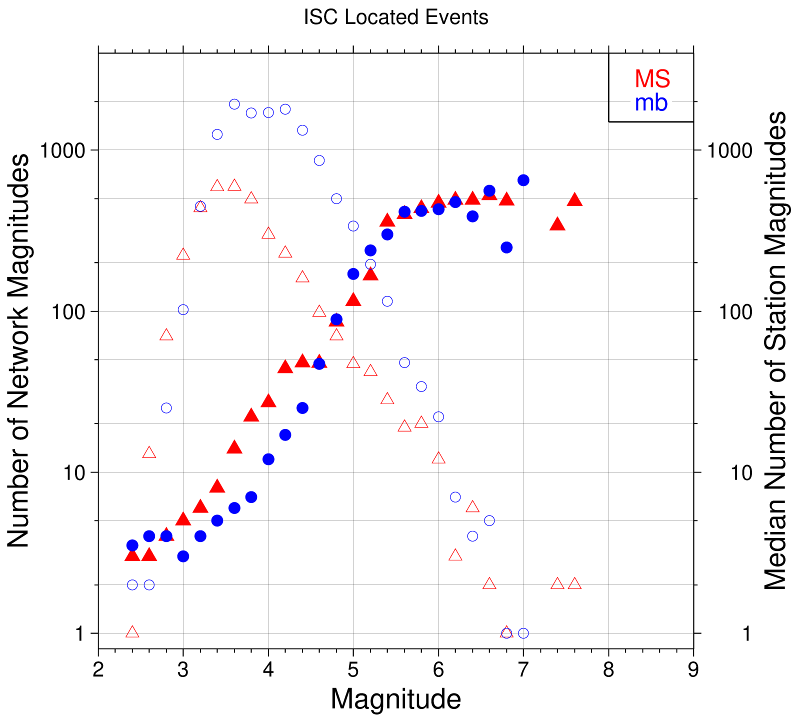

Figure 8.24: *Number of network magnitudes (open symbols) and median number of stations magnitudes (filled symbols). Blue circles refer to mb and red triangles to MS. The width of the magnitude interval δM is 0.2, and each symbol includes data with magnitude in $M \pm \delta M/2$.*

8.4 Completeness of the ISC Bulletin

We define the magnitude of completeness (hereafter M_C) as the lowest magnitude threshold above which all events are believed to be recorded. The Bulletin with events bigger than the defined M_C is assumed to be complete.

Until Issue 53, Volume II (July - December 2016) of the Summary of the ISC an estimation of M_C was computed only with the maximum curvature technique (*Woessner and Wiemer*, 2005). After the completion of the Rebuild Project and relocation of ISC hypocenters from data years 1964 to 2010 (*Storchak et al.*, 2017), the estimate of M_C for the entire ISC Bulletin is re-computed using four catalogue based methodologies (*Adamaki*, 2017, and references therein): the previously used maximum curvature for comparison (maxC), Mc based on the b-value stability (MBS technique), the Goodness of Fit Test with a 90% level of fit (GFT90) and the modified Goodness of Fit Test (mGFT). Further details on each of these methodologies and their statistical behaviour can be found in *Leptokaropoulos et al.* (2018).

The magnitudes of completeness of the ISC Bulletin for this Summary period is shown in Figure 8.25. How M_C varies for the ISC Bulletin over the years is shown in Figure 8.26. The step change in 1996 corresponds with the inclusion of the Prototype IDC (EIDC) Bulletin, followed by the Reviewed Event Bulletin (REB) of the IDC.

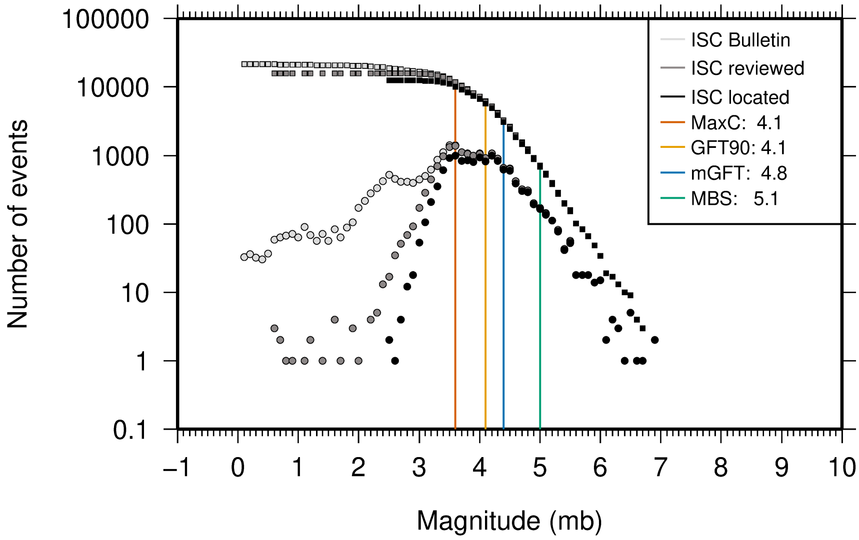

Figure 8.25: *Frequency and cumulative frequency magnitude distribution for all events in the ISC Bulletin, ISC reviewed events and events located by the ISC. The magnitude of completeness (M_C) is shown for the ISC Bulletin. Note: only events with values of mb are represented in the figure.*

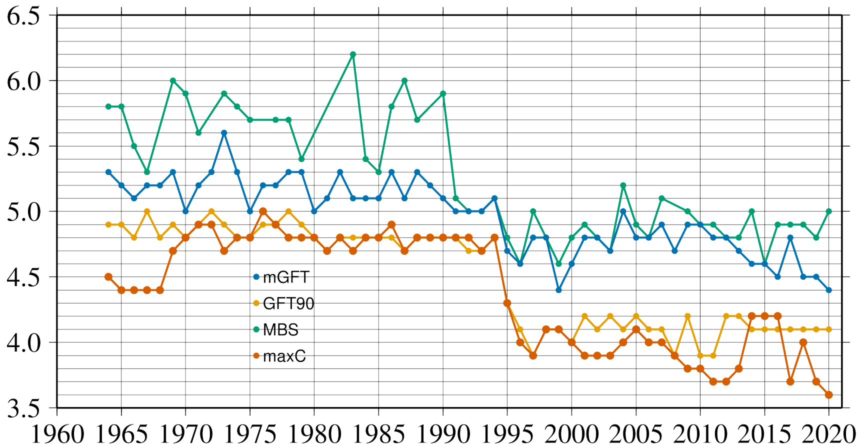

Figure 8.26: *Variation of magnitude of completeness (M_C) for each year in the ISC Bulletin. Note: M_C is calculated only using those events with values of mb.*

8.5 Magnitude Comparisons

The ISC Bulletin publishes network magnitudes reported by multiple agencies to the ISC. For events that have been located by the ISC, where enough amplitude data has been collected, the MS and mb magnitudes are calculated by the ISC (MS is computed only for depths $\leq$ 60 km). In this section, ISC magnitudes and some other reported magnitudes in the ISC Bulletin are compared.

The comparison between MS and mb computed by the ISC locator for events in this summary period is shown in Figure 8.27, where the large number of data pairs allows a colour coding of the data density. The scatter in the data reflects the fundamental differences between these magnitude scales.

Similar plots are shown in Figure 8.28 and 8.29, respectively, for comparisons of ISC mb and ISC MS with M_W from the GCMT catalogue. Since M_W is not often available below magnitude 5, these distributions are mostly for larger, global events. Not surprisingly, the scatter between mb and M_W is larger than the scatter between MS and M_W. Also, the saturation effect of mb is clearly visible for earthquakes with

$M_W > 6.5$. In contrast, MS scales well with $M_W > 6$, whereas for smaller magnitudes MS appears to be systematically smaller than M_W.

In Figure 8.30 ISC values of mb are compared with all reported values of mb, values of mb reported by NEIC and values of mb reported by IDC. Similarly in Figure 8.31, ISC values of MS are compared with all reported values of MS, values of MS reported by NEIC and values of MS reported by IDC. There is a large scatter between the ISC magnitudes and the mb and MS reported by all other agencies.

The scatter decreases both for mb and MS when ISC magnitudes are compared just with NEIC and IDC magnitudes. This is not surprising as the latter two agencies provide most of the amplitudes and periods used by the ISC locator to compute MS and mb. However, ISC mb appears to be smaller than NEIC mb for $mb < 4$ and larger than IDC mb for $mb > 4$. Since NEIC does not include IDC amplitudes, it seems these features originate from observations at the high-gain, low-noise sites reported by the IDC. For the MS comparisons between ISC and NEIC a similar but smaller effect is observed for $MS < 4.5$, whereas a good scaling is generally observed for the MS comparisons between ISC and IDC.

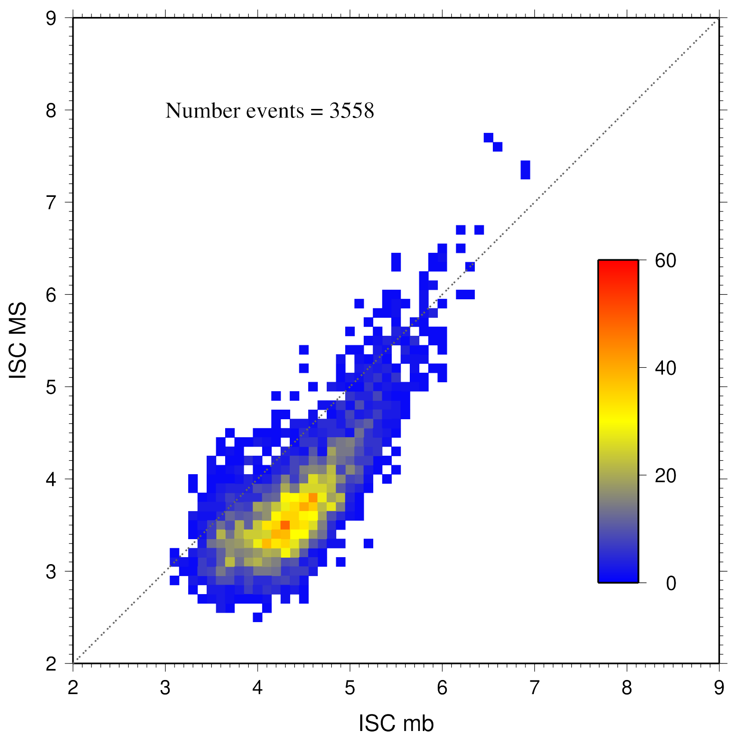

Figure 8.27: *Comparison of ISC values of MS with mb for common event pairs.*

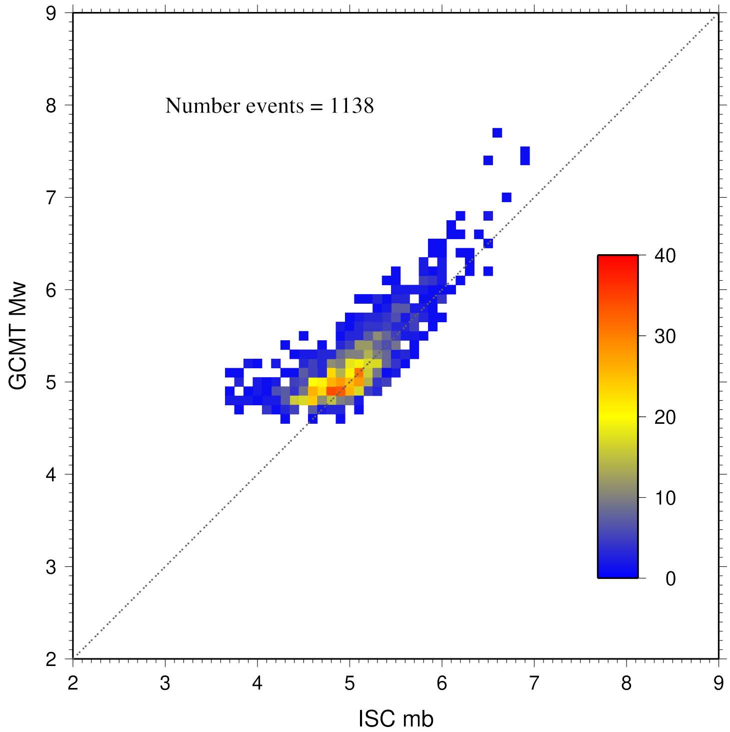

Figure 8.28: *Comparison of ISC values of mb with GCMT M_W for common event pairs.*

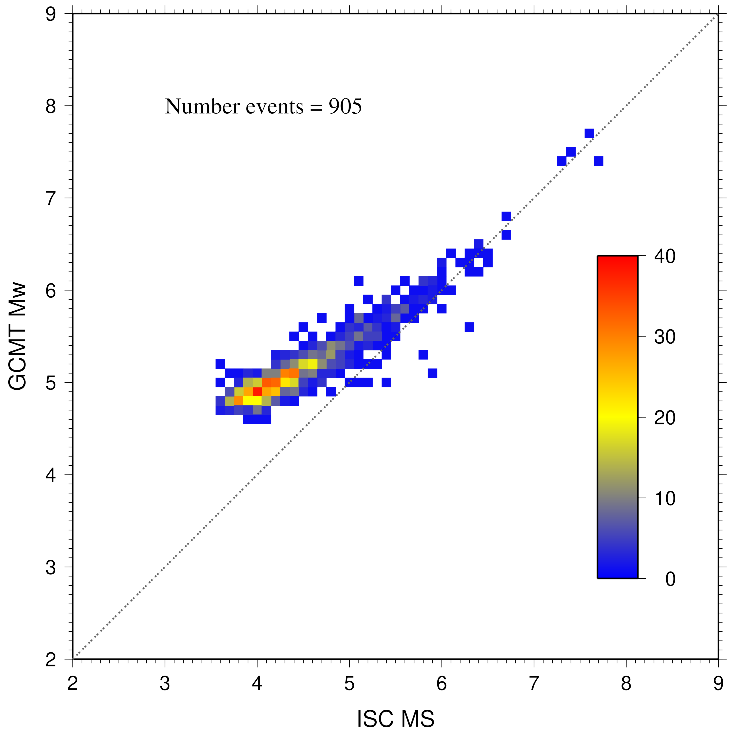

Figure 8.29: *Comparison of ISC values of MS with GCMT M_W for common event pairs.*

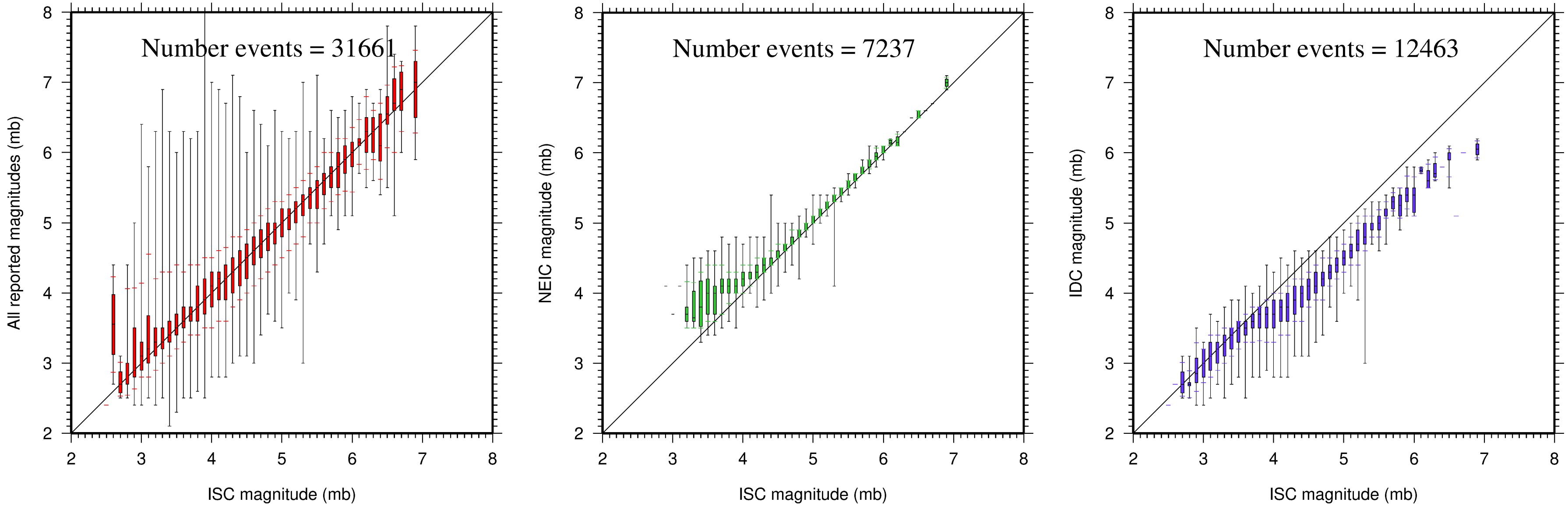

(a) (b) (c)

Figure 8.30: *Comparison of ISC magnitude data (mb) with additional agency magnitudes (mb). The statistical summary is shown in box-and-whisker plots where the 10th and 90th percentiles are shown in addition to the max and min values. (a): All magnitudes reported; (b): NEIC magnitudes; (c): IDC magnitudes.*

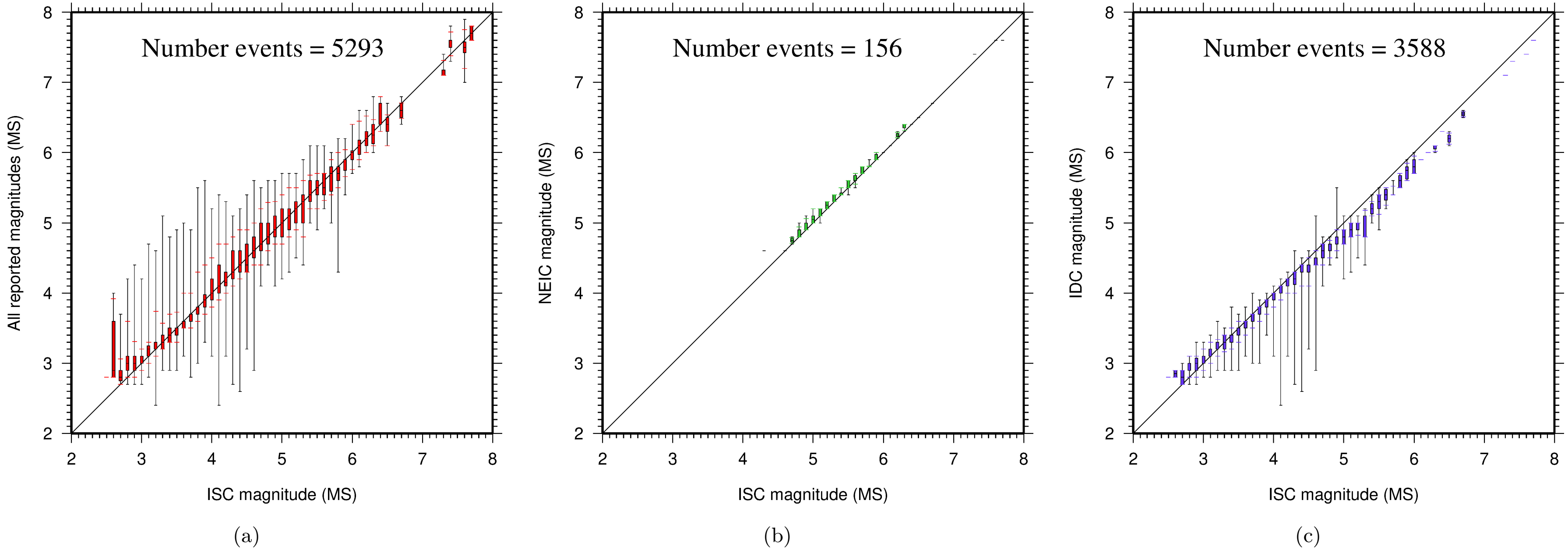

Figure 8.31: *Comparison of ISC magnitude data (MS) with additional agency magnitudes (MS). The statistical summary is shown in the box-and-whisker plots where the 10th and 90th percentiles are shown in addition to the max and min values. (a): All magnitudes reported; (b): NEIC magnitudes; (c): IDC magnitudes.*

9

The Leading Data Contributors

For the current six-month period, 150 agencies reported related bulletin data. Although we are grateful for every report, we nevertheless would like to acknowledge those agencies that made the most useful or distinct contributions to the contents of the ISC Bulletin. Here we note those agencies that:

- provided a comparatively large volume of parametric data (see Section 9.1),
- reported data that helped quite considerably to improve the quality of the ISC locations or magnitude determinations (see Section 9.2),
- helped the ISC by consistently reporting data in one of the standard recognised formats and in-line with the ISC data collection schedule (see Section 9.3).

We do not aim to discourage those numerous small networks who provide comparatively smaller yet still most essential volumes of regional data regularly, consistently and accurately. Without these reports the ISC Bulletin would not be as comprehensive and complete as it is today.

9.1 The Largest Data Contributors

We acknowledge the contribution of IDC, NEIC, GFZ, MOS, BJI, GCMT, MCSM, CLL and a few others (Figure 9.1) that reported the majority of moderate to large events recorded at teleseismic distances. The contributions of NEIC, IDC, MEX, JMA and several others are also acknowledged with respect to smaller seismic events. The contributions of JMA, AFAD, ISK, RSNC, TAP, WEL and a number of others are also acknowledged with respect to small seismic events. Note that the NEIC bulletin accumulates a contribution of all regional networks in the USA. Several agencies monitoring highly seismic regions routinely report large volumes of small to moderate magnitude events, such as those in Japan, Chinese Taipei, Turkey, Italy, Greece, New Zealand, Mexico and Columbia. Contributions of small magnitude events by agencies in regions of low seismicity, such as Finland are also gratefully received.

We also would like to acknowledge contributions of those agencies that report a large portion of arrival time and amplitude data (Figure 9.2). For small magnitude events, these are local agencies in charge of monitoring local and regional seismicity. For moderate to large events, contributions of NEIC, USArray, GFZ, MOS, IDC are especially acknowledged. Notably, four agencies (NEIC, GFZ, MOS and IDC) together reported over 70% of all amplitude measurements made for teleseismically recorded events. We hope that other agencies would also be able to update their monitoring routines in the future to include the amplitude reports for teleseismic events compliant with the IASPEI standards.

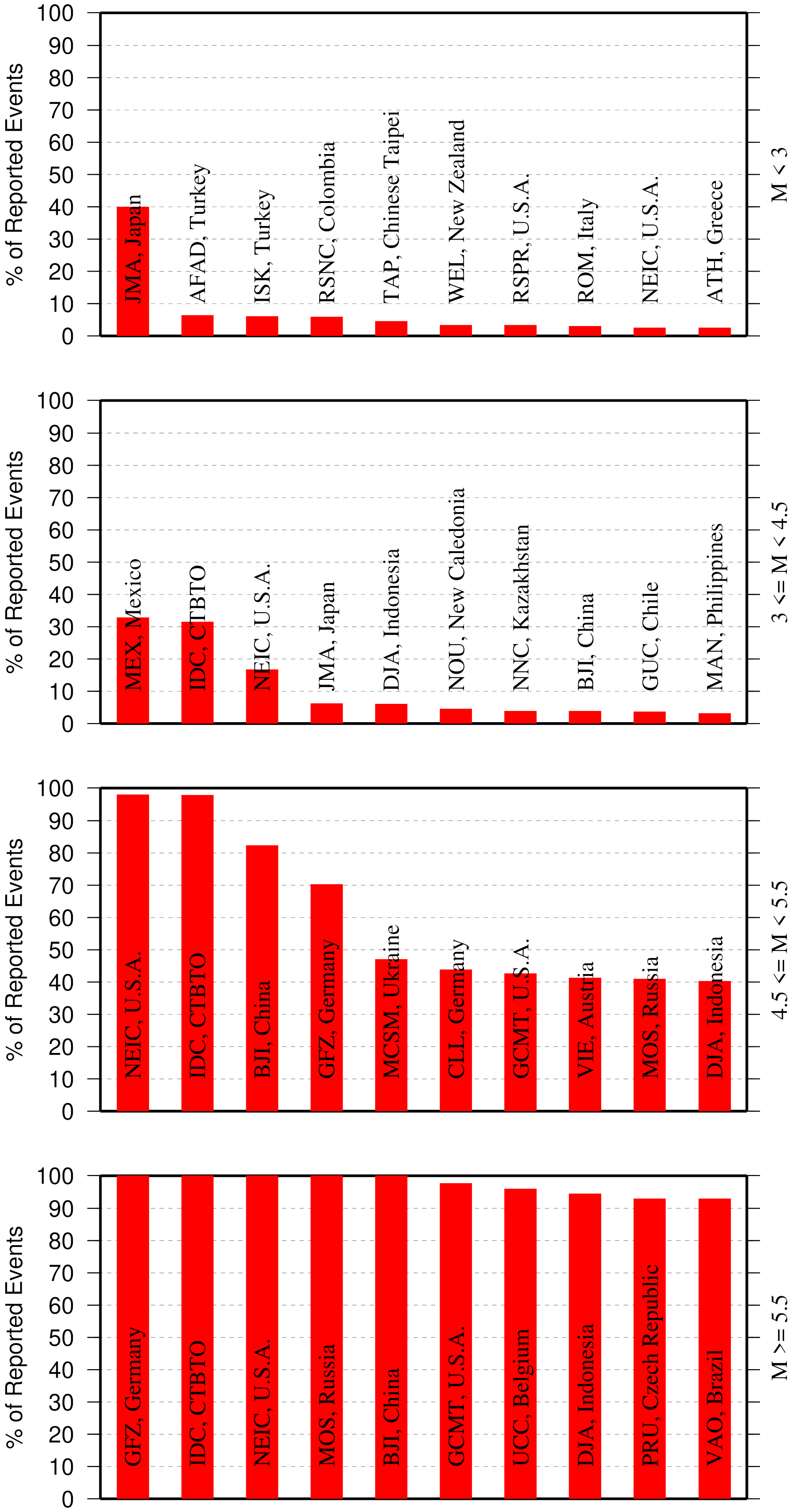

Figure 9.1: *Frequency of events in the ISC Bulletin for which an agency reported at least one item of data: a moment tensor, a hypocentre, a station arrival time or an amplitude. The top ten agencies are shown for four magnitude intervals.*

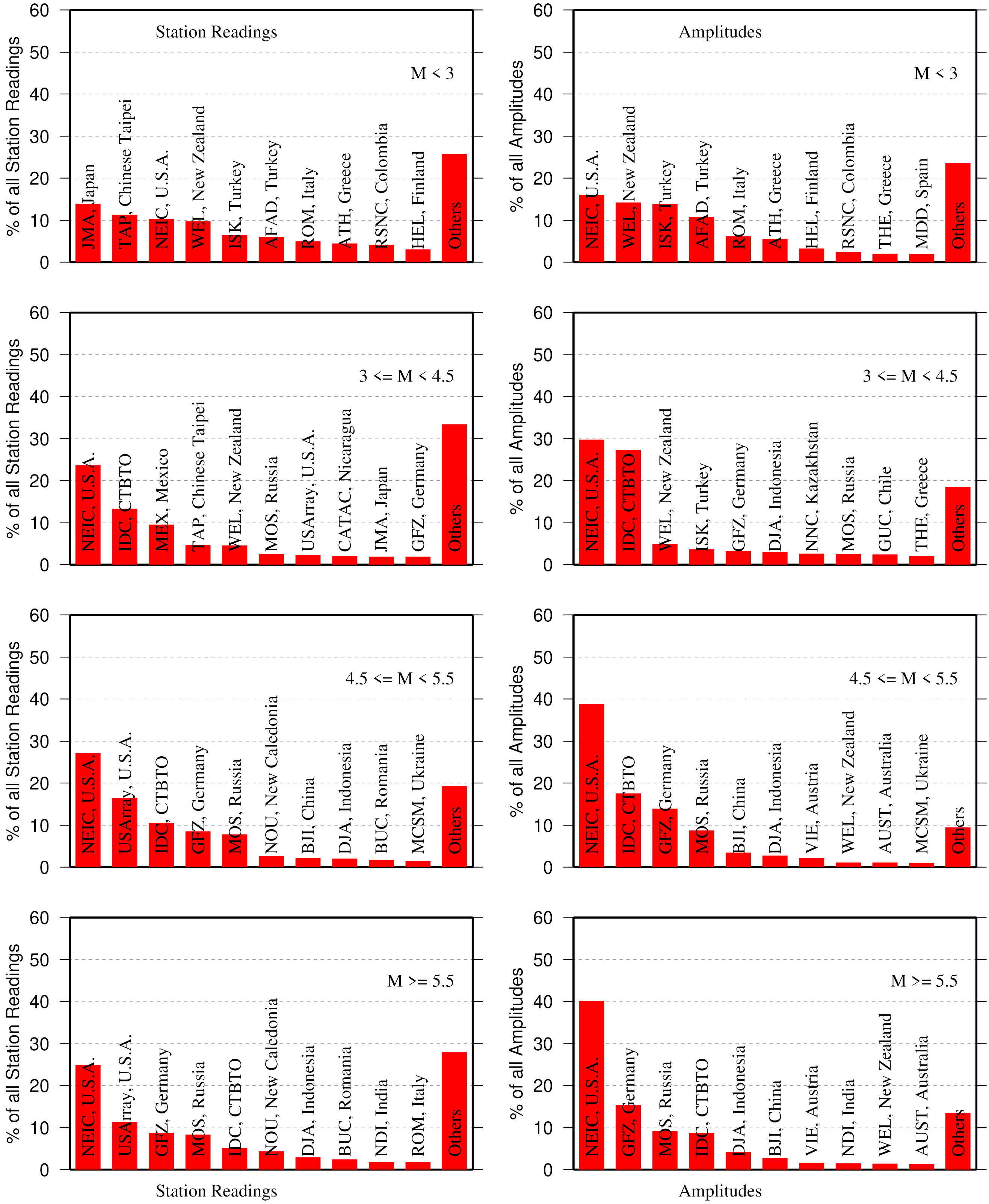

Figure 9.2: *Contributions of station arrival time readings (left) and amplitudes (right) of agencies to the ISC Bulletin. Top ten agencies are shown for four magnitude intervals.*

9.2 Contributors Reporting the Most Valuable Parameters

One of the main ISC duties is to re-calculate hypocentre estimates for those seismic events where a collective wealth of all station reports received from all agencies is likely to improve either the event location or depth compared to the hypocentre solution from each single agency. For areas with a sparse local seismic network or an unfavourable station configuration, readings made by other networks at teleseismic distances are very important. All events near mid-oceanic ridges as well as those in the majority of subduction zones around the world fall into this category. Hence we greatly appreciate the effort made by many agencies that report data for remote earthquakes (Figure 9.3). For some agencies, such as the IDC and the NEIC, it is part of their mission. For instance, the IDC reports almost every seismic event that is large enough to be recorded at teleseismic distance (20 degrees and beyond). This is largely because the International Monitoring System of primary arrays and broadband instruments is distributed at quiet sites around the world in order to be able to detect possible violations of the Comprehensive Nuclear-Test-Ban Treaty. The NEIC reported over 40% of those events as their mission requires them to report events above magnitude 4.5 outside the United States of America. For other agencies reporting distant events it is an extra effort that they undertake to notify their governments and relief agencies as well as to help the ISC and academic research in general. Hence these agencies usually report on the larger magnitude events. BJI, GFZ, MOS, NAO, CLL, VIE, UCC, AWI each reported individual station arrivals for several percent of all relevant events. We encourage other agencies to report distant events to us.

In addition to the first arriving phase we encourage reporters to contribute observations of secondary seismic phases that help constrain the event location and depth: S, Sn, Sg and pP, sP, PcP (Figure 9.4). We expect though that these observations are actually made from waveforms, rather than just predicted by standard velocity models and modern software programs. It is especially important that these arrivals are manually reviewed by an operator (as we know takes place at the IDC and NEIC), as opposed to some lesser attempts to provide automatic phase readings that are later rejected by the ISC due to a generally poor quality of unreviewed picking.

Another important long-term task that the ISC performs is to compute the most definitive values of

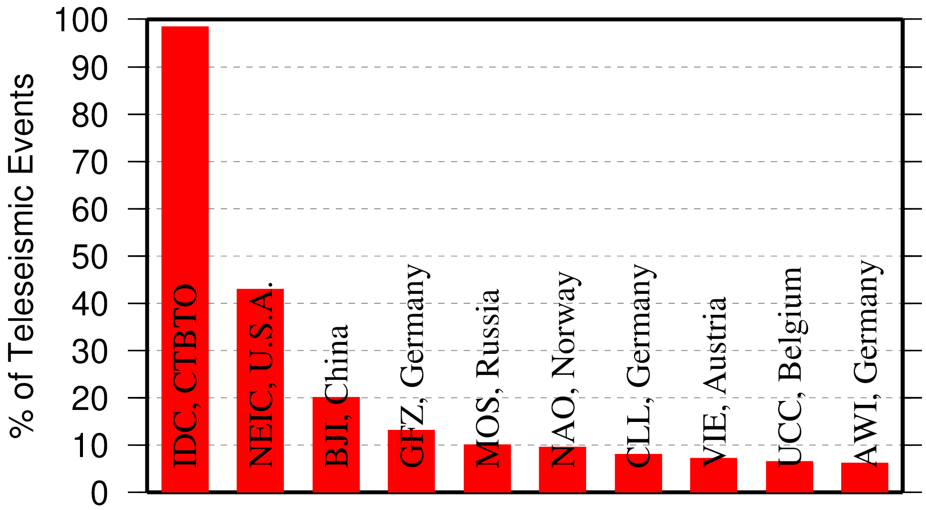

Figure 9.3: *Top ten agencies that reported teleseismic phase arrivals for a large portion of ISC events.*

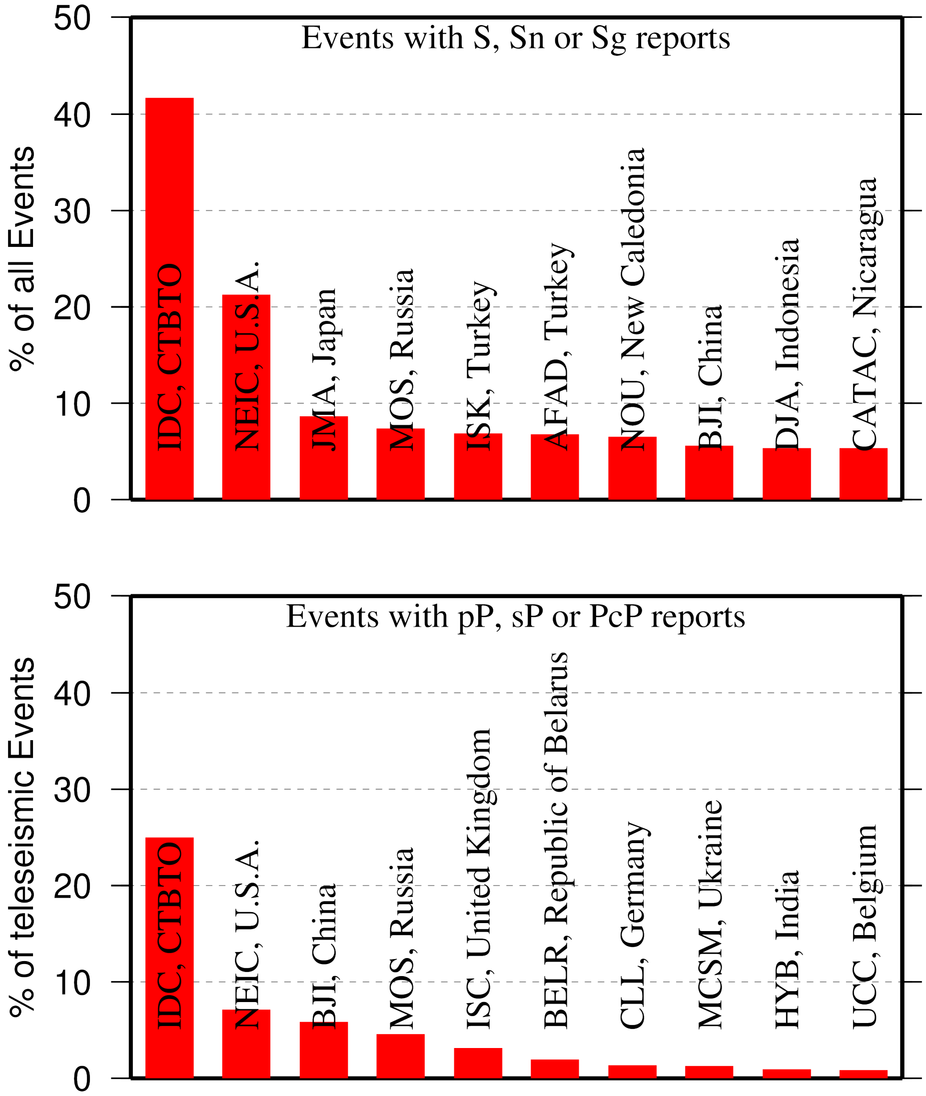

Figure 9.4: *Top ten agencies that reported secondary phases important for an accurate epicentre location (top) and focal depth determination (bottom).*

MS and mb network magnitudes that are considered reliable due to removal of outliers and consequent averaging (using alpha-trimmed median) across the largest network of stations, generally not feasible for a single agency. Despite concern over the bias at the lower end of mb introduced by the body wave amplitude data from the IDC, other agencies are also known to bias the results. This topic is further discussed in Section 8.5.

Notably, the IDC reports almost 100% of all events for which MS and mb are estimated. This is due to the standard routine that requires determination of body and surface wave magnitudes useful for discrimination purposes. NEIC, BJI, NAO, MOS, BELR, CLL and a few other agencies (Figure 9.5) are also responsible for the majority of the amplitude and period reports that contribute towards the ISC magnitudes.

The ISC only recently started to determine source mechanisms in addition to those reported by other agencies. For moment tensor magnitudes we rely on reports from other agencies (Figure 9.6).

Among other event parameters the ISC Bulletin also contains information on event type. We cannot

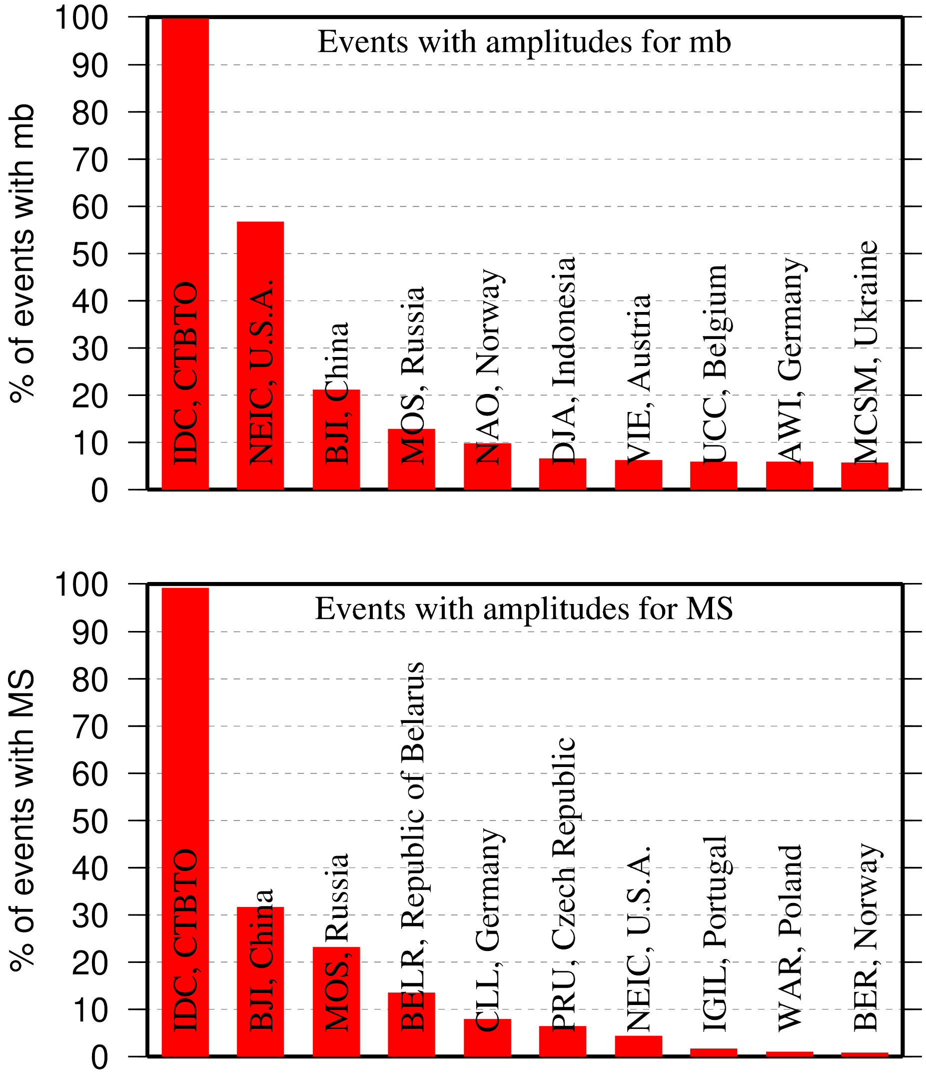

Figure 9.5: *Agencies that report defining body (top) and surface (bottom) wave amplitudes and periods for the largest fraction of those ISC Bulletin events with MS/mb determinations.*

independently verify the type of each event in the Bulletin and thus rely on other agencies to report the event type to us. Practices of reporting non-tectonic events vary greatly from country to country. Many agencies do not include anthropogenic events in their reports. Suppression of such events from reports to the ISC may lead to a situation where a neighbouring agency reports the anthropogenic event as an earthquake for which expected data are missing. This in turn is detrimental to ISC Bulletin users studying natural seismic hazard. Hence we encourage all agencies to join the agencies listed on Figure 9.7 and several others in reporting both natural and anthropogenic events to the ISC.

The ISC Bulletin also contains felt and damaging information when local agencies have reported it to us. Agencies listed on Figure 9.8 provide such information for the majority of all felt or damaging events in the ISC Bulletin.

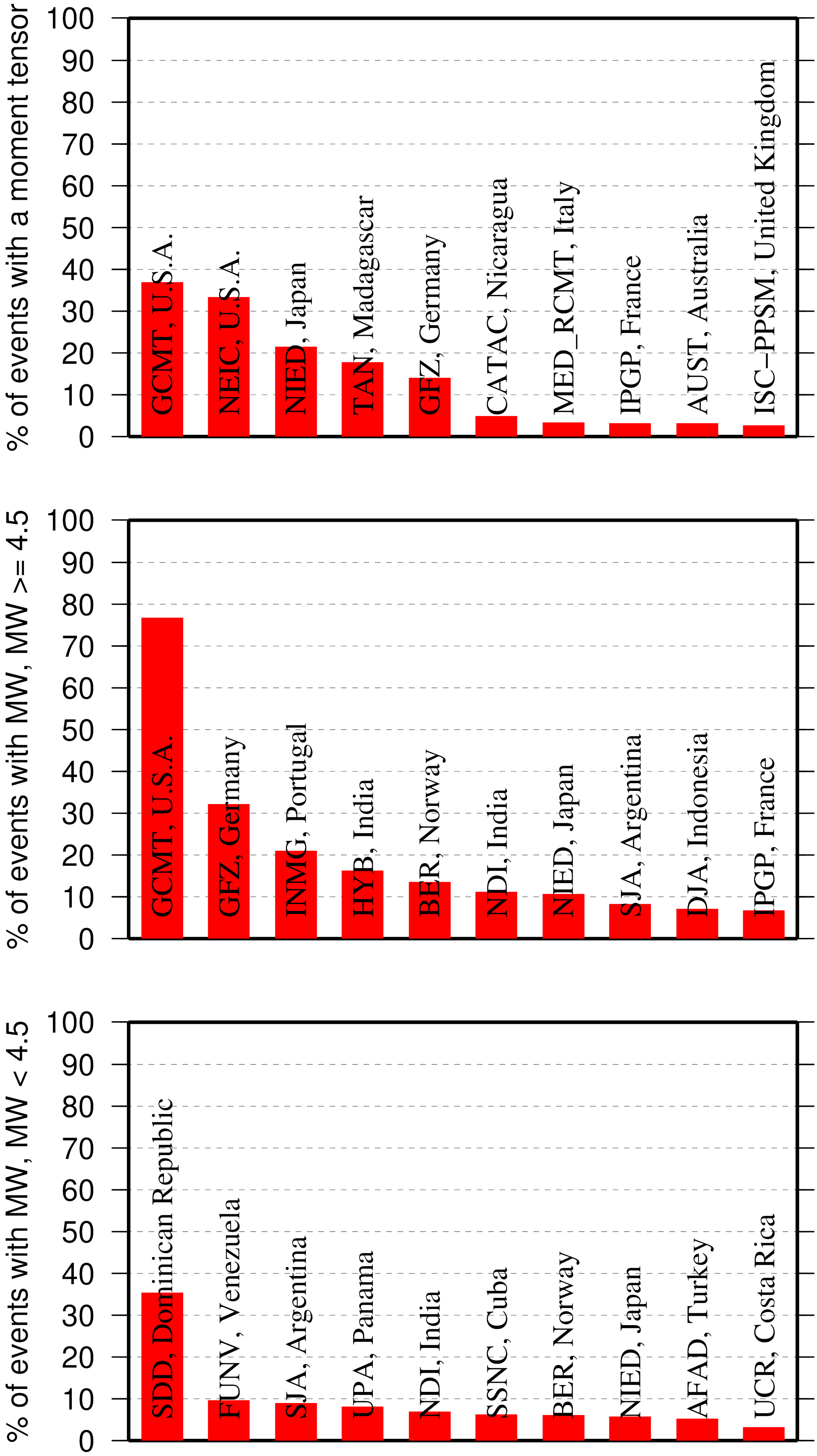

Figure 9.6: *Top ten agencies that most frequently report determinations of seismic moment tensor (top) and moment magnitude (middle/bottom for M greater/smaller than 4.5).*

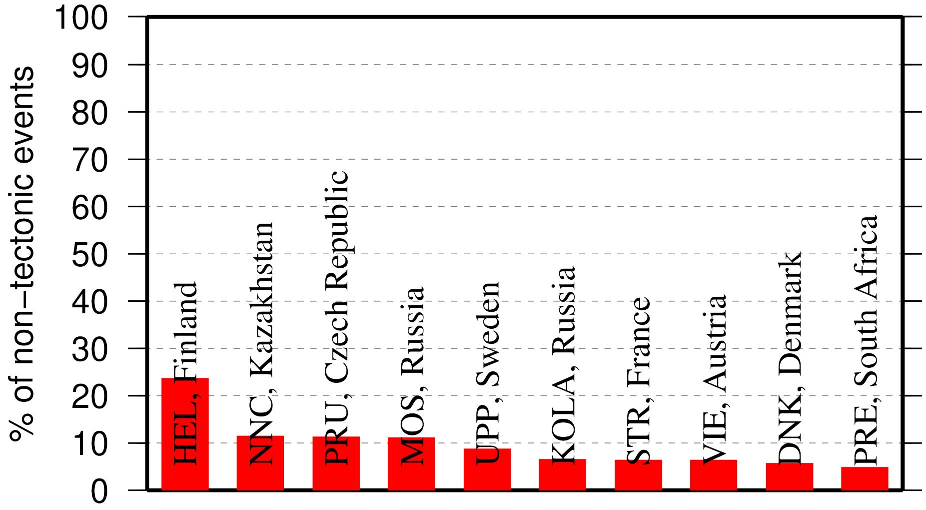

Figure 9.7: *Top ten agencies that most frequently report non-tectonic seismic events to the ISC.*

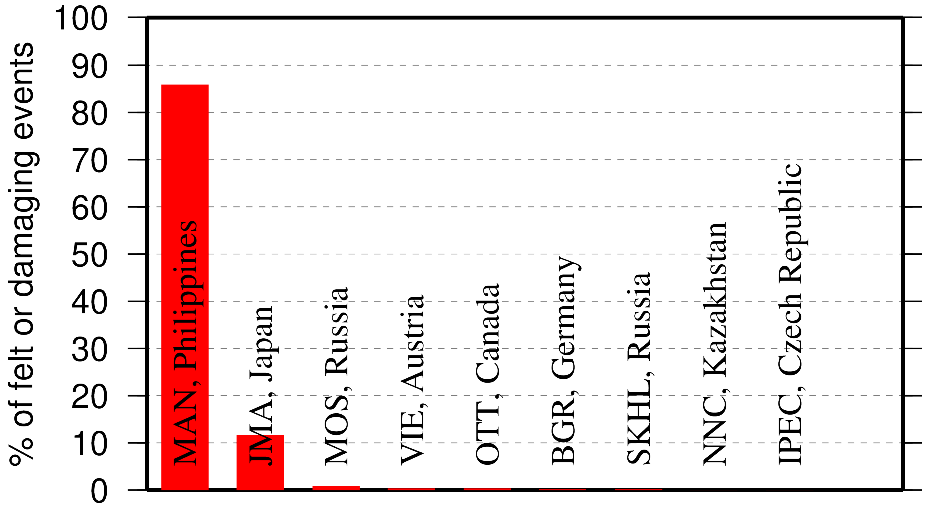

Figure 9.8: *Top ten agencies that most frequently report macroseismic information to the ISC.*

9.3 The Most Consistent and Punctual Contributors

During this six-month period, 27 agencies reported their bulletin data in one of the standard seismic formats (ISF, IMS, GSE, Nordic or QuakeML) and within the current 12-month deadline. Here we must reiterate that the ISC accepts reviewed bulletin data after a final analysis as soon as they are ready. These data, even if they arrive before the deadline, are immediately parsed into the ISC database, grouped with other data and become available to the ISC users on-line as part of the preliminary ISC Bulletin. There is no reason to wait until the deadline to send the data to the ISC. Table 9.1 lists all agencies that have been helpful to the ISC in this respect during the six-month period.

Table 9.1: *Agencies that contributed reviewed bulletin data to the ISC in one of the standard international formats before the submission deadline.*

Agency Code	Country	Average Delay from real time (days)
AUST	Australia	15
ZUR	Switzerland	17
WEL	New Zealand	18
IDC	Austria	28
ATH	Greece	28
IGIL	Portugal	31
PPT	French Polynesia	34
LDG	France	35
ECX	Mexico	35
BUC	Romania	37
NAO	Norway	44
KNET	Kyrgyzstan	49
BGS	United Kingdom	61
MDD	Spain	69
TIR	Albania	82
NEIC	U.S.A.	100
ISK	Turkey	109
SVSA	Portugal	126
INMG	Portugal	134
DSN	United Arab Emirates	167
BJI	China	167
KEA	Democratic People's Republic of Korea	175
VIE	Austria	250
NDI	India	288
BER	Norway	295
UCC	Belgium	321
IPEC	Czech Republic	328

10

Appendix

10.1 ISC Operational Procedures

10.1.1 Introduction

The relational database at the ISC is the primary source for the ISC Bulletin. This database is also the source for the ISC web-based search, the ISC CD-ROMs and this printed Summary. The ISC database is also mirrored at several institutions such as the Data Management Center of the Incorporated Research Institutions for Seismology (IRIS DMC), Earthquake Research Institute (ERI) of the University of Tokyo and a few others.

The database holds information about ISC events, both natural and anthropogenic. Information on each event may include hypocentre estimates, moment tensors, event type, felt and damaging reports and associated station observations reported by different agencies and grouped together per physical event.

The majority of the ISC events (∼80%) are small and are not reviewed by the ISC analysts. Those that are reviewed (∼20%, usually magnitude greater than 3.5) may or may not include an ISC hypocentre solution and magnitude estimates. The decision depends on whether the wealth of combined information from several agencies as compared to the data of each single agency alone warrants the ISC location. The events are called ISC events regardless of whether they have been reviewed or located by the ISC or not.

All events located by the ISC are reviewed by the ISC analysts but not the other way round. Analyst review involves an examination of the integrity of all reported parametric information. It does not involve review of waveforms. Even if waveforms from all of the ∼6,000 stations included in a typical recent month of the ISC Bulletin were freely available, it would be an unmanageable task to inspect them all.

We shall now describe briefly current processes and procedures involved in producing the Bulletin of the International Seismological Centre. These have been developed from former practices described in the Introduction to earlier issues of the ISC Bulletin to account for modern methods and technologies of data collection and analysis.

10.1.2 Data Collection

Parametric data, mainly comprising seismic event hypocentre solutions, phase arrival observations and associated magnitude data, are now mostly emailed to the ISC (seismo@isc.ac.uk) by agencies around the world. Other macroseismic and source information associated with seismic events may also be incorporated in accordance with modern standards. The process of data collection at the ISC involves the automatic parsing of these data into the ISC relational database. The ISC now has over 200 individual parsers to account for legacy and current bulletin data formats used by data reporters.

Figure 10.1 shows the 313 agencies that have reported bulletin data to the ISC, directly or via regional data centres, during the entire period of the ISC existence: these agencies are also listed in Table 10.2 of the Appendix. In Figure 10.1, corresponding countries are shown shaded in red. Please note that the continent of Antarctica appears white on the map despite a steady stream of bulletin data from Antarctic stations: the agencies that run these stations are based elsewhere.

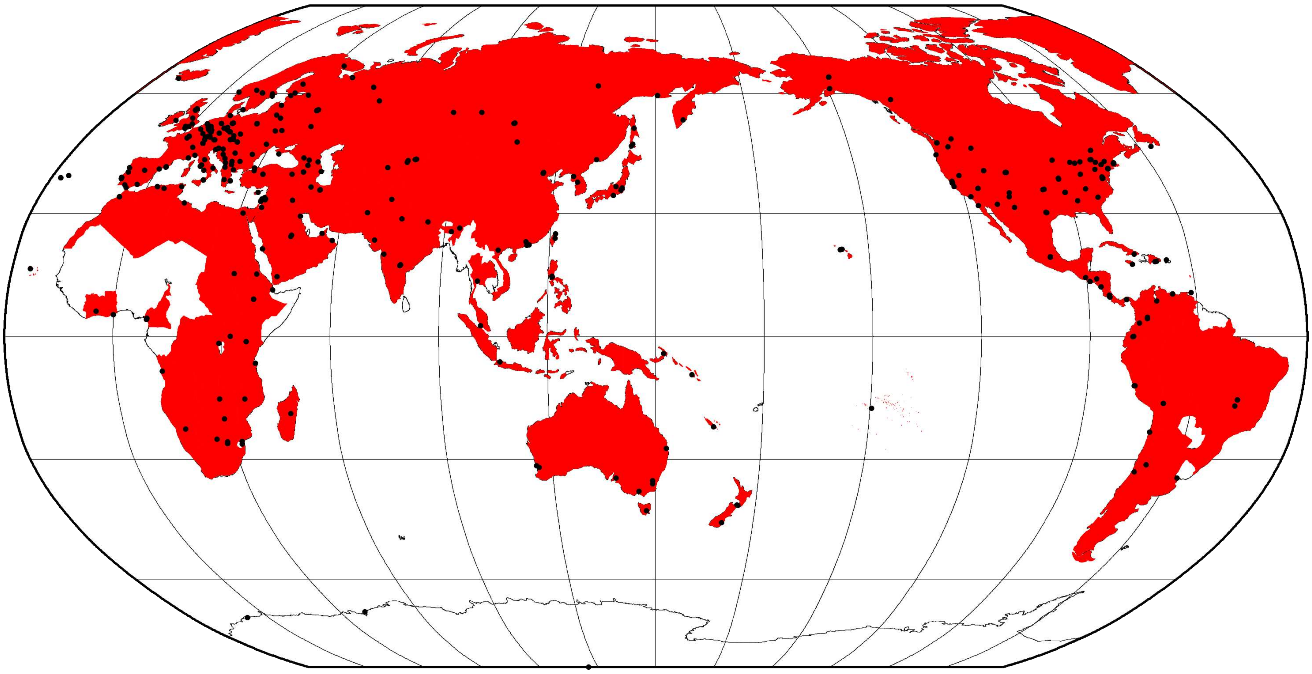

Figure 10.1: *Map of 313 agencies and corresponding countries that have reported seismic bulletin data to the ISC at least once during the entire period of the ISC operations, either directly or via regional data centres. Corresponding countries are shaded in red.*

10.1.3 ISC Automatic Procedures

Grouping

Grouping is the automatic process by which the many hypocentre solutions sent by the agencies reporting to the ISC for the same physical event are merged together into a single ISC event. This process possibly begins with an alert message and ends before a final review by ISC analysts. The process periodically runs through a set time interval of the input data stream, typically one day, looking for hypocentres in newly received data that are not yet grouped into an ISC event. Thus it considers only data more recent than the last data month reviewed by the ISC analysts. Immediately after grouping the seismic arrival associator is run on the same time interval, dealing with new phase arrival data not associated with any hypocentre.

The first stage of grouping gets a score where possible for each hypocentre to determine whether the reported hypocentre will be considered to be the primary estimate, or prime, for an ISC event. This score is based on the station arrival times reported in association with the hypocentre in four epicentral distance zones that characterise the networks of stations reporting:

1. Whole network
2. Local, 0 - 150 km
3. Near-regional, 3° - 10°
4. Teleseismic, 28° - 180°

For each distance zone, the azimuthal gap, the secondary azimuthal gap (the largest azimuthal gap filled by a single station), the minimum and maximum epicentral distance and number of stations are all used to calculate the value of dU, the normalised absolute deviation from best fitting uniformly distributed stations (*Bondár and McLaughlin*, 2009a). Clearly, this procedure can only use:

1. Bulletin data with hypocentres and sufficient associated seismic arrivals
2. Data for stations that are in the International Registry (IR)
3. Station data that are actually reported to ISC: CENC (China), for example, reports at most 24 stations, whilst many more may have been used to determine the hypocentre.

The hypocentres are then each considered in turn for grouping using one of two methods, the first by searching for a similar hypocentre, and the second by searching for the best fit of the reported phase arrival data that are associated with the candidate hypocentre. The method chosen for a reporter is based on feedback gained from ISC analysts.

For finding similar hypocentres, three sets of limits for origin-time difference and epicentral separation are used according to the type of bulletin data, be it alert, provisional or final: these limits are, respectively:

- ± 2 minutes and 10°
- ± 2 minutes and 4°
- ± 1 minutes and 2°

If there is no overlap with the hypocentre of an existing ISC event, a new event is formed. For each candidate hypocentre, a proximity score is otherwise calculated based on differences in time, t, and distance, s, between the candidate hypocentre and a hypocentre in an event with which it could potentially be grouped.

Proximity score $= 2 - (dt/dt_{max}) - (ds/ds_{max})$

where ds_{max} is the maximum distance between hypocentres and dt_{max} the maximum difference in origin time.

As long as there is no duplication of hypocentre (with the same author, origin time and location within tight limits) the candidate hypocentre together with the associated phase data is grouped with the prime hypocentre of the event and the initial dU score is used to reassess the prime hypocentre designation. Apparent duplicated hypocentre estimations, including preliminary solutions relayed by other agencies, need to be assessed to determine whether they should really be split between different events. Should there be two or more equally valid events, these can be assessed in turn and may eventually be merged together.

Grouping by fit of the associated phase arrival data is simpler. The residuals of the arrival data are calculated using ak135 travel times for all suitable prime hypocentres within the widest proximity limits given above for similar hypocentres. The hypocentre and associated phase arrival data is then grouped with the event with the best fitting prime hypocentre, which may similarly be re-designated according to the dU scores. Associations of phase arrival data are updated to be with the prime hypocentre estimate of each ISC event.

It follows that a hypocentre and associated phase arrival data submitted by a reporter will have the reported hypocentre set as the prime hypocentre in the ISC event if no other submitted hypocentre estimate is a closer match. It follows also that a hypocentre submitted without phase data can only be grouped with a similar hypocentre. Generally, early arriving data may be superseded by later arriving data: the data will still be in the ISC database but be deprecated, that is, marked as being no longer useful for further processes.

Association

Association is the automatic procedure, run routinely after grouping, that links reported phase arrivals at IR stations with the prime hypocentres of ISC events. As grouping took care of those phases associated with reported hypocentres, by associating the phases to the respective prime hypocentres of the ISC events without further checks, this procedure is only required for phase arrival observations that were sent without any association of event made for them by the reporter. Currently only 5% of arrival data is sent unassociated compared with 25% ten years ago.

If a phase arrival is found to be very similar to another already reported, it is placed in the same event, otherwise the procedure below is followed.

For associating a phase arrival, suitable events are sought with prime hypocentre origin-times in the window 40 minutes before and 100 s after the arrival time. For each phase arrival and prime hypocentre an ak135 travel-time residual is calculated for either the reported arrival phase name or an alternative from a default list if appropriate. Possible timing errors that are multiples of 60 s (a minute) are considered if the phase arrival is at a station not known to be digitally recording. A reporting likelihood is then determined based on the reported event magnitude: a magnitude default of 3.0 is used if no magnitude is given.

A final score is calculated from the residuals, from the likelihood of the phase observations for the magnitude of the event and from the S-P misfit. A phase arrival along with all other phase arrivals in that reading for the station is then associated with the prime hypocentre with the best score. If no suitable match is found, the reading remains unassociated but may be used at some later stage.

Thresholding

Thresholding is the process determining which events are to be reviewed by the ISC analysts. In former times, before email transmission of data was convenient, all events were reviewed, with magnitudes nearly always 3.5 or above. Nowadays, data contributors are encouraged to send all their data, which are stored in the ISC database. The overwhelming amount of data, including that for many more smaller events and from many more seismograph stations, led to the advent of ISC Comprehensive Bulletin, for all events, and the ISC Reviewed Bulletin, for selected events reviewed by ISC analysts. Thresholding has been under constant review since the start of the 1999 data year.

Several criteria are considered to decide which events merit review. Once a decision is made, whether or not an event is to be reviewed, further criteria are not considered.

In this section, M is the maximum magnitude reported by any agency for the event. The sequence of tests in the automatic decision process for reviewing events is currently:

- All events reported by the International Data Centre (IDC) of the Comprehensive Nuclear-Test-Ban Treaty Organization (CTBTO) are reviewed.
- If M is greater than or equal to 3.5, the event is reviewed.
- If M is less than 2.5, the event is not reviewed.
- If M is unknown, the number of data sources of hypocentres and phase arrivals is used. Care is taken here to avoid counting indirect reports arriving via agencies such as NEIC, CSEM and CASC, which compile regional and global data:
  - If the number of hypocentre authors is greater than two and the maximum epicentral distance of arrival data is greater than 10°, the event is reviewed.
  - If the number of arrival authors is greater than two and the maximum epicentral distance of arrival data is greater than 10°, the event is reviewed.
  - Otherwise the event is not reviewed.
- If M is between 2.5 and 3.5:
  - If the number of hypocentre and seismic arrival authors is less than two, the event is not reviewed.
  - If any bulletin contributing to the event has at least ten stations within 3° and the secondary azimuthal gap (the largest azimuthal gap filled by a single station) is less than 135°, the event is not reviewed.

Location by the ISC

The automatic processes group and associate incoming data into ISC events as indicated above. These data are available to users before review by the ISC analysts but there will be no ISC hypocentre solutions for any of the events. The candidate events due for review by the ISC analysts are determined by the thresholding process, which is why many smaller events remain without an ISC hypocentre solution even after the analyst review.

Several further checks of the data are made in preparation for the analyst review, and initial trial estimates for ISC hypocentres are then generated using the accumulated data. If sufficiently robust, the ISC hypocentre estimation will be retained and be made the prime solution for the event, but this, of course, will itself be subject to the analyst review.

It is important to note that not all reviewed events will have an ISC hypocentre. At least one of the criteria listed below must be met for an initial ISC location of a reviewed event to be made:

- All events with an IDC hypocentre, unless IDC is the only hypocentre author and there are less than six associated phases.
- Two or more reporters of data
- Phase data at epicentral distance $\geq 20°$

The ISC locator also needs an intial seed location; in all events except those with eight or more reporters of data where the existing prime is used, this is calculated using a Neighbourhood Algorithm (NA) (*Sambridge*, 1999; *Sambridge and Kennett*, 2001). More information about the ISC location algorithm and initial seed is given in the next section.

10.1.4 ISC Location Algorithm

The new ISC location algorithm is described in detail in *Bondár and Storchak* (2011) (doi: 10.1111/j.1365-246X.2011.05107.x, Manual www.isc.ac.uk/iscbulletin/iscloc/); here we give a short summary of the major features. Ever since the ISC came into existence in 1964, it has been committed to providing a homogeneous bulletin that benefits scientific research. Hence the location algorithm used by the ISC, except for some minor modifications, has remained largely unchanged for the past 40 years (*Adams et al.*, 1982; *Bolt*, 1960). While the ISC location procedures have served the scientific community well in the past, they can certainly be improved.

Linearised location algorithms are very sensitive to the initial starting point for the location. The old procedures made the assumption that a good initial hypocentre is available among the reported hypocentres. However, there is no guarantee that any of the reported hypocentres are close to the global minimum in the search space. Furthermore, attempting to find a free-depth solution was futile when the data had no resolving power for depth (e.g. when the first arrival is not within the inflection point of the P travel-time curve). When there was no depth resolution, the algorithm would simply pick a point on the origin time – depth trade-off curve. The old ISC locator assumed that the observational errors are independent. The recent years have seen a phenomenal growth both in the number of reported events and phases, owing to the ever-increasing number of stations worldwide. Similar ray paths will produce correlated travel-time prediction errors due to unmodelled heterogeneities in the Earth, resulting in underestimated location uncertainties and for unfavourable network geometries, location bias. Hence, accounting for correlated travel-time prediction errors becomes imperative if we want to improve (or simply maintain) location accuracy as station networks become progressively denser. Finally, publishing network magnitudes that may have been derived from a single station measurement was rather prone to producing erroneous event magnitude estimates.

To meet the challenge imposed by the ever-increasing data volume from heavily unbalanced networks we introduced a new ISC location algorithm to ensure the efficient handling of data and to further improve the location accuracy of events reviewed by the ISC. The new ISC location algorithm

- Uses all ak135 (*Kennett et al.*, 1995) predicted phases (including depth phases) in the location;
- Obtains the initial hypocentre guess via the Neighbourhood Algorithm (NA) (*Sambridge*, 1999; *Sambridge and Kennett*, 2001);
- Performs iterative linearised inversion using an *a priori* estimate of the full data covariance matrix to account for correlated model errors (*Bondár and McLaughlin*, 2009b);
- Attempts a free-depth solution if and only if there is depth resolution, otherwise it fixes the depth to a region-dependent default depth;
- Scales uncertainties to 90% confidence level and calculates location quality metrics for various distance ranges;
- Obtains a depth-phase depth estimate based on reported surface reflections via depth-phase stacking (*Murphy and Barker*, 2006);
- Provides robust network magnitude estimates with uncertainties.

Seismic Phases

One of the major advantages of using the ak135 travel-time predictions (*Kennett et al.*, 1995) is that they do not suffer from the baseline difference between P, S and PKP phases compared with the Jeffreys-Bullen tables (*Jeffreys and Bullen*, 1940). Furthermore, ak135 offers an abundance of phases from the IASPEI Standard Seismic List (*Storchak et al.*, 2003; 2011) that can be used in the location, most notably the PKP branches and depth-sensitive phases. Elevation and ellipticity corrections (*Dziewonski and Gilbert*, 1976; *Engdahl et al.*, 1998; *Kennett et al.*, 1996), using the WG84 ellipsoid parameters, are added to the ak135 predictions. For depth phases, bounce point (elevation correction at the surface reflection point) and water depth (for pwP) corrections are calculated using the algorithm of *Engdahl et al.* (1998). We use the ETOPO1 global relief model (*Amante and Eakins*, 2009) to obtain the elevation or the water depth at the bounce point.

Phase picking errors are described by *a priori* measurement error estimates derived from the inspection of the distribution of ground truth residuals (residuals calculated with respect to the ground truth location) from the IASPEI Reference Event List (*Bondár and McLaughlin*, 2009a). For phases that do not have a sufficient number of observations in the ground truth database we establish *a priori* measurement errors so that the consistency of the relative weighting schema is maintained. First-arriving P-type phases (P, Pn, Pb, Pg) are picked more accurately than later phases, so their measurement error estimates are the smallest, 0.8 s. The measurement error for first-arriving S-phases (S, Sn, Sb, Sg) is set to 1.5 s.

Phases traversing through or reflecting from the inner/outer core of the Earth have somewhat larger (1.3 s for PKP, PKS, PKKP, PKKS and P'P' branches as well as PKiKP, PcP and PcS, and 1.8 s for SKP, SKS, SKKP, SKKS and S'S' branches as well as SKiKP, ScP and ScS) measurement error estimates to account for possible identification errors among the various branches. Free-surface reflections and conversions (PnPn, PbPb, PgPg, PS, PnS, PgS and SnSn, SbSb, SgSg, SP, SPn, SPg) are observed less frequently and with larger uncertainty, and therefore suffer from large, 2.5 s, measurement errors. Similarly, a measurement error of 2.8 s is assigned to the longer period and typically emergent diffracted phases (Pdif, Sdif, PKPdif). The *a priori* measurement error for the commonly observed depth phases (pP, sP, pS, sS and pwP) is set to 1.3 s, while the remaining depth phases (pPKP, sPKP, pSKS, sSKS branches and pPb, sPb, sSb, pPn, sPn, sSn) have the measurement error estimate set to 1.8 s. We set the measurement error estimate to 2.5 s for the less reliable depth phases (pPg, sPg, sSg, pPdif, pSdif, sPdif and sSdif). Note that we also allow for distance-dependent measurement errors. For instance, to account for possible phase identification errors at far-regional distances the *a priori* measurement error for Pn and P is increased from 0.8 s to 1.2 s and for Sn and S from 1.5 s to 1.8 s between 15° and 28°. The measurement errors between 40° and 180° are set to 1.3 s and 1.8 s for the prominent PP and SS arrivals respectively, but they are increased to 1.8 s and 2.5 s between 25° and 40°.

The relative weighting scheme (Figure 10.2) described above ensures that arrivals picked less reliably or prone to phase identification errors are down-weighted in the location algorithm. Since the ISC works with reported parametric data with wildly varying quality, we opted for a rather conservative set of *a priori* measurement error estimates.

Correlated Travel-Time Prediction Error Structure

Most location algorithms, either linearised or non-linear, assume that all observational errors are independent. This assumption is violated when the separation between stations is less than the scale length of local velocity heterogeneities. When correlated travel-time prediction errors are present, the data covariance matrix is no longer diagonal, and the redundancy in the observations reduces the effective number of degrees of freedom. Thus, ignoring the correlated error structure inevitably results in underestimated location uncertainty estimates. For events located by an unbalanced seismic network this may also lead to a biased location estimate. *Chang et al.* (1983) demonstrated that accounting for correlated error structure in a linearised location algorithm is relatively straightforward once an estimate of the non-diagonal data covariance matrix is available. To determine the data covariance matrix we follow the approach described by *Bondár and McLaughlin* (2009b). They assume that the similarity between ray paths is well approximated by the station separation. This simplifying assumption allows for the estimation of covariances between station pairs from a generic P variogram model derived from ground truth residuals. Because the overwhelming number of phases in the ISC Bulletin is teleseismic P, we expect that the generic variogram model will perform reasonably well anywhere on the globe.

Since in this representation the covariances depend only on station separations, the covariance matrix (and its inverse) needs to be calculated only once. We assume that different phases owing to the different ray paths they travel along as well as station pairs with a separation larger than 1000 km are uncorrelated. Hence, the data covariance matrix is a sparse, block-diagonal matrix. Furthermore, if the stations in each phase block are ordered by their nearest neighbour distance, the phase blocks themselves become

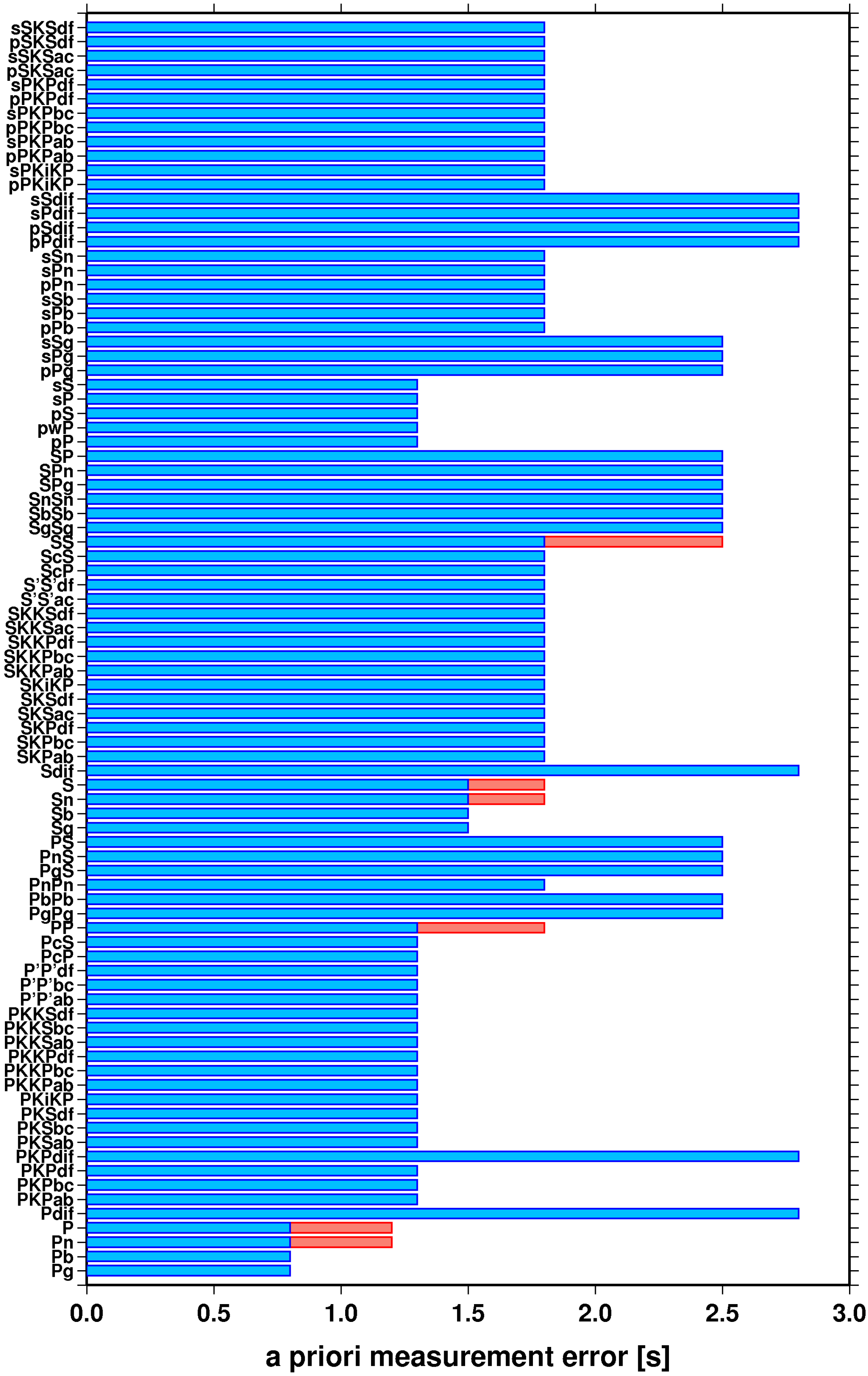

Figure 10.2: A priori *measurement error estimates for phases used in the location algorithm. The red coloured errors are distance-dependent, which are applied for distances when phase identification errors may occur (see text).*

block-diagonal. To reduce the computational time of inverting large matrices we exploit the inherent block-diagonal structure by inverting the covariance matrix block-by-block. The *a priori* measurement error variances are added to the diagonal of the data covariance matrix.

Depth Resolution

In principle, depth can be resolved if there is a mixture of upgoing and downgoing waves emanating from the source, that is, if there are stations covering the distance range where the vertical partial derivative of the travel-time of the first-arriving phase changes sign (local networks), or if there are phases with vertical slowness of opposite sign (depth phases). Core reflections, such as PcP, and to a lesser extent, secondary phases (S in particular) could also help in resolving the depth.

We developed a number of criteria to test whether the reported data for an event have sufficient depth resolution:

- local network: one or more stations within 0.2° with time-defining phases
- depth phases: five or more time-defining depth phases reported by at least two agencies (to reduce a chance of misinterpretation by a single inexperienced analyst)
- core reflections: five or more time-defining core reflections (PcP, ScS) reported by at least two agencies
- local/near regional S: five or more time-defining S and P pairs within 3°

We attempt a free-depth solution if any of the above criteria are satisfied; otherwise we fix the depth to a default depth dependent on the epicentre location. This will preferably be the grid depth based on the ISC default depth grid (Figure 10.3). Where no grid depth is available the default depth is set to either 10 km or 35 km based on the GRN (See Figure 10.4. A list of GRN's can be found in Section 10.2.2). The default depth grid was derived from the EHB (*Engdahl et al.*, 1998) free-depth solutions, including the fixed-depth EHB earthquakes that were flagged as having reliable depth estimate (personal communication with Bob Engdahl), as well as from free-depth solutions obtained by the new locator when locating the entire ISC Bulletin data-set. As Figure 10.3 indicates, the default depth grid provides a reasonable depth estimate where seismicity is well established. Note that the depths of known anthropogenic events and landslides are fixed to the surface.

Depth-Phase Stack

While we use depth phases directly in the location, the depth-phase stacking method (*Murphy and Barker*, 2006) provides an independent means to obtain robust depth estimates. Because the depth obtained from the depth-phase stacking method implicitly depends on the epicentre itself, we perform the depth-phase stack only twice: first, with respect to the initial location in order to obtain a reasonable starting point for the depth in the grid search described in the following section; second, with respect to the final location to obtain the final estimate for the depth-phase constrained depth.

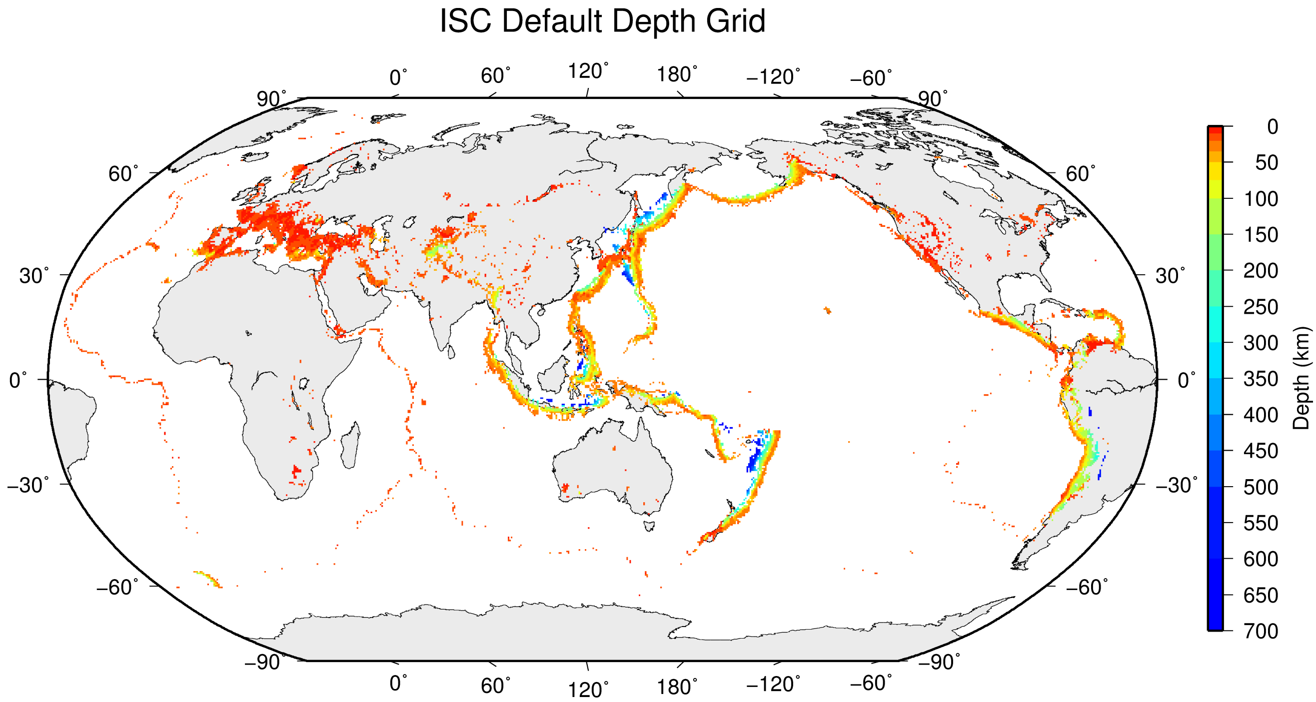

Figure 10.3: *Default depths on a 0.5×0.5 degree grid derived from EHB free-depth solutions and EHB events flagged as reliable depth, as well as free-depth solutions from the entire ISC Bulletin located with the new locator.*

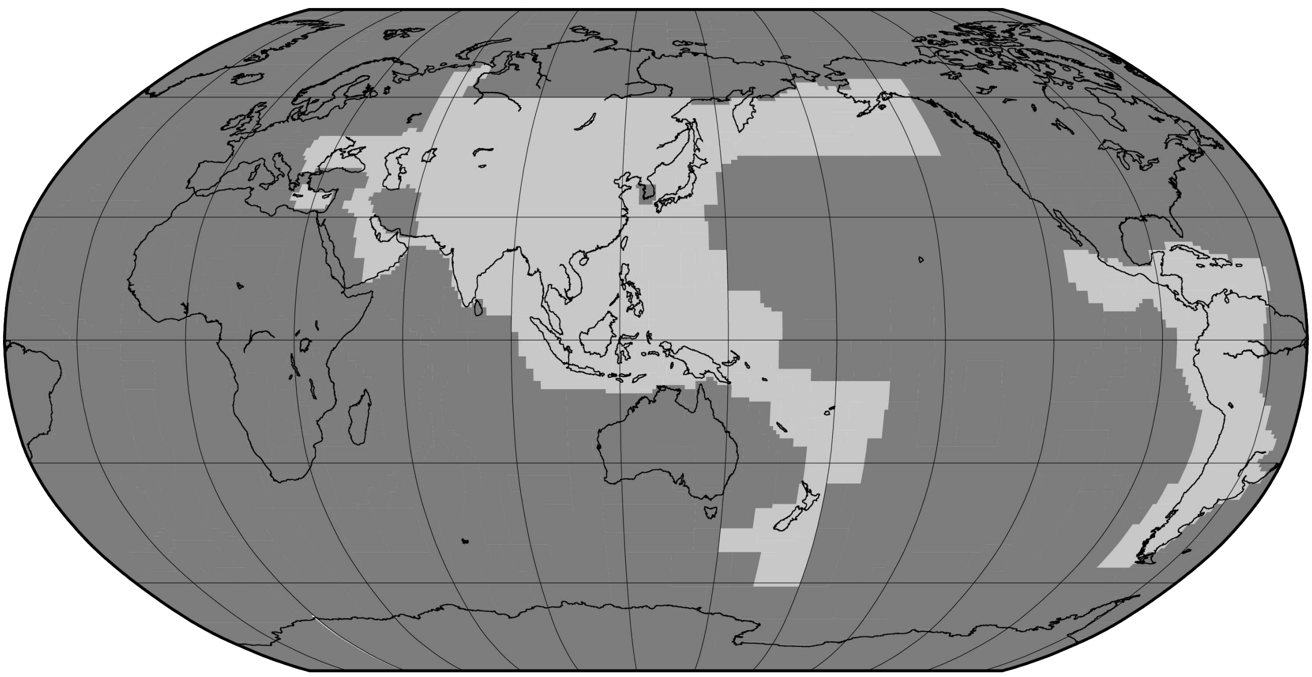

Figure 10.4: *Default depths by Flinn-Engdahl geographic regions. Dark grey regions are set to 10 km and light grey to 35 km*

Initial Hypocentre

For poorly recorded events the reported hypocentres may exhibit a large scatter and they could suffer from large location errors, especially if they are only recorded teleseismically. In order to obtain a good initial hypocentre guess for the linearised location algorithm we employ the Neighbourhood Algorithm (NA) (*Sambridge*, 1999; *Sambridge and Kennett*, 2001). NA is a nonlinear grid search method capable of exploring a large search space and rapidly closing in on the global optimum. *Kennett* (2006) discusses in detail the NA algorithm and its use for locating earthquakes.

We perform a search around the median of reported hypocentre parameters with a generously defined search region – within a 2° radius circle around the median epicentre, 10 s around the median origin time and 150 km around the median reported depth. These default search parameters were obtained by trial-and-error runs to achieve a compromise between execution time and allowance for gross errors in the median reported hypocentre parameters. Note that if our test for depth resolution fails, we fix the depth to the region-dependent default depth. The initial hypocentre estimate will be the one with the smallest L1-norm misfit among the NA trial hypocentres. Once close to the global optimum, we proceed with the linearised location algorithm to obtain the final solution and corresponding formal uncertainties.

Iterative Linearised Location Algorithm

We adopt the location algorithm described in detail in *Bondár and McLaughlin* (2009b). Recall that in the presence of correlated travel-time prediction errors the data covariance matrix is no longer diagonal. Using the singular value decomposition of the data covariance matrix we construct a projection matrix that orthogonalises the data set and projects redundant observations into the null space. In other words, we solve the inversion problem in the eigen coordinate system in which the transformed observations are independent.

The model covariance matrix yields the four-dimensional error ellipsoid whose projections provide the two-dimensional error ellipse and one-dimensional errors for depth and origin time. These uncertainties are scaled to the 90% confidence level. Note that since we projected the system of equations into the eigen coordinate system, the number of independent observations is less than the total number of observations. Hence, the estimated location error ellipses necessarily become larger, providing a more realistic representation of the location uncertainties. The major advantage of this approach is that the projection matrix is calculated only once for each event location.

Validation Tests

To demonstrate improvements due to the new location procedures, we located some 7,200 GT0-5 events in the IASPEI Reference Event List (*Bondár and McLaughlin*, 2009a) both with the old ISC locator (which constitutes the baseline) and with the new location algorithm. We also located the entire (1960-2010) ISC Bulletin, including four years of the International Seismological Summary (ISS, the predecessor of the ISC) catalogue (*Villaseñor and Engdahl*, 2005; 2007).

The location of GT events demonstrated that the new ISC location algorithm provides small but consistent location improvements, considerable improvements in depth determination and significantly more accurate formal uncertainty estimates. Even using a 1-D model and a variogram model that fits teleseismic observations we could achieve realistic uncertainty estimates, as the 90% confidence error ellipses cover the true locations 80-85% of the time. The default depth grid provides reasonable depth estimates where there is seismicity. We have shown that the location and depth accuracy obtained by the new algorithm matches or surpasses the EHB accuracy.

We noted above that the location improvements for the ground truth events are consistent, but minor. This is not surprising as most of the events in the IASPEI Reference Event List are very well-recorded with a small azimuthal gap and dominated by P-type phases. In these circumstances we could expect significant location improvements only for heavily unbalanced networks where large numbers of correlated ray paths conspire to introduce location bias. On the other hand, the ISC Bulletin represents a plethora of station configurations ranging from reasonable to the most unfavourable network geometries. Hence, we could expect more dramatic location improvements when locating the entire ISC Bulletin. Although in this case we cannot measure the improvement in location accuracy due to the lack of ground truth information, we show that with the new locator we obtain significantly better clustering of event locations (Figure 10.5), thus providing an improved view of the seismicity of the Earth.

Magnitude Calculation

Currently the ISC locator calculates body and surface wave magnitudes. MS is calculated for shallow events (depth $<$ 60 km) only. At least three station magnitudes are required for a network (mb or MS) magnitude. The network magnitude is defined as the median of the station magnitudes, and its uncertainty is defined as the standard median absolute deviation (SMAD) of the alpha-trimmed (*alpha* $=$ 20%) station magnitudes.

The station magnitude is defined as the median of reading magnitudes for a station. The reading magnitude is defined as the magnitude computed from the maximal log(A/T) in a reading. Amplitude magnitudes are calculated for each reported amplitude-period pair.

Body-Wave Magnitudes

Body-wave magnitudes are calculated for each reported amplitude-period pair, provided that the phase is in the list of phases that can contribute to mb (P, pP, sP, AMB, IAmb, pmax), the station is between the epicentral distances $21 - 100°$ and the period is less than 3 s.

A reading contains all parametric data reported by a single agency for an event at a station, and it may have several reported amplitude and periods. The amplitudes are measured as zero-to-peak values in nanometres. For each pair an amplitude mb is calculated.

$$mb_{amp} = log(A/T) + Q(\Delta, h) - 3 \tag{10.1}$$

If no amplitude-period pairs are reported for a reading, the body-wave magnitude is calculated using the reported logat values for $log(A/T)$.

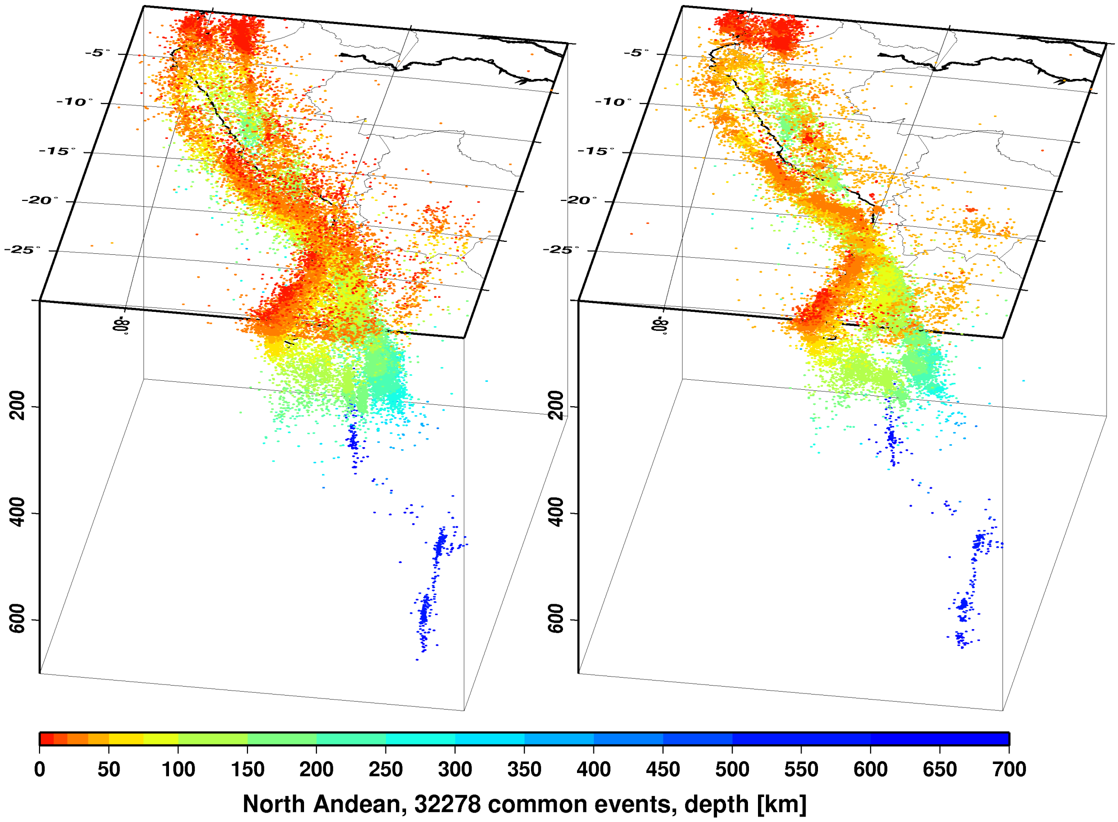

(a)

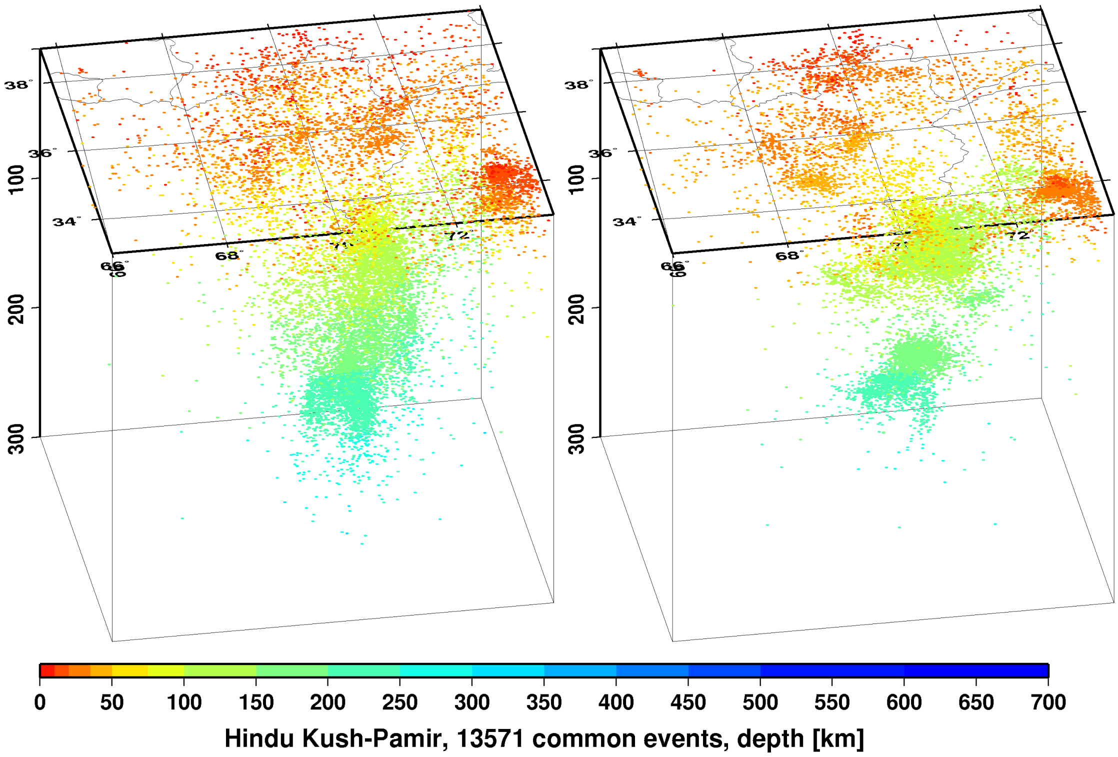

(b)

Figure 10.5: *Comparison of seismicity maps for common events in the reviewed ISC Bulletin (old locator, left) and the located ISC Bulletin (new locator, right) for the North Andean (a) and Hindu Kush - Pamir regions (b). The events are better clustered when located with the new locator.*

$$mb_{amp} = logat + Q(\Delta, h) - 3 \tag{10.2}$$

where the magnitude attenuation $Q(\Delta, h)$ value is calculated using the Gutenberg-Richter tables (*Gutenberg and Richter*, 1956).

For each reading the ISC locator finds the reported amplitude-period pair for which A/T is maximal:

$$mb_{rd} = log(max(A/T)) + Q(\Delta, h) - 3 \tag{10.3}$$

Or, if no amplitude-period pairs were reported for the reading:

$$mb_{rd} = max(logat) + Q(\Delta, h) - 3 \tag{10.4}$$

Several agencies may report data from the same station. The station magnitude is defined as the median of the reading magnitudes for a station.

$$mb_{sta} = median(mb_{rd}) \tag{10.5}$$

Once all station mb values are determined, the station magnitudes are sorted and the lower and upper alpha percentiles are made non-defining. The network mb and its uncertainty are then calculated as the median and the standard median absolute deviation (SMAD) of the alpha-trimmed station magnitudes, respectively.

Surface-Wave Magnitudes

Surface-wave magnitudes are calculated for each reported amplitude-period pair, provided that the phase is in the list of phases that can contribute to MS (*AMS, IAMs_20, LR, MLR, M, L*), the station is between the epicentral distances $20 - 160°$ and the period is between $10 - 60$ s.

For each reported amplitude-period pair MS is calculated using the Prague formula (*Vaněk et al.*, 1962). Amplitude MS is calculated for each component (Z, E, N) separately.

$$MS_{amp} = log(A/T) + 1.66 * log(\Delta) + 0.3 \tag{10.6}$$

To calculate the reading MS, the ISC locator first finds the reported amplitude-period pair for which A/T is maximal on the vertical component.

$$MS_Z = log(max(A_Z/T_Z)) + 1.66 * log(\Delta) + 0.3 \tag{10.7}$$

Then it finds the max(A/T) for the E and N components for which the period measured on the horizontal components is within ±5s from the period measured on the vertical component.

$$MS_E = log(max(A_E/T_E)) + 1.66 * log(\Delta) + 0.3 \tag{10.8}$$

$$MS_N = log(max(A_N/T_N)) + 1.66 * log(\Delta) + 0.3 \tag{10.9}$$

The horizontal MS is calculated as

$$max(A/T)h = \begin{cases} \sqrt{2(max(A_E/T_E))^2} & \text{if } MS_N \text{ does not exist} \\ \sqrt{(max(A_E/T_E))^2 + (max(A_N/T_N))^2} & \text{if } MS_E \text{ and } MS_N \text{ exist} \\ \sqrt{2(max(A_N/T_N))^2} & \text{if } MS_E \text{ does not exist} \end{cases} \tag{10.10}$$

$$MS_H = log(max(A/T)_H) + 1.66 * log(\Delta) + 0.3 \tag{10.11}$$

The reading MS is defined as

$$MS = \begin{cases} (MS_Z + MS_H)/2 & \text{if } MS_Z \text{ and } MS_H \text{ exist} \\ MS_H & \text{if } MS_Z \text{ does not exist} \\ MS_Z & \text{if } MS_H \text{ does not exist} \end{cases} \tag{10.12}$$

Several agencies may report data from the same station. The station magnitude is defined as the median of the reading magnitudes for a station.

$$MS_{sta} = median(MS_{rd}) \tag{10.13}$$

Once all station MS values are determined, the station magnitudes are sorted and the lower and upper alpha percentiles are made non-defining. The network MS and its uncertainty are calculated as the median and the standard median absolute deviation (SMAD) of the alpha-trimmed station magnitudes, respectively.

10.1.5 Review Process

Typically, for each month, the ISC analysts now review approximately 10-20% of the events in the ISC database, currently 3,500-5,000 per data month. This review is done about 24 months behind real time to allow for the comprehensive collection of data from networks and data centres worldwide.

Users of the ISC Bulletin can be assured that all ISC Bulletin events with an ISC hypocentre solution have been reviewed by the ISC analysts. Not all reviewed events will end up having an ISC hypocentre solution, but events that have not been reviewed are flagged accordingly.

At the beginning of analysis of each data month, events that need to be reviewed by an analyst are flagged based on the thresholding procedure described in Section 10.1.3. These events are split into daily blocks on average consisting of $100 - 150$ to events. They are then analysed and if necessary edited by an analyst. After all blocks in a data month have been reviewed, they are being assessed again by a different analyst to spot any potential inconsistencies that might have been overlooked in the first run.

Analysis is done with the help of the Visual Bulletin Analysis System (VBAS) developed at ISC. For each event it shows the reported hypocentres, magnitudes and phase arrivals as well as an ISC solution for the hypocentre, if there is one, along with phase arrival-time residuals and error estimates. Amongst other visual aids, VBAS plots graphs of travel time curves, seismicity maps, depth distributions of reported hypocentres and station geometry.

The analysts have the capability to execute a variety of commands that can be used to merge or split events, to move phase arrivals or hypocentres from one event to another or to modify the reported phase names. There are also several commands to change the starting depth or location in the location algorithm.

The main tasks in reviewing the ISC Bulletin are to:

1. Check that the grouping of hypocentres and association of phase arrivals is appropriate.
2. Check that the depth and location is appropriate for the region and reported phase arrivals.
3. Check that no data are missing for an event, given the region and magnitude, and that included data are appropriate.
4. Examine the phase arrival-time residuals to check that the ISC hypocentre solution is appropriate.
5. Look for outliers in the observations and for misassociated phases.
6. Check that the azimuthal coverage for ISC hypocentres is at least 45 deg.

As well as examining each event closely, it is also important to scan the hypocentres and phase arrivals of adjacent events, close in time and space, to ensure that there is uniformity in the composition of the events. In some cases, two events should be merged into one event, as apparent in some other case. In other cases, one apparent event needs to be split into two events, when the automatic grouping has erroneously created one event with more than one reported hypocentre out of the observations for two real events that are distinct but closely occurring.

Misassociated phase arrivals are returned to the unassociated data stream, if not immediately placed by the analyst in another event where they belong, These unassociated phases are then available to be associated with some other event if the time and location is appropriate. The analysts also check that no phase is associated to more than one event.

Towards the end of the monthly analysis, the ISC 'Search' procedure runs, attempting to build events from the remaining set of unassociated phase arrivals. The algorithm is based on the methodology of *Engdahl and Gunst* (1966). Candidate events are validated or rejected by attempting to find ISC hypocentres for them using the ISC locator. The surviving events are then reviewed. Those events with phase arrival observations reported by stations from at least two networks are added to the ISC Bulletin if the solutions meet the standards set by the ISC analysts. These events have only an ISC determination of hypocentre.

At the end of analysis for a data month, a set of final checks is run for quality control, with the results reviewed by an analyst and the defects rectified. These are checks for inconsistencies and errors to ensure the general integrity of the ISC Bulletin.

10.1.6 Probabilistic Point Source Model (ISC-PPSM)

From data month January 2019 we have begun routinely calculating the earthquake moment tensor, source time function (STF) and depth for moderate magnitude (M_W 5.8 – 7.2) earthquakes. The resulting catalogue is refered to as ISC-PPSM (International Seismological Centre - Probabilistic Point Source Model). This point source calculation is performed using a Bayesian inversion technique based on the methods proposed by *Stähler and Sigloch* (2014; 2016). There are three main purposes of the ISC-PPSM catalogue:

1. Quantifying the uncertainties in the earthquake moment tensor.
2. Providing new constraints on the earthquake STF, along with full error estimation.
3. Adding new depth resolution, especially for relatively shallow ($<$ 40 km depth) moderate magnitude earthquakes, where surface reflected depth phases are subsumed into the earthquake STF.

The first purpose is motivated by the range of moment tensor solutions that can be reported by different agencies or methods for the same earthquake (e.g., *Lentas et al.* (2019)). It is clear that given the variability in the data and methods these different earthquake mechanisms may not be reconciled in all cases. Instead, we aim to quantify the full range of plausible earthquake mechanisms for a given event.

The second role of the ISC-PPSM catalogue is to provide new parameterised estimates of the earthquake STF. By parameterising the STF, we allow the range of plausible STFs to be assessed, but also reduce the sensitivity to near source reverberations (such as water depth phases). It is hoped that this will provide a new resource for full waveform tomographic studies, as well as earthquake physics studies.

Thirdly, and of most significance to the wider ISC operations, ISC-PPSM offers new depth resolution for remote shallow moderate magnitude earthquakes, where the depth of an ISC hypocentre would otherwise be fixed to a default or grid depth (e.g., *Bondár and Storchak* (2011)). As ISC-PPSM solves for both the earthquake depth and STF, the tradeoffs between depth and STF length are directly addressed. In cases where no free depth solution is possible, the ISC-PPSM depth can be fixed to by an analyst during the review process.

To allow the ISC-PPSM depth to be used in the main ISC review process, we calculate preliminary ISC-PPSM results ahead of the review process. For the preliminary ISC-PPSM result, the earthquake latitude and longitude are fixed to the USGS-PDE epicenter. After the main ISC review process, we recalculate the ISC-PPSM solution at the location of the reviewed ISC epicenter. After checking that the revised ISC-PPSM depths are consistent with any earthquake depths that were fixed to preliminary ISC-PPSM, we publish the revised ISC-PPSM solution. If the depths are not consistent to within 1 km, we relocate the ISC hypocentre at the revised ISC-PPSM depth.

10.1.7 History of Operational Changes

The following operational changes are listed here for historical archiving purpose. Some of them have effectively become irrelevant as a result of further changes.

- From data-month January 2001 onwards, both P and S groups of arrival times are used in location.
- From data-month September 2002 onwards, the printed ISC Bulletins have been generated directly from the ISC Relational Database.
- From data-month October 2002, a new location program ISCloc has been used in operations. Also, the IASPEI standard phase list has now been adopted by the ISC. Please see Section 10.2.1 for details.
- From data-month January 2003 onwards, an updated regionalisation scheme has been adopted (*Young et al.*, 1996).
- From data-month January 2006 the ISC hypocentres are computed using the *ak135* earth velocity model (*Kennett et al.*, 1995) and then reviewed by ISC seismologists. The ISC still produces the hypocentre solutions based on Jeffreys-Bullen travel time tables (agency code ISCJB), yet these solutions are no longer reviewed.

  Currently, the ISC is re-computing the entire ISC Bulletin as part of the Rebuild Project using *ak135* and the new location program (Section 10.1.4) in order to assure homogeneity and consistency of the data in the ISC Bulletin.
- From data-month January 2009, a new location program (*Bondár and Storchak*, 2011) has been used in operations. The new program uses all predicted *ak135* phases and accounts for correlated model errors. An overview of the location algorithm is provided in this volume (Section 10.1.4).
- As of February 2020, the ISC Bulletin for the period 1964-2010 has been completely rebuilt (*Storchak et al.*, 2017; 2020): all ISC hypocentres and magnitude have been recalculated using the algorithm by *Bondár and Storchak* (2011); many new previously unavailable datasets added based on extensive international correspondence with networks, data centres, temporary deployment managers and individual researchers; the Bulletin has been cleaned from phantom and poorly constrained events; many station readings have been added or corrected.

10.2 IASPEI Standards

10.2.1 Standard Nomenclature of Seismic Phases

The following list of seismic phases was approved by the IASPEI Commission on Seismological Observation and Interpretation (CoSOI) and adopted by IASPEI on 9th July 2003. More details can be found in *Storchak et al.* (2003) and *Storchak et al.* (2011). Ray paths for some of these phases are shown in Figures 10.6–10.11.

Crustal Phases	
Pg	At short distances, either an upgoing P wave from a source in the upper crust or a P wave bottoming in the upper crust. At larger distances also, arrivals caused by multiple P-wave reverberations inside the whole crust with a group velocity around 5.8 km/s.
Pb	Either an upgoing P wave from a source in the lower crust or a P wave bottoming in the lower crust (alt: P*)

Pn	Any P wave bottoming in the uppermost mantle or an upgoing P wave from a source in the uppermost mantle
PnPn	Pn free-surface reflection
PgPg	Pg free-surface reflection
PmP	P reflection from the outer side of the Moho
PmP*N*	PmP multiple free surface reflection; *N* is a positive integer. For example, PmP2 is PmPPmP.
PmS	P to S reflection/conversion from the outer side of the Moho
Sg	At short distances, either an upgoing S wave from a source in the upper crust or an S wave bottoming in the upper crust. At larger distances also, arrivals caused by superposition of multiple S-wave reverberations and SV to P and/or P to SV conversions inside the whole crust.
Sb	Either an upgoing S wave from a source in the lower crust or an S wave bottoming in the lower crust (alt: S*)
Sn	Any S wave bottoming in the uppermost mantle or an upgoing S wave from a source in the uppermost mantle
SnSn	Sn free-surface reflection
SgSg	Sg free-surface reflection
SmS	S reflection from the outer side of the Moho
SmS*N*	SmS multiple free-surface reflection; *N* is a positive integer. For example, SmS2 is SmSSmS.
SmP	S to P reflection/conversion from the outer side of the Moho
Lg	A wave group observed at larger regional distances and caused by superposition of multiple S-wave reverberations and SV to P and/or P to SV conversions inside the whole crust. The maximum energy travels with a group velocity of approximately 3.5 km/s
Rg	Short-period crustal Rayleigh wave

Mantle Phases

P	A longitudinal wave, bottoming below the uppermost mantle; also an upgoing longitudinal wave from a source below the uppermost mantle
PP	Free-surface reflection of P wave leaving a source downward
PS	P, leaving a source downward, reflected as an S at the free surface. At shorter distances the first leg is represented by a crustal P wave.
PPP	Analogous to PP
PPS	PP which is converted to S at the second reflection point on the free surface; travel time matches that of PSP
PSS	PS reflected at the free surface
PcP	P reflection from the core-mantle boundary (CMB)
PcS	P converted to S when reflected from the CMB
PcP*N*	PcP reflected from the free surface *N* - 1 times; *N* is a positive integer. For example PcP2 is PcPPcP.
P*z*+P	(alt: P*z*P) P reflection from outer side of a discontinuity at depth *z*; *z* may be a positive numerical value in km. For example, P660+P is a P reflection from the top of the 660 km discontinuity.
P*z*-P	P reflection from inner side of a discontinuity at depth *z*. For example, P660-P is a P reflection from below the 660 km discontinuity, which means it is precursory to PP.
P*z*+S	(alt:P*z*S) P converted to S when reflected from outer side of discontinuity at depth *z*
P*z*-S	P converted to S when reflected from inner side of discontinuity at depth *z*
PScS	P (leaving a source downward) to ScS reflection at the free surface
Pdif	P diffracted along the CMB in the mantle (old: Pdiff)
S	Shear wave, bottoming below the uppermost mantle; also an upgoing shear wave from a source below the uppermost mantle
SS	Free-surface reflection of an S wave leaving a source downward
SP	S, leaving a source downward, reflected as P at the free surface. At shorter distances the second leg is represented by a crustal P wave.
SSS	Analogous to SS

SSP	SS converted to P when reflected from the free surface; travel time matches that of SPS
SPP	SP reflected at the free surface
ScS	S reflection from the CMB
ScP	S converted to P when reflected from the CMB
ScS*N*	ScS multiple free-surface reflection; *N* is a positive integer. For example ScS2 is ScSScS.
S*z*+S	S reflection from outer side of a discontinuity at depth *z*; *z* may be a positive numerical value in km. For example S660+S is an S reflection from the top of the 660 km discontinuity. (alt: S*z*S)
S*z*-S	S reflection from inner side of discontinuity at depth *z*. For example, S660-S is an S reflection from below the 660 km discontinuity, which means it is precursory to SS.
S*z*+P	(alt: S*z*P) S converted to P when reflected from outer side of discontinuity at depth *z*
S*z*-P	S converted to P when reflected from inner side of discontinuity at depth *z*
ScSP	ScS to P reflection at the free surface
Sdif	S diffracted along the CMB in the mantle (old: Sdiff)

Core Phases

PKP	Unspecified P wave bottoming in the core (alt: P')
PKPab	P wave bottoming in the upper outer core; ab indicates the retrograde branch of the PKP caustic (old: PKP2)
PKPbc	P wave bottoming in the lower outer core; bc indicates the prograde branch of the PKP caustic (old: PKP1)
PKPdf	P wave bottoming in the inner core (alt: PKIKP)
PKPpre	A precursor to PKPdf due to scattering near or at the CMB (old: PKhKP)
PKPdif	P wave diffracted at the inner core boundary (ICB) in the outer core
PKS	Unspecified P wave bottoming in the core and converting to S at the CMB
PKSab	PKS bottoming in the upper outer core
PKSbc	PKS bottoming in the lower outer core
PKSdf	PKS bottoming in the inner core
P'P'	Free-surface reflection of PKP (alt: PKPPKP)
P'N	PKP reflected at the free surface N - 1 times; N is a positive integer. For example, P'3 is P'P'P'. (alt: PKPN)
P'z-P'	PKP reflected from inner side of a discontinuity at depth z outside the core, which means it is precursory to P'P'; z may be a positive numerical value in km
P'S'	(alt: PKPSKS) PKP converted to SKS when reflected from the free surface; other examples are P'PKS, P'SKP
PS'	P (leaving a source downward) to SKS reflection at the free surface (alt: PSKS)
PKKP	Unspecified P wave reflected once from the inner side of the CMB
PKKPab	PKKP bottoming in the upper outer core
PKKPbc	PKKP bottoming in the lower outer core
PKKPdf	PKKP bottoming in the inner core
PNKP	P wave reflected N - 1 times from inner side of the CMB; N is a positive integer.
PKKPpre	A precursor to PKKP due to scattering near the CMB
PKiKP	P wave reflected from the inner core boundary (ICB)
PKNIKP	P wave reflected N - 1 times from the inner side of the ICB
PKJKP	P wave traversing the outer core as P and the inner core as S
PKKS	P wave reflected once from inner side of the CMB and converted to S at the CMB
PKKSab	PKKS bottoming in the upper outer core
PKKSbc	PKKS bottoming in the lower outer core
PKKSdf	PKKS bottoming in the inner core
PcPP'	PcP to PKP reflection at the free surface; other examples are PcPS', PcSP', PcSS', PcPSKP, PcSSKP. (alt: PcPPKP)
SKS	unspecified S wave traversing the core as P (alt: S')
SKSac	SKS bottoming in the outer core
SKSdf	SKS bottoming in the inner core (alt: SKIKS)
SPdifKS	SKS wave with a segment of mantleside Pdif at the source and/or the receiver side of the ray path (alt: SKPdifS)
SKP	Unspecified S wave traversing the core and then the mantle as P
SKPab	SKP bottoming in the upper outer core
SKPbc	SKP bottoming in the lower outer core
SKPdf	SKP bottoming in the inner core
S'S'	Free-surface reflection of SKS (alt: SKSSKS)
S'N	SKS reflected at the free surface N - 1 times; N is a positive integer
S'z-S'	SKS reflected from inner side of discontinuity at depth z outside the core, which means it is precursory to S'S'; z may be a positive numerical value in km.
S'P'	(alt: SKSPKP) SKS converted to PKP when reflected from the free surface; other examples are S'SKP, S'PKS.
S'P	(alt: SKSP) SKS to P reflection at the free surface
SKKS	Unspecified S wave reflected once from inner side of the CMB
SKKSac	SKKS bottoming in the outer core
SKKSdf	SKKS bottoming in the inner core
SNKS	S wave reflected N - 1 times from inner side of the CMB; N is a positive integer.

SKiKS	S wave traversing the outer core as P and reflected from the ICB
SKJKS	S wave traversing the outer core as P and the inner core as S
SKKP	S wave traversing the core as P with one reflection from the inner side of the CMB and then continuing as P in the mantle
SKKPab	SKKP bottoming in the upper outer core
SKKPbc	SKKP bottoming in the lower outer core
SKKPdf	SKKP bottoming in the inner core
ScSS'	ScS to SKS reflection at the free surface; other examples are ScPS', ScSP', ScPP', ScSSKP, ScPSKP. (alt: ScSSKS)

Near-source Surface reflections (Depth Phases)

pP*y*	All P-type onsets (P*y*), as defined above, which resulted from reflection of an upgoing P wave at the free surface or an ocean bottom. WARNING: The character *y* is only a wild card for any seismic phase, which could be generated at the free surface. Examples are pP, pPKP, pPP, pPcP, etc.
sP*y*	All P*y* resulting from reflection of an upgoing S wave at the free surface or an ocean bottom; for example, sP, sPKP, sPP, sPcP, etc.
pS*y*	All S-type onsets (S*y*), as defined above, which resulted from reflection of an upgoing P wave at the free surface or an ocean bottom; for example, pS, pSKS, pSS, pScP, etc.
sS*y*	All S*y* resulting from reflection of an upgoing S wave at the free surface or an ocean bottom; for example, sSn, sSS, sScS, sSdif, etc.
pwP*y*	All P*y* resulting from reflection of an upgoing P wave at the ocean's free surface
pmP*y*	All P*y* resulting from reflection of an upgoing P wave from the inner side of the Moho

Surface Waves

L	Unspecified long-period surface wave
LQ	Love wave
LR	Rayleigh wave
G	Mantle wave of Love type
G*N*	Mantle wave of Love type; *N* is integer and indicates wave packets traveling along the minor arcs (odd numbers) or major arc (even numbers) of the great circle
R	Mantle wave of Rayleigh type
R*N*	Mantle wave of Rayleigh type; *N* is integer and indicates wave packets traveling along the minor arcs (odd numbers) or major arc (even numbers) of the great circle
PL	Fundamental leaking mode following P onsets generated by coupling of P energy into the waveguide formed by the crust and upper mantle SPL S wave coupling into the PL waveguide; other examples are SSPL, SSSPL.

Acoustic Phases

H	A hydroacoustic wave from a source in the water, which couples in the ground
HPg	H phase converted to Pg at the receiver side
HSg	H phase converted to Sg at the receiver side
HRg	H phase converted to Rg at the receiver side
I	An atmospheric sound arrival which couples in the ground
IPg	I phase converted to Pg at the receiver side
ISg	I phase converted to Sg at the receiver side
IRg	I phase converted to Rg at the receiver side
T	A tertiary wave. This is an acoustic wave from a source in the solid earth, usually trapped in a low-velocity oceanic water layer called the SOFAR channel (SOund Fixing And Ranging).
TPg	T phase converted to Pg at the receiver side
TSg	T phase converted to Sg at the receiver side
TRg	T phase converted to Rg at the receiver side

Amplitude Measurement Phases

The following set of amplitude measurement names refers to the IASPEI Magnitude Standard (see www.iaspei.org/commissions/CSOI/Summary_of_WG_recommendations.pdf) compliance to which is indicated by the presence of leading letter I. The absence of leading letter I indicates that a measurement is non-standard. Letter A indicates a measurement in *nm* made on a displacement seismogram, whereas letter V indicates a measurement in *nm/s* made on a velocity seismogram.

IAML	Displacement amplitude measured according to the IASPEI standard for local magnitude ML
IAMs_20	Displacement amplitude measured according to IASPEI standard for surface-wave magnitude $MS(20)$
IVMs_BB	Velocity amplitude measured according to IASPEI standard for broadband surface-wave magnitude $MS(BB)$
IAmb	Displacement amplitude measured according to IASPEI standard for short-period teleseismic body-wave magnitude mb
IVmB_BB	Velocity amplitude measured according to IASPEI standard for broadband teleseismic body-wave magnitude $mB(BB)$
AX_IN	Displacement amplitude of phase of type X (e.g., PP, S, etc), measured on an instrument of type IN (e.g., SP - short-period, LP - long-period, BB - broadband)
VX_IN	Velocity amplitude of phase of type X and instrument of type IN (as above)
A	Unspecified displacement amplitude measurement
V	Unspecified velocity amplitude measurement
AML	Displacement amplitude measurement for nonstandard local magnitude
AMs	Displacement amplitude measurement for nonstandard surface-wave magnitude
Amb	Displacement amplitude measurement for nonstandard short-period body-wave magnitude
AmB	Displacement amplitude measurement for nonstandard medium to long-period body-wave magnitude
END	Time of visible end of record for duration magnitude

Unidentified Arrivals

x	unidentified arrival (old: i, e, NULL)
rx	unidentified regional arrival (old: i, e, NULL)
tx	unidentified teleseismic arrival (old: i, e, NULL)
Px	unidentified arrival of P type (old: i, e, NULL, (P), P?)
Sx	unidentified arrival of S type (old: i, e, NULL, (S), S?)

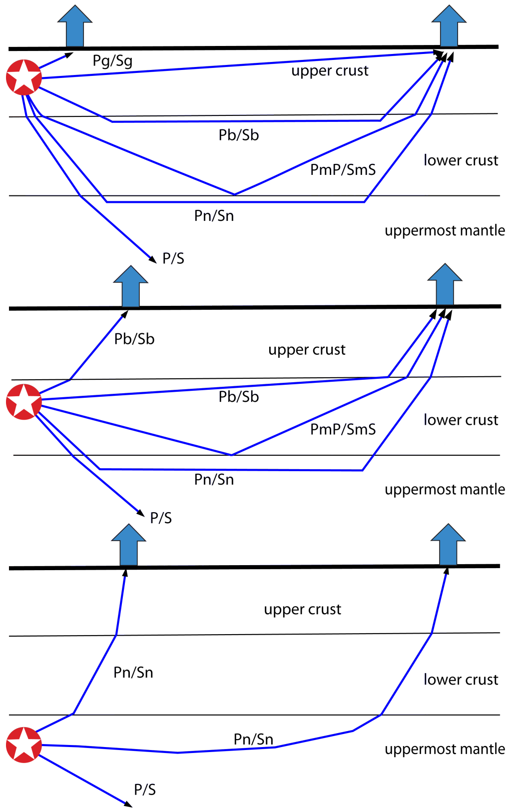

Figure 10.6: *Seismic 'crustal phases' observed in the case of a two-layer crust in local and regional distance ranges (0°<D< about 20°) from the seismic source in the: upper crust (top); lower crust (middle); and uppermost mantle (bottom).*

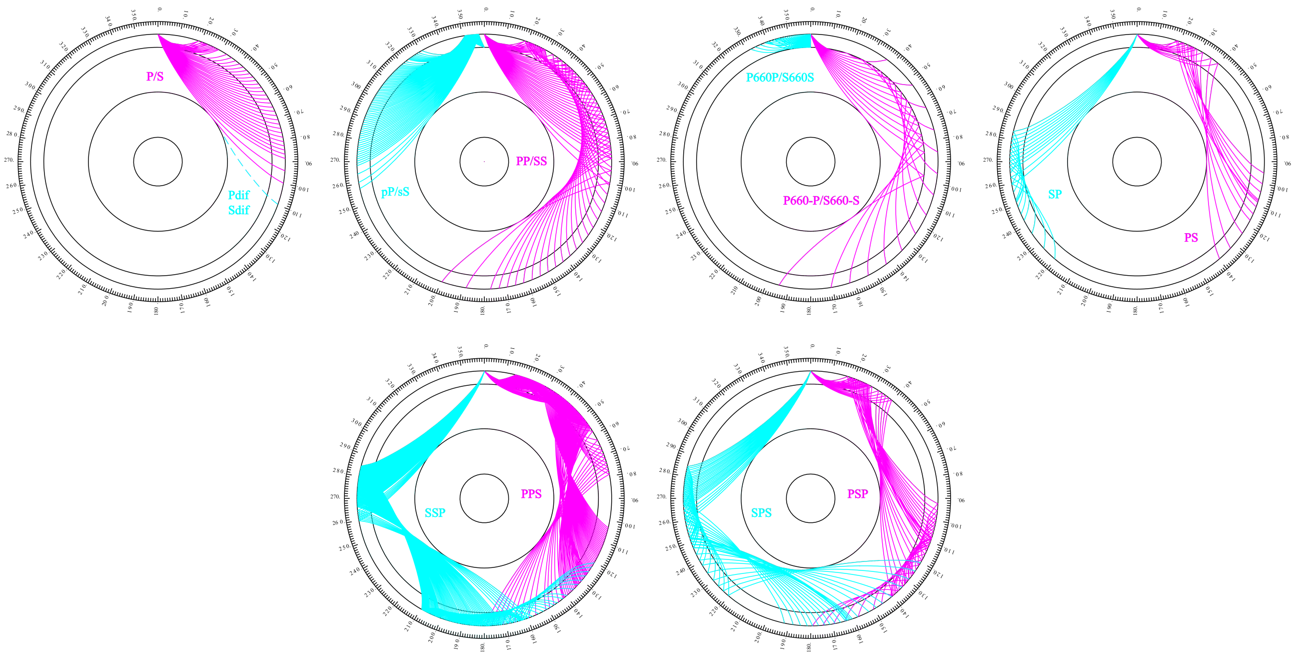

Figure 10.7: *Mantle phases observed at the teleseismic distance range D > about 20°.*

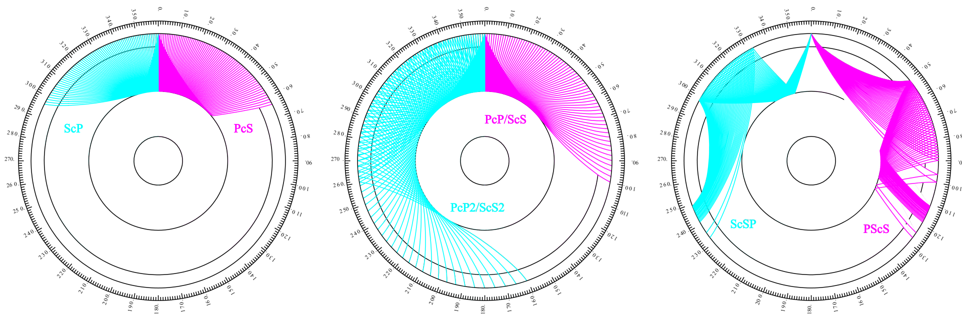

Figure 10.8: *Reflections from the Earth's core.*

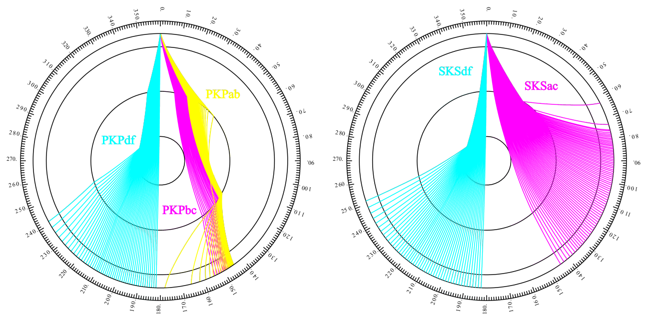

Figure 10.9: *Seismic rays of direct core phases.*

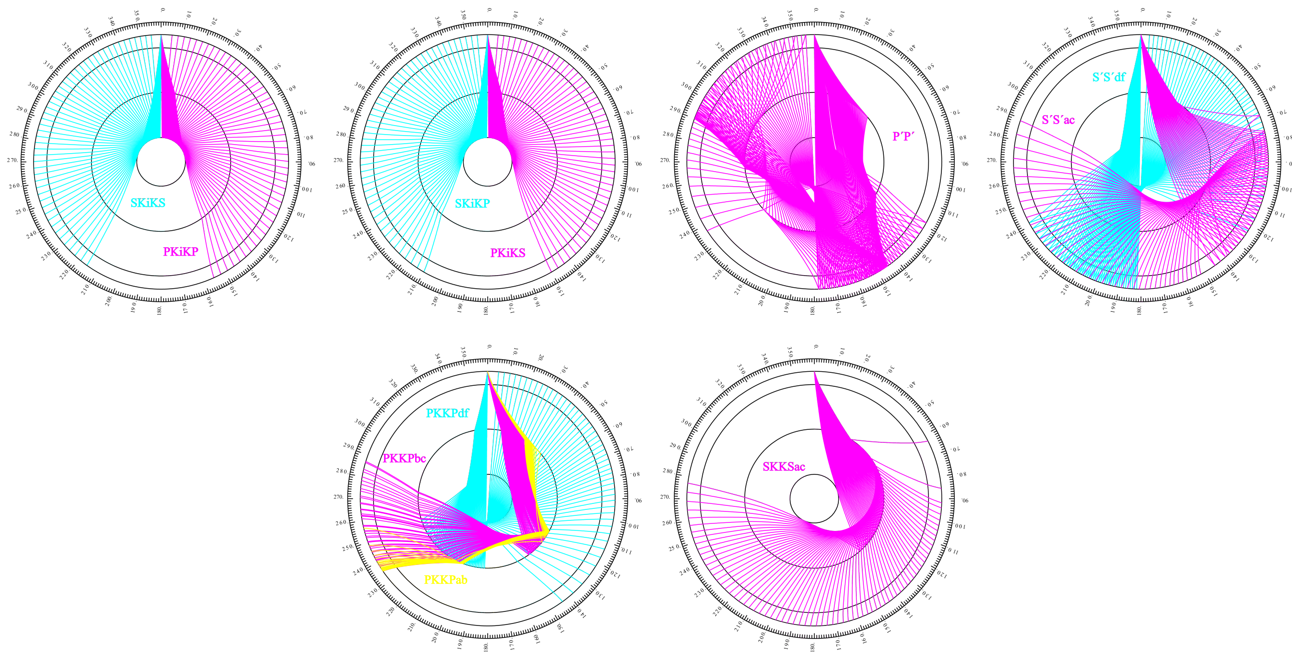

Figure 10.10: *Seismic rays of single-reflected core phases.*

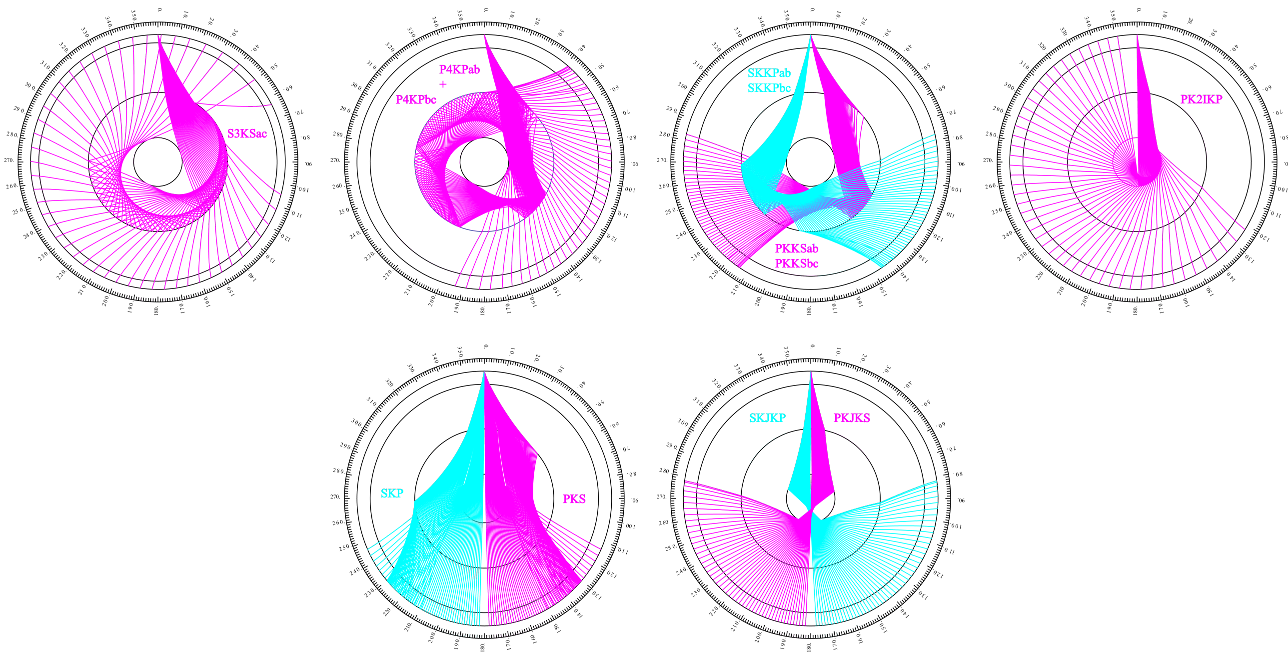

Figure 10.11: *Seismic rays of multiple-reflected and converted core phases.*

10.2.2 Flinn-Engdahl Regions

The Flinn-Engdahl regions were first proposed by *Flinn and Engdahl* (1965), with the standard defined by *Flinn et al.* (1974). The latest version of the schema, published by *Young et al.* (1996), divides the Earth into 50 seismic regions (Figure 10.12), which are further subdivided producing a total of 754 geographical regions (listed below). The geographic regions are numbered 1 to 757 with regions 172, 299 and 550 no longer in use. The boundaries of these regions are defined at one-degree intervals.

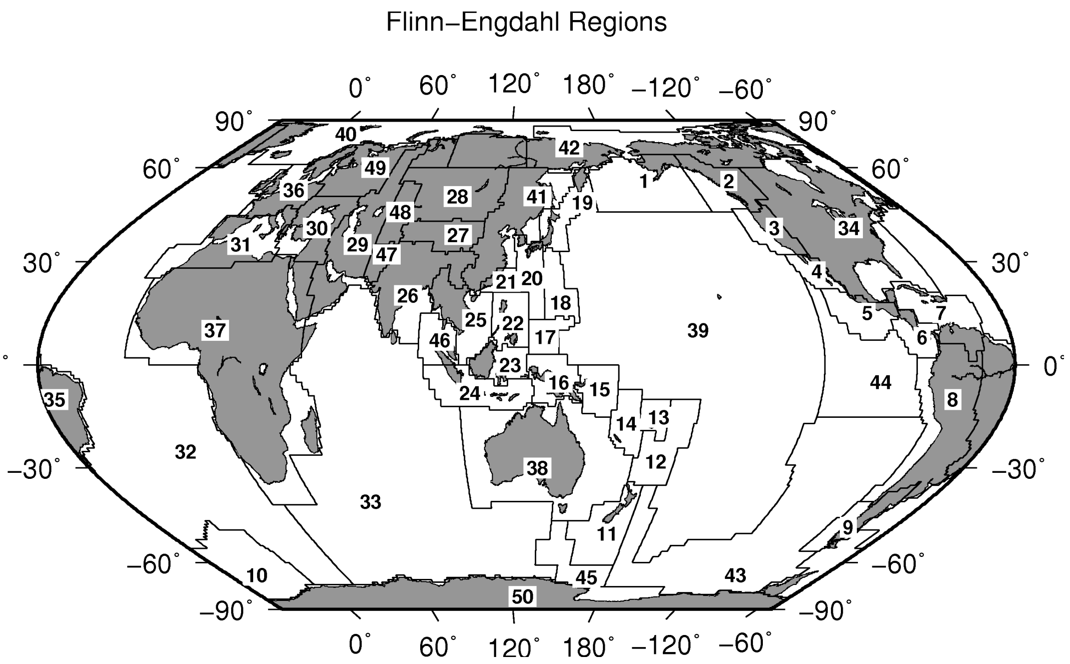

Figure 10.12: *Map of all Flinn-Engdahl seismic regions.*

Seismic Region 1
Alaska-Aleutian Arc
1. Central Alaska
2. Southern Alaska
3. Bering Sea
4. Komandorsky Islands region
5. Near Islands
6. Rat Islands
7. Andreanof Islands
8. Pribilof Islands
9. Fox Islands
10. Unimak Island region
11. Bristol Bay
12. Alaska Peninsula
13. Kodiak Island region
14. Kenai Peninsula
15. Gulf of Alaska
16. South of Aleutian Islands
17. South of Alaska

Seismic Region 2
Eastern Alaska to Vancouver Island
18. Southern Yukon Territory
19. Southeastern Alaska
20. Off coast of southeastern Alaska
21. West of Vancouver Island
22. Queen Charlotte Islands region
23. British Columbia
24. Alberta
25. Vancouver Island region
26. Off coast of Washington
27. Near coast of Washington
28. Washington-Oregon border region
29. Washington

Seismic Region 3
California-Nevada Region
30. Off coast of Oregon
31. Near coast of Oregon
32. Oregon
33. Western Idaho
34. Off coast of northern California
35. Near coast of northern California
36. Northern California
37. Nevada
38. Off coast of California
39. Central California
40. California-Nevada border region
41. Southern Nevada
42. Western Arizona
43. Southern California
44. California-Arizona border region
45. California-Baja California border region
46. Western Arizona-Sonora border region

Seismic Region 4
Lower California and Gulf of California
47. Off west coast of Baja California
48. Baja California
49. Gulf of California
50. Sonora
51. Off coast of central Mexico
52. Near coast of central Mexico

Seismic Region 5
Mexico-Guatemala Area
53. Revilla Gigedo Islands region
54. Off coast of Jalisco
55. Near coast of Jalisco
56. Near coast of Michoacan
57. Michoacan
58. Near coast of Guerrero
59. Guerrero
60. Oaxaca
61. Chiapas
62. Mexico-Guatemala border region
63. Off coast of Mexico
64. Off coast of Michoacan
65. Off coast of Guerrero
66. Near coast of Oaxaca
67. Off coast of Oaxaca
68. Off coast of Chiapas
69. Near coast of Chiapas
70. Guatemala
71. Near coast of Guatemala
730. Northern East Pacific Rise

Seismic Region 6
Central America
72. Honduras
73. El Salvador
74. Near coast of Nicaragua
75. Nicaragua
76. Off coast of central America
77. Off coast of Costa Rica
78. Costa Rica
79. North of Panama
80. Panama-Costa Rica border region
81. Panama
82. Panama-Colombia border region
83. South of Panama

Seismic Region 7
Caribbean Loop
84. Yucatan Peninsula
85. Cuba region
86. Jamaica region
87. Haiti region
88. Dominican Republic region
89. Mona Passage
90. Puerto Rico region
91. Virgin Islands
92. Leeward Islands
93. Belize
94. Caribbean Sea
95. Windward Islands
96. Near north coast of Colombia
97. Near coast of Venezuela
98. Trinidad
99. Northern Colombia
100. Lake Maracaibo
101. Venezuela
731. North of Honduras

Seismic Region 8
Andean South America
102. Near west coast of Colombia
103. Colombia
104. Off coast of Ecuador
105. Near coast of Ecuador
106. Colombia-Ecuador border region
107. Ecuador
108. Off coast of northern Peru
109. Near coast of northern Peru
110. Peru-Ecuador border region
111. Northern Peru
112. Peru-Brazil border region
113. Western Brazil
114. Off coast of Peru
115. Near coast of Peru
116. Central Peru
117. Southern Peru
118. Peru-Bolivia border region
119. Northern Bolivia
120. Central Bolivia
121. Off coast of northern Chile
122. Near coast of northern Chile
123. Northern Chile
124. Chile-Bolivia border region
125. Southern Bolivia
126. Paraguay
127. Chile-Argentina border region
128. Jujuy Province
129. Salta Province
130. Catamarca Province
131. Tucuman Province
132. Santiago del Estero Province
133. Northeastern Argentina
134. Off coast of central Chile
135. Near coast of central Chile
136. Central Chile
137. San Juan Province
138. La Rioja Province
139. Mendoza Province

140. San Luis Province
141. Cordoba Province
142. Uruguay

Seismic Region 9
Extreme South America
143. Off coast of southern Chile
144. Southern Chile
145. Southern Chile-Argentina border region
146. Southern Argentina

Seismic Region 10
Southern Antilles
147. Tierra del Fuego
148. Falkland Islands region
149. Drake Passage
150. Scotia Sea
151. South Georgia Island region
152. South Georgia Rise
153. South Sandwich Islands region
154. South Shetland Islands
155. Antarctic Peninsula
156. Southwestern Atlantic Ocean
157. Weddell Sea
732. East of South Sandwich Islands

Seismic Region 11
New Zealand Region
158. Off west coast of North Island
159. North Island
160. Off east coast of North Island
161. Off west coast of South Island
162. South Island
163. Cook Strait
164. Off east coast of South Island
165. North of Macquarie Island
166. Auckland Islands region
167. Macquarie Island region
168. South of New Zealand

Seismic Region 12
Kermadec-Tonga-Samoa Area
169. Samoa Islands region
170. Samoa Islands
171. South of Fiji Islands
172. West of Tonga Islands (REGION NOT IN USE)
173. Tonga Islands
174. Tonga Islands region
175. South of Tonga Islands
176. North of New Zealand
177. Kermadec Islands region
178. Kermadec Islands
179. South of Kermadec Islands

Seismic Region 13
Fiji Area
180. North of Fiji Islands
181. Fiji Islands region
182. Fiji Islands

Seismic Region 14
Vanuatu (New Hebrides)
183. Santa Cruz Islands region
184. Santa Cruz Islands
185. Vanuatu Islands region
186. Vanuatu Islands
187. New Caledonia
188. Loyalty Islands
189. Southeast of Loyalty Islands

Seismic Region 15
Bismarck and Solomon Islands
190. New Ireland region
191. North of Solomon Islands
192. New Britain region
193. Bougainville-Solomon Islands region
194. D'Entrecasteaux Islands region
195. South of Solomon Islands

Seismic Region 16
New Guinea
196. Irian Jaya region
197. Near north coast of Irian Jaya
198. Ninigo Islands region
199. Admiralty Islands region
200. Near north coast of New Guinea
201. Irian Jaya
202. New Guinea
203. Bismarck Sea
204. Aru Islands region
205. Near south coast of Irian Jaya
206. Near south coast of New Guinea
207. Eastern New Guinea region
208. Arafura Sea

Seismic Region 17
Caroline Islands to Guam
209. Western Caroline Islands
210. South of Mariana Islands

Seismic Region 18
Guam to Japan
211. Southeast of Honshu
212. Bonin Islands region
213. Volcano Islands region
214. West of Mariana Islands
215. Mariana Islands region
216. Mariana Islands

Seismic Region 19
Japan-Kurils-Kamchatka
217. Kamchatka Peninsula
218. Near east coast of Kamchatka Peninsula
219. Off east coast of Kamchatka Peninsula
220. Northwest of Kuril Islands
221. Kuril Islands
222. East of Kuril Islands
223. Eastern Sea of Japan
224. Hokkaido region
225. Off southeast coast of Hokkaido
226. Near west coast of eastern Honshu
227. Eastern Honshu
228. Near east coast of eastern Honshu
229. Off east coast of Honshu
230. Near south coast of eastern Honshu

Seismic Region 20
Southwestern Japan and Ryukyu Islands
231. South Korea
232. Western Honshu
233. Near south coast of western Honshu
234. Northwest of Ryukyu Islands
235. Kyushu
236. Shikoku
237. Southeast of Shikoku
238. Ryukyu Islands
239. Southeast of Ryukyu Islands
240. West of Bonin Islands
241. Philippine Sea

Seismic Region 21
Taiwan
242. Near coast of southeastern China
243. Taiwan region
244. Taiwan
245. Northeast of Taiwan
246. Southwestern Ryukyu Islands
247. Southeast of Taiwan

Seismic Region 22
Philippines
248. Philippine Islands region
249. Luzon
250. Mindoro
251. Samar
252. Palawan
253. Sulu Sea
254. Panay

255. Cebu
256. Leyte
257. Negros
258. Sulu Archipelago
259. Mindanao
260. East of Philippine Islands

Seismic Region 23
Borneo-Sulawesi
261. Borneo
262. Celebes Sea
263. Talaud Islands
264. North of Halmahera
265. Minahassa Peninsula, Sulawesi
266. Northern Molucca Sea
267. Halmahera
268. Sulawesi
269. Southern Molucca Sea
270. Ceram Sea
271. Buru
272. Seram

Seismic Region 24
Sunda Arc
273. Southwest of Sumatera
274. Southern Sumatera
275. Java Sea
276. Sunda Strait
277. Jawa
278. Bali Sea
279. Flores Sea
280. Banda Sea
281. Tanimbar Islands region
282. South of Jawa
283. Bali region
284. South of Bali
285. Sumbawa region
286. Flores region
287. Sumba region
288. Savu Sea
289. Timor region
290. Timor Sea
291. South of Sumbawa
292. South of Sumba
293. South of Timor

Seismic Region 25
Myanmar and Southeast Asia
294. Myanmar-India border region
295. Myanmar-Bangladesh border region
296. Myanmar
297. Myanmar-China border region
298. Near south coast of Myanmar
299. Southeast Asia (REGION NOT IN USE)
300. Hainan Island
301. South China Sea
733. Thailand
734. Laos
735. Kampuchea
736. Vietnam
737. Gulf of Tongking

Seismic Region 26
India-Xizang-Szechwan-Yunnan
302. Eastern Kashmir
303. Kashmir-India border region
304. Kashmir-Xizang border region
305. Western Xizang-India border region
306. Xizang
307. Sichuan
308. Northern India
309. Nepal-India border region
310. Nepal
311. Sikkim
312. Bhutan
313. Eastern Xizang-India border region
314. Southern India
315. India-Bangladesh border region
316. Bangladesh
317. Northeastern India
318. Yunnan
319. Bay of Bengal

Seismic Region 27
Southern Xinjiang to Gansu
320. Kyrgyzstan-Xinjiang border region
321. Southern Xinjiang
322. Gansu
323. Western Nei Mongol
324. Kashmir-Xinjiang border region
325. Qinghai

Seismic Region 28
Alma-Ata to Lake Baikal
326. Southwestern Siberia
327. Lake Baykal region
328. East of Lake Baykal
329. Eastern Kazakhstan
330. Lake Issyk-Kul region
331. Kazakhstan-Xinjiang border region
332. Northern Xinjiang
333. Tuva-Buryatia-Mongolia border region
334. Mongolia

Seismic Region 29
Western Asia
335. Ural Mountains region
336. Western Kazakhstan
337. Eastern Caucasus
338. Caspian Sea
339. Northwestern Uzbekistan
340. Turkmenistan
341. Iran-Turkmenistan border region
342. Turkmenistan-Afghanistan border region
343. Turkey-Iran border region
344. Iran-Armenia-Azerbaijan border region
345. Northwestern Iran
346. Iran-Iraq border region
347. Western Iran
348. Northern and central Iran
349. Northwestern Afghanistan
350. Southwestern Afghanistan
351. Eastern Arabian Peninsula
352. Persian Gulf
353. Southern Iran
354. Southwestern Pakistan
355. Gulf of Oman
356. Off coast of Pakistan

Seismic Region 30
Middle East-Crimea-Eastern Balkans
357. Ukraine-Moldova-Southwestern Russia region
358. Romania
359. Bulgaria
360. Black Sea
361. Crimea region
362. Western Caucasus
363. Greece-Bulgaria border region
364. Greece
365. Aegean Sea
366. Turkey
367. Turkey-Georgia-Armenia border region
368. Southern Greece
369. Dodecanese Islands
370. Crete
371. Eastern Mediterranean Sea
372. Cyprus region
373. Dead Sea region
374. Jordan-Syria region
375. Iraq

Seismic Region 31
Western Mediterranean Area
376. Portugal
377. Spain

378. Pyrenees
379. Near south coast of France
380. Corsica
381. Central Italy
382. Adriatic Sea
383. Northwestern Balkan Peninsula
384. West of Gibraltar
385. Strait of Gibraltar
386. Balearic Islands
387. Western Mediterranean Sea
388. Sardinia
389. Tyrrhenian Sea
390. Southern Italy
391. Albania
392. Greece-Albania border region
393. Madeira Islands region
394. Canary Islands region
395. Morocco
396. Northern Algeria
397. Tunisia
398. Sicily
399. Ionian Sea
400. Central Mediterranean Sea
401. Near coast of Libya

Seismic Region 32
Atlantic Ocean

402. North Atlantic Ocean
403. Northern Mid-Atlantic Ridge
404. Azores Islands region
405. Azores Islands
406. Central Mid-Atlantic Ridge
407. North of Ascension Island
408. Ascension Island region
409. South Atlantic Ocean
410. Southern Mid-Atlantic Ridge
411. Tristan da Cunha region
412. Bouvet Island region
413. Southwest of Africa
414. Southeastern Atlantic Ocean
738. Reykjanes Ridge
739. Azores-Cape St. Vincent Ridge

Seismic Region 33
Indian Ocean

415. Eastern Gulf of Aden
416. Socotra region
417. Arabian Sea
418. Lakshadweep region
419. Northeastern Somalia
420. North Indian Ocean
421. Carlsberg Ridge
422. Maldive Islands region
423. Laccadive Sea
424. Sri Lanka
425. South Indian Ocean
426. Chagos Archipelago region
427. Mauritius-Reunion region
428. Southwest Indian Ridge
429. Mid-Indian Ridge
430. South of Africa
431. Prince Edward Islands region
432. Crozet Islands region
433. Kerguelen Islands region
434. Broken Ridge
435. Southeast Indian Ridge
436. Southern Kerguelen Plateau
437. South of Australia
740. Owen Fracture Zone region
741. Indian Ocean Triple Junction
742. Western Indian-Antarctic Ridge

Seismic Region 34
Eastern North America

438. Saskatchewan
439. Manitoba
440. Hudson Bay
441. Ontario
442. Hudson Strait region
443. Northern Quebec
444. Davis Strait
445. Labrador
446. Labrador Sea
447. Southern Quebec
448. Gaspe Peninsula
449. Eastern Quebec
450. Anticosti Island
451. New Brunswick
452. Nova Scotia
453. Prince Edward Island
454. Gulf of St. Lawrence
455. Newfoundland
456. Montana
457. Eastern Idaho
458. Hebgen Lake region, Montana
459. Yellowstone region
460. Wyoming
461. North Dakota
462. South Dakota
463. Nebraska
464. Minnesota
465. Iowa
466. Wisconsin
467. Illinois
468. Michigan
469. Indiana
470. Southern Ontario
471. Ohio
472. New York
473. Pennsylvania
474. Vermont-New Hampshire region
475. Maine
476. Southern New England
477. Gulf of Maine
478. Utah
479. Colorado
480. Kansas
481. Iowa-Missouri border region
482. Missouri-Kansas border region
483. Missouri
484. Missouri-Arkansas border region
485. Missouri-Illinois border region
486. New Madrid region, Missouri
487. Cape Girardeau region, Missouri
488. Southern Illinois
489. Southern Indiana
490. Kentucky
491. West Virginia
492. Virginia
493. Chesapeake Bay region
494. New Jersey
495. Eastern Arizona
496. New Mexico
497. Northwestern Texas-Oklahoma border region
498. Western Texas
499. Oklahoma
500. Central Texas
501. Arkansas-Oklahoma border region
502. Arkansas
503. Louisiana-Texas border region
504. Louisiana
505. Mississippi
506. Tennessee
507. Alabama
508. Western Florida
509. Georgia
510. Florida-Georgia border region
511. South Carolina
512. North Carolina
513. Off east coast of United States
514. Florida Peninsula
515. Bahama Islands
516. Eastern Arizona-Sonora border region
517. New Mexico-Chihuahua border region
518. Texas-Mexico border region
519. Southern Texas
520. Near coast of Texas
521. Chihuahua
522. Northern Mexico
523. Central Mexico
524. Jalisco
525. Veracruz
526. Gulf of Mexico
527. Bay of Campeche

Seismic Region 35
Eastern South America
528. Brazil
529. Guyana
530. Suriname
531. French Guiana

Seismic Region 36
Northwestern Europe
532. Eire
533. United Kingdom
534. North Sea
535. Southern Norway
536. Sweden
537. Baltic Sea
538. France
539. Bay of Biscay
540. The Netherlands
541. Belgium
542. Denmark
543. Germany
544. Switzerland
545. Northern Italy
546. Austria
547. Czech and Slovak Republics
548. Poland
549. Hungary

Seismic Region 37
Africa
550. Northwest Africa (REGION NOT IN USE)
551. Southern Algeria
552. Libya
553. Egypt
554. Red Sea
555. Western Arabian Peninsula
556. Chad region
557. Sudan
558. Ethiopia
559. Western Gulf of Aden
560. Northwestern Somalia
561. Off south coast of northwest Africa
562. Cameroon
563. Equatorial Guinea
564. Central African Republic
565. Gabon
566. Congo
567. Zaire
568. Uganda
569. Lake Victoria region
570. Kenya
571. Southern Somalia
572. Lake Tanganyika region
573. Tanzania
574. Northwest of Madagascar
575. Angola
576. Zambia
577. Malawi
578. Namibia
579. Botswana
580. Zimbabwe
581. Mozambique
582. Mozambique Channel
583. Madagascar
584. South Africa
585. Lesotho
586. Swaziland
587. Off coast of South Africa
743. Western Sahara
744. Mauritania
745. Mali
746. Senegal-Gambia region
747. Guinea region
748. Sierra Leone
749. Liberia region
750. Cote d'Ivoire
751. Burkina Faso
752. Ghana
753. Benin-Togo region
754. Niger
755. Nigeria

Seismic Region 38
Australia
588. Northwest of Australia
589. West of Australia
590. Western Australia
591. Northern Territory
592. South Australia
593. Gulf of Carpentaria
594. Queensland
595. Coral Sea
596. Northwest of New Caledonia
597. New Caledonia region
598. Southwest of Australia
599. Off south coast of Australia
600. Near coast of South Australia
601. New South Wales
602. Victoria
603. Near southeast coast of Australia
604. Near east coast of Australia
605. East of Australia
606. Norfolk Island region
607. Northwest of New Zealand
608. Bass Strait
609. Tasmania region
610. Southeast of Australia

Seismic Region 39
Pacific Basin
611. North Pacific Ocean
612. Hawaiian Islands region
613. Hawaiian Islands
614. Eastern Caroline Islands region
615. Marshall Islands region
616. Enewetak Atoll region
617. Bikini Atoll region
618. Gilbert Islands region
619. Johnston Island region
620. Line Islands region
621. Palmyra Island region
622. Kiritimati region
623. Tuvalu region
624. Phoenix Islands region
625. Tokelau Islands region
626. Northern Cook Islands
627. Cook Islands region
628. Society Islands region
629. Tubuai Islands region
630. Marquesas Islands region
631. Tuamotu Archipelago region
632. South Pacific Ocean

Seismic Region 40
Arctic Zone
633. Lomonosov Ridge
634. Arctic Ocean
635. Near north coast of Kalaallit Nunaat
636. Eastern Kalaallit Nunaat
637. Iceland region
638. Iceland
639. Jan Mayen Island region
640. Greenland Sea
641. North of Svalbard
642. Norwegian Sea
643. Svalbard region
644. North of Franz Josef Land
645. Franz Josef Land
646. Northern Norway
647. Barents Sea
648. Novaya Zemlya
649. Kara Sea
650. Near coast of northwestern Siberia
651. North of Severnaya Zemlya
652. Severnaya Zemlya
653. Near coast of northern Siberia
654. East of Severnaya Zemlya
655. Laptev Sea

Seismic Region 41
Eastern Asia
656. Southeastern Siberia
657. Priamurye-Northeastern China border region
658. Northeastern China
659. North Korea

660. Sea of Japan
661. Primorye
662. Sakhalin Island
663. Sea of Okhotsk
664. Southeastern China
665. Yellow Sea
666. Off east coast of southeastern China

Seismic Region 42
Northeastern Asia, Northern Alaska to Greenland

667. North of New Siberian Islands
668. New Siberian Islands
669. Eastern Siberian Sea
670. Near north coast of eastern Siberia
671. Eastern Siberia
672. Chukchi Sea
673. Bering Strait
674. St. Lawrence Island region
675. Beaufort Sea
676. Northern Alaska
677. Northern Yukon Territory
678. Queen Elizabeth Islands
679. Northwest Territories
680. Western Kalaallit Nunaat
681. Baffin Bay
682. Baffin Island region

Seismic Region 43
Southeastern and Antarctic Pacific Ocean

683. Southeastcentral Pacific Ocean
684. Southern East Pacific Rise
685. Easter Island region
686. West Chile Rise
687. Juan Fernandez Islands region
688. East of North Island
689. Chatham Islands region
690. South of Chatham Islands
691. Pacific-Antarctic Ridge
692. Southern Pacific Ocean
756. Southeast of Easter Island

Seismic Region 44
Galapagos Area

693. Eastcentral Pacific Ocean
694. Central East Pacific Rise
695. West of Galapagos Islands
696. Galapagos Islands region
697. Galapagos Islands
698. Southwest of Galapagos Islands
699. Southeast of Galapagos Islands
757. Galapagos Triple Junction region

Seismic Region 45
Macquarie Loop

700. South of Tasmania
701. West of Macquarie Island
702. Balleny Islands region

Seismic Region 46
Andaman Islands to Sumatera

703. Andaman Islands region
704. Nicobar Islands region
705. Off west coast of northern Sumatera
706. Northern Sumatera
707. Malay Peninsula
708. Gulf of Thailand

Seismic Region 47
Baluchistan

709. Southeastern Afghanistan
710. Pakistan
711. Southwestern Kashmir
712. India-Pakistan border region

Seismic Region 48
Hindu Kush and Pamir

713. Central Kazakhstan
714. Southeastern Uzbekistan
715. Tajikistan
716. Kyrgyzstan
717. Afghanistan-Tajikistan border region
718. Hindu Kush region
719. Tajikistan-Xinjiang border region
720. Northwestern Kashmir

Seismic Region 49
Northern Eurasia

721. Finland
722. Norway-Murmansk border region
723. Finland-Karelia border region
724. Baltic States-Belarus-Northwestern Russia
725. Northwestern Siberia
726. Northern and central Siberia

Seismic Region 50
Antarctica

727. Victoria Land
728. Ross Sea
729. Antarctica

10.2.3 IASPEI Magnitudes

The ISC publishes a diversity of magnitude data. Although trying to be as complete and specific as possible, preference is now given to magnitudes determined according to standard procedures recommended by the Working Group on Magnitude Measurements of the IASPEI Commission on Seismological Observation and Interpretation (CoSOI). So far, such standards have been agreed upon for the local magnitude ML, the local-regional mb_Lg, and for two types each of body-wave (mb and mB_BB) and surface-wave magnitudes (Ms_20 and Ms_BB). With the exception of ML, all other standard magnitudes are measured on vertical-component records only. BB stands for direct measurement on unfiltered velocity broadband records in a wide range of periods, provided that their passband covers at least the period range within which mB_BB and Ms_BB are supposed to be measured. Otherwise, a deconvolution has to be applied prior to the amplitude and period measurement so as to assure that this specification is met. In contrast, mb_Lg, mb and Ms_20 are based on narrowband amplitude measurements around periods of 1 s and 20 s, respectively.

ML is consistent with the original definition of the local magnitude by *Richter* (1935) and mB_BB in close agreement with the original definition of medium-period body-wave magnitude mB measured in a wide range of periods between some 2 to 20 s and calibrated with the *Gutenberg and Richter* (1956) Q-function for vertical-component P waves. Similarly, Ms_BB is best tuned to the unbiased use of the IASPEI (1967) recommended standard magnitude formula for surface-wave amplitudes in a wide range of periods and distances, as proposed by its authors *Vaněk et al.* (1962). In contrast, mb and Ms_20 are chiefly based on measurement standards defined by US agencies in the 1960s in conjunction with the global deployment of the World-Wide Standard Seismograph Network (WWSSN), which did not include medium or broadband recordings. Some modifications were made in the 1970s to account for IASPEI recommendations on extended measurement time windows for mb. Although not optimal for calibrating narrow-band spectral amplitudes measured around 1 s and 20 s only, mb and Ms_20 use the same original calibrations functions as mB_BB and Ms_BB. But mb and Ms_20 data constitute by far the largest available magnitude data sets. Therefore they continue to be used, with appreciation for their advantages (e.g., mb is by far the most frequently measured teleseismic magnitude and often the only available and reasonably good magnitude estimator for small earthquakes) and their shortcomings (see section 3.2.5.2 of Chapter 3 in NMSOP-2).

Abbreviated descriptions of the standard procedures for ML, mb_Lg, mb, mB_BB and Ms_BB are summarised below. For more details, including also the transfer functions of the simulation filters to be used, see www.iaspei.org/commissions/CSOI/Summary_WG-Recommendations_20130327.pdf.

All amplitudes used in the magnitude formulas below are in most circumstances to be measured as one-half the maximum deflection of the seismogram trace, peak-to-adjacent-trough or trough-to-adjacent-peak, where the peak and trough are separated by one crossing of the zero-line: this measurement is sometimes described as "one-half peak-to-peak amplitude." The periods are to be measured as twice the time-intervals separating the peak and adjacent-trough from which the amplitudes are measured. The amplitude-phase arrival-times are to be measured and reported too as the time of the zero-crossing between the peak and adjacent-trough from which the amplitudes are measured. The issue of amplitude and period measuring procedures, and circumstances under which alternative procedures are acceptable or preferable, is discussed further in Section 5 of IS 3.3 and in section 3.2.3.3 of Chapter 3 of NMSOP-2.

Amplitudes measured according to recommended IASPEI standard procedures should be reported with the following ISF amplitude "phase names": IAML, IAmb_Lg, IAmb, IAMs_20, IVmB_BB and IVMs_BB. "I" stands for "International" or "IASPEI", "A" for displacement amplitude, measured in nm, and "V" for velocity amplitude, measured in nm/s. Although the ISC will calculate standard surface-wave magnitudes only for earthquakes shallower than 60 km, contributing agencies or stations are encouraged to report standard amplitude measurements of IAMs_20 and IVMs_BB for deeper earthquakes as well.

Note that the commonly known classical calibration relationships have been modified in the following to be consistent with displacements measured in nm, and velocities in nm/s, which is now common with high-resolution digital data and analysis tools. With these general definitions of the measurement parameters, where R is hypocentral distance in km (typically less than 1000 km), Δ is epicentral distance in degrees and h is hypocentre depth in km, the standard formulas and procedures read as follows:

ML:

$$ML = \log_{10}(A) + 1.11 \log_{10} R + 0.00189R - 2.09 \tag{10.14}$$

for crustal earthquakes in regions with attenuative properties similar to those of southern California, and with A being the maximum trace amplitude in nm that is measured on output from a horizontal-component instrument that is filtered so that the response of the seismograph/filter system replicates that of a Wood-Anderson standard seismograph (but with a static magnification of 1). For the normalised simulated response curve and related poles and zeros see Figure 1 and Table 1 in IS 3.3 of NMSOP-2.

Equation (10.14) is an expansion of that of *Hutton and Boore* (1987). The constant term in equation (10.14), −2.09, is based on an experimentally determined static magnification of the Wood-Anderson of 2080 (see *Uhrhammer and Collins* (1990)), rather than the theoretical magnification of 2800 that was specified by the seismograph´s manufacturer. The formulation of equation (10.14) assures that reported ML amplitude data are not affected by uncertainty in the static magnification of the Wood-Anderson seismograph.

For seismographic stations containing two horizontal components, amplitudes are measured independently from each horizontal component and each amplitude is treated as a single datum. There is no effort to measure the two observations at the same time, and there is no attempt to compute a vector average. For crustal earthquakes in regions with attenuative properties that are different from those of coastal California and for measuring magnitudes with vertical-component seismographs the constants in the above equation have to be re-determined to adjust for the different regional attenuation and travel paths as well as for systematic differences between amplitudes measured on horizontal and vertical seismographs.

mb_Lg:

$$mb\_Lg = \log_{10}(A) + 0.833 \log_{10} R + 0.434\gamma(R - 10) - 0.87 \tag{10.15}$$

where A = "sustained ground-motion amplitude" in nm, defined as the third largest amplitude in the time window corresponding to group velocities of 3.6 to 3.2 km/s, in the period (T) range 0.7 s to 1.3

s; R = epicentral distance in km, γ = coefficient of attenuation in km^{-1}. γ is related to the quality factor Q through the equation $\gamma = \pi/(QUT)$, where U is group velocity and T is the wave period of the L_g wave. γ is a strong function of crustal structure and should be determined specifically for the region in which the mb_Lg is to be used. A and T are measured on output from a vertical-component instrument that is filtered so that the frequency response of the seismograph/filter system replicates that of a WWSSN short-period seismograph (see Figure 1 and Table 1 in IS 3.3 of NMSOP-2). Arrival times with respect to the origin of the seismic disturbance are used, along with epicentral distance, to compute group velocity U.

mb:

$$mb = \log_{10}(A/T) + Q(\Delta, h) - 3.0 \tag{10.16}$$

where A = vertical component P-wave ground amplitude in nm measured at distances $20° \leq \Delta \leq 100°$ and calculated from the maximum trace-amplitude with $T < 3$ s in the entire P-phase train (time spanned by P, pP, sP, and possibly PcP and their codas, and ending preferably before PP). A and T are measured on output from an instrument that is filtered so that the frequency response of the seismograph/filter system replicates that of a WWSSN short-period seismograph (see Figure 1 and Table 1 in IS 3.3 of NMSOP-2). A is determined by dividing the maximum trace amplitude by the magnification of the simulated WWSSN-SP response at period T.

$Q(\Delta, h)$ = attenuation function for PZ (P-waves recorded on vertical component seismographs) established by *Gutenberg and Richter* (1956) in the tabulated or algorithmic form as used by the U.S. Geological Survey/National Earthquake Information Center (USGS/NEIC) (see Table 2 in IS 3.3 and program description PD 3.1 in NMSOP-2);

mB_BB:

$$mB\_BB = \log_{10}(Vmax/2\pi) + Q(\Delta, h) - 3.0 \tag{10.17}$$

where $Vmax$ = vertical component ground velocity in nm/s at periods between 0.2 s $< T <$ 30 s, measured in the range $20° \leq \Delta \leq 100°$. $Vmax$ is calculated from the maximum trace-amplitude in the entire P-phase train (see mb), as recorded on a seismogram that is proportional to velocity at least in the period range of measurements. $Q(\Delta, h)$ = attenuation function for PZ established by *Gutenberg and Richter* (1956) (see 10.16). Equation (10.16) differs from the equation for mB of *Gutenberg and Richter* (1956) by virtue of the $log_{10}(Vmax/2\pi)$ term, which replaces the classical $\log_{10}(A/T)_{max}$ term. Contributors should continue to send observations of A and T to ISC.

Ms_20:

$$Ms\_20 = \log_{10}(A/T) + 1.66\log_{10}\Delta + 0.3 \tag{10.18}$$

where A = vertical-component ground displacement in nm at $20° \leq \Delta \leq 160°$ epicentral distance measured from the maximum trace amplitude of a surface-wave phase having a period T between 18 s and 22 s on a waveform that has been filtered so that the frequency response of the seismograph/filter replicates that of a WWSSN long-period seismograph (see Figure 1 and Table 1 in IS 3.3 of NMSOP-2). A is determined by dividing the maximum trace amplitude by the magnification of the simulated WWSSN-LP response at period T. Equation (10.18) is formally equivalent to the Ms equation proposed by *Vaněk et al.* (1962) but is here applied to vertical motion measurements in a narrow range of periods.

Ms_BB:

$$Ms\_BB = \log_{10}(Vmax/2\pi) + 1.66\log_{10}\Delta + 0.3 \tag{10.19}$$

where $Vmax$ = vertical-component ground velocity in nm/s associated with the maximum trace-amplitude in the surface-wave train at periods between 3 s $< T <$ 60 s as recorded at distances $2° \leq \Delta \leq 160°$ on a seismogram that is proportional to velocity in that range of considered periods. Equation (10.19) is based on the Ms equation proposed by *Vaněk et al.* (1962), but is here applied to vertical motion measurements and is used with the $\log_{10}(Vmax/2\pi)$ term replacing the $\log_{10}(A/T)_{max}$ term of the original. As for mB_BB, observations of A and T should be reported to ISC.

Mw:

$$Mw = (\log_{10} M_0 - 9.1)/1.5 \tag{10.20}$$

Moment magnitude Mw is calculated from data of the scalar seismic moment M_0 (when given in Nm), or

$$Mw = (\log_{10} M_0 - 16.1)/1.5 \tag{10.21}$$

its CGS equivalent when M_0 is in dyne·cm.

Please note that the magnitude nomenclature used in this Section uses the IASPEI standards as the reference. However, the magnitude type is typically written in plain text in most typical data reports and so it is in this document. Moreover, writing magnitude types in plain text allows us to reproduce the magnitude type as stored in the database and provides a more direct identification of the magnitude type reported by different agencies. A short description of the common magnitude types available in this Summary is given in table 7.6.

10.2.4 The IASPEI Seismic Format (ISF)

The ISF is the IASPEI approved standard format for the exchange of parametric seismological data (hypocentres, magnitudes, phase arrivals, moment tensors etc.) and is one of the formats used by the ISC. It was adopted as standard in August 2001 and is an extension of the International Monitoring System 1.0 (IMS1.0) standard, which was developed for exchanging data used to monitor the Comprehensive Nuclear-Test-Ban Treaty. An example of the ISF is shown in Listing 10.1.

Bulletins which use the ISF are comprised of origin and arrival information, provided in a series of data blocks. These include: a bulletin title block; an event title block; an origin block; a magnitude sub-block; an effect block; a reference block; and a phase block.

Within these blocks an important extension of the IMS1.0 standard is the ability to add additional comments and thus provide further parametric information. The ISF comments are distinguishable within the open parentheses required for IMS1.0 comments by beginning with a hash mark (#) followed by a keyword identifying the type of formatted comment. Each additional line required in the ISF comment begins with the hash (within the comment parentheses) followed by blank spaces at least as long as the keyword. Optional lines within the comment are signified with a plus sign (+) instead of a hash mark. The keywords include `PRIME` (to designate a prime origin of a hypocentre); `CENTROID` (to indicate the centroid origin); `MOMTENS` (moment tensor solution); `FAULT_PLANE` (fault plane solution); `PRINAX` (principal axes); `PARAM` (an origin parameter e.g. hypocentre depth given by a depth phase).

The ISC has now moved to ISF 2.1 as the default format for searches, this provides more detail primarily for the identification of arrivals. An essential change with the planned use of network codes from data year 2021.

The full documentation for the ISF 1 and 2.1 is maintained at the ISC and can be downloaded from:
www.isc.ac.uk/standards/isf/download/isf21.pdf
www.isc.ac.uk//standards/isf/download/isf.pdf

The documentation for the IMS1.0 standard can be downloaded from:
www.isc.ac.uk/standards/isf/download/ims1_0.pdf

Listing 10.1: *Example of an ISF 2.1 formatted event*

```
DATA_TYPE BULLETIN ISF2.1:short
Reviewed ISC Bulletin
Event   619631664 Andreanof Islands
   Date       Time        Err   RMS Latitude Longitude  Smaj  Smin  Az Depth   Err Ndef Nsta Gap  mdist  Mdist Qual   Author      OrigID
2021/01/03 12:38:45.00          0.980  51.1100 -179.7400                    20.0           1      318  32.20  68.70     uk BJI         615527075
2021/01/03 12:38:47.10   0.97          51.2380 -179.7850   6.6   3.9 106  23.0         226                                 MOS         616002310
2021/01/03 12:38:48.00                 51.1850 -179.8390                    21.0                                           IPGP        614752189
2021/01/03 12:38:48   f                51.2200 -179.7930f                    2.7   0.5                            m i    ISC-PPSM    619290698
 (#MOMTENS sc    M0 fCLVD    MRR    MTT    MPP    MRT    MTP    MPR NST1 NST2 Author   )
 (#             eM0 eCLVD    eRR    eTT    ePP    eRT    eTP    ePR NCO1 NCO2 Duration )
 (#        18 5.310         0.128  0.327 -0.216  0.249  0.515  0.296   62      ISC-PPSM )
 (#                         0.207  0.242  0.328  0.177  0.152  0.207                    )
 (#FAULT_PLANE Typ Strike   Dip    Rake  NP  NS Plane Author   )
 (#                 21.10 87.60  125.20               ISC-PPSM )
 (+                114.50 35.30    4.20                        )
 (#STF N_samp   FS  mo_norm STF_units  NST    NWV  Author   )
 (#       256   10  1.04e10    Nm/s     62     62  ISC-PPSM )
 (#NORMALISED_STF (8 col, 32 lines)
 (#  0.002090  0.036500  0.077460  0.119480  0.162860  0.207420  0.252510  0.297000 )
 (#  0.339360  0.377810  0.410530  0.435920  0.452820  0.460700  0.459820  0.451200 )
.
.
 (#  0.000500  0.000640  0.000830  0.001060  0.001330  0.001630  0.001970  0.002260 )
 (#  0.002600  0.002870  0.003070  0.003280  0.003460  0.003600  0.003700  0.003740 )
2021/01/03 12:38:48.69   0.30 1.383  51.1476 -179.7638  4.53 3.236 177  25.2  1.69 2041 2350  26   2.06 160.04 m i ke ISC         619187305
 (#PRIME)
 (#PARAM pP_DEPTH=25.0+4.6)

Magnitude  Err Nsta Author      OrigID
mb      5.8      93 BJI         615527075
mB      6.2      74 BJI         615527075
.
.
mB_BB   6.5         BGR         618932975
Ms      5.8         BGR         618932975
Mww     6.1 0.1   46 NEIC        615855125
mb      5.9 0.1  628 ISC         619187305
MS      5.9 0.1  488 ISC         619187305

Sta     Dist  EvAz Phase        Time      TRes  Azim AzRes   Slow   SRes Def   SNR       Amp   Per Qual Magnitude    ArrID    Agy   Deploy   Ln Auth  Rep   PCh ACh L   Lat        Lon       Elev     Depth
ADK     2.06  67.9 Pn       12:39:23.1     1.5                           T__                       m__               868429551 FDSN IU       00 AEIC  NEIC  BHZ ??? _  51.8823 -176.6842   129.0     0.0
.
.
MAPS    8.27  66.2 Pn       12:40:49.61    2.7                           T__                       m__               868429348 FDSN AV       -- AEIC  NEIC  BHZ ??? _  53.8082 -166.9407   333.0     0.0
MAPS    8.27  66.2 Pn       12:40:50.0     3.1                           T__                        __               869293237 ISC  IR       -- PTWC  PTWC  ??? ??? _  53.8082 -166.9407     0.0     0.0
MGOD    8.30  66.4 Pn       12:40:50.04    2.7                           T__                       m__               868429349 FDSN AV       -- AEIC  NEIC  BHZ ??? _  53.7938 -166.8780   650.0     0.0
MGOD    8.31  66.4 Pn       12:40:49.8     2.4                           T__                        __               869293236 ISC  IR       -- PTWC  PTWC  ??? ??? _  53.7947 -166.8725     0.0     0.0
MSW     8.38  65.7 Pn       12:40:51.27    2.8                           T__                       m__               868429350 FDSN AV       -- AEIC  NEIC  BHZ ??? _  53.9148 -166.7880   423.0     0.0
.
.
FUORN  82.23 353.0 P        12:51:08.125   0.5                           T__            158.7  1.78 a__ mb      5.8  887040354 FDSN CH          GFZ   GFZ   BHZ BHZ _  46.6203   10.2635  2286.0     0.0
CNGN   82.29  79.8 P        12:51:08.695   0.5                           T__             43.0  1.16 a__ mb      5.4  887040356 FDSN NU          GFZ   GFZ   BHZ BHZ _  12.5012  -86.6993   510.0     0.0
HUMR   82.32 342.4 P        12:51:07.363  -0.5                           T__                       c_                876829539 ISC  IR       -- BUC   BUC   ??? ??? _  44.5281   24.9804     0.0     0.0
HUMR   82.32 342.4 P        12:51:06.92   -0.9                           T__            167.3  1.59 a__ mb      5.8  887040350 FDSN RO          GFZ   GFZ   BHZ BHZ _  44.5281   24.9804   247.0     0.0
DRE    82.37 350.6 P        12:51:07.56   -0.6                           T__             84.3  1.60 a__ mb      5.6  887040352 FDSN OX          GFZ   GFZ   HHZ HHZ _  46.1733   13.6450   810.0     0.0
.
.
OTAV   96.91  81.0 IAMs_20  13:44:16.741                                 ___                       a__               868429973 FDSN IU       00 NEIC  NEIC  LHZ LHZ _   0.2376  -78.4508  3495.0     0.0
OTAV   96.91  81.0 P        12:52:19.42    0.9                           T__                        _e               890748234 ISC  IR       -- VAO   VAO   B?Z ??? _   0.2376  -78.4508     0.0     0.0
OTAV   96.91  81.0 P        12:52:19.749   1.3                           T__                        __               892078544 ISC  IR       -- OSUNB OSUNB ??? ??? _   0.2376  -78.4508     0.0     0.0
OTAV   96.91  81.0 S        13:03:38.834  -0.9                           T__                        __               892078544 ISC  IR       -- OSUNB OSUNB ??? ??? _   0.2376  -78.4508     0.0     0.0
.
.
PTGB  132.32  76.7 PKiKP    12:58:01.04   -0.5                           T__                        _e               890748236 ISC  IR       -- VAO   VAO   H?N ??? _ -24.7161  -52.0648     0.0     0.0
PTGB  132.32  76.7 PKPdf    12:58:00.846   0.4                           T__                        __               892078547 ISC  IR       -- OSUNB OSUNB ??? ??? _ -24.7161  -52.0648     0.0     0.0
CANS  132.36  67.4 PKPdf    12:58:01.03    0.4                           T__                        __               892078525 ISC  IR       -- OSUNB OSUNB ??? ??? _ -20.2896  -46.3921     0.0     0.0
ITQB  133.02  85.3 PKiKP    12:58:02.261  -0.4                           T__                        __               892078533 ISC  IR       -- OSUNB OSUNB ??? ??? _ -29.6714  -56.6241    80.0     0.0
GUA01 133.06  57.6 PKPdf    12:58:02.21    0.3                           T__                        __               892078531 ISC  IR       -- OSUNB OSUNB ??? ??? _ -16.5835  -39.8053     0.0     0.0
COYC  133.41 112.9 IAMs_20  13:46:48.189                                 ___                       a__               868429657 FDSN G        00 NEIC  NEIC  LHZ LHZ _ -45.5730  -72.0814   235.0     0.0
COYC  133.41 112.9 PKiKP    12:58:03.8     0.9                           T__              0.2      a__               887040460 FDSN G        00 GFZ   GFZ   BHZ BHZ _ -45.5730  -72.0814   235.0     0.0
.
.
VNA3  159.34 170.9 PKPab    12:59:20.797  -0.1                           T__             28.6  0.92  c_              848409489 ISC  IR       -- AWI   AWI   BHZ BHZ _ -71.2428   -9.6687     0.0     0.0
VNA3  159.34 170.9 sPKPab   12:59:31.707   1.2                           T__             37.9  0.88  c_              848409489 ISC  IR       -- AWI   AWI   BHZ BHZ _ -71.2428   -9.6687     0.0     0.0
VNA3  159.34 170.9 PKPdf    12:58:41.928  -1.3                           T__              0.3      a__               887040472 FDSN AW          GFZ   GFZ   BHZ BHZ _ -71.2420   -9.6660   566.0     0.0
NVL   159.60 191.0 PKPab    12:59:19.4    -2.6                           T__                        _e               870843797 ISC  IR       --       MOS   S?Z ??? _ -70.7667   11.8333     0.0     0.0
NVL   159.60 191.0 pmax                                                  ___             23.0  1.00  __              870843797 ISC  IR       --       MOS   S?Z S?Z _ -70.7667   11.8333     0.0     0.0
VNA2  159.85 172.7 PKPab    12:59:23.322   0.2 186.7        2.44         T__             33.4  0.80  c_              848409490 ISC  IR       -- AWI   AWI   BHZ BHZ _ -70.9252   -7.3927     0.0     0.0
VNA2  159.85 172.7 PKPdf    12:58:38.128  -5.7                           T__              0.3      a__               887040470 FDSN AW          GFZ   GFZ   BHZ BHZ _ -70.9250   -7.3930   442.0     0.0
VNA1  160.04 171.7 PKPab    12:59:25.322   1.4                           T__             62.3  1.08  c_              848409491 ISC  IR       -- AWI   AWI   BHZ BHZ _ -70.6503   -8.2624     0.0     0.0

STOP

Agencies whose data contributed towards the results of this search:

 AUST      Geoscience Australia                                                      Australia
 AWI       Alfred Wegener Institute for Polar and Marine Research                    Germany
 .
 .
 WAR       Institute of Geophysics, Polish Academy of Sciences                       Poland
 WEL       Institute of Geological and Nuclear Sciences                              New Zealand
```

10.2.5 Ground Truth (GT) Events

Accurate locations are crucial in testing Earth models derived from body and surface wave tomography as well as in location calibration studies. 'Ground Truth' (GT) events are well-established source locations and origin times. A database of IASPEI reference events (GT earthquakes and explosions) is hosted at the ISC (www.isc.ac.uk). A full description of GT selection criteria can be found in *Bondár and McLaughlin* (2009a).

The events are coded by category GT0, GT1, GT2 or GT5, where the epicentre of a GTX event is known to within X km to a 95% confidence level. A map of all IASPEI reference events is shown in Figure 10.13 and the types of event are categorised in Figure 10.14. GT0 are explosions with announced locations and origin times. GT1 and GT2 are typically explosions, mine blasts or rock bursts either associated to explosion phenomenology located upon overhead imagery with seismically determined origin times, or precisely located by in-mine seismic networks. GT1-2 events are assumed to be shallow, but depth is unknown.

The database consists of nuclear explosions of GT0–5 quality, adopted from the Nuclear Explosion Database (*Bennett et al.*, 2010); GT0–5 chemical explosions, rock bursts, mine-induced events, as well as a few earthquakes, inherited from the reference event set by *Bondár et al.* (2004); GT5 events (typically earthquakes with crustal depths) which have been identified using either the method of *Bondár et al.* (2008) (2,275 events) or *Bondár and McLaughlin* (2009a) (updated regularly from the EHB catalogue (*Engdahl et al.*, 1998)), which uses the following criteria:

- 10 or more stations within 150 km from the epicentre
- one or more stations within 10 km
- $\Delta U \leq 0.35$
- a secondary azimuthal gap $\leq 160°$

where ΔU is the network quality metric defined as the mean absolute deviation between the best-fitting uniformly distributed network of stations and the actual network:

$$\Delta U = \frac{4\sum |esaz_i - (unif_i + b)|}{360N}, 0 \leq \Delta U \leq 1 \qquad (10.22)$$

where N is the number of stations, $esaz_i$ is the ith event-to-station azimuth, $unif_i = 360i/N$ for $i = 0$, ..., $N-1$, and $b = avg\,(esaz_i) - avg\,(unif_i)$. ΔU is normalised so that it is 0 when the stations are uniformly distributed in azimuth and 1 when all the stations are at the same azimuth.

The seismological community is invited to participate in this project by nominating seismic events for the reference event database. Submitters may be contacted for further confirmation and for arrival time data. The IASPEI Reference Event List will be periodically published both in written and electronic form with proper acknowledgement of all submitters.

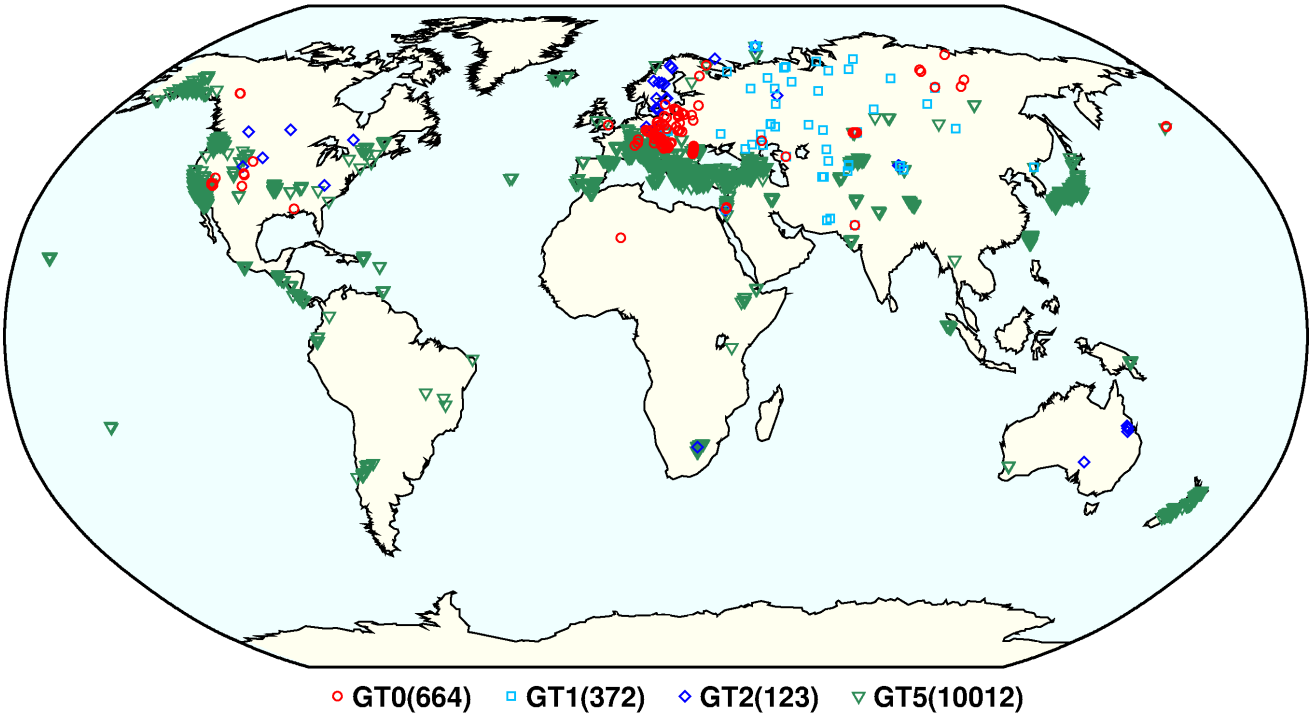

Figure 10.13: *Map of all IASPEI Reference Events as of January 2023.*

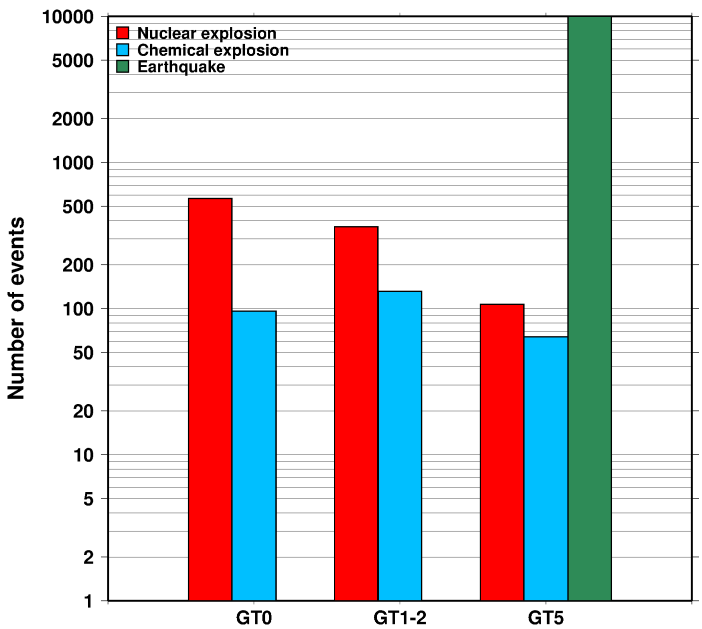

Figure 10.14: *Histogram showing the event types within the IASPEI Reference Event list as of January 2023.*

10.2.6 Nomenclature of Event Types

The nomenclature of event types currently used in the ISC Bulletin takes its origin from the IASPEI International Seismic Format (ISF).

Event type codes are composed of a leading character that generally indicates the confidence with which the type of the event is asserted and a trailing character that generally gives the type of the event. The leading and trailing characters may be used in any combination.

The **leading** characters are:

- s = suspected
- k = known
- f = felt (implies known)
- d = damaging (implies felt and known)

The **trailing** characters are:

- c = meteoritic event
- e = earthquake
- h = chemical explosion
- i = induced event
- l = landslide
- m = mining explosion
- n = nuclear explosion
- r = rock burst
- x = experimental explosion

A chemical explosion might be for mining or experimental purposes, and it is conceivable that other types of event might be assigned two or more different event type codes. This is deliberate, and matches the ambiguous identification of events in existing databases.

In addition, the code `uk` is used for events of unknown type and `ls` is used for known landslides.

The frequency of the different event types designated in the ISC Bulletin since 1964 is indicated in Figure 10.15.

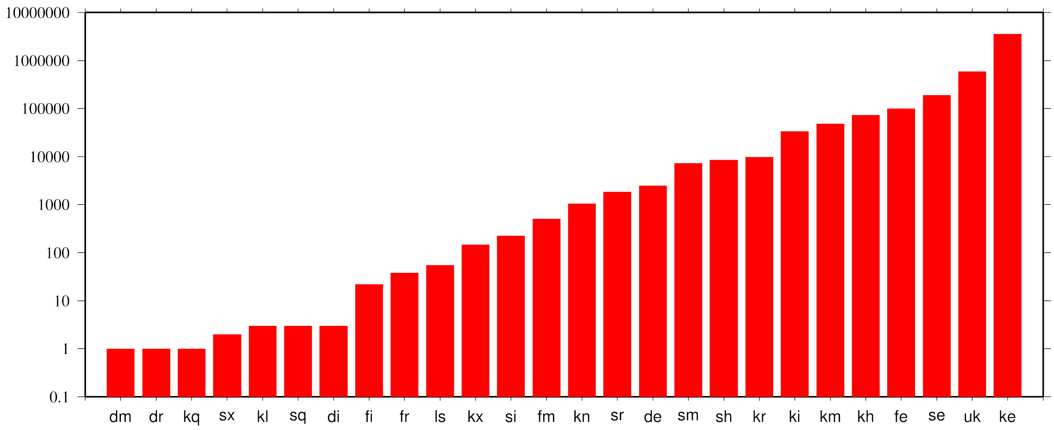

Figure 10.15: *Event types in the ISC Bulletin*

There are currently plans to revise this nomenclature as part of the coordination process between the National Earthquake Information Center (NEIC/USGS), European-Mediterranean Seismological Centre (CSEM) and the ISC.

10.3 Tables

Table 10.2: *Listing of all 391 agencies that have directly reported to the ISC. The 150 agencies highlighted in bold have reported data to the ISC Bulletin for the period of this Bulletin Summary.*

Agency Code	Agency Name
AAA	Alma-ata, Kazakhstan
AAE	University of Addis Ababa, Ethiopia
AAM	University of Michigan, USA
ADE	Primary Industries and Resources SA, Australia
ADH	Observatorio Afonso Chaves, Portugal
AEIC	Alaska Earthquake Information Center, USA
AFAD	**Disaster and Emergency Management Presidency, Turkey**
AFAR	The Afar Depression: Interpretation of the 1960-2000 Earthquakes, Israel
AFUA	University of Alabama, USA
ALG	Algiers University, Algeria
ANDRE	USSR
ANF	USArray Array Network Facility, USA
ANT	Antofagasta, Chile
ARE	Instituto Geofisico del Peru, Peru
ARO	Observatoire Géophysique d'Arta, Djibouti
ASIES	**Institute of Earth Sciences, Academia Sinica, Chinese Taipei**
ASL	Albuquerque Seismological Laboratory, USA
ASM	University of Asmara, Eritrea
ASRS	**Altai-Sayan Seismological Centre, GS SB RAS, Russia**
ATA	The Earthquake Research Center Ataturk University, Turkey
ATH	**National Observatory of Athens, Greece**
AUST	**Geoscience Australia, Australia**
AVETI	USSR
AWI	**Alfred Wegener Institute for Polar and Marine Research, Germany**

Table 10.2: *Continued.*

Agency Code	Agency Name
AZER	**Republican Seismic Survey Center of Azerbaijan National Academy of Sciences, Azerbaijan**
BCIS	Bureau Central International de Sismologie, France
BDF	Observatório Sismológico da Universidade de Brasília, Brazil
BELR	**Centre of Geophysical Monitoring of the National Academy of Sciences of Belarus, Republic of Belarus**
BEO	**Republicki seizmoloski zavod, Serbia**
BER	**University of Bergen, Norway**
BERK	Berkheimer H, Germany
BGR	**Bundesanstalt für Geowissenschaften und Rohstoffe, Germany**
BGS	**British Geological Survey, United Kingdom**
BGSI	**Botswana Geoscience Institute, Botswana**
BHUJ2	Study of Aftershocks of the Bhuj Earthquake by Japanese Research Team, Japan
BIAK	Biak earthquake aftershocks (17-Feb-1996), USA
BJI	**China Earthquake Networks Center, China**
BKK	**Thai Meteorological Department, Thailand**
BNS	Erdbebenstation, Geologisches Institut der Universität, Köl, Germany
BOG	Universidad Javeriana, Colombia
BRA	**Geophysical Institute, Slovak Academy of Sciences, Slovakia**
BRG	**Seismological Observatory Berggießhübel, TU Bergakademie Freiberg, Germany**
BRK	Berkeley Seismological Laboratory, USA
BRS	Brisbane Seismograph Station, Australia
BUC	**National Institute for Earth Physics, Romania**
BUD	Geodetic and Geophysical Research Institute, Hungary
BUEE	Earth & Environment, USA
BUG	Institute of Geology, Mineralogy & Geophysics, Germany
BUL	**Goetz Observatory, Zimbabwe**
BUT	Montana Bureau of Mines and Geology, USA
BYKL	**Baykal Regional Seismological Centre, GS SB RAS, Russia**
CADCG	Central America Data Centre, Costa Rica
CAN	Australian National University, Australia
CANSK	Canadian and Scandinavian Networks, Sweden
CAR	Instituto Sismologico de Caracas, Venezuela
CASC	Central American Seismic Center, Costa Rica
CATAC	**Central American Tsunami Advisory Center, Nicaragua**
CENT	Centennial Earthquake Catalog, USA
CERI	Center for Earthquake Research and Information, USA
CFUSG	**Inst. of Seismology and Geodynamics, V.I. Vernadsky Crimean Federal University, Republic of Crimea**
CLL	**Geophysikalisches Observatorium Collm, Germany**
CMWS	Laboratory of Seismic Monitoring of Caucasus Mineral Water Region, GSRAS, Russia
CNG	Seismographic Station Changalane, Mozambique
CNRM	**Centre National de Recherche, Morocco**
COSMOS	Consortium of Organizations for Strong Motion Observations, USA
CRAAG	**Centre de Recherche en Astronomie, Astrophysique et Géophysique, Algeria**

Table 10.2: *Continued.*

Agency Code	Agency Name
CSC	University of South Carolina, USA
CSEM	Centre Sismologique Euro-Méditerranéen (CSEM/EMSC), France
CUPWA	**Curtin University, Australia**
DASA	Defense Atomic Support Agency, USA
DBN	Koninklijk Nederlands Meteorologisch Instituut, Netherlands
DDA	General Directorate of Disaster Affairs, Turkey
DHMR	Yemen National Seismological Center, Yemen
DIAS	**Dublin Institute for Advanced Studies, Ireland**
DJA	**Badan Meteorologi, Klimatologi dan Geofisika, Indonesia**
DMN	**National Seismological Centre, Nepal, Nepal**
DNAG	USA
DNK	**Geological Survey of Denmark and Greenland, Denmark**
DRS	Dagestan Branch, Geophysical Survey, Russian Academy of Sciences, Russia
DSN	**Dubai Seismic Network, United Arab Emirates**
DUSS	Damascus University, Syria, Syria
EAF	East African Network, Unknown
EAGLE	Ethiopia-Afar Geoscientific Lithospheric Experiment, Unknown
EBR	Observatori de l'Ebre, Spain
EBSE	Ethiopian Broadband Seismic Experiment, Unknown
ECGS	European Center for Geodynamics and Seismology, Luxembourg
ECX	**Centro de Investigación Científica y de Educación Superior de Ensenada, Mexico**
EFATE	OBS Experiment near Efate, Vanuatu, USA
EHB	Engdahl, van der Hilst and Buland, USA
EIDC	Experimental (GSETT3) International Data Center, USA
EKA	Eskdalemuir Array Station, United Kingdom
ENT	Geological Survey and Mines Department, Uganda
EPSI	Reference events computed by the ISC for EPSI project, United Kingdom
ERDA	Energy Research and Development Administration, USA
EST	Geological Survey of Estonia, Estonia
EUROP	Unknown
EVBIB	Data from publications listed in the ISC Event Bibliography, Unknown
FBR	Fabra Observatory, Spain
FCIAR	**Federal Center for Integrated Arctic Research, Russia**
FDF	Fort de France, Martinique
FIA0	Finessa Array, Finland
FOR	Unknown Historical Agency, Unknown - historical agency
FUBES	Earth Science Dept., Geophysics Section, Germany
FUNV	**Fundación Venezolana de Investigaciones Sismológicas, Venezuela**
FUR	Geophysikalisches Observatorium der Universität München, Germany
GBZT	Marmara Research Center, Turkey
GCG	**INSIVUMEH, Guatemala**
GCMT	**The Global CMT Project, USA**
GDNRW	Geologischer Dienst Nordrhein-Westfalen, Germany
GEN	**Dipartimento per lo Studio del Territorio e delle sue Risorse (RSNI), Italy**
GEOAZ	UMR Géoazur, France

Table 10.2: Continued.

Agency Code	Agency Name
GEOMR	GEOMAR, Germany
GFZ	**Helmholtz Centre Potsdam GFZ German Research Centre For Geosciences**, **Germany**
GII	**The Geophysical Institute of Israel**, **Israel**
GOM	Observatoire Volcanologique de Goma, Democratic Republic of the Congo
GRAL	**National Council for Scientific Research**, **Lebanon**
GSDM	Geological Survey Department Malawi, Malawi
GSET2	Group of Scientific Experts Second Technical Test 1991, April 22 - June 2, Unknown
GTFE	German Task Force for Earthquakes, Germany
GUC	**Centro Sismológico Nacional, Universidad de Chile**, **Chile**
HAN	Hannover, Germany
HDC	Observatorio Vulcanológico y Sismológico de Costa Rica, Costa Rica
HEL	**Institute of Seismology, University of Helsinki**, **Finland**
HFS	Hagfors Observatory, Sweden
HFS1	Hagfors Observatory, Sweden
HFS2	Hagfors Observatory, Sweden
HIMNT	Himalayan Nepal Tibet Experiment, USA
HKC	**Hong Kong Observatory**, **Hong Kong**
HLUG	Hessisches Landesamt für Umwelt und Geologie, Germany
HLW	**National Research Institute of Astronomy and Geophysics**, **Egypt**
HNR	Ministry of Mines, Energy and Rural Electrification, Solomon Islands
HON	Pacific Tsunami Warning Center - NOAA, USA
HRVD	Harvard University, USA
HRVD_LR	Department of Geological Sciences, Harvard University, USA
HVO	Hawaiian Volcano Observatory, USA
HYB	**National Geophysical Research Institute**, **India**
HYD	National Geophysical Research Institute, India
IAG	Instituto Andaluz de Geofisica, Spain
IASBS	Institute for Advanced Studies in Basic Sciences, Iran
IASPEI	IASPEI Working Group on Reference Events, USA
ICE	Instituto Costarricense de Electricidad, Costa Rica
IDC	**International Data Centre, CTBTO**, **Austria**
IDG	Institute of Dynamics of Geosphere, Russian Academy of Sciences, Russia
IEC	Institute of the Earth Crust, SB RAS, Russia
IEPN	Institute of Environmental Problems of the North, Russian Academy of Sciences, Russia
IFREE	Institute For Research on Earth Evolution, Japan
IGGSL	Seismology Lab, Institute of Geology & Geophysics, Chinese Academy of Sciences, China
IGIL	**Instituto Dom Luiz, University of Lisbon**, **Portugal**
IGKR	Institute of Geology,Komi Science Centre,Ural Branch,Russian Academy of Sciences, Russia
IGQ	**Servicio Nacional de Sismología y Vulcanología**, **Ecuador**
IGS	Institute of Geological Sciences, United Kingdom
INAM	Instituto Nacional de Meteorologia e Geofisica - INAMET, Angola

***Table 10.2:** Continued.*

Agency Code	Agency Name
INDEPTH3	International Deep Profiling of Tibet and the Himalayas, USA
INET	Instituto Nicaraguense de Estudios Territoriales - INETER, Nicaragua
INMG	**Instituto Português do Mar e da Atmosfera, I.P.**, **Portugal**
INMGC	Instituto Nacional de Meteorologia e Geofísica, Cape Verde
IPEC	**The Institute of Physics of the Earth (IPEC)**, **Czech Republic**
IPER	Institute of Physics of the Earth, Academy of Sciences, Moscow, Russia
IPGP	**Institut de Physique du Globe de Paris**, **France**
IPRG	Institute for Petroleum Research and Geophysics, Israel
IRIS	**IRIS Data Management Center**, **USA**
IRSM	Institute of Rock Structure and Mechanics, Czech Republic
ISC	**International Seismological Centre**, **United Kingdom**
ISC-PPSM	**International Seismological Centre Probabilistic Point Source Model**, **United Kingdom**
ISK	**Kandilli Observatory and Research Institute**, **Turkey**
ISN	**Iraqi Meteorological and Seismology Organisation**, **Iraq**
ISS	International Seismological Summary, United Kingdom
IST	Institute of Physics of the Earth, Technical University of Istanbul, Turkey
ISU	**Institute of Seismology, Academy of Sciences, Republic of Uzbekistan**, **Uzbekistan**
ITU	Faculty of Mines, Department of Geophysical Engineering, Turkey
JEN	Geodynamisches Observatorium Moxa, Germany
JMA	**Japan Meteorological Agency**, **Japan**
JOH	Bernard Price Institute of Geophysics, South Africa
JSN	**Jamaica Seismic Network**, **Jamaica**
JSO	**Jordan Seismological Observatory**, **Jordan**
KBC	Institut de Recherches Géologiques et Minières, Cameroon
KEA	**Korea Earthquake Administration**, **Democratic People's Republic of Korea**
KEW	Kew Observatory, United Kingdom
KHC	Institute of Geophysics, Czech Academy of Sciences, Czech Republic
KISR	Kuwait Institute for Scientific Research, Kuwait
KLM	Malaysian Meteorological Service, Malaysia
KMA	**Korea Meteorological Administration**, **Republic of Korea**
KNET	**Kyrgyz Seismic Network**, **Kyrgyzstan**
KOLA	**Kola Regional Seismic Centre, GS RAS**, **Russia**
KRAR	Krasnoyarsk Scientific Research Inst. of Geology and Mineral Resources, Russia, Russia
KRL	Geodätisches Institut der Universität Karlsruhe, Germany
KRNET	**Institute of Seismology, Academy of Sciences of Kyrgyz Republic**, **Kyrgyzstan**
KRSC	**Kamchatka Branch of the Geophyiscal Survey of the RAS**, **Russia**
KRSZO	**Geodetic and Geophysical Reasearch Institute, Hungarian Academy of Sciences**, **Hungary**
KSA	Observatoire de Ksara, Lebanon
KUK	Geological Survey Department of Ghana, Ghana
LAO	Large Aperture Seismic Array, USA
LDG	**Laboratoire de Détection et de Géophysique/CEA**, **France**
LDN	University of Western Ontario, Canada

Table 10.2: Continued.

Agency Code	Agency Name
LDO	Lamont-Doherty Earth Observatory, USA
LED	Landeserdbebendienst Baden-Württemberg, Germany
LEDBW	Landeserdbebendienst Baden-Württemberg, Germany
LER	Besucherbergwerk Binweide Station, Germany
LIB	Tripoli, Libya
LIC	Station Géophysique de Lamto, Ivory Coast
LIM	Lima, Peru
LIS	Instituto de Meteorologia, Portugal
LIT	**Geological Survey of Lithuania**, **Lithuania**
LJU	**Slovenian Environment Agency**, **Slovenia**
LPA	**Universidad Nacional de La Plata**, **Argentina**
LPZ	Observatorio San Calixto, Bolivia
LRSM	Long Range Seismic Measurements Project, Unknown
LSZ	Geological Survey Department of Zambia, Zambia
LVSN	**Latvian Seismic Network**, **Latvia**
MAN	**Philippine Institute of Volcanology and Seismology**, **Philippines**
MAT	The Matsushiro Seismological Observatory, Japan
MATSS	USSR
MCO	**Macao Meteorological and Geophysical Bureau**, **Macao, China**
MCSM	**Main Centre for Special Monitoring**, **Ukraine**
MDD	**Instituto Geográfico Nacional**, **Spain**
MED_RCMT	**MedNet Regional Centroid - Moment Tensors**, **Italy**
MERI	Maharashta Engineering Research Institute, India
MES	Messina Seismological Observatory, Italy
MEX	**Instituto de Geofísica de la UNAM**, **Mexico**
MIRAS	**Mining Institute of the Ural Branch of the Russian Academy of Sciences**, **Russia**
MNH	Institut für Angewandte Geophysik der Universitat Munchen, Germany
MOLD	Institute of Geophysics and Geology, Moldova
MOS	**Geophysical Survey of Russian Academy of Sciences**, **Russia**
MOZ	Direccao Nacional de Geologia, Mozambique
MOZAR	, Mozambique
MRB	**Institut Cartogràfic i Geològic de Catalunya**, **Spain**
MSI	Messina Seismological Observatory, Italy
MSSP	Micro Seismic Studies Programme, PINSTECH, Pakistan
MSUGS	Michigan State University, Department of Geological Sciences, USA
MUN	Mundaring Observatory, Australia
NAI	University of Nairobi, Kenya
NAM	**The Geological Survey of Namibia**, **Namibia**
NAO	**Stiftelsen NORSAR**, **Norway**
NCEDC	Northern California Earthquake Data Center, USA
NDI	**National Centre for Seismology of the Ministry of Earth Sciences of India**, **India**
NEIC	**National Earthquake Information Center**, **USA**
NEIS	National Earthquake Information Service, USA
NERS	**North Eastern Regional Seismological Centre, Magadan, GS RAS**, **Russia**
NIC	**Cyprus Geological Survey Department**, **Cyprus**

Table 10.2: Continued.

Agency Code	Agency Name
NIED	**National Research Institute for Earth Science and Disaster Resilience, Japan**
NKSZ	USSR
NNC	**National Nuclear Center, Kazakhstan**
NORS	North Ossetia (Alania) Branch, Geophysical Survey, Russian Academy of Sciences, Russia
NOU	**IRD Centre de Nouméa, New Caledonia**
NSSC	National Syrian Seismological Center, Syria
NSSP	**National Survey of Seismic Protection, Armenia**
OBM	Institute of Astronomy and Geophysics, Mongolian Academy of Sciences, Mongolia
OGAUC	Centro de Investigação da Terra e do Espaço da Universidade de Coimbra, Portugal
OGSO	Ohio Geological Survey, USA
OMAN	**Sultan Qaboos University, Oman**
ORF	Orfeus Data Center, Netherlands
OSPL	**Observatorio Sismologico Politecnico Loyola, Dominican Republic**
OSUB	Osservatorio Sismologico Universita di Bari, Italy
OSUNB	**Observatory Seismological of the University of Brasilia, Brazil**
OTT	**Canadian Hazards Information Service, Natural Resources Canada, Canada**
PAL	Palisades, USA
PAS	California Institute of Technology, USA
PDA	Universidade dos Açores, Portugal
PDG	**Institute of Hydrometeorology and Seismology of Montenegro, Montenegro**
PEK	Peking, China
PGC	Pacific Geoscience Centre, Canada
PJWWP	**Private Observatory of Pawel Jacek Wiejacz, D.Sc., Poland**
PLV	**Institute of Geophysics, Viet Nam Academy of Science and Technology, Viet Nam**
PMEL	Pacific seismicity from hydrophones, USA
PMR	Alaska Tsunami Warning Center,, USA
PNNL	Pacific Northwest National Laboratory, USA
PNSN	**Pacific Northwest Seismic Network, USA**
PPT	**Laboratoire de Géophysique/CEA, French Polynesia**
PRE	**Council for Geoscience, South Africa**
PRU	**Institute of Geophysics, Czech Academy of Sciences, Czech Republic**
PTO	Instituto Geofísico da Universidade do Porto, Portugal
PTWC	**Pacific Tsunami Warning Center, USA**
QCP	**Manila Observatory, Philippines**
QUE	Pakistan Meteorological Department, Pakistan
QUI	Escuela Politécnica Nacional, Ecuador
RAB	Rabaul Volcanological Observatory, Papua New Guinea
RBA	Université Mohammed V, Morocco
REN	MacKay School of Mines, USA
REY	**Icelandic Meteorological Office, Iceland**

Table 10.2: Continued.

Agency Code	Agency Name
RHSSO	**Republic Hydrometeorological Service, Seismological Observatory, Banja Luka**, **Bosnia and Herzegovina**
RISSC	**Laboratory of Research on Experimental and Computational Seimology**, **Italy**
RMIT	Royal Melbourne Institute of Technology, Australia
ROC	Odenbach Seismic Observatory, USA
ROM	**Istituto Nazionale di Geofisica e Vulcanologia**, **Italy**
RRLJ	Regional Research Laboratory Jorhat, India
RSMAC	Red Sísmica Mexicana de Apertura Continental, Mexico
RSNC	**Red Sismológica Nacional de Colombia**, **Colombia**
RSPR	**Red Sísmica de Puerto Rico**, **USA**
RYD	King Saud University, Saudi Arabia
SAPSE	Southern Alps Passive Seismic Experiment, New Zealand
SAR	Sarajevo Seismological Station, Bosnia and Herzegovina
SARA	**SARA Electronic Instrument s.r.l.**, **Italy**
SBDV	USSR
SCB	**Observatorio San Calixto**, **Bolivia**
SCEDC	Southern California Earthquake Data Center, USA
SCSIO	Key Laboratory of Ocean and Marginal Sea Geology, South China Sea, China
SDD	**Universidad Autonoma de Santo Domingo**, **Dominican Republic**
SEA	Geophysics Program AK-50, USA
SET	Setif Observatory, Algeria
SFS	**Real Instituto y Observatorio de la Armada**, **Spain**
SGS	**Saudi Geological Survey**, **Saudi Arabia**
SHL	Central Seismological Observatory, India
SIGU	**Subbotin Institute of Geophysics, National Academy of Sciences**, **Ukraine**
SIK	Seismic Institute of Kosovo, Unknown
SIO	Scripps Institution of Oceanography, USA
SJA	**Instituto Nacional de Prevención Sísmica**, **Argentina**
SJS	Instituto Costarricense de Electricidad, Costa Rica
SKHL	**Sakhalin Experimental and Methodological Seismological Expedition, GS RAS**, **Russia**
SKL	Sakhalin Complex Scientific Research Institute, Russia
SKO	**Seismological Observatory Skopje**, **North Macedonia**
SLC	Salt Lake City, USA
SLM	Saint Louis University, USA
SNET	**Servicio Nacional de Estudios Territoriales**, **El Salvador**
SNM	New Mexico Institute of Mining and Technology, USA
SNSN	Saudi National Seismic Network, Saudi Arabia
SOF	**National Institute of Geophysics, Geology and Geography**, **Bulgaria**
SOMC	Seismological Observatory of Mount Cameroon, Cameroon
SOME	**Seismological Experimental Methodological Expedition**, **Kazakhstan**
SPA	USGS - South Pole, Antarctica
SPGM	Service de Physique du Globe, Morocco

Table 10.2: Continued.

Agency Code	Agency Name
SPITAK	, Armenia
SRI	Stanford Research Institute, USA
SSN	Sudan Seismic Network, Sudan
SSNC	**Servicio Sismológico Nacional Cubano, Cuba**
SSS	Centro de Estudios y Investigaciones Geotecnicas del San Salvador, El Salvador
STK	Stockholm Seismological Station, Sweden
STR	**EOST / RéNaSS, France**
STU	Stuttgart Seismological Station, Germany
SVSA	**Sistema de Vigilância Sismológica dos Açores, Portugal**
SYO	**National Institute of Polar Research, Japan**
SZGRF	Seismologisches Zentralobservatorium Gräfenberg, Germany
TAC	Estación Central de Tacubaya, Mexico
TAN	**Antananarivo, Madagascar**
TANZANIA	Tanzania Broadband Seismic Experiment, USA
TAP	**Central Weather Bureau (CWB), Chinese Taipei**
TAU	University of Tasmania, Australia
TEH	**Tehran University, Iran**
TEIC	Center for Earthquake Research and Information, USA
THE	**Department of Geophysics, Aristotle University of Thessaloniki, Greece**
THR	**International Institute of Earthquake Engineering and Seismology (IIEES), Iran**
TIF	**Institute of Earth Sciences/ National Seismic Monitoring Center, Georgia**
TIR	**Institute of Geosciences, Polytechnic University of Tirana, Albania**
TRI	**Istituto Nazionale di Oceanografia e di Geofisica Sperimentale (OGS), Italy**
TRN	**The Seismic Research Centre, Trinidad and Tobago**
TTG	Titograd Seismological Station, Montenegro
TUL	Oklahoma Geological Survey, USA
TUN	**Institut National de la Météorologie, Tunisia**
TVA	Tennessee Valley Authority, USA
TXNET	**Texas Seismological Network, University of Texas at Austin, USA**
TZN	University of Dar Es Salaam, Tanzania
UAF	Department of Geosciences, USA
UATDG	The University of Arizona, Department of Geosciences, USA
UAV	Red Sismológica de Los Andes Venezolanos, Venezuela
UCB	University of Colorado, Boulder, USA
UCC	**Royal Observatory of Belgium, Belgium**
UCDES	Department of Earth Sciences, United Kingdom
UCR	**Sección de Sismología, Vulcanología y Exploración Geofísica, Costa Rica**
UCSC	Earth & Planetary Sciences, USA
UESG	School of Geosciences, United Kingdom
UGN	Institute of Geonics AS CR, Czech Republic
ULE	University of Leeds, United Kingdom

Table 10.2: Continued.

Agency Code	Agency Name
UNAH	Universidad Nacional Autonoma de Honduras, Honduras
UPA	**Universidad de Panama**, **Panama**
UPIES	Institute of Earth- and Environmental Science, Germany
UPP	**University of Uppsala**, **Sweden**
UPSL	**University of Patras, Department of Geology**, **Greece**
UREES	Department of Earth and Environmental Science, USA
USAEC	United States Atomic Energy Commission, USA
USCGS	United States Coast and Geodetic Survey, USA
USGS	United States Geological Survey, USA
UTEP	Department of Geological Sciences, USA
UUSS	The University of Utah Seismograph Stations, USA
UVC	Universidad del Valle, Colombia
UWMDG	University of Wisconsin-Madison, Department of Geoscience, USA
VAO	**Instituto Astronomico e Geofísico**, **Brazil**
VIE	**Zentralanstalt für Meteorologie und Geodynamik (ZAMG)**, **Austria**
VKMS	Lab. of Seismic Monitoring, Voronezh region, GSRAS & Voronezh State University, Russia
VLA	Vladivostok Seismological Station, Russia
VSI	University of Athens, Greece
VUW	Victoria University of Wellington, New Zealand
WAR	**Institute of Geophysics, Polish Academy of Sciences**, **Poland**
WASN	USA
WBNET	**Institute of Geophysics, Czech Academy of Sciences**, **Czech Republic**
WEL	**Institute of Geological and Nuclear Sciences**, **New Zealand**
WES	Weston Observatory, USA
WUSTL	Washington University Earth and Planentary Sciences, USA
YARS	**Yakutiya Regional Seismological Center, GS SB RAS**, **Russia**
ZAG	**Seismological Survey of the Republic of Croatia**, **Croatia**
ZEMSU	USSR
ZUR	**Swiss Seismological Service (SED)**, **Switzerland**
ZUR_RMT	Zurich Moment Tensors, Switzerland

Table 10.3: *Phases reported to the ISC. These include phases that could not be matched to an appropriate* ak135 *phases. Those agencies that reported at least 10% of a particular phase are also shown.*

Reported Phase	Total	Agencies reporting
P	4307264	
S	2132602	JMA (15%), TAP (15%)
IAML	915597	NEIC (54%), AFAD (21%)
NULL	795804	NEIC (47%), IDC (24%)
IAmb	501782	NEIC (96%)
AML	488923	ROM (98%)
Pg	363938	ISK (36%)
Pn	299994	NEIC (33%), ISK (28%)
Sg	256463	ISK (21%), STR (12%)
LR	140870	IDC (72%), BJI (24%)
pmax	120644	MOS (71%), BJI (29%)
Sn	80667	IDC (16%)
IAMs_20	72746	NEIC (97%)
SG	70774	HEL (54%), PRU (25%)
PG	64434	HEL (57%), PRU (18%), IPEC (12%)
smax	40587	HEL (78%), MOS (14%)
Lg	39788	NNC (65%), IDC (22%)
PKP	35899	IDC (40%), VIE (14%)
PN	30435	MOS (40%), HEL (33%)
T	26373	IDC (97%)
SN	21792	HEL (78%), OTT (14%)
IAmb_Lg	20753	NEIC (100%)
IVmb_Lg	19386	MDD (100%)
pP	17517	BJI (29%), IDC (17%), ISC1 (12%), VIE (11%)
MLR	15230	MOS (100%)
PKPbc	15003	IDC (70%)
PKIKP	13970	MOS (98%)
PcP	13773	IDC (62%)
A	13642	JMA (56%), SKHL (44%)
SB	12051	HEL (100%)
PP	11936	BJI (21%), IDC (20%), BELR (16%)
PB	9992	HEL (100%)
SPECP	9800	AFAD (100%)
SS	8638	MOS (36%), BELR (23%), BJI (21%)
PKPdf	6929	NEIC (42%), INMG (18%)
x	6897	BRG (27%), TRN (19%), CLL (18%), NDI (12%)
L	6782	BJI (79%), WAR (13%)
sP	5904	BJI (68%), ISC1 (15%)
Sb	5064	IRIS (91%)
PKPab	5049	IDC (55%), INMG (15%)
Trac	4850	OTT (100%)
ScP	4670	IDC (66%), IRIS (13%), BJI (11%)
AMS	4191	PRU (73%), CLL (20%)
PKiKP	4023	IDC (37%), VIE (30%)
PPP	3900	MOS (53%), BELR (41%)
AMB	3572	SKHL (87%), BJI (12%)
Amp	3495	BRG (100%)
LRM	3233	BELR (100%)
LG	3199	BRA (76%), OTT (24%)
SSS	3142	BELR (53%), MOS (38%)
Pdiff	2803	IRIS (50%), IDC (17%), VIE (15%)
*PP	2796	MOS (100%)
PKP2	2498	MOS (100%)
Pb	2426	IRIS (81%), NAO (13%)
PKKPbc	2301	IDC (93%)
LQ	2057	BELR (68%), PPT (15%), INMG (11%)
I	1742	IDC (100%)
PKhKP	1709	IDC (100%)
IVmb_VC	1670	MDD (100%)
sS	1600	BJI (77%), BELR (17%)
pPKP	1553	VIE (37%), IDC (33%), BJI (15%)
SKS	1427	BJI (37%), BELR (27%), VIE (14%), PRU (13%)
Smax	1149	BYKL (100%)
SKPbc	1060	IDC (92%)
IVMs_BB	1014	BER (81%)
Pmax	974	BYKL (88%)
IVmB_BB	918	BER (80%), SSNC (15%)
X	859	JMA (89%)
ScS	850	BJI (66%), IDC (17%)
PKPPKP	803	IDC (98%)

Table 10.3: (continued)

Reported Phase	Total	Agencies reporting
PS	766	MOS (45%), BELR (23%), CLL (16%)
Sgmax	748	NERS (100%)
PKKP	692	IDC (47%), VIE (40%)
Pdif	666	BJI (28%), NEIC (18%)
SKP	634	IDC (43%), VIE (17%), INMG (12%)
END	596	ROM (100%)
AMs_VX	564	NEIC (100%)
SKSac	545	BER (40%), AWI (21%), CLL (11%)
tx	497	INMG (95%)
PKHKP	470	MOS (100%)
PDIFF	460	PRU (42%), BRA (33%), IPEC (21%)
pPKPbc	454	IDC (78%), BGR (11%)
AMd	448	TIR (100%)
PKPAB	442	PRU (100%)
*SS	440	MOS (100%)
*SP	420	MOS (100%)
SP	410	MOS (22%), BER (21%), BGR (15%)
p	363	MAN (68%), ROM (32%)
pPKiKP	354	VIE (66%), BELR (20%)
max	349	BYKL (100%)
AMP	335	UPA (46%), BER (42%)
sPKP	297	BJI (77%), BELR (13%)
PKPDF	291	PRU (100%)
SKKS	282	BELR (54%), BJI (40%)
PKP2bc	251	IDC (100%)
s	239	MAN (100%)
Pgmax	220	NERS (100%)
SKKPbc	220	IDC (93%)
PKKPab	216	IDC (98%)
AmB	199	KEA (100%)
P3KPbc	193	IDC (100%)
PPS	177	CLL (59%), MOS (18%), LPA (15%)
PmP	177	BGR (59%), ZUR (41%)
PcS	171	BJI (96%)
MSG	159	HEL (100%)
SKPdf	151	CLL (25%), BER (23%), INMG (22%), AWI (19%)
SSSS	146	CLL (100%)
P4KPbc	141	IDC (100%)
SmS	139	BGR (75%), ZUR (25%)
m	139	SIGU (100%)
PKS	130	BELR (48%), BJI (48%)
pPKPab	125	IDC (48%), CLL (31%)
pPKPdf	124	AWI (44%), CLL (19%), UCC (13%)
SKKP	104	BELR (44%), IDC (31%), VIE (18%)
IAMLHF	100	BER (100%)
H	100	IDC (99%)
PKPpre	97	NEIC (61%), PRU (28%), CLL (11%)
IVmB	97	BER (100%)
PCP	90	LPA (46%), PRU (39%)
pPP	86	LPA (59%), CLL (30%)
PKPf	83	BRG (100%)
SKPab	75	IDC (59%), INMG (32%)
PKPb	74	BRG (100%)
SKKSac	68	CLL (59%), HYB (26%)
Px	64	CLL (100%)
Sdif	64	CLL (58%), INMG (20%), BELR (14%)
pPdiff	62	VIE (77%), BGR (11%)
SKIKS	62	LPA (100%)
SKIKP	59	LPA (100%)
sPKiKP	58	BELR (69%)
PKP2ab	58	IDC (100%)
PKIKS	56	LPA (100%)
IAML_BB	56	THR (100%)
sPP	54	CLL (94%)
E	53	YARS (47%), INMG (40%)
PKKPdf	52	AWI (88%)
r	49	BRG (100%)
SCS	44	LPA (95%)
P'P'	44	VIE (95%)
Pif	43	BRG (100%)
pPcP	42	IDC (90%)

Table 10.3: (continued)

Reported Phase	Total	Agencies reporting
P3KP	41	IDC (100%)
SME	39	BJI (100%)
SKSdf	38	HYB (53%), AWI (16%)
SMN	38	BJI (100%)
SgSg	38	BYKL (100%)
PPPP	35	CLL (100%)
ATPG	35	OSPL (100%)
ASSG	35	OSPL (100%)
SKiKP	35	IDC (83%)
ATSG	35	OSPL (100%)
ASPG	35	OSPL (100%)
sSKS	34	BELR (97%)
PPMZ	32	BJI (100%)
Sdiff	31	BGR (94%)
PSKS	30	CLL (97%)
sSS	30	CLL (93%)
(sP)	28	CLL (100%)
PSP	28	LPA (96%)
PgPg	28	BYKL (100%)
Rg	27	IDC (63%), BRG (22%)
SKSa	26	BRG (100%)
pwP	24	ISC1 (100%)
rx	24	SKHL (88%)
R	22	AWI (100%)
SDIFF	21	LPA (81%), IPEC (19%)
sPdiff	20	VIE (95%)
PKPdif	20	CLL (65%), LJU (35%)
AMl	19	TIR (100%)
(PP)	19	CLL (100%)
sPKPdf	17	HYB (47%), CLL (41%), AWI (12%)
PKPB	17	PRU (100%)
i	17	INMG (100%)
(SS)	17	CLL (100%)
Pn_1	17	ATH (100%)
BAZ	15	BER (80%), DNK (20%)
MSN	15	HEL (73%), BER (27%)
PKPPKPdf	15	CLL (100%)
S'S'	14	SVSA (100%)
Sif	14	BRG (100%)
PKSdf	14	CLL (86%), BER (14%)
RG	13	HEL (54%), IPEC (46%)
Pn_2	12	ATH (100%)
P*	12	MOS (50%), BGR (42%)
pPKPf	12	BRG (100%)
Sx	11	CLL (100%)
PKKS	11	BELR (91%)
SPP	11	CLL (64%), BELR (18%), MOS (18%)
pPdif	11	CLL (55%), BELR (45%)
(S)	11	CFUSG (100%)
x2	11	ISC1 (100%)
(Pg)	11	CLL (82%), CFUSG (18%)
sPPP	10	CLL (100%)
(pP)	10	CLL (100%)
PKSbc	10	SOME (60%), CLL (40%)
sSdif	10	CLL (70%), BELR (30%)
P(2)	10	CLL (100%)
PKP1	9	PPT (67%), LDG (33%)
PKPlp	9	CLL (100%)
sSSS	9	CLL (100%)
Plp	8	CLL (100%)
(Pn)	8	CLL (100%)
(PKPdf)	8	CLL (100%)
IVMs	8	BER (100%)
sPdif	8	CLL (62%), BELR (38%)
(Sg)	7	CLL (57%), CFUSG (43%)
(P)	7	CFUSG (100%)
sPKPbc	6	AWI (67%), CLL (33%)
SKSP	6	CLL (67%), BRG (33%)
Pn_3	6	ATH (100%)
SKPa	6	NAO (100%)
AP	6	MOS (100%)

Table 10.3: (continued)

Reported Phase	Total	Agencies reporting
PKPmax	6	CLL (100%)
(PKPbc)	6	CLL (100%)
P'P'bc	6	AWI (100%)
(PKiKP)	6	CLL (100%)
PPPrev	5	CLL (100%)
(Sn)	5	CLL (100%)
SKKSa	5	BRG (100%)
PPmax	5	CLL (100%)
PKPc	5	PJWWP (100%)
sPS	5	CLL (60%), BRG (40%)
x1	4	ISC1 (100%)
sSKPdf	4	CLL (100%)
sPKPab	4	AWI (50%), INMG (25%), CLL (25%)
R2	4	CLL (100%)
SKKPdf	4	CLL (50%), AWI (50%)
del	4	KNET (100%)
SKSp	4	BRA (75%), WAR (25%)
Pn_0	4	ATH (100%)
(pPKPdf)	4	CLL (100%)
pSKKSac	4	CLL (100%)
(pPKPab)	4	CLL (100%)
SH	4	SYO (100%)
LH	4	CLL (100%)
(PKPab)	4	CLL (100%)
(SSS)	4	CLL (100%)
(sS)	4	CLL (100%)
AMPG	4	BGS (50%), DNK (25%), BER (25%)
SCP	3	IPEC (100%)
SKKSdf	3	CLL (67%), HYB (33%)
PDIF	3	PRU (100%)
APKP	3	MOS (100%)
pS	3	WAR (67%), CLL (33%)
IVMsBB	3	HYB (67%), DNK (33%)
pSKSac	3	CLL (100%)
(SSSS)	3	CLL (100%)
PPdif	3	BER (100%)
pPif	3	BRG (100%)
sPPPP	3	CLL (100%)
S*	3	BJI (67%), BGR (33%)
sPPS	2	CLL (100%)
Pg_3	2	ATH (100%)
(P	2	CFUSG (100%)
IVmBBB	2	HYB (100%)
sSKSac	2	CLL (100%)
IAMl	2	SSNC (100%)
SKKPf	2	BRG (100%)
pPPS	2	CLL (100%)
P9	2	NDI (50%), UPA (50%)
(sPP)	2	CLL (100%)
SSmax	2	CLL (100%)
SKPf	2	BRG (100%)
pPS	2	CLL (100%)
AMb	2	ISN (50%), LVSN (50%)
sSSSS	2	CLL (100%)
Station	2	AWI (100%)
(PKPdif)	2	CLL (100%)
PSPS	2	CLL (100%)
PSS	2	BRG (50%), CLL (50%)
pPKPb	2	BRG (100%)
SKSSKSac	2	CLL (100%)
Sglp	2	CLL (100%)
PKPdf(2)	2	CLL (100%)
PKPa	2	NAO (100%)
LV	2	CLL (100%)
SKPlp	2	CLL (100%)
PPlp	2	CLL (100%)
SKPPKPdf	2	CLL (100%)
PnA	2	THR (100%)
Sg_2	2	ATH (100%)
SA	2	SJA (100%)
(pPKiKP)	2	CLL (100%)

Table 10.3: (continued)

Reported Phase	Total	Agencies reporting
P4KP	2	IDC (100%)
sSif	2	BRG (100%)
AMSG	2	BGS (100%)
PKKPf	1	BRG (100%)
PP(2)	1	LPA (100%)
pSPP	1	CLL (100%)
sSKSdf	1	CLL (100%)
sSKSP	1	CLL (100%)
M	1	LJU (100%)
PKKPbc2	1	CLL (100%)
PnPn	1	KRSZO (100%)
pSKSdf	1	CLL (100%)
PGN	1	HEL (100%)
Unk	1	FCIAR (100%)
(sPPP)	1	CLL (100%)
(PcP)	1	CLL (100%)
pScP	1	CLL (100%)
(sSS)	1	CLL (100%)
SnFF	1	INMG (100%)
(sPKPdf)	1	CLL (100%)
(sSP)	1	CLL (100%)
rg	1	BRG (100%)
(SKSdf)	1	CLL (100%)
(SKPdf)	1	CLL (100%)
pPKPlp	1	CLL (100%)
sp	1	CLL (100%)
PKKPb	1	BRG (100%)
PPP(2)	1	LPA (100%)
(PSSrev)	1	CLL (100%)
pPPPrev	1	CLL (100%)
sSKKSac	1	CLL (100%)
SSPrev	1	CLL (100%)
SKKPab	1	BELR (100%)
sPKP2	1	BJI (100%)
Pmlp	1	CLL (100%)
PRKPbc	1	CLL (100%)
pSdiff	1	CLL (100%)
XP	1	MOS (100%)
SKPPKPbc	1	CLL (100%)
D	1	MOS (100%)
SDIF	1	PRU (100%)
PPk	1	CLL (100%)
(pPPS)	1	CLL (100%)
P(3)	1	CLL (100%)
PPPmax	1	CLL (100%)
PcP(2)	1	CLL (100%)
sPSS	1	CLL (100%)
(PPPP)	1	CLL (100%)
(PSKS)	1	CLL (100%)
sScS	1	CLL (100%)
sSP	1	CLL (100%)
i-	1	INMG (100%)
(SP)	1	CLL (100%)
(sPPS)	1	CLL (100%)
(PPS)	1	CLL (100%)
SKPdf(2)	1	CLL (100%)
PKPPKPab	1	CLL (100%)
(SKSac)	1	CLL (100%)
SbSb	1	KRSZO (100%)
sPSSrev	1	CLL (100%)
S(3)	1	CLL (100%)
(Pdif)	1	CLL (100%)
sSKSa	1	BRG (100%)
sPSKS	1	CLL (100%)
PKPdF	1	INMG (100%)
(SKPab)	1	CLL (100%)
P(4)	1	CLL (100%)
Pe	1	SSNC (100%)
Sg_3	1	ATH (100%)
pPKSdf	1	CLL (100%)
PIkP	1	SYO (100%)

Table 10.3: *(continued)*

Reported Phase	Total	Agencies reporting
(PKP)	1	CLL (100%)
SS(2)	1	LPA (100%)
pPPP	1	CLL (100%)
PSSrev	1	CLL (100%)
pPKKPbc	1	CLL (100%)
PKPabd	1	PJWWP (100%)
SPS	1	CLL (100%)
Pg_2	1	ATH (100%)
(SKKSdf)	1	CLL (100%)
pPKPdf2	1	CLL (100%)
sPKPf	1	BRG (100%)
(PSS)	1	CLL (100%)
sSKPbc	1	CLL (100%)
PPSmax	1	CLL (100%)
(SKSP)	1	CLL (100%)
pPKSbc	1	CLL (100%)

Table 10.4: Reporters of amplitude data

Agency	Number of reported amplitudes	Number of amplitudes in ISC located events	Number used for ISC mb	Number used for ISC MS
NEIC	1071621	324773	213087	34227
IDC	556245	525730	130190	73016
ROM	477855	11360	0	0
WEL	275872	43293	9	0
AFAD	188447	17037	0	0
ISK	159772	25929	0	0
GFZ	153275	153086	0	0
MOS	109980	105899	50709	9982
NNC	84059	31578	63	0
BJI	76253	74427	21065	24481
DJA	67688	54371	11287	0
ATH	66315	11713	0	0
RSNC	66276	17483	1980	0
AUST	54987	10088	7109	0
THE	53764	21404	0	0
VIE	50980	29422	10206	0
SOME	49348	19299	3017	0
INMG	40298	14534	4090	3
GUC	33230	7839	17	0
SVSA	32115	952	214	0
HEL	32038	1793	1	0
SDD	29087	9668	0	0
SSNC	23438	4309	55	0
TXNET	22108	385	0	0
MDD	21079	3485	0	0
JSO	15846	1989	90	0
JMA	15104	14914	0	0
NDI	15081	11291	3172	219
SJA	13935	12970	0	0
MAN	13641	2055	0	0
PRE	13387	628	0	0
MCSM	13020	12853	5220	0
LDG	12284	1497	0	0
BER	11792	5172	1493	415
PRU	10322	4026	0	2152
DNK	9513	5798	4712	46
SKHL	9303	4583	0	0
ZUR	8943	409	0	0
OSPL	8637	4174	0	0
MRB	8636	214	0	0
AWI	7572	4060	1800	0
BELR	7569	5078	736	1232
LJU	6831	300	0	0
PDG	6717	3725	0	0
PPT	6324	5447	339	0
BUC	6152	2060	0	0

Table 10.4: *Continued.*

Agency	Number of reported amplitudes	Number of amplitudes in ISC located events	Number used for ISC *mb*	Number used for ISC *MS*
BGR	5922	5636	4219	0
NIC	5347	3257	0	0
OTT	4850	527	0	0
KRSZO	4611	661	0	0
NOU	4563	4477	2869	0
YARS	4435	394	1	0
BGS	3994	2361	1708	316
WBNET	3934	0	0	0
UCC	3671	2908	2477	0
BRG	3495	497	0	0
ECX	3226	282	0	0
TIR	2935	832	0	0
KNET	2928	1351	0	0
CLL	2671	2381	339	503
IPEC	2605	513	0	0
BYKL	2391	1408	0	0
CFUSG	2104	1951	0	0
GCG	2102	1736	0	0
BKK	2028	1011	6	0
SCB	1880	265	0	0
NAO	1786	1768	1232	0
ASRS	1581	892	0	0
BGSI	1456	332	0	0
LVSN	1438	275	0	0
SKO	1302	391	0	0
IGIL	1187	586	136	153
NERS	1011	647	0	0
UPA	985	42	0	0
THR	967	905	0	0
WAR	906	317	0	180
SIGU	787	488	0	0
KEA	679	344	0	60
FCIAR	602	227	15	0
MIRAS	595	90	0	0
DMN	535	412	0	0
SNET	395	95	0	0
NAM	382	78	0	0
ISN	359	299	0	0
PLV	104	53	0	0
HYB	101	101	0	0
PJWWP	22	21	0	0
KMA	1	1	0	0

11

Glossary of ISC Terminology

- Agency/ISC data contributor

  An academic or government institute, seismological organisation or company, geological/meteorological survey, station operator or author that reports or contributed data in the past to the ISC or one of its predecessors. Agencies may contribute data to the ISC directly, or indirectly through other ISC data contributors.

- Agency code

  A unique, maximum eight-character code for a data reporting agency (e.g. NEIC, GFZ, BUD) or author (e.g. ISC, ISC-EHB, IASPEI). Often the agency code is the commonly used acronym of the reporting institute.

- Arrival

  A phase pick at a station is characterised by a phase name and an arrival time.

- Associated phase

  Associated phase arrival or amplitude measurements represent a collection of observations belonging to (i.e. generated by) an event. The complete set of observations are associated to the prime hypocentre.

- Azimuthal gap/Secondary azimuthal gap

  The azimuthal gap for an event is defined as the largest angle between two stations with defining phases when the stations are ordered by their event-to-station azimuths. The secondary azimuthal gap is the largest azimuthal gap a single station closes.

- BAAS

  Seismological bulletins published by the British Association for the Advancement of Science (1913-1917) under the leadership of H.H. Turner. These bulletins are the predecessors of the ISS Bulletins and include reports from stations distributed worldwide.

- Bulletin

  An ordered list of event hypocentres, uncertainties, focal mechanisms, network magnitudes, as well as phase arrival and amplitude observations associated to each event. An event bulletin may list all the reported hypocentres for an event. The convention in the ISC Bulletin is that the preferred (prime) hypocentre appears last in the list of reported hypocentres for an event.

- Catalogue

  An ordered list of event hypocentres, uncertainties and magnitudes. An event catalogue typically lists only the preferred (prime) hypocentres and network magnitudes.

- CoSOI/IASPEI

  Commission on Seismological Observation and Interpretation, a commission of IASPEI that prepares and discusses international standards and procedures in seismological observation and interpretation.

- Defining/Non-defining phase

  A defining phase is used in the location of the event (time-defining) or in the calculation of the network magnitude (magnitude-defining). Non-defining phases are not used in the calculations because they suffer from large residuals or could not be identified.

- Direct/Indirect report

  A data report sent (e-mailed) directly to the ISC, or indirectly through another ISC data contributor.

- Duplicates

  Nearly identical phase arrival time data reported by one or more agencies for the same station. Duplicates may be created by agencies reporting observations from other agencies, or several agencies independently analysing the waveforms from the same station.

- Event

  A natural (e.g. earthquake, landslide, asteroid impact) or anthropogenic (e.g. explosion) phenomenon that generates seismic waves and its source can be identified by an event location algorithm.

- Grouping

  The ISC algorithm that organises reported hypocentres into groups of events. Phases associated to any of the reported hypocentres will also be associated to the preferred (prime) hypocentre. The grouping algorithm also attempts to associate phases that were reported without an accompanying hypocentre to events.

- Ground Truth

  An event with a hypocentre known to certain accuracy at a high confidence level. For instance, GT0 stands for events with exactly known location, depth and origin time (typically explosions); GT5 stands for events with their epicentre known to 5 km accuracy at the 95% confidence level, while their depth and origin time may be known with less accuracy.

- Ground Truth database

  On behalf of IASPEI, the ISC hosts and maintains the IASPEI Reference Event List, a bulletin of ground truth events.

- IASPEI

  International Association of Seismology and Physics of the Earth Interior, www.iaspei.org.

- International Registry of Seismograph Stations (IR)

  Registry of seismographic stations, jointly run by the ISC and the World Data Center for Seismology, Denver (NEIC). The registry provides and maintains unique five-letter codes for stations participating in the international parametric and waveform data exchange.

- ISC Bulletin

  The comprehensive bulletin of the seismicity of the Earth stored in the ISC database and accessible through the ISC website. The bulletin contains both natural and anthropogenic events. Currently the ISC Bulletin spans more than 50 years (1960-to date) and it is constantly extended by adding both recent and past data. Eventually the ISC Bulletin will contain all instrumentally recorded events since 1900.

- ISC Governing Council

  According to the ISC Working Statutes the Governing Council is the governing body of the ISC, comprising one representative for each ISC Member.

- ISC-located events

  A subset of the events selected for ISC review are located by the ISC. The rules for selecting an event for location are described in Section 10.1.3; ISC-located events are denoted by the author ISC.

- ISC Member

  An academic or government institute, seismological organisation or company, geological/meteorological survey, station operator, national/international scientific organisation that contribute to the ISC budget by paying membership fees. ISC members have voting rights in the ISC Governing Council.

- ISC-reviewed events

  A subset of the events reported to the ISC are selected for ISC analyst review. These events may or may not be located by the ISC. The rules for selecting an event for review are described in Section 10.1.3. Non-reviewed events are explicitly marked in the ISC Bulletin by the comment following the prime hypocentre "Event not reviewed by the ISC".

- ISF

  International Seismic Format (www.isc.ac.uk/standards/isf). A standard bulletin format approved by IASPEI. The ISC Bulletin is presented in this format at the ISC website.

- ISS

  International Seismological Summary (1918-1963). These bulletins are the predecessors of the ISC Bulletin and represent the major source of instrumental seismological data before the digital era. The ISS contains regionally and teleseismically recorded events from several hundreds of globally distributed stations.

- Network magnitude

The event magnitude reported by an agency or computed by the ISC locator. An agency can report several network magnitudes for the same event and also several values for the same magnitude type. The network magnitude obtained with the ISC locator is defined as the median of station magnitudes of the same magnitude type.

- Phase

  A maximum eight-character code for a seismic, infrasonic, or hydroacoustic phase. During the ISC processing, reported phases are mapped to standard IASPEI phase names. Amplitude measurements are identified by specific phase names to facilitate the computation of body-wave and surface-wave magnitudes.

- Prime hypocentre

  The preferred hypocentre solution for an event from a list of hypocentres reported by various agencies or calculated by the ISC.

- Reading

  Parametric data that are associated to a single event and reported by a single agency from a single station. A reading typically includes one or more phase names, arrival time and/or amplitude/period measurements.

- Report/Data report

  All data that are reported to the ISC are parsed and stored in the ISC database. These may include event bulletins, focal mechanisms, moment tensor solutions, macroseismic descriptions and other event comments, as well as phase arrival data that are not associated to events. Every single report sent to the ISC can be traced back in the ISC database via its unique report identifier.

- Shide Circulars

  Collections of station reports for large earthquakes occurring in the period 1899-1912. These reports were compiled through the efforts of J. Milne. The reports are mainly for stations of the British Empire equipped with Milne seismographs. After Milne's death, the Shide Circulars were replaced by the Seismological Bulletins of the BAAS.

- Station code

  A unique, maximum five-character code for a station. The ISC Bulletin contains data exclusively from stations registered in the International Registry of Seismograph Stations.

12

Acknowledgements

We thank our colleagues at the Institute of Geophysics and Geology of the University of Leipzig in Germany for kindly accepting our invitation and preparing an article for this issue of the Summary.

We are also grateful to the developers of the Generic Mapping Tools (GMT) suite of software (Wessel et al., 2019) that was used extensively for producing the figures.

Finally, we thank the ISC Member Institutions, Data Contributors, Funding Agencies (including NSF Award EAR-1811737 and Royal Society Award INT004) and Sponsors for supporting the long-term operation of the ISC.

References

Adamaki, A. (2017), Seismicity Analysis Using Dense Network Data : Catalogue Statistics and Possible Foreshocks Investigated Using Empirical and Synthetic Data, Ph.D. thesis, Uppsala University, urn:nbn:se:uu:diva-328057.

Adams, R. D., A. A. Hughes, and D. M. McGregor (1982), Analysis procedures at the International Seismological Centre, *Physics of the Earth and Planetary Interiors*, *30*, 85–93.

Amante, C., and B. W. Eakins (2009), ETOPO1 1 arc-minute global relief model: procedures, data sources and analysis, *NOAA Technical Memorandum NESDIS NGDC-24*, NOAA.

Balfour, N., R. Baldwin, and A. Bird (2008), Magnitude calculations in Antelope 4.10, *Analysis Group Note of Geological Survey of Canada*, pp. 1–13.

Bennett, T. J., V. Oancea, B. W. Barker, Y.-L. Kung, M. Bahavar, B. C. Kohl, J. . Murphy, and I. K. Bondár (2010), The nuclear explosion database NEDB: a new database and web site for accessing nuclear explosion source information and waveforms, *Seismological Research Letters*, *81*, https://doi.org/10.1785/gssrl.81.1.12.

Bisztricsany, E. A. (1958), A new method for the determination of the magnitude of earthquakes, *Geofiz. Kozl*, pp. 69–76.

Bolt, B. A. (1960), The revision of earthquake epicentres, focal depths and origin time using a high-speed computer, *Geophysical Journal of the Royal Astronomical Society*, *3*, 434–440.

Bondár, I., and K. McLaughlin (2009a), A new ground truth data set for seismic studies, *Seismological Research Letters*, *80*, 465–472.

Bondár, I., and K. McLaughlin (2009b), Seismic location bias and uncertainty in the presence of correlated and non-Gaussian travel-time errors, *Bulletin of the Seismological Society of America*, *99*, 172–193.

Bondár, I., and D. Storchak (2011), Improved location procedures at the International Seismological Centre, *Geophysical Journal International*, *186*, 1220–1244.

Bondár, I., E. R. Engdahl, X. Yang, H. A. A. Ghalib, A. Hofstetter, V. Kirchenko, R. Wagner, I. Gupta, G. Ekström, E. Bergman, H. Israelsson, and K. McLaughlin (2004), Collection of a reference event set for regional and teleseismic location calibration, *Bulletin of the Seismological Society of America*, *94*, 1528–1545.

Bondár, I., E. Bergman, E. R. Engdahl, B. Kohl, Y.-L. Kung, and K. McLaughlin (2008), A hybrid multiple event location technique to obtain ground truth event locations, *Geophysical Journal International*, *175*, https://doi.org/10.1111/j.1365246X.2008.03867x.

Bormann, P., and J. W. Dewey (2012), The new IASPEI standards for determining magnitudes from digital data and their relation to classical magnitudes, IS 3.3, *New Manual of Seismological Observatory Practice 2 (NMSOP-2), P. Bormann (Ed.)*, pp. 1–44, https://doi.org/10.2312/GFZ.NMSOP-2_IS_3.3,10.2312/GFZ.NMSOP-2.

Bormann, P., and J. Saul (2008), The new IASPEI standard broadband magnitude mB, *Seism. Res. Lett*, *79*(5), 698–705.

Bormann, P., R. Liu, X. Ren, R. Gutdeutsch, D. Kaiser, and S. Castellaro (2007), Chinese national network magnitudes, their Relation to NEIC magnitudes and recommendations for new IASPEI magnitude standards, *Bulletin of the Seismological Society of America*, *97*(1B), 114–127, https://doi.org/10.1785/012006007835.

Bormann, P., R. Liu, Z. Xu, R. Ren, and S. Wendt (2009), First application of the new IASPEI teleseismic magnitude standards to data of the China National Seismographic Network, *Bulletin of the Seismological Society of America*, *99*, 1868–1891, https://doi.org/10.1785/0120080010.

Chang, A. C., R. H. Shumway, R. R. Blandford, and B. W. Barker (1983), Two methods to improve location estimates - preliminary results, *Bulletin of the Seismological Society of America*, *73*, 281–295.

Choy, G. L., and J. L. Boatwright (1995), Global patterns of readiated seismic energy and apparent stress, *J. Geophys. Res.*, *100*(B9), 18,205–18,228.

Dziewonski, A. M., and F. Gilbert (1976), The effect of small, aspherical perturbations on travel times and a re-examination of the correction for ellipticity, *Geophysical Journal of the Royal Astronomical Society*, *44*, 7–17.

Dziewonski, A. M., T.-A. Chou, and J. H. Woodhouse (1981), Determination of earthquake source parameters from waveform data for studies of global and regional seismicity, *J. Geophys. Res.*, *86*, 2825–2852.

Engdahl, E. R., and R. H. Gunst (1966), Use of a high speed computer for the preliminary determination of earthquake hypocentres, *Bulletin of the Seismological Society of America*, *56*, 325–336.

Engdahl, E. R., and A. Villaseñor (2002), Global seismicity: 1900-1999, *International Handbook of Earthquake Engineering and Seismology, International Geophysics series*, *81A*, 665–690.

Engdahl, E. R., R. van der Hilst, and R. Buland (1998), Global teleseismic earthquake relocation with improved travel times and procedures for depth determination, *Bulletin of the Seismological Society of America*, *88*, 722–743.

Flinn, E. A., and E. R. Engdahl (1965), Proposed basis for geographical and seismic regionalization, *Reviews of Geophysics*, *3*(1), 123–149.

Flinn, E. A., E. R. Engdahl, and A. R. Hill (1974), Seismic and geographical regionalization, *Bulletin of the Seismological Society of America*, *64*, 771–993.

Gutenberg, B. (1945a), Amplitudes of P, PP and S and magnitude of shallow earthquakes, *Bulletin of the Seismological Society of America*, *35*, 57–69.

Gutenberg, B. (1945b), Magnitude determination of deep-focus earthquakes, *Bulletin of the Seismological Society of America*, *35*, 117–130.

Gutenberg, B. (1945c), Amplitudes of surface waves and magnitudes of shallow earthquakes, *Bulletin of the Seismological Society of America*, *35*, 3–12.

Gutenberg, B., and C. F. Richter (1956), Magnitude and Energy of earthquakes, *Ann. Geof.*, *9*, 1–5.

Hutton, L. K., and D. M. Boore (1987), The ML scale in southern California, *Bulletin of the Seismological Society of America*, *77*, 2074–2094.

IASPEI (2005), Summary of Magnitude Working group recommendations on standard procedures for determining earthquake magnitudes from digital data, http://www.iaspei.org/commissions/CSOI.html#wgmm,http://www.iaspei.org/commissions/CSOI/summary_of_WG_recommendations_2005.pdf.

IASPEI (2013), Summary of magnitude working group recommendations on standard procedures for determining earthquake magnitudes from digital data, http://www.iaspei.org/commissions/CSOI/Summary_of_WG_recommendations_20130327.pdf.

IDC (1999), IDC processing of seismic, hydroacoustic and infrasonic data, *IDC Documentation*.

Jeffreys, H., and K. E. Bullen (1940), *Seismological Tables*, British Association for the Advancement of Science.

Kanamori, H. (1977), The energy release in great earthquakes, *J. Geophys. Res.*, *82*, 2981–2987.

Kennett, B. L. N. (2006), Non-linear methods for event location in a global context, *Physics of the Earth and Planetary Interiors*, *158*, 45–64.

Kennett, B. L. N., E. R. Engdahl, and R. Buland (1995), Constraints on seismic velocities in the Earth from traveltimes, *Geophysical Journal International*, *122*, 108–124.

Kennett, B. L. N., E. R. Engdahl, and R. Buland (1996), Ellipticity corrections for seismic phases, *Geophysical Journal International*, *127*, 40–48.

Lee, W. H. K., R. Bennet, and K. Meagher (1972), A method of estimating magnitude of local earthquakes from signal duration, *U.S. Geol. Surv.*, Open-File Rep.

Lentas, K., D. D. Giacomo, J. Harris, and D. A. Storchak (2019), The ISC Bulletin as a comprehensive source of earthquake source mechanisms, *Earth System Science Data*, *11*(2), 565–578, https://doi.org/10.5194/essd-11-565-2019.

Leptokaropoulos, K. M., A. K. Adamaki, R. G. Roberts, C. G. Gkarlaouni, and P. M. Paradisopoulou (2018), Impact of magnitude uncertainties on seismic catalogue properties, *Geophysical Journal International*, *213*(2), 940–951, https://doi.org/10.1093/gji/ggy023.

Murphy, J. R., and B. W. Barker (2006), Improved focal-depth determination through automated identication of the seismic depth phases pP and sP, *Bulletin of the Seismological Society of America*, *96*, 1213–1229.

NMSOP-2 (2012), *New Manual of Seismological Observatory Practice (NMSOP-2)*, IASPEI, GFZ, German Research Centre for Geosciences, Potsdam, https://doi.org/10.2312/GFZ.NMSOP-2.

Nuttli, O. W. (1973), Seismic wave attenuation and magnitude relations for eastern North America, *J. Geophys. Res.*, *78*, 876–885.

Richter, C. F. (1935), An instrumental earthquake magnitude scale, *Bulletin of the Seismological Society of America*, *25*, 1–32.

Ringdal, F. (1976), Maximum-likelihood estimation of seismic magnitude, *Bulletin of the Seismological Society of America*, *66*(3), 789–802.

Sambridge, M. (1999), Geophysical inversion with a neighbourhood algorithm, *Geophysical Journal International*, *138*, 479–494.

Sambridge, M., and B. L. N. Kennett (2001), Seismic event location: non-linear inversion using a neighbourhood algorithm, *Pure and Applied Geophysics*, *158*, 241–257.

Storchak, D. A., J. Schweitzer, and P. Bormann (2003), The IASPEI standard seismic phases list, *Seismological Research Letters*, *74*(6), 761–772.

Storchak, D. A., J. Schweitzer, and P. Bormann (2011), Seismic phase names: IASPEI Standard, in *Encyclopedia of Solid Earth Geophysics*, edited by H.K. Gupta, pp. 1162–1173, Springer.

Storchak, D. A., J. Harris, L. Brown, K. Lieser, B. Shumba, R. Verney, D. Di Giacomo, and E. I. M. Korger (2017), Rebuild of the Bulletin of the International Seismological Centre (ISC), part 1: 1964–1979, *Geoscience Letters*, *4*(32), https://doi.org/10.1186/s40562-017-0098-z.

Storchak, D. A., J. Harris, L. Brown, K. Lieser, B. Shumba, and D. Di Giacomo (2020), Rebuild of the Bulletin of the International Seismological Centre (ISC)-part 2: 1980–2010, *Geoscience Letters*, *7*(18), https://doi.org/10.1186/s40562-020-00164-6.

Stähler, S., and K. Sigloch (2014), Fully probabilistic seismic source inversion–Part 1: Efficient parameterisation, *Solid Earth*, *5*(2), 1055–1069, https://doi.org/10.5194/se-5-1055-2014.

Stähler, S., and K. Sigloch (2016), Fully probabilistic seismic source inversion–Part 2: Modelling errors and station covariances, *Solid Earth*, *7*(6), 1521–1536, https://doi.org/10.5194/se-7-1521-2016.

Tsuboi, C. (1954), Determination of the Gutenberg-Richter's magnitude of earthquakes occurring in and near Japan, *Zisin (J. Seism. Soc. Japan), Ser. II*(7), 185–193.

Tsuboi, S., K. Abe, K. Takano, and Y. Yamanaka (1995), Rapid determination of Mw from broadband P waveforms, *Bulletin of the Seismological Society of America*, *85*(2), 606–613.

Uhrhammer, R. A., and E. R. Collins (1990), Synthesis of Wood-Anderson Seismograms from Broadband Digital Records, *Bulletin of the Seismological Society of America*, *80*(3), 702–716.

Vaněk, J., A. Zapotek, V. Karnik, N. V. Kondorskaya, Y. V. Riznichenko, E. F. Savarensky, S. L. Solov'yov, and N. V. Shebalin (1962), Standardization of magnitude scales, *Izvestiya Akad. SSSR., Ser. Geofiz.*(2), 153–158, Pages 108–111 in the English translation.

Villaseñor, A., and E. R. Engdahl (2005), A digital hypocenter catalog for the International Seismological Summary, *Seismological Research Letters*, *76*, 554–559.

Villaseñor, A., and E. R. Engdahl (2007), Systematic relocation of early instrumental seismicity: Earthquakes in the International Seismological Summary for 1960–1963, *Bulletin of the Seismological Society of America*, *97*, 1820–1832.

Woessner, J., and S. Wiemer (2005), Assessing the quality of earthquake catalogues: estimating the magnitude of completeness and its uncertainty, *Bulletin of the Seismological Society of America*, *95*(2), https://doi.org/10/1785/012040007.

Young, J. B., B. W. Presgrave, H. Aichele, D. A. Wiens, and E. A. Flinn (1996), The Flinn-Engdahl regionalisation scheme: the 1995 revision, *Physics of the Earth and Planetary Interiors*, *96*, 223–297.

sara

www.sara.pg.it

Strong motion


Seismic stations


Modal analysis


Strong motion network - Turkey

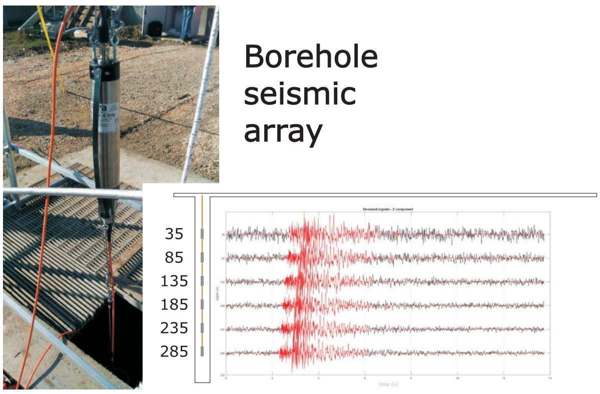

Borehole seismic array

Broad band seismometers:
- observatory grade
- compact
- borehole

SARA electronic instruments s.r.l.
your reliable and friendly partner in earthquake monitoring and geophysical exploration

sara

www.sara.pg.it

contact us at: info@sara.pg.it
or by telephone: +39 075 5051014

Weak motion sensor and
microtremor (HVSR)
Nodal systems - Terrabot

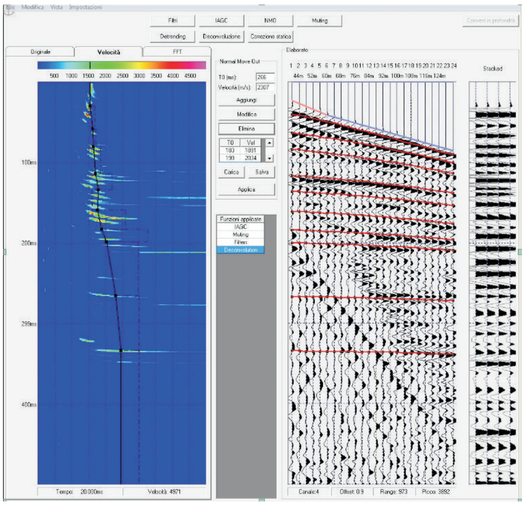

Geophysical exploration software

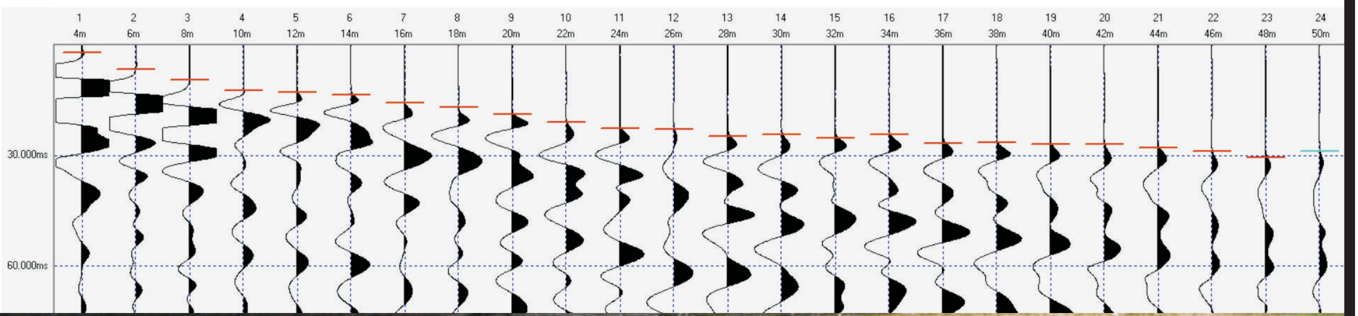

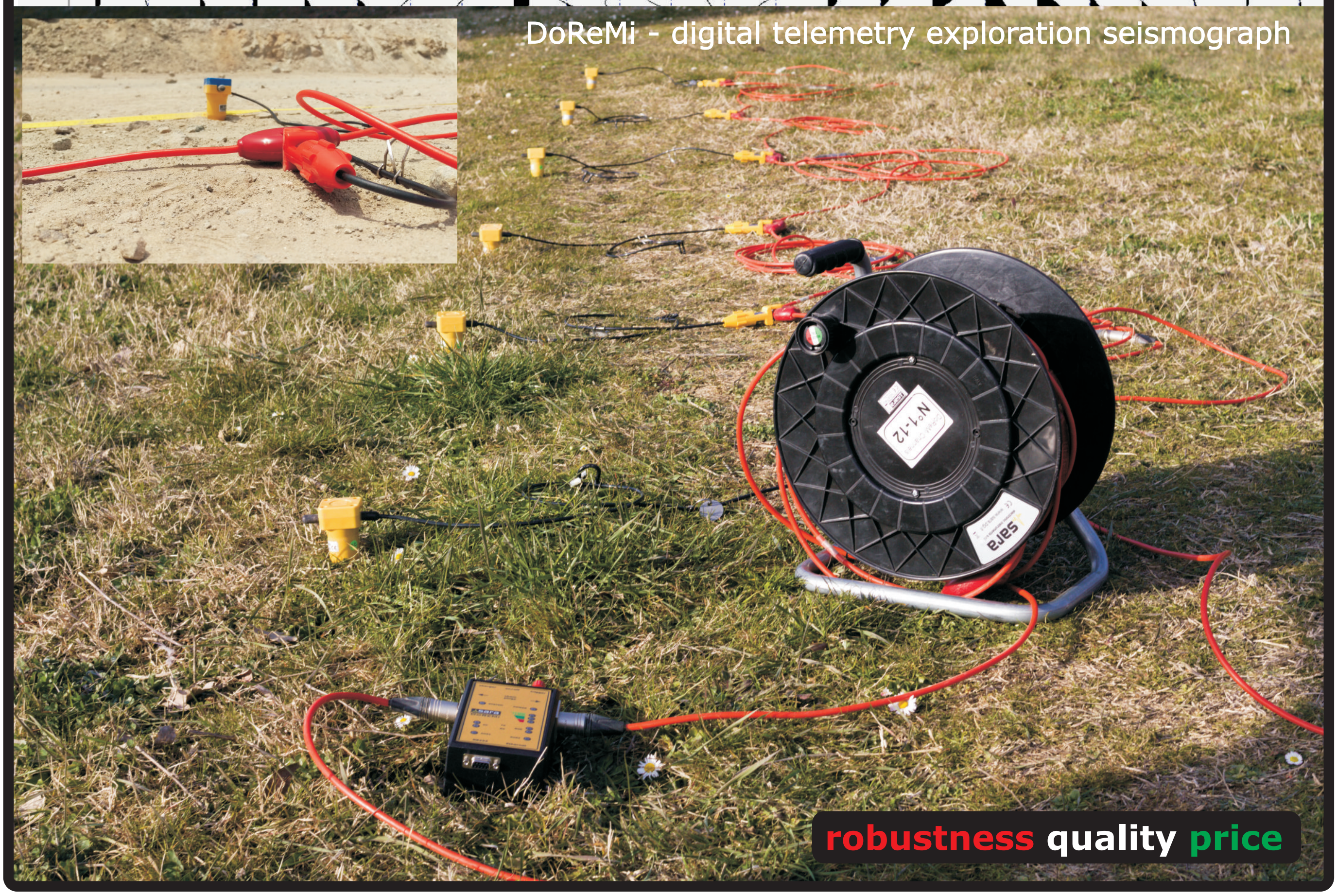

DoReMi - digital telemetry exploration seismograph

PERFECTLY PAIRED

arolla + **nair** slim

VE series broadband seismometer

GMS series recorder / digitiser

The **arolla** broadband seismometer features a compact and lightweight design, yet it is rugged and versatile, making it an ideal choice for many applications. Weak-motion, broadband seismometers have the highest sensitivity among seismometers over long periods, and are able to pick up even small tremors at great distances.

The culmination of years of experience designing reliable, high-precision, low-noise seismic equipment enabled the creation of **arolla**.

Best paired with **arolla** is **nair** slim—GeoSIG's latest generation seismic recorder that offers highest performance, excellent operational flexibility and enhanced connectivity. GeoSIG's **nair** slim is a self-contained instrument that acquires and processes data in real time. It boasts an impressive 146db (0.01-30Hz), making it suitable for weak motion precision recording. A set comprising **arolla** and **nair** slim is fully compatible with existing GeoSIG systems that may already be in place. Also, its simple upgrade path makes **nair** slim "future proof."

A winning combination: **arolla** and **nair** slim!

GeoSIG
swiss made to measure

For more information, contact us at info@geosig.com

GeoSIG

swiss made to measure

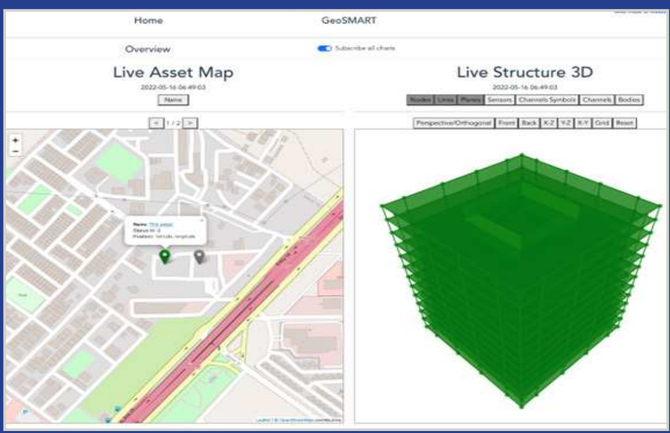

GeoSMART Offers Peak Performance

GeoSMART is an innovative graphical application that provides **tools** for realtime structural health monitoring for civil engineering structures. GeoSMART, with its “smart” features, can **monitor** and display the status of a structure that is equipped with GeoSIG measuring instruments. GeoSMART is S2HM in a Box; it has been designed to meet fundamental engineering requirements with respect to **structural health** monitoring applications.

Main Features of GeoSMART

- Support for any type of sensor such as acceleration, velocity, displacement, tilt, wind, temperature, strain, and many more.
- User-friendly web-interface for an intuitive experience.
- 3D representation of any structure with live status.
- Interactive zoom, rotate, pan, visibility and projection.
- Multiple structures on live interactive map.
- Real-time continuous data acquisition and processing.
- Storage and direct download of all data and graphics.
- Data export for long-term storage.
- Sliding window-based continuous frequency analyses: Amplitude, Spectrogram and Response Spectra.
- Rigid body motions in translations and rotations.
- Interpolations for non-instrumented areas.
- Interstory drift ratios and torsion.
- Exceedance of predefined threshold levels or curves.
- Plot of archive data and statistical information.
- Live screen indicators and HTML formatted emails.
- Individualised notifications to users / user groups.
- Customisable messages such as action plans.
- Reports including actual images of plotted graphics.
- Hardware relays to start or shutdown any process.
- Advanced user accessible powerful database.
- API to fetch and externally manipulate the stored data.

GeoSIG Ltd | Wiesenstrasse 39
8952 Schlieren, Switzerland
T: +41 44 810 2150 | F: + 41 44 810 2350
www.geosig.com

For more information, contact us at info@geosig.com